Identification of metabolic genes essential for proliferation of clear cell Renal Cell Carcinoma (ccRCC) cells

Heike Miess

University College London

and

Cancer Research UK London Research Institute

PhD Supervisor: Prof Almut Schulze

A thesis submitted for the degree of

Doctor of Philosophy

University College London

September 2014

Declaration

I, Heike Miess, confirm that the work presented in this thesis is my own, apart from the following:

The screen was performed in collaboration with the High Throughput Screening (HTS) facility headed by Dr Michael Howell at the Cancer Research UK London Research Institute. Optimisation of transfection reagents was performed by Dr Ming Jiang (HTS), who also assisted during the screen. Screen data analysis was performed by Dr Rebecca Saunders (HTS).

Cell cycle analysis via FACS (cytohistochemistry, FACS analysis with subsequent data analysis) was performed by members of the FACS facility at the Cancer Research UK London Research Institute.

Bioinformatic analysis of the ccRCC TCGA data set was performed by Richard Mitter from the Bioinformatics and Biostatistics (BABS) facility at Cancer Research UK London Research Institute.

Where information has been derived from other sources, I confirm that this has been indicated in the thesis.

Abstract

Kidney cancer accounts for 2-3% of adult malignancies with clear cell renal cell carcinoma (ccRCC) being the most common histological subtype (70-80% of cases). Interestingly, ccRCCs show a highly distinct metabolic phenotype making this disease stand out amongst other cancer types. The underlying causes of the aberrant metabolism in ccRCC are not fully understood, but metabolic transformation could provide novel strategies for targeted therapies in this disease. The pVHL tumour suppressor is located on chromosome 3p21, which is frequently lost in ccRCC. pVHL is a negative regulator of the Hypoxia-inducible factor (HIF), which orchestrates the cellular response to oxygen deprivation and might contribute to the aberrant metabolic phenotype of ccRCC cells.

In order to reveal metabolic weaknesses in ccRCC, a customised RNAi screen targeting 230 different metabolic enzymes, regulators and nutrient transporters was performed. The screen was performed in a panel of 5 ccRCC pVHL-null cell lines and included their counterparts with reconstituted pVHL, in order to also identify potential vulnerabilities that depend on VHL function. With this approach, several genes that are essential for ccRCC cell viability but dispensable for the survival of non-malignant renal epithelial cells were identified. It was found that ccRCC cell lines are highly sensitive to ablation of components of the glutathione-dependent reactive oxygen species (ROS) detoxification system. Silencing of enzymes of the glutathione biosynthesis pathway or different glutathione peroxidases (GPXs) severely impaired cell viability. One of the precursors of glutathione biosynthesis is glutamate, which is generated from glutamine by glutaminase (GLS). Interestingly, there is evidence that ccRCCs are highly dependent on the MYC oncogene, which induces many enzymes within the glutaminolysis pathway. Indeed, we found that glutamine starvation or chemical inhibition of GLS reduced proliferation and viability of ccRCC cells, confirming the importance of this pathway in ccRCC.

In conclusion, the study reported in this thesis provides insight into the metabolic dependencies of ccRCC cells and emphasises the need for a solid anti-oxidant system for ccRCC cell survival and proliferation. Concomitantly, the reliance of ccRCC cells on glutamine and glutathione is a vulnerability that could potentially be exploited for diagnostic and/or therapeutical applications.

Acknowledgements

First and foremost I would like to thank my supervisor Almut Schulze for inviting me to be part of the Gene Expression Analysis (GEA) Lab, for all the scientific discussions, advice and support throughout the last 4 years. I learned a lot in this stimulating and engaging environment. Unfortunately, for the last year we had only a long-distant relationship, nevertheless, she maintained to be approachable. I'm convinced her new lab in Würzburg, DE will continue the successful research that started in the LRI.

I sincerely thank Julian Downward for his offer to join the Signal Transduction Lab (STL) for my final PhD year to enable me finishing in the LRI as well as for all the support and advice he has given me first as a thesis committee member and then as a secondary supervisor during my PhD time. It is very much appreciated!

I would also like to thank my first secondary supervisor Charles Swanton for helpful scientific input, discussions and support over the last 4 years.

I would also like to thank my examiners Gyorgy Szabadkai and Miguel Martins for taking the time to evaluate my research and scientific understanding.

I would like to thank all past GEA lab members: Emma, Caroline, Claudio, Franzi, Susana, Barrie and Beatrice. It was a pleasure working with you. I learned a lot from you and with you. Claudio I have to thank for giving me a warm welcome to London and the LRI by introducing me to the Catalan/STL crew. Beatrice, a very special thank you for making working in the lab smoothly, as you always made sure that we had what we needed and that we got what we wanted ASAP but also for your continuous technical help and advice. Barrie, a BIG THANK YOU! from me to you for all your help, encouragement, advice, support inside and outside of the lab. You're scientific input into this work was/is invaluable. You're good mood and positivity was infectious and just what the lab needed. I'll miss the old Barrie.

I thank past and present members of the STL lab, Esther, Elza, Miguel, Miriam, George for welcoming me in London first and Ralph, Maggie, Alice, Matt, Danïel, Dave and Pat for welcoming me later in the lab and making the transition from the 1st to the 2nd floor as smooth as possible, for all the entertaining Friday night Pub socials at the George but also for sharing reagents, scientific advice and help. I'd like to say a BIG THANK YOU! to Miriam, Clare, and Davide for all their encouragement, scientific input and advice inside and outside of work and for being great people to hang out with also outside the lab.

Thank you, past and present members of the TCT lab, Andrew, Rebecca, Marco, Eva and Nnenna, for technical help, reagents and discussions; Sally, Carlos and Andy for entertaining discussions that made the long tissue-culture days during the last year just that little bit more bearable.

I thank all the core facilities I had a chance to interact with: equipment park, cell services, light microscopy, BABS, particularly Richard Mitter for bioinformatical analyses of the TCGA dataset and Stuart for trying to teach me statistics, as well as the FACS lab, particularly Andy Filby for his help, advice and patience.
I am indebted to the High Throughput Facility, and would like to say a BIG thank you particularly to Mike Howell and Ming Jiang for all their help in planning, setting up and executing the screen as well as the continuous interest, advice and support thereafter – oh, and not to forget, the countless Acumen, Cellomics and IncuCyte runs they started for me. I also thank Becky Saunders for analysing and reanalysing and patiently reanalysing my screen data.
I have to thank the first floor lab aids, actually, the best LRI lab aids in my opinion anyway, Ian and Chris. Always super helpful, always super friendly, always there for a distracting chat, and, if you are in Chris' good books, you can awe a card trick or two.

I thank Sally Leevers for advice and the (student) admin team (Sabina Ebbols, Rachel Coulthard, Andrew Brown, Alice Birch, Sophia Kontakkis, David Bacon, Emma Rainbow) for keeping bureaucracy for us students to a minimum, for organising all sorts of things and for keeping us in check re deadlines.

I thank my fellow students and great friends especially Alessandra, Mariana, Gary, Richard, Rafal, for having deep conversations, weird conversations, nonsense conversations… for sharing many happy moments, for listening, support and encouragement, especially during the last few months; just for being there and sharing the experience. I am grateful to have met all of you and all the other PhDs in the 2010 year group and across the years. I hope we'll keep in touch, also once we're scattered around the world again.

Last but by far not least, I thank my family, particularly my parents, Karin and Christian, my grandparents and the best sister in the world, Henrike, with all my heart for always being there for me, for having faith in me, for believing in me, for supporting me, no matter what. They made me what I am today and I wouldn't be where I am today if it wasn't for them.

Ich möchte meiner Familie, v.a. meinen Eltern, Karin und Christian und meinen Grosseltern herzlichst für jegliche Unterstützung, gutes Zureden, an mich glauben ob nah oder fern von Herzen DANKE! sagen. Ihr habt mich zu dem gemacht was ich heute bin.

Finally, I'd like to address and thank everybody who I have not mentioned by name (there is actually a space limit) but whom I met along the way and who influenced me in one way or another. Thanks for your contribution to my life! Be assured you left a mark!

Table of Contents

Table of Figures

List of Tables

Chapter 1: Introduction

1.1 Cancer – cell proliferation out of control

Under normal conditions, cell proliferation is a highly controlled process required for tissue growth and regeneration. Cell proliferation is stimulated through growth factors such as epidermal growth factor (EGF), platelet-derived growth factor (PDGF), insulin-like growth factor (IGF), vascular endothelial growth factor (VEGF), tumour growth factor α (TGF-α) or other mitogens and inhibited by growth inhibitory factors, such as TGF-β. Growth factors engage intracellular signalling cascades that eventually lead to regulation of gene expression and modulation of the cell cycle. Moreover, if the cell senses stress or accumulated damage, such as DNA breaks, lipid oxidation or protein misfolding, cell cycle checkpoints get induced and stall cell cycle progression to provide time for damage repair. Is the damage beyond repair, apoptosis (the best described form of programmed cell death) is induced to remove the faulty cell from the system.

Cancer cells are fast proliferating cells that are literally 'out of control'. They display increased growth factor signalling through increased expression of activating mutations in components of growth factor signalling pathways. Furthermore, cancerous cells acquired means to overrule cell cycle regulation, most often through mutations in p53, and evade apoptosis. A summary of common phenotypes, 10 have been defined so far, that contribute to malignant transformation from normal cells to tumour cells is depicted in Figure 1.1 and is described in more detail in the Hallmarks of Cancer (Hanahan and Weinberg, 2011, Hanahan and Weinberg, 2000).

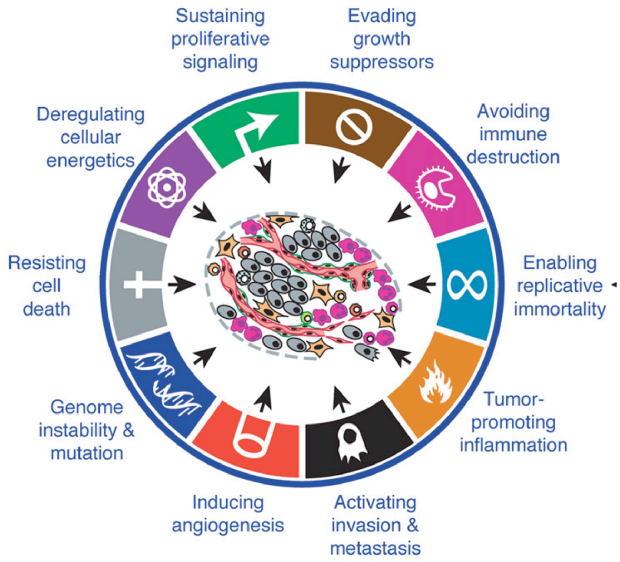

Figure 1.1: The Hallmarks of Cancer
Schematic overview of events frequently occurring in the process of malignant transformation and important in tumour maintenance. Events can be cell intrinsic, arise from extrinsic stimuli or are mediated through cell-cell interactions. Schematic was modified after (Hanahan and Weinberg, 2011) with permission.

Two signalling cascades frequently deregulated in cancer, the RAS/MAP kinase and the PI3K/AKT/mTOR pathway, are initiated by growth factor binding to a suitable growth factor receptor tyrosine kinase (RTK). Subsequent phosphorylation/activation events eventually lead to changes in gene expression promoting cell survival, growth and proliferation (Figure 1.2) (Cully et al., 2006).

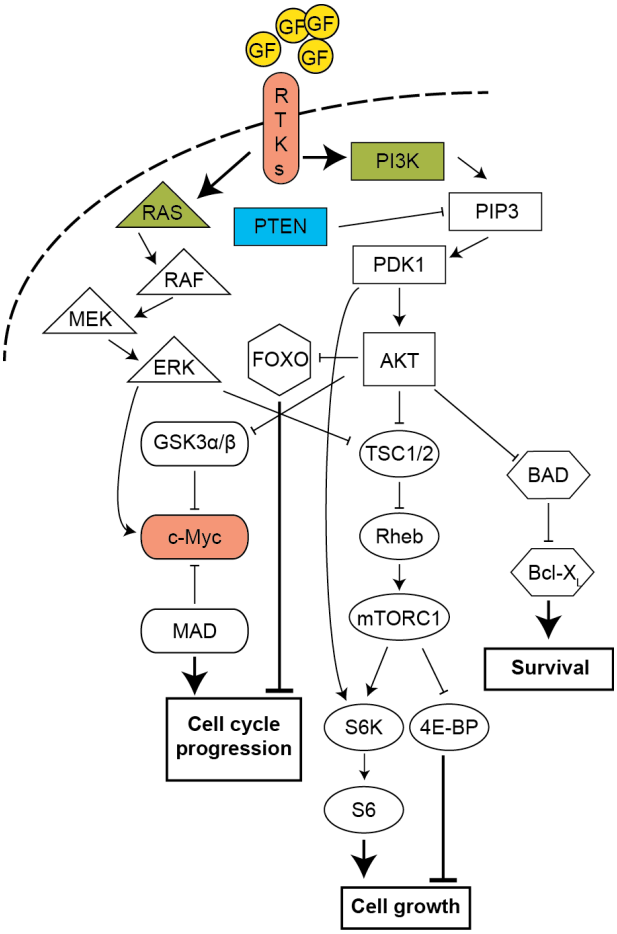

Figure 1.2: Frequently deregulated growth factor signalling in cancer cells
Schematic of receptor tyrosine kinase (RTK) downstream signalling to promote cell growth, proliferation and survival. Upon stimulation through growth factors (GF), RTKs activate RAS or PI3K through phosphorylation. The PI3K/AKT cascade leads to cell cycle progression via inhibition of GSK3 resulting in the stabilisation and activation of c-Myc. Inhibition of FOXO proteins by AKT also leads to cell cycle progression. Activation of the mTOR pathway by AKT induces protein translation, ribosomal biogenesis and cell growth, while inhibition of pro-apoptotic BCL2 proteins promotes cell survival. The RAS/MAP kinase cascade stimulates cell growth and proliferation via positively regulating the mTOR pathway and c-MYC, respectively. Highlighted in red are proteins that are frequently upregulated in cancer; highlighted in green are proteins that are often activated in tumours due to genetic mutations and highlighted in blue, PTEN, is frequently lost in cancer.

1.2 Cancer – cellular metabolism rewired

Metabolic requirements differ according to the cell type. In resting differentiated cells, metabolism is tuned to generate enough energy to maintain structural integrity and fulfil the cells' physiological role. If the cellular function is production or storage of certain substances, the metabolic network is adapted accordingly. In contrast, proliferating cells adapt their metabolism towards generation of macromolecules such as proteins, lipids and nucleic acids, which are needed for cellular growth and division (Thompson et al., 2005, Vander Heiden et al., 2009). Adequate nutrient supply is essential for execution

of metabolic reactions. Nutrients, i.e. carbohydrates, amino acids and fatty acids, are taken up through food and, following resorption in the gut, are transported with the blood to sites of consumption, where they are taken up by the cells through specific transporters. Furthermore, cells rely on sufficient oxygen supply, also provided by the blood stream. Under normal conditions, nutrient and oxygen supply is warranted through an elaborate and efficient vascular system. Growing solid tumours, however, can outgrow the vasculature resulting in inefficient nutrient supply and hypoxic areas.

1.2.1 Cancer cells are hooked on aerobic glycolysis

During the 1920s, Otto Warburg observed that cancer cells displayed high glucose consumption rates concomitant with high lactate secretion rates, a sign of high glycolytic flux (Warburg, 1956a, Warburg, 1956b). This would not be surprising would it not have occurred under ample oxygen conditions. In normal, differentiated cells, under ample oxygen conditions, the tricarboxylic acid (TCA) cycle with associated oxidative phosphorylation (OXPHOS) along the electron transport chain (ETC) in the mitochondria is the main site of adenosine triphosphate (ATP, cellular energy-storing molecule) generation (Figure 1.3A). Glycolysis, the multi-step conversion of glucose to pyruvate, is prevalent in situations when oxygen is limited as it is an anaerobic process (Figure 1.3A and Figure 1.4). Glycolysis generates less ATP than oxidative phosphorylation but ATP generation is faster (Curi et al., 1988). While conversion of a single glucose molecule to CO_2 yields a total of ~36 ATP molecules (corresponding to 2 ATP, 8 NADH, 2 $FADH_2$) via the mitochondrial TCA cycle and OXPHOS; the net yield from glycolysis for a glucose molecule is only 2 ATP and 2 NADH molecules. Concluding that cancer cells have dysfunctional mitochondria, Warburg defined cancer as a metabolic disease and cancer-characteristic aerobic glycolysis ever since became known as the Warburg Effect (Warburg, 1956b) (Figure 1.3B).

This cancer-characteristic high rate of glucose uptake that exceeds the glucose uptake of resting cells formed the basis of 2-fluoro-2-deoxy-D-glucose (^{18}F)-positron emission tomography ([^{18}F]-FDG-PET), a diagnostic method for detection of tumour lesions in the body (Som et al., 1980, Kelloff et al., 2005). ^{18}F-FDG is a glucose analogue coupled to a positron-emitting radioactive fluorine-18 isotope, which, once it is taken up by a

cell, is trapped in the cell cytoplasm following hexokinase (HK)-mediated phosphorylation and can be visualised using PET scanning technology.

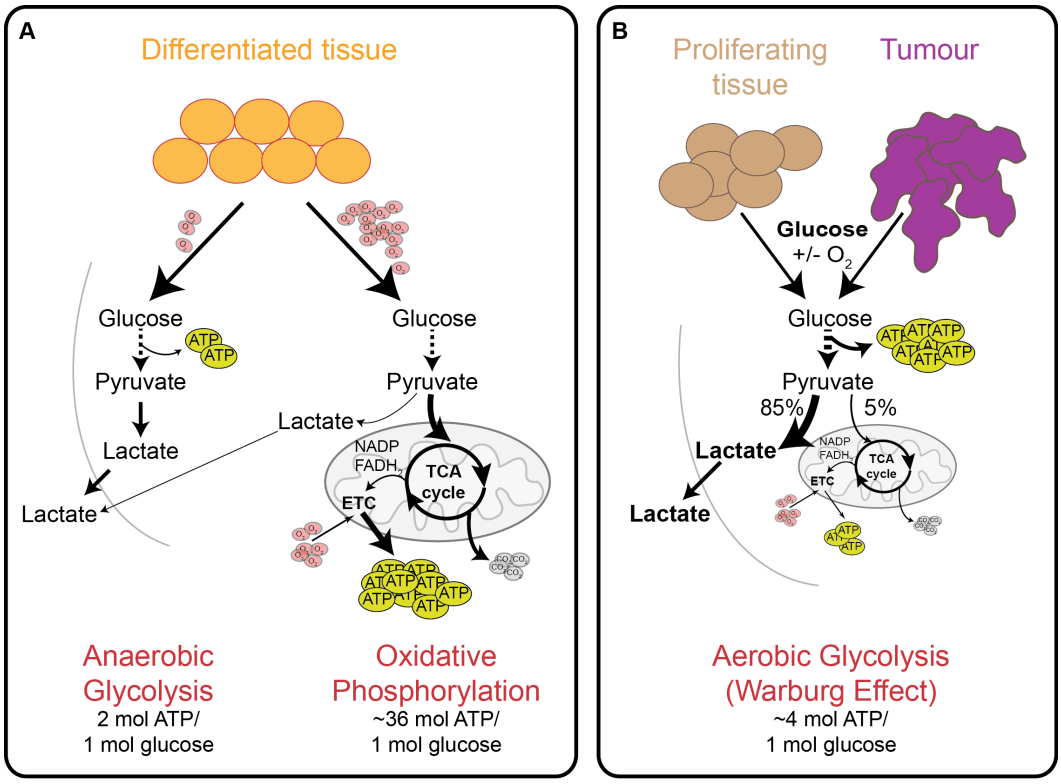

Figure 1.3: Glucose utilisation for energy production in differentiated and proliferative tissue

(A) Under normal oxygen conditions, differentiated, non-proliferating cells use the tricarboxylic acid (TCA) cycle with associated oxidative phosphorylation via the electron transport chain (ETC) as main energy source to fuel cellular homeostasis and function. Only if oxygen levels get low in the microenvironment, cells switch to anaerobic glycolysis. (B) In contrast, proliferating cells and cancer cells often show the so-called Warburg Effect, whereby they mainly rely on glycolysis independent of the oxygen concentration in the microenvironment. In terms of ATP/energy production glycolysis is less efficient, however, intermediates from glucose catabolism serve as precursors for many macromolecules. Actively cycling cells may switch to an increased glycolytic flux to accommodate for efficient cell mass accumulation, which enables cell growth and division.

Although Warburg's theory of cancer being a metabolic disease was proven wrong in the 1960s with the establishment of genetic mutations being causal for tumourigenesis, it took scientists almost 30 years from Warburg's initial observation to realise the importance of metabolism in the context of cancer. In recent years, cancer metabolism gained increasing appreciation so much that it was included in the revised version of the Hallmarks of Cancer (Figure 1.1) (Hanahan and Weinberg, 2000, Hanahan and Weinberg, 2011).

1.2.2 Glycolysis provides precursors for anabolic processes

One reason for why cancer cells operate on such high glycolytic rates is the high demand of building blocks for macromolecules (Lunt and Vander Heiden, 2011, Moreno-Sanchez et al., 2007). Intermediates of glycolysis serve as precursors for the biosynthesis of nucleotides, amino acids (AAs) or phospholipids. Glucose-6-phosphate (G6P) and fructose-6-phosphate (F6P) for example are precursors for purine and pyrimidine biosynthesis via the oxidative arm of the pentose phosphate pathway (PPP). In addition, theses reactions generate NADPH as by-product, which is essential for maintaining cellular redox homeostasis, as it is an important cofactor for enzyme-mediated redox reactions (Figure 1.4). The glycolytic intermediate 3-phosphoglycerate (3PG) is a precursor of serine, which itself is a substrate/precursor for purine and pyrimidine, glycine and cysteine as well as sphingolipids and folate, connecting glycolysis with the PPP, AA biosynthesis and one-carbon metabolism (Locasale, 2013) (Figure 1.4). Another glycolytic intermediate, glyceraldehyde-3-phosphate, is converted to glycerol-3-phosphate and phosphatidic acid and supports phospholipid synthesis, while pyruvate can be converted into alanine (Figure 1.4).

With glycolysis having such a central role in macromolecule biosynthesis, it is not surprising that cancer cells found a way to circumvent the tight regulation of this process, often through upregulation of glycolytic enzymes due to aberrant transcriptional regulation.

In many caner cells, enhanced glucose uptake necessary for increased glycolytic flux is accommodated through upregulation of glucose transporters (GLUT1-5), especially of GLUT1 and GLUT3 (Yamamoto et al., 1990). Hexokinase 2 (HK2), one of the four glycolytic enzyme isoforms (HK1-3 and GCK) that commits glucose to the glycolytic pathway through irreversible conversion to G6P, is also frequently upregulated in different cancer cells (Peng et al., 2008, Wolf et al., 2011).

The rate-controlling reversible conversion of F6P to fructose-2,6-bisphosphate (F2,6BP) and back is mediated by bifunctional 6-phosphofructo-2-kinase/fructose-2,6-bisphosphatases (PFKFBs). F6P is an allosteric activator of phosphofructokinase 1 (PFK1), which converts F6P into F1,6BP and enhances glycolytic flux. The ATP-dependent phosphorylation of F6P is catalysed by the PFK2 activity, while F2,6BP

dephosphorylation is carried out by the FBPase activity. There are four members of the PFKFB homodimeric enzyme family, PFKFB1-4. All but PFKFB3 have equal PFK2 and FBPase activity, while in the PFKFB3 isoform the PFK2 activity dominates (Okar and Lange, 1999, Okar et al., 2001). Many cancer types show high expression of PFKFB3 as adaptation to sustain high-rate glycolysis (Atsumi et al., 2002, Kessler et al., 2008, Minchenko et al., 2005). However, metastatic prostate cancer cells rely on the PFKFB4 FBPase activity to provide the PPP with substrates for NADPH production to sustain cellular redox balance (Ros et al., 2012).

Under hypoxic conditions, pyruvate is converted into lactate instead of entering the TCA cycle in mitochondria. The conversion to lactate is catalysed by lactate dehydrogenase (LDH). There are two LDH isoforms, LDHA and LDHB, and LDHA has been found upregulated in several tumour types (Augoff and Grabowski, 2004, Fantin et al., 2006, Koukourakis et al., 2009).

GLUT1/3, PFKFB3 and LDHA are targets of the transcription factor hypoxia inducible factor 1 (HIF-1), which regulates a metabolic switch from oxidative respiration to anaerobic glycolysis in response to low oxygen levels. HIF activity is often aberrantly high in cancers and will be discussed in more detail below.

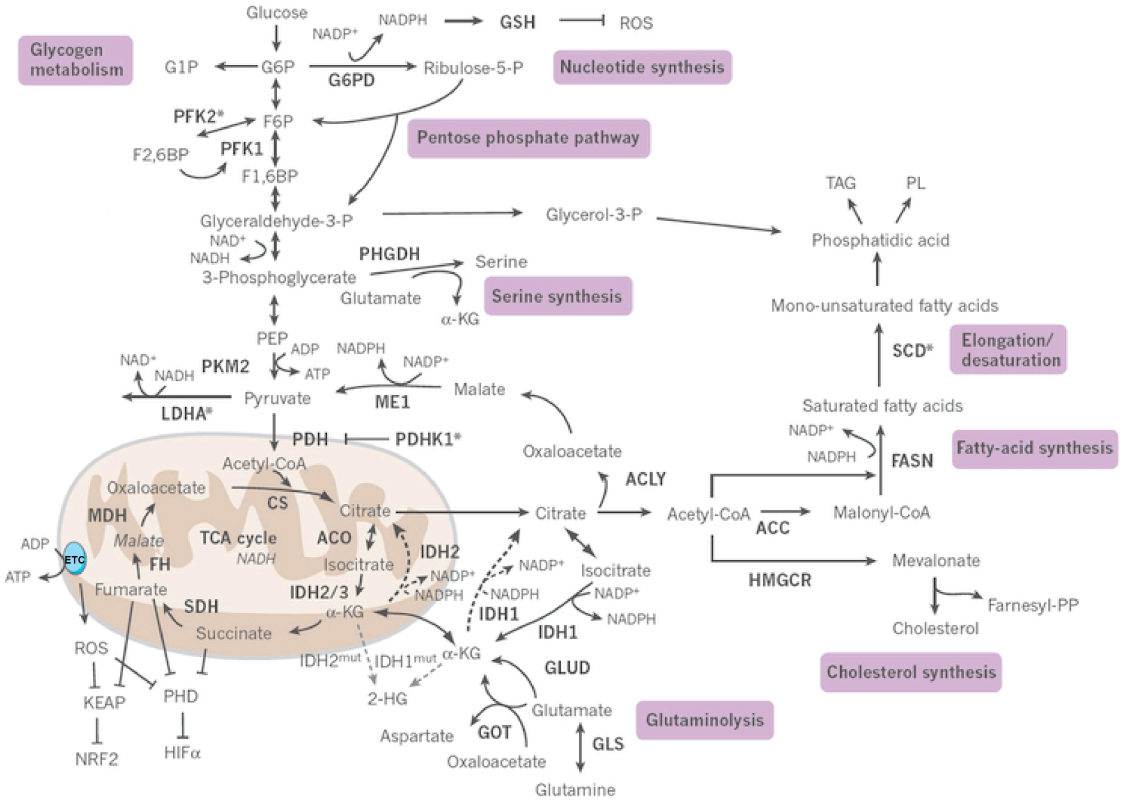

Figure 1.4: Overview of the main metabolic activities in cancer cells

The main metabolic pathways that contribute to the production of macromolecules in mammalian cells are nucleotide synthesis, the pentose phosphate pathway, glycogen and serine synthesis, glutaminolysis, cholesterol synthesis, fatty-acid synthesis and elongation/desaturation. The enzymes involved in these pathways are shown in bold, those induced in response to hypoxia are marked with an asterisk. Metabolic enzymes in the TCA cycle, fumarate hydratase (FH) and succinate dehydrogenase (SDH), can act as tumour suppressors. 2-hydroxyglutarate (2-HG) is produced from α-ketoglutarate (α-KG) by the mutant forms of isocitrate dehydrogenase 1 (IDH1) and IDH2 enzymes that are found in cancer (grey dashed arrow). Reductive carboxylation of α-KG by IDH1 and IDH2 produces citrate for lipid synthesis in hypoxic cells (black dashed arrow). ACC, acetyl-CoA carboxylase; ACLY, ATP citrate lyase; ACO, aconitase; CA9, carbonic anhydrase 9; CoA, coenzyme A; CS, citrate synthase; FASN, fatty-acid synthase; F1,6BP, fructose-1,6-bisphosphate; F2,6BP, fructose-2,6-bisphosphate; F6P, fructose-6-phosphate; GLS, glutaminase; GLUD, glutamate dehydrogenase 1; GOT, glutamic-oxaloacetic transaminase; GSH, glutathione; G1P, glucose-1-phosphate; G6P, glucose-6-phosphate; G6PD, G6P dehydrogenase; HIF, hypoxia inducible factor; HMGCR, 3-hydroxy-3-methylglutaryl-CoA reductase; KEAP, kelch-like ECH-associated protein 1; LDHA, lactate dehydrogenase A; MDH, malate dehydrogenase; ME1, malic enzyme 1; NRF2, nuclear factor (erythroid-derived 2)-like 2; PDH, pyruvate dehydrogenase; PDHK1, pyruvate dehydrogenase kinase; PEP, phosphoenolpyruvate; PFK, phosphofructokinase; PHD, prolyl hydroxylases; PHGDH, phosphoglycerate dehydrogenase; PKM2, pyruvate kinase M2; PL, phospholipids; ROS, reactive oxygen species; SCD, stearoyl-CoA desaturase; TAG, triacylglycerides. Figure and legend taken from and modified after (Schulze and Harris, 2012) with permission.

1.2.3 Glutaminolysis provides precursors for anabolic processes

Besides glucose, glutamine, the most abundant AA, is another important cellular carbon source for anabolic processes and additionally provides nitrogen for the synthesis of non-essential AAs and nucleotides. Following uptake by the cell through specialised transporters such as solute carrier family 1 member 5 (SLC1A5), glutamine is converted to glutamate and ammonia via glutaminase (GLS). The process by which glutamine is shunted into other metabolic pathways following conversion to glutamate is termed glutaminolysis. The transcriptional programme of mitochondrial glutaminolysis is regulated by the proto-oncogenen c-MYC. Consequently, MYC transformed cells are referred to as glutamine addicted, as glutamine withdrawal is highly detrimental to theses cells, even more than glucose withdrawal (Dang, 2009, Dang, 2012, Wise et al., 2008, Yuneva et al., 2007).

The amino-group of glutamate can be transferred to oxaloacetate, in a reaction catalysed by glutamic-oxaloacetic transaminase (GOT), to form aspartate. Alternatively, glutamate can be converted to α-ketogluterate (α-KG) by glutamate dehydrogenase (GLUD). α-KG can then enter the mitochondria to replenish the TCA cycle for ATP/energy generation or to generate TCA cycle intermediates required for biosynthetic processes, such as citrate, a process called anaplerosis (DeBerardinis et al., 2007). However, α-KG can also undergo isocitrate dehydrogenase (IDH)-mediated reductive decarboxylation (NADPH-dependent) to directly yield citrate, a precursor of fatty acid synthesis (DeBerardinis et al., 2007, Mullen et al., 2012). There are three IDH isoforms, IDH1-3, with IDH1 being mainly cytoplasmic, while the other two are localised to the mitochondrial compartment. Hypoxic cancer cells and clear cell renal cell carcinoma cells were found to make use of this reductive glutamine metabolism for lipogenesis (Mullen et al., 2012, Wise et al., 2008).

1.2.4 Cancer cells reactivate *de novo* lipid synthesis

Apart from hepatocytes and adipocytes, most cells within the adult human body are not capable of lipogenesis but rely almost exclusively on external lipid supply, in form of free fatty acids (fFAs) or low-density lipoproteins (LDLs), via the blood stream. The expression of enzymes involved in *de novo* lipid synthesis is mostly regulated by sterol

regulatory element (SRE)-binding proteins (SREBP) (Eberle et al., 2004, Horton, 2002). SREBPs are basic-helix-loop-helix-leucine zipper transcription factors, that come in three isoforms: SREBP1a, SREBP1c and SREBP2, whereby the two SREBP1 isoforms are generated through alternative splicing of the same gene locus (Brown and Goldstein, 1997). Although all isoforms have largely overlapping functions, SREBP1c mainly regulates fatty acid, triacylglycerol and phospholipid synthesis, while SREBP2 controls cholesterol synthesis (Bengoechea-Alonso and Ericsson, 2007, Horton, 2002). The activation of all SREBP isoforms is cholesterol dependent and SREBPs are processed, accumulate in the nucleus and become transcriptionally active when cholesterol is limited (Espenshade et al., 2002). In addition, SREBP1 is also activated upon insulin-stimulated PI3K/AKT/mTORC1 signal transduction, linking the regulation of protein synthesis with lipid production (Li et al., 2010, Porstmann et al., 2008, Peterson et al., 2011, Yecies and Manning, 2011). Moreover, the finding that p53 can cooperate with SREBP2 to drive transformation in breast epithelial cells by inducing enzymes of the mevalonate (cholesterol) pathway links lipogenesis to tumourigenesis (Freed-Pastor et al., 2012). Indeed, reports have shown, that cancer cells reactivate *de novo* lipid synthesis even in the presence of ample exogenous lipid supply and present increased expression of enzymes involved in lipid synthesis such as ATP citrate lyase (ACLY), acetyl-coA carboxylase (ACC) and fatty acid synthase (FASN) (Medes et al., 1953, Menendez and Lupu, 2007, Yahagi et al., 2005, Yoon et al., 2007). The exact role of lipid synthesis in cancer still needs to be explored, but it is reasonable to assume that lipogenesis contributes to generation of biological membranes, energy via FA-oxidation/β-oxidation, protein modifications and second messengers to support cell growth and proliferation (Santos and Schulze, 2012, Baenke et al., 2013).

1.2.5 Pentose Phosphate Pathway is important for sustaining redox balance

The PPP is split into two phases: the oxidative and the non-oxidative arm. In the oxidative part, G6P is firstly converted to 6-phosphoglucono-δ-lactone by glucose-6-phosphate dehydrogenase (G6PD), generating one molecule of nicotinamide adenine dinucleotide phosphate (NADPH). Next, the lactone is hydrolysed by 6-phosphogluconolactonase (PGLS) to 6-phosphogluconate (6PG). Finally, ribulose-5-

phosphate (R5P) is generated through decarboxylation of 6PG by 6-phosphogluconate dehydrogenase (6PGD), yielding another NADPH molecule. In the oxidative PPP arm, R5P is converted back to the glycolysis intermediates F6P by transaldolase (TALDO) or to glyceraldehyde-3-phosphate by transketolase (TKTL) (Figure 1.4).

The PPP is particularly important in proliferating cells to guarantee the supply of riboses for nucleotide biosynthesis and DNA replication. In resting, non-cycling cells, the PPP becomes rewired to produce mainly NADPH as the demand for nucleotides drops. However, the oxidative PPP branch is one of only four reactions that generate the co-factor NADPH in the cytosol. The conversion of malate to pyruvate by malic enzyme 1 (ME1) and the conversion of isocitrate to α-KG by IDH1 and the one-carbon metabolism are the other sources of NADPH (Fan et al., 2014, Lewis et al., 2014). NADPH, besides nicotinamide adenine dinucleotide (NADH), is important for cellular redox homeostasis as it serves as reducing agent in many enzyme-mediated redox reactions. The relative ratios of $NADPH/NADP^+$ and $NADH/NAD^+$ are indicators of cellular redox state (Feron, 2009). In the context of cancer metabolism, it has been suggested that NADPH production is rate-limiting for proliferation (Vander Heiden et al., 2009). One reason for this is the high NADPH amount needed for *de novo* lipid synthesis (14mol NADPH per 1mol palmitoyl-CoA), the other for being essential for the recycling of glutathione, the most abundant non-enzymatic antioxidant in the cell.

1.3 HIF signalling pathway

Many solid tumours display hypoxic areas, i.e. areas where the partial oxygen pressure is below that of normal surrounding tissue, as they outgrow the local vascular system (Bristow and Hill, 2008). In the developing organism hypoxia is a driver for vascularisation but it can also contribute to the maintenance of cells in an undifferentiated state (Covello et al., 2006). Hypoxia is also important in wound healing as it promotes keratinocyte migration to the lesion and subsequent epithelial restoration (Benizri et al., 2008). Hence, cells developed an oxygen sensing and context-dependent responding system. The main cellular response to low oxygen tensions is orchestrated by hypoxia-inducible factor (HIF). HIF is a heterodimeric transcription factor consisting of the constantly expressed HIF-1β subunit, also known as aryl hydrocarbon receptor

nuclear translocator (ARNT), and the oxygen-sensitive HIF-α subunit. There are three HIF-α subunits: HIF-1α, HIF-2α and several splice variants of HIF-3α.

Both, HIF-α and ARNT contain a basic helix-loop-helix (bHLH) domain followed by a Per/ARNT/Sim (PAS) domain in the N-terminus, which are essential for DNA binding and heterodimerisation (Jiang et al., 1996). HIF-1/2α have two transactivation domains, one in the C-terminus (CAD) and one in the N-terminus (NAD), while HIF-3α lacks the CAD and ARNT only has one transactivation domain (TAD) in the C-terminus (Semenza, 1999a, Gu et al., 1998, Hara et al., 2001, Maynard and Ohh, 2004, Semenza, 1999b). Furthermore, the HIF-α subunits contain a unique oxygen-dependent degradation (ODD) domain. Under hypoxic conditions (molecular oxygen tensions below local homeostatic oxygen concentrations), HIF-α is stable, translocates to the nucleus, binds to ARNT and recruits transcriptional co-activators p300/CBP to its CAD. The HIF transcription factor complex binds to hypoxia-response elements (HRE, 5'-RCGTG-3') in target enhancer/promoter sequences of numerous genes (>800 already identified) inducing a transcriptional programme to adapt to hypoxia (Xia et al., 2009, Schodel et al., 2011, Semenza, 2011). HIF upregulates genes involved in angiogenesis and erythropoiesis (e.g. VEGFA, PDGF, inducible nitric oxide synthase (iNOS) and erythropoietin (EPO)) to enhance reoxygenation by increasing blood supply. In addition, HIF also induces glycolytic enzymes (e.g. GLUT1/3, HK2, PDHK1, PFKFB3 and LDHA) to reduce oxygen consumption via energy/ATP production (Bertout et al., 2008, Kaelin, 2008, Porporato et al., 2011). Under normoxic conditions, prolyl hydroxylase domain-containing proteins, PHD1-3, catalyse the hydroxylation of conserved proline residues within the ODD domain (P402 and P564), marking HIF-α for proteasomal degradation (Bruick and McKnight, 2001, Jaakkola et al., 2001). PHD1-3, members of the α-KG-dependent oxygenase superfamily, are also referred to as oxygen sensors, as their enzymatic activity strongly depends on molecular oxygen tension. Apart from oxygen and α-KG, PHD activity is dependent on ascorbate and Fe^{2+} (Schofield and Ratcliffe, 2004). Contrary, cytosolic accumulation of succinate, fumarate and ROS has inhibitory effects on PHD activity (Kaelin and Ratcliffe, 2008, Selak et al., 2005). In addition, the HIF-1α isoforms can also be hydroxylated on a specific aspargine residue (A803) in the CAD by factor inhibiting HIF-1 (FIH1) (Mahon et al., 2001).

The prolyl-hydroxylated HIF-α subunit is recognised by the von Hippel-Lindau protein (pVHL) (Maxwell et al., 1999). pVHL is part of a hydroxylated prolyl-motive specific

E3 ubiquitin ligase, a complex that comprises, apart from pVHL, of elongin B, elongin C and cullin-2. pVHL is considered to be a tumour suppressor gene, as germline mutation in the *VHL* gene causes familial von Hippel-Lindau disease, a hereditary cancer syndrome. Clear cell renal cell carcinomas (ccRCC), the most common subtype of renal cancer, is characterised by heterozygous loss of the *VHL* gene located on the short arm of chromosome 3 (3p26-25) (Latif et al., 1993). *VHL* mutations analysed so far all seem to impair either the ubiquitin ligase complex assembly or binding to the HIF-α substrate (Kishida et al., 1995, Lonergan et al., 1998, Clifford et al., 2001, Knauth et al., 2006, Li et al., 2007). Hence, loss of pVHL leads to loss of pVHL-mediated degradation of HIF-α via the 26S proteasome, resulting in HIF stabilisation and activation of HIF-target genes. ccRCC thus represents a pseudo-hypoxic state in which angiogenesis and glycolysis are promoted even in the presence of ample oxygen in the microenvironment (Figure 1.5). Consequently, ccRCC is a suitable model to study HIF signalling and metabolic remodelling.

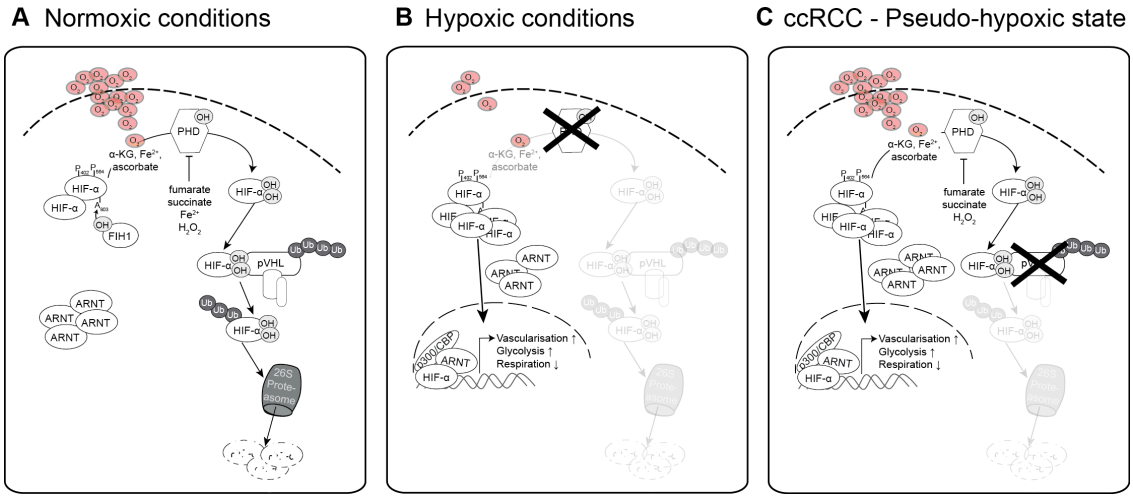

Figure 1.5: HIF pathway regulation under normoxic and hypoxic conditions and in ccRCC
(A) Under normoxic conditions, HIF-α is hydroxylated on conserved proline residues by prolyl-hydroxylases (PHDs). This phosphorylation pattern is recognised by pVHL, a component of an E3-ubiquitin ligase complex, which ubiquinates HIF-α and targets it for proteasomal degradation. (B) If oxygen levels drop, PHDs cannot longer hydroxylate HIF-α, so that it is stabilised and can translocate to the nucleus where it binds to ARNT and p300/CBP and induces transcription of target genes involved in vascularisation and glycolysis. (C) Most ccRCCs lack functional pVHL and, although HIF-α is hydroxylated by PHDs, the E3-ubiquitin ligase complex is not able to mark it for degradation. HIF accumulates, translocates to the nucleus and induces a transcriptional program in adaptation to hypoxia despite ample oxygen in the microenvironment.

Although HIF-1α and HIF-2α have overlapping functions in that they both induce a cellular response to a hypoxic environment, they also differentially regulate distinct subsets of genes in a context dependent manner (Hu et al., 2002, Raval et al., 2005).

HIF-1α has been found to be induced quickly upon oxygen deprivation and orchestrates an immediate acute response to hypoxia. To tune down oxygen consumption, HIF-1α induces a metabolic switch from oxidative phosphorylation to glycolysis. HIF-2α, on the other hand, is induced during prolonged hypoxia and activates angiogenesis by inducing VEGF and EPO expression. HIF-2α was also found to induce the stem cell factor OCT4 (Covello et al., 2006), transforming growth factor α (TGFα) and cyclin D1 (Raval et al., 2005) as well as mTORC1 activity (Elorza et al., 2012). Furthermore, ccRCCs expressing both HIF-α isoforms show increased MAP kinase and PI3K/AKT/mTOR signalling, while ccRCCs expressing only the HIF-2α isoform reveal hyperactive c-MYC (Gordan et al., 2008).

Interestingly, there is evidence for the two HIF-α isoforms antagonising each other. Not only do the two isoforms reciprocally regulate each other's protein levels (Mandriota et al., 2002, Raval et al., 2005) but they also have opposing effects on c-MYC activity (Gordan et al., 2007a, Gordan et al., 2007b, Gordan et al., 2008, Koshiji et al., 2004, Zhang et al., 2007). c-MYC, a transcription factor regulating cell cycle progression but also mitochondrial biogenesis and respiration, is upregulated in 40% of human cancers. While HIF-1α inhibits, HIF-2α promotes c-MYC activity. Apart from being able to induce the expression of MXI, a repressor of c-MYC activity (Ferber et al., 2012), HIF-1α can also negatively regulate c-MYC through promoting its proteasomal degradation (Zhang et al., 2007) or by replacing c-MYC from its binding partner Sp1, thereby increasing transcription of p21 amongst others (Koshiji et al., 2004).

Both HIF-α isoforms can interact with the c-MYC binding partner MAX, but these interactions lead to opposing effects. HIF-1α inhibits c-MYC/MAX complex formation leading to cell cycle arrest by inducing expression of the negative cell cycle regulators p21 and p27, and reducing the expression of the positive regulators cyclin D2 and E2F.

Contrary, HIF-2α stabilises c-MYC by complexing with MAX, causing a dose-dependent stabilisation of the c-MYC/MAX complex and an induction/repression of cyclin D2, E2F1, p21 and p27 promoting cell cycle progression and proliferation (Gordan et al., 2007a, Gordan et al., 2007b). In keeping with this observation, it has been suggested, that HIF-2α acts as driver in pVHL-defective ccRCC tumourigenesis, as HIF-1α expression decreases in the course of tumour development due to frequent loss of HIF-1α on chromosome 14q, while HIF-2α expression increases concomitantly and can override pVHL's tumour suppressor activity (Kondo et al., 2002, Mandriota et

al., 2002, Maranchie et al., 2002, Raval et al., 2005, Keith et al., 2012). Moreover, preclinical models have shown that ablation of HIF-2α is sufficient to suppress tumour formation by pVHL-defective ccRCC cells (Kondo et al., 2002, Zimmer et al., 2004). Finally, a genome-wide association study provided evidence that *HIF2A/EPAS* polymorphisms can be linked to the risk of renal carcinoma (Purdue et al., 2011).

In contrast to the other two HIF-α isoforms, not much is known about HIF-3α so far. Lacking the CAD it has been suggested that it is less potent in transcriptional regulation than HIF-1/2α in the human kidney (Hara et al., 2001). Instead, it has been shown that the alternatively spliced variant HIF-3α4 that lacks ODD, NAD and CAD has a negative effect on HIF-1α transcriptional response. Furthermore, the same study showed that mRNA levels of this HIF-3α isoform were downregulated in most of the tested primary ccRCC tumour specimens, and an important role of HIF-3α4 in inhibiting ccRCC tumourigenesis was suggested (Maynard et al., 2005).

1.4 Clear cell renal cell carcinoma - ccRCC

1.4.1 ccRCC – Incidence, prognosis and treatment

Kidney cancer accounts for ~2% of all cancers yearly diagnosed worldwide (Figure 1.6A) (Ljungberg et al., 2011). In the UK from 2000-2002 to 2009-2011, kidney cancer incidences increased 27% in men and 38% in women, making it the 8^{th}/9^{th} most frequent cancer type in men/women, respectively (Cancer Research UK statistics) (Figure 1.6C). Kidney cancer incidence is higher in men than in women and is rare below the age of 50 but frequent in patients above 60. The overall survival rate for kidney cancer is low (56% for 5-year and 50% for 10-year survival; Figure 1.6B), due to the lack of early symptoms and diagnostic markers and frequent resistance towards conventional radiation and chemotherapy. Kidney cancer is often only diagnosed in an advanced disease stage, or after metastases have already formed (25-30%). Hence, initial treatment is partial or radical nephrectomy, depending on size and staging of the tumour. In some cases, surgical excision can be accompanied or replaced with more targeted therapies. Sunitinib (Sutent; RTK inhibitor), Pazopanib (Votrient; RTK inhibitor), interferon (if cancer is very small) are considered first line drug treatments, whereas Bevacizumab (Avastin; recombinant humanised monoclonal antibody against

VEGFA), Temsirolimus (Torisel; mTOR inhibitor), Everolimus (Afinitor; mTOR inhibitor), Sorafenib (Nexavar; tyrosine kinase inhibitor) and interleukin 2 are given to patients with metastatic phenotype and disease reoccurrence (Singer et al., 2013).

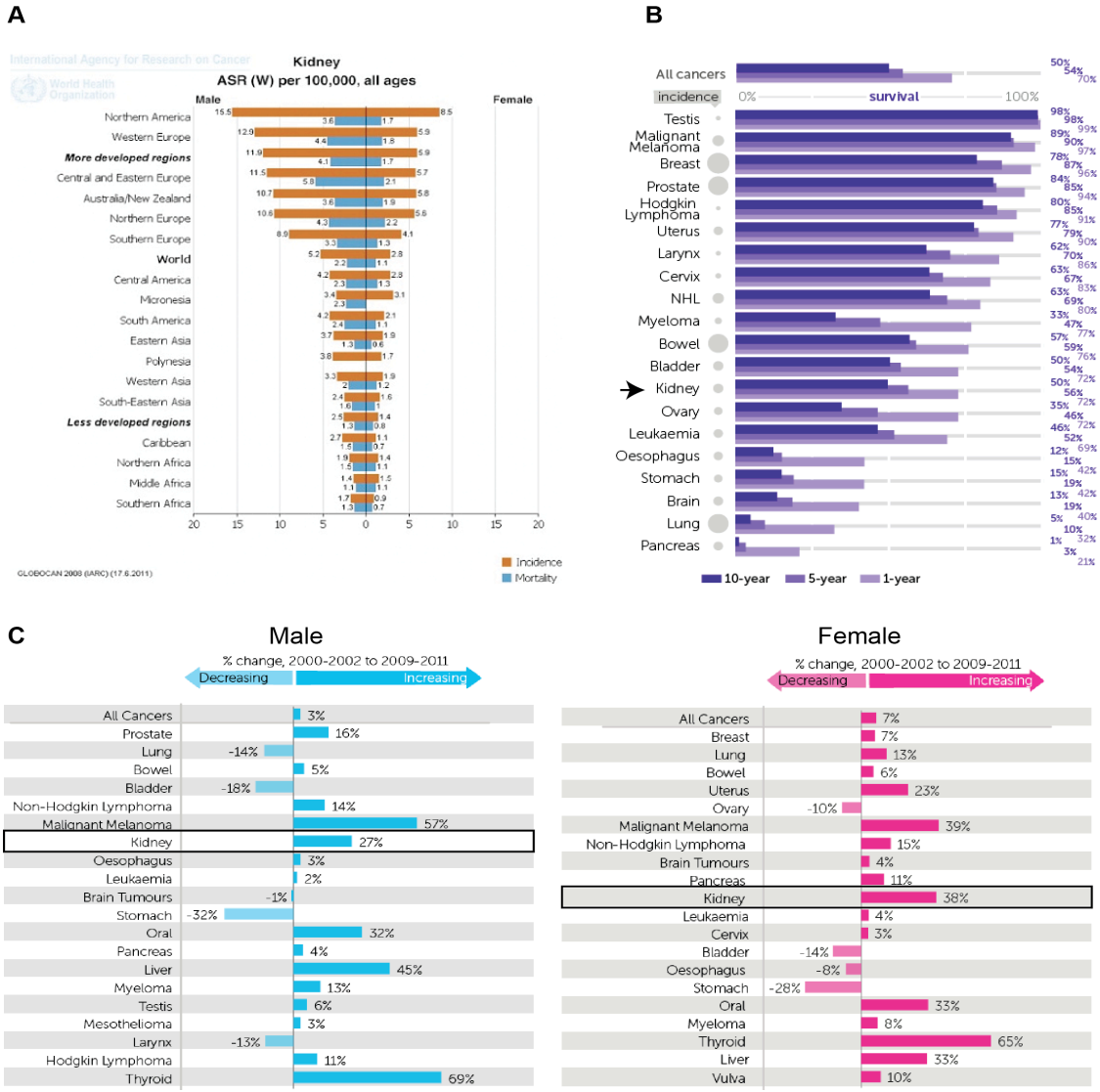

Figure 1.6 Kidney cancer statistics

(A) Worldwide kidney cancer incidence and mortality rates. Copied from (Ljungberg et al., 2011). (B) Age-standardised one-, five-and ten-year net survival for selected cancers in adults (aged 15-99), England and Wales, 2010-2011; Prepared by Cancer Research UK; Original data sources: Cancer Research UK Cancer Survival Group, London School of Hygiene and Tropical Medicine. Personal communication, 2014; (C) The 20 most commonly diagnosed cancers: 2000-2002 and 2009-2011. Percentage change in European age-standardised incidence rates per 100,000 population (male and females, UK); Prepared by Cancer Research UK; Original data sources: 1. Office for National Statistics. Cancer Statistics: Registrations Series MB1. http://www.ons.gov.uk/ons; 2. Welsh Cancer Intelligence and Surveillance Unit. http://www.wcisu.wales.nhs.uk; 3.Information Services Division Scotland. Cancer Information Programme. www.isdscotland.org/cancer; 4. N. Ireland Cancer Registry. www.qub.ac.uk/nicr.

Kidney cancer can be split into two main cancer types: renal cell carcinoma (RCC) and urothelial cell carcinoma (UCC) of the renal pelvis. RCC, an adenocarcinoma

originating from the proximal convoluted tubule epithelium (site of waste transport from blood to urine) is the most common kidney cancer in adults and accounts for 90-95% of all cases; UCC accounts for most of the remaining cases. Histologically, there are four distinguishable RCC sub-types: conventional or clear cell RCC (ccRCC), the most common subtype accounting for 75% of all RCC cases, papillary RCC (15% of cases), chromophobic RCC (5% of cases) and collecting duct RCC (2% of cases). ccRCC can be subdivided further into hereditary and sporadic ccRCC. Underlying hereditary ccRCC is the von Hippel-Lindau (VHL) disease, a rare autosomal-dominant tumour syndrome resulting from germ line mutations in the *VHL* gene on chromosome 3p25. Individuals with VHL disease develop highly vascularised tumours in multiple organs - depending on the location of the mutation, but 45% of them develop ccRCC (Clifford et al., 2001, Hoffman et al., 2001, Lonser et al., 2003, Neumann and Bender, 1998). Non-familial ccRCC also show a high frequency of bi-allelic *VHL* inactivation (Kim and Kaelin, 2004, Kondo et al., 2002). Risk factors associated with sporadic ccRCC include hypertension, obesity, smoking and, especially, continuous dialysis following cystic renal disease.

1.4.2 Metabolic and epigenetic reprogramming is characteristic for ccRCC tumourigenesis

The Cancer Genome Atlas (TCGA) Research Network recently published a comprehensive molecular characterisation of ccRCC resulting from the analysis of ≥ 400 primary nephrectomy specimens from ccRCC patients; with overlapping and complimentary findings published by Sato and colleagues at the same time confirming the universality of these events in ccRCC pathogenesis.

One of their findings was the observation that, although, somatic copy number alterations (SCNAs) occurred at fewer sites compared to other tumour types, the observed SCNAs frequently involved entire chromosome arms or chromosomes as opposed to focal alterations (Cancer Genome Atlas Research, 2013). It was confirmed that fractional loss of chromosome 3p, was the most frequent event, observed in 91% of all samples (Zbar et al., 1987). In addition to *VHL*, chromosome 3p also comprises genes encoding PBRM1, BAP1 and SETD2, three chromatin and histone modifying proteins that were recently identified to be frequently altered in ccRCC (Dalgliesh et al.,

2010, Guo et al., 2012, Varela et al., 2011). The previously reported fractional loss of chromosome 14q, including the pVHL target *HIF1A* (Shen et al., 2011), was found in almost half of the cases. Loss of *HIF1A* was suggested to drive more aggressive tumours in ccRCC, contrary to what has been observed in other tumour types (Semenza, 2003, Shen et al., 2011). The previously reported focal gain of chromosome 5q was confirmed in 67% of the cases, whereby 5q35 was refined as region of interest (Presti and Carroll, 1991, Presti et al., 1991a, Cancer Genome Atlas Research, 2013). Finally, the study from Sato and colleagues identified a gain of chromosome 7q in 41% of cases and 20% of cases show a loss of 8p with or without loss of 8q (Sato et al., 2013). In addition to these sites of accumulated events of focal loss/gain, more sporadic losses or amplifications of specific loci were found. Gene losses include *CUL3* on 2q36, *CDKN2A* (p16) and *CDKN2B* on 9p21 and *PTEN* on 10q23, while *MDM4*, a p53 regulator, on 1q32, *c-MYC* on 8q24 and *JAK2* on 9p24 were gained. Furthermore, whole-exome sequencing revealed 19 significantly mutated genes, including VHL, PBRM1, SETD2, KDM5C, BAP1, ATM, P53, PTEN, PIK3CA, MTOR and TET2 highlighting the contribution of metabolic regulators and DNA modifying enzymes in ccRCC tumourigenesis (Cancer Genome Atlas Research, 2013, Sato et al., 2013). Several integrative pathway analyses pointed out that besides the HIF1A/ARNT also the MYC/MAX, SP1, FOXM1 and JUN/FOS transcriptional response are hyperactive in ccRCC (Cancer Genome Atlas Research, 2013). With respect to signalling cascades, the PI3K/AKT/MTOR axis was found to be impaired in 28% of the analysed core set samples. This impairment was based on mutually exclusive gene alterations with respect to copy number alterations, somatic mutations and mRNA expression (Cancer Genome Atlas Research, 2013, Sato et al., 2013).

Analysis of protein and mRNA expression levels as potential predictive marker for clinical outcome reiterated that a shift towards increased lipogenesis as result of reduced levels of AMPK and its complex components together with increased ACC levels correlate with poor prognosis (Tong et al., 2011). In addition, downregulation of TCA cycle genes, particularly pyruvate dehydrogenase 4 (PDHK4), dihydrolipoamide S-acetyltransferase (DLAT), aconitase 2 (ACO2) and α-KG dehydrogenase (OGDH) and upregulation of PPP genes, especially G6PD, PGLS, TKT and TALDO as well as increased glutamine import via SLC1A5 also correlate with worse clinical outcome (Figure 1.7) (Cancer Genome Atlas Research, 2013).

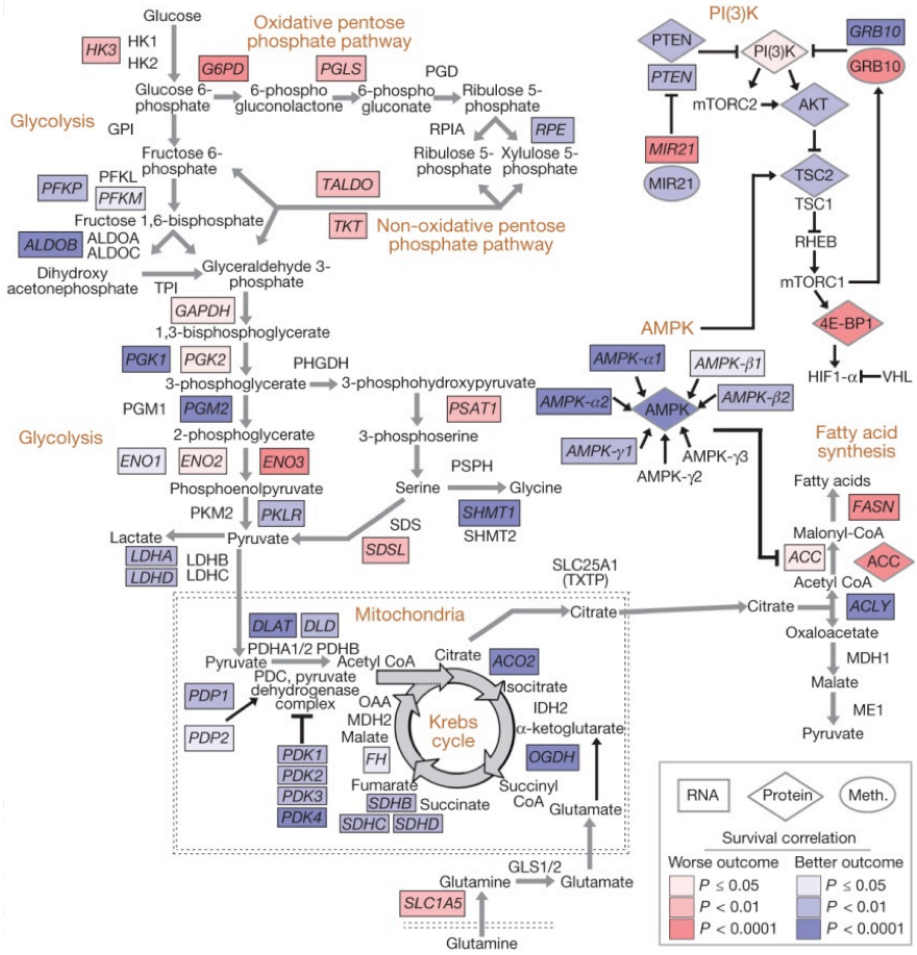

Figure 1.7: Molecular correlates of patient survival involve metabolic pathways

When viewed in the context of metabolism, the molecular survival correlates highlight a widespread metabolic shift, with tumours altering their usage of key pathways and metabolites (red and blue shading representing the correlation of increased gene expression with worse or better survival respectively, univariate Cox based on extended cohort). Worse survival correlates with upregulation of pentose phosphate pathway genes (*G6PD*, *PGLS*, *TALDO* and *TKT*), fatty acid synthesis genes (*ACC* and *FASN*), and PI(3)K pathway enhancing genes (*MIR21*). Better survival correlates with upregulation of AMPK complex genes, multiple TCA cycle genes and PI(3)K pathway inhibitors (*PTEN*, *TSC2*). Additionally, specific promoter methylation events, including hypermethylation of PI(3)K pathway repressor *GRB10*, associate with outcome. (Figure and legend was adapted from (Cancer Genome Atlas Research, 2013)).

Furthermore, a systems biology approach that applied genome-scale metabolic modelling of cancer cells, revealed that ccRCC has a unique metabolic phenotype that distinguishes this disease from other cancer types in that ccRCCs displayed unique alterations in nucleotide, one-carbon and glycerophospholipid metabolism with regard to transcript and protein level (Gatto et al., 2014). Moreover, these alterations were associated with recurrent loss of heterozygosity (LOH) in multiple metabolic genes adjacent to *VHL*, suggesting that it is not exclusively the pVHL/HIF axis that initiates tumour formation and contributes to the distinct ccRCC metabolic phenotype.

1.4.3 ccRCC mouse models

Evidence for pVHL not being the exclusive driver of ccRCC was provided by several studies aiming to generate ccRCC mouse models. For example, attempts to recapitulate ccRCC tumourigenesis in mouse by inactivating *Vhl* in kidney epithelia only resulted in a mild phenotype (Frew and Krek, 2008, Hsu, 2012). More promising results were obtained through a conditional *Vhl* knockout mediated by a proximal tubule-specific *phosphoenolpyruvate carboxykinase* (*Pepck*)-Cre driver, which resulted in renal microcysts in ~25% of mice (Rankin et al., 2006). In addition, conditional ablation of *Vhl* outside of the proximal tubule using Cre recombinase expression under the Ksp-cadherin-promoter (distal tubules and collecting duct-specific expression) resulted in hydronephrosis but no further abnormalities (Shao et al., 2002). Only combined Ksp1.3-Cre –mediated ablation of *Vhl* and *Pten* led to hyper-proliferation of the urothelium and multiple epithelial tubule cysts in the kidney cortex and medulla (Frew et al., 2008), suggesting that ablation of *VHL* alone is unable to drive tumour formation. A recent study by Pritchett and colleagues showed that conditional ablation of *Vhl* in collecting ducts and distal tubules using Hoxb7-driven Cre recombinase expression resulted in highly penetrant tubular phenotypes, interstitial inflammation and fibrosis after 2 months (Pritchett et al., 2014). Furthermore, knockout of *Hif-1α* in addition to *Vhl* was able to rescue this phenotype (although fibrosis only modestly), while double knockout of *Vhl* and *Hif-2α* did not alter the phenotype, hinting to an important role of HIF-1α in kidney cancer initiation (Pritchett et al., 2014). Indeed, the so-called TRACK (transgenic model of cancer of the kidney) mouse model was found to recapitulate ccRCC histological morphology (Fu et al., 2011). TRACK mice express a constitutively active triple mutant (P402A, P564A and N803A) human HIF-1α under the *type 1 γ-glutamyl transpeptidase* (*GGT* or *γGT*) promoter, which is expressed exclusively in the kidney proximal tube. TRACK mice show distorted tubular structures and accumulation of ‘clear’ cells in the outer renal cortex (30-50% coverage). These kidney lesions resemble human VHL disease on histological (accumulation of lipids and glycogen in the cytoplasm in ‘clear’ cells) and molecular (increased expression of HIF-1α downstream targets CAIX, Glut-1 and VEGF) level. These data support the conclusion that constitutively active HIF-1α is a driving force in ccRCC tumourigenesis.

Aim

The aim of this study was to investigate potential metabolic vulnerabilities of clear cell renal cell carcinoma (ccRCC). To identify these vulnerabilities, a screening approach was taken. The applied functional screen comprises of an siRNA library targeting 240 metabolite transporters and metabolic enzymes and regulators. With loss of functional pVHL being a central characteristic in ccRCC, identification of possible metabolic vulnerabilities that are dependent on pVHL loss was one of the aims. Another aim was finding potential correlations between different metabolic vulnerabilities and the different HIF-α isoforms, as they clearly have distinguishable roles in ccRCC tumourigenesis. In the following, the questions that will be addressed are:

- What differences and commonalities do different ccRCC cell lines show with regards to HIF-α isoform expression and stabilisation? How does reintroduction of functional pVHL change this pattern?
- What differences and commonalities do different cell lines show in their dependencies to different nutrients and energy/ATP producing pathways? Does reintroduction of functional pVHL influence this behaviour?
- Does the loss of any other metabolic enzyme, metabolic regulator or metabolite transporter synergise with the loss of pVHL or correlate with one HIF-α isoform or the other to negatively influence the survival and proliferation of ccRCC cells?
- How do the identified genes cause loss of cell viability? What is the underlying mechanism? Is there a pattern emerging when comparing the different ccRCC cell lines?
- How can the identified vulnerability be exploited?

Chapter 2:
Materials & Methods

2.1 Cell culture

2.1.1 Cell lines

The 5 isogenic clear cell Renal Cell Carcinoma (ccRCC) cell lines RCC4, UMRC2, A498, 786-O, 769-P, which either contain a pVHL-expression construct or an empty vector (EV) were obtained from the laboratory of William Kaelin Jr. (Iliopoulos et al., 1995). The parental ccRCC cell lines RCC4, UMRC2, A498, 786-O as well as CAKI1, TK10, A.704, UMRC3, ACHN and HEK293 were obtained from the LRI Clare Hall Cell Services facility. 769-P, CAKI2, UO31 were a gift from Marco Gerlinger, Translational Cancer Therapeutics, CRUK LRI. Finally, the HPV-16 transformed but non-tumourigenic proximal tubular cell line HK-2 (Cat. No. CRL-2190^{TM}) was purchased from the American Type Culture Collection (ATCC).

2.1.2 Culture conditions

All ccRCC cell lines were maintained in DMEM supplemented with 4.5 g/l D-Glucose, 0.11 g/l Sodium Pyruvate (Gibco), 4mM Glutamine (Clare Hall Cell Services facility), 100Units/ml Penicillin / 100 µg/ml Streptomycin (Gibco), 10% Fetal Bovine Serum (FBS) (Gibco, Cat. No. 10270-106). HK-2 cells were maintained in Keratinocyte-Serum Free Medium (KSFM) with L-Glutamine (Gibco, Cat. No. 17005-034) supplemented with 5 ng/ml Human Recombinant EGF and 50 ng/ml Bovine Pituitary Extract (BPE) (both Gibco, Cat. No. 37000-015) and were grown on collagen-coated cell culture dishes (BD Bioscience, Cat. No. 734-0280). All cell lines were maintained in a humid incubator at 37°C and 5% CO_2 for 6-8 weeks before they were discarded and exchanged with newly thawed cells.

Only HK-2 cells are sensitive to trypsin and need pelleting (centrifugation for 5 min at 1000rpm) and removal of the trypsin-containing supernatant (SN) before transferring to a new petri dish.

2.1.3 Culture of cell lines in hypoxic conditions

For treatment of cell lines in hypoxic conditions, cells were placed into a hypoxia chamber (Ruskinn Invivo$_2$ 500, Bridgend, UK). All ccRCC cell lines were cultured under 0.1% oxygen conditions if not stated differently for the indicated time periods. Upon plating, cells were usually allowed to attach before placing them into the hypoxia chamber.

2.1.4 Storage and recovery of cells

All cancer cell lines were cryo-preserved in freezing medium containing 50% FBS, 40% full growth medium and 10% Dimethyl sulfoxide (DMSO, Sigma). HK-2 cells were frozen in full growth medium (KSFM) containing 7.5% DMSO.
Following trypsinisation, cells were spun down for 5 min at 1000rpm to remove residual trypsin, resuspended in the appropriate freezing medium and distributed to cryogenic vials (Nunc, ThermoFisher Scientific) in 1 ml aliquots. Cells were gradually frozen in isopropanol-containing cryogenic freezing containers (Nalgene, ThermoFisher Scientific) at -80°C before they were transferred to liquid nitrogen tanks for long-term storage.
For recovery, cryogenic vials containing frozen cells were placed in a 37°C water bath for ~3 min to thaw. Cell suspensions were then transferred to 5 ml pre-warmed culture medium, spun down for 5 min at 1000 rpm to remove residual DMSO. Obtained cell pellet was resuspended in fresh culture medium and transferred to appropriate tissue culture vessels. Cells were media changed the next day in order to remove dead cells.
Cells were passaged at least twice after thawing before they were used for an experiment.

2.1.5 Determination of live cell number

For plating a given cell number in experimental set-ups, cells were counted either using a Vi-CELL® XR Cell Viability Analyzer (Beckman Coulter) or a Countess® Automated Cell Counter (Invitrogen). Most of the time, the Vi-CELL® was used for ccRCC cell counting. For this automated cell counting device, 500 µl cell suspension following

trypsinisation were transferred into a Vi-CELL® sample vial and placed in the instrument for cell number determination using the 'Default' setting.
The Countess® Automated Cell Counter was used for HK-2 cells and for determining cell numbers for the screen as it requires less cell suspension volume as the Vi-CELL®. For this, following trypsinisation, 10 µl cell suspension was mixed well with 10 µl Trypan Blue (0.4%, Invitrogen). 10 µl of this mix was transferred to a disposable counting chamber (Invitrogen) which was inserted into the Countess® device for cell number determination.

2.1.6 Starvation of ccRCC cell lines

For starvation/nutrient –dependency studies, DMEM lacking glucose, glutamine and sodium-pyruvate was obtained from the LRI Clare Hall Cell Services facility. This medium was supplemented before usage with 100 Units/ml Penicillin / 100 µg/ml Streptomycin (Gibco), 10 % FBS and one or any combination of the following nutrients: 25 mM D-glucose (Invitrogen), 1 mM sodium pyruvate (Gibco), 4 mM glutamine (Clare Hall Cell Services facility). Both regular and dialysed FBS (Invitrogen) were used and is indicated, respectively.

For lipid starvation, DMEM was supplemented before usage with 25mM D-glucose (Invitrogen), 1 mM sodium pyruvate (Gibco), 4 mM glutamine (Clare Hall Cell Services facility) and 10 % regular FBS was substituted with either 1 % lipoprotein-deficient FCS (LPDS, Bioscience UK) or 10 % lipid depleted FBS (LDS). LDS was generated using Liposorb™ resin from Calbiochem (Darmstadt, DE) according to manufacturer's instructions.

For starvation experiments, cells were plated in 96-well plates at 2000 cells/well in 100 µl common growth medium. The next day, cells were washed 2x in PBS before addition of 200 µl DMEM with the desired nutrient supplementation. Cells were maintained at 37°C/ 5% CO_2 during the duration of the experiment. After 96 h, cells were fixed over night at -20°C with 80% ice-cold EtOH (in ddH_2O).

2.2 siRNA transfections

A list of siRNAs used in this study can be found in Table 2.1.

2.2.1 Reverse siRNA transfection for cell viability experiments

In order to determine the effect on cell viability upon ablating a specific gene, siRNA transfection was employed. A reverse siRNA transfection protocol was performed in black clear bottom 96-well plates (BD Falcon) using 37.5 nM of siRNA (Dharmacon siGENOME® set of 4 upgrade; 2 nM were resuspended in 100 µl 1x siRNA-buffer for a final stock concentration of 20 µM before mixing a small aliquot of the 4 individual oligonucleotides in a 1:1:1:1 ratio to obtain a SMARTpool, all ThermoFisher Scientific) and 0.1 µl (0.2 µl for HK-2 cells) Dharmafect2 transfection reagent (Dharmacon, ThermoFisher Scientific) per 100 µl reaction volume per well.

Briefly, for a 96-well format 0.1875 µl siRNA SMARTpool (20µM stock) were mixed with 9.8 µl OptiMEM (Invitrogen) and incubated for 5 min. Meanwhile, 0.1 µl of Dharmafect2 transfection reagent (0.2 µl for HK-2 cells) were mixed with 9.9 µl OptiMEM (9.8 µl for HK-2 cells) and then added to the siRNA/OptiMEM mix, vortexed and incubated for at least 20 min (for up to 2 h) before transferring 20 µl of this siRNA/Dharmafect2/OptiMEM to a well of a 96-well plate. In parallel, cells were trypsinised, counted (ccRCCs with Vi-CELL® and HK-2 with Countess®) and resuspended in a volume of culture medium (containing 10 % FBS) that would yield a cell concentration of 25 cells per µl. 80 µl of this cell suspension was then added on top of the 20 µl siRNA/Dharmafect2/OptiMEM transfection mix. After plating, the plates were kept for ≥ 30 min at RT before placing them in a humid 37°C/5 % CO_2 incubator. Approximately 24 h later, 100 µl fresh culture medium was added to the cells. Cells were fixed 96 h post transfection by aspirating the culture medium, adding 100 µl -20°C-cold 80 % EtOH/ddH_2O and keeping them at least over night at -20°C.

2.2.2 Reverse siRNA transfection for total RNA and protein extractions

Transfections aimed for total RNA and/or protein extractions were performed in 6-well plates according to the protocol as described in 2.2.1, with adapted transfection reagent amounts used per well. For a 6-well plate, 2.6 µl siRNA SMARTpool were mixed with 147.4 µl OptiMEM and incubated for 5 min. In the meantime, 1.5 µl Dahrmafect2 transfection reagent (3 µl for HK-2 cells) were mixed with 148.5 µl OptiMEM (147 µl for HK-2 cells). siRNA and Dharmafect2 mix were then added together, vortexed and incubated for ≥ 20 min before transferring the 300 µl to a well. In parallel, cells were trypsinised, counted and resuspended in culture medium (containing 10 % FBS) so that a suspension with 125 cells/µl was achieved. 1.2 ml of this cell suspension was added on top of the 300 µl siRNA/Dharmafect2/OptiMEM transfection mix. Following plating, plates were kept for ≥ 30 min at RT, before placing them in a humid 37°C/5 % CO_2 incubator. Approximately 24 h later, 1 ml fresh culture medium was added to the cells. To check knockdown (KD) efficiency, cells were lysed 48 h post transfection.

In case of time course analyses, cells were transfected all at the same time and harvested 24, 48, 72, 96, 120 hours post transfection or as specified in the respective figure legend.

2.2.3 Reverse siRNA transfection of two genes simultaneous

For co-silencing of two genes simultaneously, procedure as described in 2.2.1 and 2.2.2 was followed using half the concentration, i.e.18.75 nM (cell viability, 96-well plate) or 1.3 nM (RNA/protein extraction, 6-well plate) of each of the siRNA SMARTpools in order to keep the final siRNA concentration in the transfection reaction at 37.5 nM per 100 µl and 2.6 nM per 1.5 ml. In these experiments, the single (control) knockdowns were complemented 1:1 with scrambled siRNA.

Table 2.1: siGENOME siRNAs used in this study

Gene Symbol	Entrez Gene ID	Pool Number	Duplex Number	Sequence
CAT	847	MU-010021-01	D-010021-01 D-010021-02 D-010021-03 D-010021-04	CACAUGACAUUACCAAAUA GGAAUCCAGUUAAUUACUU GAGCACAGCAUCCAAUAUU GGACAUCGCCACAUGAAUG
CPT1A	1374	MU-009749-02	D-009749-01 D-009749-02 D-009749-05 D-009749-18	GAGAGAACCUCAUCAAUUU GAAGAAGGAUACAGAAGUG GGACAGCUACGCCAAAUCU UGACAACGAUGUACGCCAA
CPT1B	1375	MU-010266-01	D-010266-04 D-010266-17 D-010266-18 D-010266-19	CAAGUAACUAUGUGAGUGA GAUCAUGUAUCGCCGUAAA GGACUGAGACUGUGCGUUC CAUGAUUGCAGGCGAGAAC
FOXO1	2308	MU-003006-03	D-003006-05 D-003006-06 D-003006-07 D-003006-21	CCAGGCAUCUCAUAACAAA CCAGAUGCCUAUACAAACA GGAGGUAUGAGUCAGUAUA AGGACAAUAAGUCGAGUUA
FOXO3	2309	MU-003008-02	D-003008-05 D-003008-07 D-003008-21 D-003008-22	CGAAUCAGCUGACGACAGU GUACUCAACUAGUGCAAAC CAGUAAAGAGGUACGAAAA UGCAUUAACUUGCGGUAUU
FOXO4/MLLT7	4303	MU-003016-02	D-003016-05 D-003016-06 D-003016-07 D-003016-08	GGACUGGACUUCAACUUUG CCACGAAGCAGUUCAAAUG GAGAAGCGACUGACACUUG GACCAGAGAUCGCUAACCA
G6PD	2539	MU-008181-02	D-008181-01 D-008181-02 D-008181-03 D-008181-05	GAGAGUGGGUUUCCAGUAU CAACAUCGCCUGCGUUAUC CGUGAGGCCUGGCGUAUUU UGACCUACGGCAACAGAUA
GCLC	2729	MU-009212-03	D-009212-03 D-009212-05 D-009212-06 D-009212-20	CUUCUAAGCCGGAUCAUAU GAGUAUGGGAGUUACAUGA UGAGGGAGUUUAUCGCAAA CAAGAAAUAUCCGACAUAG
GLS	2744	MU-004548-00	D-004548-01 D-004548-02 D-004548-03 D-004548-04	AGACAUGGUUGGUAUAUUAUU UGAAUAAGAUGGCUGGUAAUU GGUGGUUUCUGCCCAAUUAUU GAAUAACACUCCCAUGGAUUU
GPX1	2876	MU-008982-00	D-008982-01 D-008982-02 D-008982-03 D-008982-04	GCAAGGUACUACUUAUCGA UGAAUUCCCUCAAGUACGU GGAGAACGCCAAGAACGAA GCAACCAGUUUGGGCAUCA
GPX2	2877	MU-011675-00	D-011675-01 D-011675-02 D-011675-03 D-011675-01	GAACGAGCAUCCUGUCUUC GAAGGUAGAUUUCAAUACG CAGGAGAACUGUCAGAAUG GCAGGGCCGUGCUGAUUGA
GPX3	2878	MU-006485-01	D-006485-01 D-006485-02 D-006485-03 D-006485-04	GUACGGAGCCCUCACCAUU GGAUGUCAAUGGAGAGAAA AGGAAGAGCUUGCACCAUU GAGGCUUUGUCCCUAAUUU
GPX4	2879	MU-011676-01	D-011676-01 D-011676-03 D-011676-04 D-011676-17	CAACGUGGCCUCCCAGUGA GUAACGAAGAGAUCAAAGA CGUCAAAUUCGAUAUGUUC GCUGCGUGGUGAAGCGCUA
GPX5	2880	MU-009445-01	D-009445-03 D-009445-04 D-009445-17 D-009445-18	GCAAGCACAUCCUCUUCGU UGGCGUACUUGAAGCAAUU AGGCCAUCGCACUUAAUAA GGGAGGAUUUGUACCUAGU

Gene Symbol	Entrez Gene ID	Pool Number	Duplex Number	Sequence
GPX6	257202	MU-019309-00	D-019309-01 D-019309-02 D-019309-03 D-019309-04	GCAAGCACGUCCUGUUUGU GCAGUUCAAUACCCACUAG GCGAGGAGUACAUCCAAUU AUAGGAAGGUGGAUUGCAA
GPX7	2882	MU-009875-01	D-009875-01 D-009875-02 D-009875-03 D-009875-04	GAAGCGAGAAGACUUAUAA ACAAGGAGAUUGAGAGCUU GCACCUACAGUGUCUCAUU GGACUUCUACGACUUCAAG
GPX8	493869	MU-034902-01	D-034902-17 D-034902-18 D-034902-19 D-034902-20	GUAUAAAGGCAAAGUUUCA CUAAAAUUCCUCAAACCUA GGUUAGACAAGUGAUCAUA GUGUAUGACUGAAAUUUCU
GSR	2936	MU-009647-01	D-009647-01 D-009647-02 D-009647-03 D-009647-04	GAACACAGCUGUCCACUCU GAUUAUGGCUUUCCAAGUU GAUACGGCAUGAUAAGGUA UCAAUUGGCGUGUUAUUAA
GSS	2937	MU-009586-00	D-009586-01 D-009586-02 D-009586-03 D-009586-04	CAAAGAAGCUGGCAAGAUC CGACGAACAUUUGAAGAUA CUACAUGCCUCGUCAGUAC GCAUCUACUUCGAACCAAA
LMNA	4000	MU-004978-01	D-001050-01	GGUGGUGACGAUCUGGGCU
ME1	4199	MU-009348-02	D-009348-02 D-009348-03 D-009348-19 D-009348-05	CAUCUGACAUUGAGAAAUU AGUAAGAGGUUCUGAAUAU CCUUGCAGCUCUUCGAAUA GGUAAAUUGGCUCUAUAUA
MYC	4609	MU-003282-07	D-003282-14 D-003282-15 D-003282-16 D-003282-35	AACGUUAGCUUCACCAACA GGAACUAUGACCUCGACUA GAACACACAACGUCUUGGA CUACCAGGCUGCGCGCAAA
NFE2L2	4780	MU-003755-02	D-003755-01 D-003755-02 D-003755-04 D-003755-05	
PDHK1	5163	MU-005019-00	D-005019-01 D-005019-02 D-005019-03 D-005019-04	GGAAGUCCAUCUCAUCGAAUU GGAACACCAUGCCAACAGAUU GAUCAGAAACCGACACAAUUU GAUCAGUGAAUGCUUGUGAUU
PLK1	5347	MU-003290-01	D-003290-05 D-003290-06 D-003290-07 D-003290-08	CAACCAAAGUCGAAUAUGA CAAGAAGAAUGAAUACAGU GAAGAUGUCCAUGGAAAUA CAACACGCCUCAUCCUCUA
SEPSECS	51091	MU-015559-00	D-015559-01 D-015559-02 D-015559-03 D-015559-04	CAAGAUGUAUCCAGGAAGA CCAAAGGCAAAGUAUAUUA AAGGGUGCCUGAUAGAUUA GGCUCGAGUUGGUAGAAUA
SLC1A5	6510	MU-007429-01	D-007429-02 D-007429-03 D-007429-17 D-007429-18	GGAUGUGGGUUUACUCUUU GUUCUGGUCUCCUGGAUCA GAGAGGAAUAUCACCGGAA CAGUCAACCUCCCGGUCGA
SLC7A9	11136	MU-007619-02	D-007619-02 D-007619-04 D-007619-05 D-007619-18	UCAAUUACAUCACAGAAGA GAAGCUACGUCCAGAACAU GACAUAAACUCGUUAGUCA CGUGAUGACUGCCACCGAA
SLC7A11	23657	MU-007612-01	D-007612-01 D-007612-02 D-007612-03 D-007612-04	GGAAGUCUUUGGUCCAUUA GGAGUUAUGCAGCUAAUUA GGGAACAACUAUAAAGAAA UGACAAAUGUGGCCUACUU
SLC16A4	9122	M-007406-00	D-007406-01 D-007406-02 D-007406-03 D-007406-04	GACAGGAGCCCUUAUAUUA GAAACACACUGCCAUGAGA GAAGAAAGUGAUAAGGUUA UGACAUACUUGGAGAGAAA

Gene Symbol	Entrez Gene ID	Pool Number	Duplex Number	Sequence
SOD1	6647	MU-008364-01	D-008364-05 D-008364-06 D-008364-07 D-008364-08	UCGUUUGGCUUGUGGUGUA ACAAAGAUGGUGUGGCCGA GUGCAGGGCAUCAUCAAUU UUAAUCCUCUAUCCAGAAA
SOD2	6648	MU-009784-02	D-009784-03 D-009784-04 D-009784-19 D-009784-20	AAAGAUACAUGGCUUGCAA GUAAUCAACUGGGAGAAUG ACCAGGAGGCGUUGGCCAA GGAUUGAUGUGUGGGAGCA
TXNRD2	10587	MU-009089-01	D-009089-01 D-009089-03 D-009089-04 D-009089-17	GAAAGAGAUUCUGCUGUCA UGGGAGGCCUGAUCCAAGA GCCGAUCACAUCAUCAUUG GCACACGGUUUGCGGCGUU
UBB	7314	MU-013382-01	D-013382-01 D-013382-02 D-013382-03 D-013382-17	GCCGUACUCUUUCUGACUA GUAUGCAGAUCUUCGUGAA GACCAUCACUCUGGAGGUG CCCAGUGACACCAUCGAAA
RISC-free siRNA			D-001220-01	N/A
siGENOME non-targeting siRNA1 siRNA2 siRNA3 siRNA4			 D-001210-01 D-001210-02 D-001210-03 D-001210-04	 AUGAACGUGAAUUGCUCAA UAAGGCUAUGAAGAGAUAC AUGUAUUGGCCUGUAUUAG UAGCGACUAAACACAUCAA
On TARGET Plus (siOTP, non-targeting) siControl1 siControl2 siControl3 siControl4			 D-001810-01 D-001810-02 D-001810-03 D-001810-04	 UGGUUUACAUGUCGACUAA UGGUUUACAUGUUUUCUGA UGGUUUACAUGUUUUCCUA UGGUUUACAUGUUGUGUGA

2.3 siRNA screening

2.3.1 Determination of optimal transfection reagent

The UMRC2, A498, 786-O, and 769-P isogenic cell line pairs as well as the HK-2 cells were screened with a library of 23 transfection reagents (TR) (Table 2.2) by Dr. Ming Jiang from the CRUK LRI High Throughput Screening (HTS) facility in search for the optimal transfection reagent. For this, cells were reverse transfected on a 96-well plate format with 37.5 nM LaminA/C using the TR library at two different concentrations (0.1 µl and 0.3 µl). 48 h post transfection, cells were fixed with 80% -20°C-cold ethanol over night at -20°C. Cells were then stained with an antibody against LaminA/C (see Table 2.5 for details) and DAPI. Immunofluorescence intensities of LaminA/C as readout for knockdown efficiency and number of positive DAPI-stained nuclei as readout for cell number, was computed using a Cellomics ArrayScan V^T (Thermo Scientific).

Table 2.2: Transfection reagents used in this study

Transfection Reagent	Manufacturer
CodeBreaker™	Promega
DharmaFect 1	ThermoFisher Scientific
DharmaFect 2	ThermoFisher Scientific
DharmaFect 3	ThermoFisher Scientific
DharmaFect 4	ThermoFisher Scientific
DreamFect Gold	Oz Biosciences (Marseille, France)
FuGENE®	Promega
GeneEraser™	Agilent
GeneSilencer®	Genlantis (San Diego, CA, USA)
HiPerFect®	Qiagen (Germantwon, MD, USA)
INTERFERin®	Polyplus (Illkirch, France)
Lipofectamine	Invitrogen
Lipofectamine™ 2000	Invitrogen
Lipofectamine™ RNAiMAX	Invitrogen
Lullaby®	Oz Biosciences
METAFECTENE®	Cambio (Cambridge, UK)
N-TER™ Nanoparticle	Sigma-Aldrich
Oligofectamine™	Invitrogen
RiboJuice™	Merck Millipore
siIMPORTER™	Merck Millipore
siLentFect	Bio-Rad
siPORT™ Amine	Ambion
siPORT™ NeoFX™	Ambion
TransIT-siQUEST®	Mirusbio (Madison, Wi, USA)
TransIT-TKO®	Mirusbio

2.3.2 Screening protocol

Day 2 prior to screening

All 10 cell lines used in the screen were passaged under standard tissue culture conditions into 2× 75 cm^2 flasks and incubated at 37ºC, 5% CO_2 for 2/3 days to let the cells reach 90% confluence.

(Note: A 1:4 split from 90 % confluence into 75 cm^2 flask, allows 90% confluence within 48 h with a total of ~5-8×10^6 live cells per 75 cm^2.)

Day of screening

The aliquoted siRNA library containing 10 µl of 375 nM siRNA/Hank's Buffer Salt Solution (HBSS) mix were thawed for 20 min at room temperature (RT) and centrifuged for 1 min at 1500 rpm. 10 µl of the transfection reagent mix (0.1 µl

Dharmafect2/OptiMEM (Invitrogen)) was added to each well of each plate used at the time using a WellMate 8-channel microplate dispenser (ThermoFisher Scientific). While the plates with the 20 µl siRNA/HBSS:Dharmafect2/OptiMEM transfection mix were left to incubate for 20 min at RT, the cells were prepared. One cell line pair was processed at the time. Cells were rinsed with PBS, trypsinised and centrifuged for 5 min at 1000 rpm to remove the trypsin. Cells were counted using the Countess® and resuspended in 100 ml freshly prepared growth medium yielding a cell density of 2.5×10^4 cells/ml. 80 µl of this cell suspension per well was dispersed over the nine 96-well plates constituting the siRNA library (3 plates in triplicates) using a WellMate (speed = high). The final reaction volume was 100 µl per well with a final siRNA concentration of 37.5nM.
(Note: RCC4, UMRC2 and 786-O ± pVHL were transfected on one day and A498 and 769-P ± pVHL were transfected a week later.)

Day 1 post screening

100 µl freshly prepared full growth media was added per well using a WellMate (speed = 3).

Day 4 post screening

96 hours post reverse siRNA transfection, cells were fixed with 100 µl/well of 80% -20°C-cold EtOH. Therefore, the culture medium was aspirated using a microplate washer (Bio Tek) and 100 µl/well of ice-cold EtOH was added using a WellMate (speed = 3). Plates were sealed and stored at -20°C until ready to process further.

Day X post screening

The plates were processed in two batches: 3 pairs (i.e. 54 plates) in the morning and 2 pairs (i.e. 36 plates) in the afternoon. Using a microplate washer, EtOH was aspirated and cells were washed 3x with 100 µl PBS, RT. Subsequently, a WellMate dispersed 30 µl/well DAPI solution (100 ng/ml in PBS) (speed = 1) and cells were incubated for 1 h. Next, the staining solution was aspirated and the cells were washed 2x with 100 µl PBS using a microplate washer. Finally, 100 µl PBS was added with a WellMate (speed = 1). Plates were sealed with aluminium foil and fed into an Acumen X^3 laser

scanning imaging cytometer (TTP Labtech, Hertfordshire, UK) to determine DAPI staining intensity as readout for cell number.

2.3.3 Screen data analysis

The raw cell number values obtained from the Acumen X^3 were analysed by Dr. Rebecca Saunders from the CRUK LRI HTS facility using the cellHTS2 software package (Bioconductor) (Boutros et al., 2006). Firstly, raw cell number values were centred to the respective plate median based only on sample wells without inclusion of the 16 control wells. Next, Z-Scores were calculated using the median absolute deviation (MAD) of the population. A $Z\text{-Score}_{(MAD)}$ close to 0 indicates that the given measurement is very similar to the median of the population, a negative $Z\text{-Score}_{(MAD)}$ indicates a loss in cell number while a positive $Z\text{-Score}_{(MAD)}$ represents a gain in cell number compared to the population median. $Z\text{-Scores}_{(MAD)} \leq -1.7$ and ≥ 1.7 were considered to indicate significant effects on cell number compared to the population median. These $Z\text{-Score}_{(MAD)}$ values were used to define hits in the course of the screen data analysis. For screen quality evaluation, Spearman Rank Correlation analyses were performed on a plate-by-plate basis of the individual replicates to check for reproducibility within the experiment. A Spearman Rank factor above 0.65 was considered to indicate good correlation.
For more details on the screen analysis and quality control see Chapter 4, sections 4.3.2 and 4.3.3.

2.4 Small molecule inhibitor treatment

Drug response studies were performed in a 96-well plate format. Cells were plated at a cell density of 2000 cells/well in 100 µl growth medium. The next day, 100 µl/well of fresh growth medium containing the respective drug in twice the concentration than desired was added to the cells. Cells were incubated with the respective drug for 72 h before over night fixation at -20°C in 100 µl 80% ice-cold EtOH. Fixed cells were washed 2x with 150 µl PBS, stained with 50 µl DAPI (100 ng/ml)/PBS solution for $\geq$ 20 min, washed again 2x in 100 µl PBS before adding a final 100 µl PBS. Plates were

then sealed and analysed for cell number counts using an Acumen X^3 laser scanning imaging cytometer.

A complete list with small molecule inhibitors and other chemicals used to treat cells in this study is depicted in Table 2.3.

Table 2.3: Chemical inhibitors, small molecules and supplements used for cell treatment

Reagent	Supplier	Solvent	Stock solution	Description
(+)-Etomoxir sodium salt hydrate	Invitrogen	DMSO	100 mM	CPT1 inhibitor -> inhibits β-oxidation
2-Deoxy-D-Glucose	Sigma Aldrich	ddH_2O	1 M	Glucose analogue
4-hydroxy-2,2,6,6-tetramethyl-piperidine-N-oxyl (TEMPOL)	Sigma-Aldrich	ddH_2O	1 M	Antioxidant; SOD2 mimetic
Antimycin A	DMSO	DMSO	100 mM	ETC Complex III inhibitor
Bezafibrate	Sigma-Aldrich	DMSO	500 mM	PPARα agonist
BPTES	Sigma-Aldrich	DMSO	10 mM	GLS inhibitor
BrdU	Sigma-Aldrich	PBS	30 mM	
BSO	Sigma-Aldrich	ddH_2O	100 mM	GCLC inhibitor
Carbonyl cyanide-*4*-(trifluoro-methoxy)phenyl hydrazone (FCCP)	Sigma-Aldrich	DMSO	20 mM	Disruption of mitochondrial membrane potential
Carnitine	Sigma-Aldrich	ddH_2O	50 mM	Supports β-oxidation
Cdk4/6 inhibitor		DMSO	25 mM	Induces cell cycle arrest in G1
D-Glucose	Sigma-Aldrich	ddH_2O	10% (355 mM)	
DMOG	Sigma Aldrich	DMSO	1 M	PHD inhibitor
Doxirubicine		ddH_2O	100 µM	Intercalates into the DNA and causes DNA damage
Ebselen	Sigma Aldrich	DMSO	100 mM	Antioxidant; GPX mimetic
L-Glutathione reduced	Sigma-Aldrich	ddH_2O		Antioxidant
Hydrogen peroxide	Sigma-Aldrich	ddH_2O	30 wt%	Reactive oxygen species
L-Cysteine hydrochloride, non-animal source, anhydrous	Sigma-Aldrich	ddH_2O		Amino acid
MG-132	Calbiochem	ddH_2O	20 mM	Proteasome inhibitor
N-Acetyl-L-cysteine (NAC)	Sigma-Aldrich	ddH_2O	1 M	Antioxidant; Precursor for Cysteine
Sodium Palmitate	Sigma-Aldrich			Fatty acid
Oligomycin A	Invitrogen	DMSO	100 mM	ATP synthase inhibitor
Pyocyanin	Sigma-Aldrich	DMSO	100 mM	ROS generator
Rotenone		DMSO	10 mM	ETC Complex I inhibitor
Sodium pyruvate	Sigma-Aldrich	ddH_2O	100 mM	
Luperox® TBH70x Tert-Butyl Hydroperoxide	Sigma-Aldrich	ddH_2O	70 wt%	Reactive oxygen species
α-Ketoglutaric acid (α-KG)	Sigma-Aldrich	ddH_2O		TCA cycle intermediate

2.5 Kinetic Caspase-3/7 Apoptosis assay

For analysis of real time apoptosis induction following siRNA treatment, a CellPlayerTM Kinetic Caspase-3/7 Apoptosis Assay Kit (Essen Bioscience, Cat no. 4440) was employed. This reagent is a fusion of an activated caspase-3/7 motif (DEVD) to NucView™488, a DNA intercalating dye. Just before placing cells in an Essen

BioScience IncuCyte™ system, the Caspase-3/7 substrate was added as a 1:500 dilution directly to the medium (10 μM final concentration). This inert, non- fluorescent substrate is cell permeable and its cleavage upon induction of apoptosis results in a green fluorescent DNA dye. Quantification of fluorescence accumulation was analysed using the IncuCyte™ FLR object counting algorithm.

2.6 Fluorescence-activated cell sorting (FACS) analysis

2.6.1 Cell cycle analysis

Cell cycle analysis was performed using the intercalating fluorescent agent propidium idodide (PI, Ex/Em = 535/617 nm) to measure DNA content using FACS.
Cells were reverse transfected with 37.5 nM SMARTpool siRNA targeting GPX1 and GPX3 in a 6-well format. For harvesting, cells were trypsinised, spun down at 1000 rpm for 5 min and washed 1x PBS before fixing in ice-cold 70 % EtOH over night at 4ºC. Before FACS analysis, cells were washed 2x in ice-cold PBS and treated with 50 μl ribonuclease (100 μg/ml, Sigma) for 5 min to ensure staining of only DNA. Cells were subsequently stained with 200 μl PI (50 μg/ml in PBS, Sigma) and analysed immediately on an LSRII flow cytometer.

2.6.2 BrdU pulse-chase analysis

For tracing cell cycle duration, 5-bromo-2-deoxyuridine (BrdU) –pulse chase analysis was performed. Therefore, cells were incubated with 30 μM BrdU for 15 min (labels cells in S-phase), then washed 2x with PBS and replenished with fresh medium. Cells were trypsinised, washed 2x in PBS and fixed in 70% EtOH over night at 4ºC immediately for time point 0 h and then after 2, 4, 6 and 8 h. Immunofluorescence (IF) against DNA-incorporated BrdU (anti-BrdU antibody, Becton Dickinson) was performed following antigen retrieval with 2 M Hydrochloric acid (1:4 HCL in ddH_2O); PI staining was complenmetary. Fluorescent intensity was analysed on a FORTESSA FACS analyser.
NOTE: Cell cycle analysis, i.e. PI staining and IF against BrdU and subsequent FACS analysis was performed by members of the LRI FACS laboratory.

2.6.3 Reactive oxygen species (ROS) detection

(A) H_2DCFDA

$1.5x10^5$ cells were reverse transfected with 37.5 nM siRNA for 48 h in a 6-well format. Treatment with 1 mM H_2O_2 for 10 min prior to H_2DCFDA addition was used as a positive control for ROS induction. Cells were incubated with 5 μM cell permeable 6-carboxy-2',7'-dichlorodihydrofluorescein diacetate (Carboxy-H_2DCFDA; Ex/Em = 495/529 nm; Molecular Probes), a chemically reduced, acetylated form of fluorescein that is used as an indication of the presence of reactive oxygen species (ROS), for 30 min at 37ºC in the dark. Stained cells were then trypsinised, washed 1x in PBS to remove residual trypsin and media and resuspended in 300 μl cold PBS. Immediately before analysing on an LSRII FACS analyser, DAPI was added to exclude dead cells. Cells were kept on ice and in dark while waiting to be analysed.

(B) Cellular ROS/Superoxide detection (Abcam, ab139476)

30 min prior trypsinisation cells were treated with 200 μM Pyocyanin (a ROS inducer) and AntimycineA (superoxide inducer) respectively, as positive control for ROS/Superoxide induction. Cells were washed 2x in PBS and incubated with the ROS/Superoxide fluorescent dye combination for 30 min at 37°C and in the dark. Cells do not need to be washed to remove residual dye, but were analysed directly with an LSRII FACS analyser. The green ROS probe requires Ex/Em = 490/525 nm (Fluorescine), while the orange Superoxide probe requires Ex/Em = 550/620 nm (Rhodamine) filter sets for detection.

2.7 Immunocytochemistry to detect DNA damage

Accumulation of phospho-Histone H2A.X (γ-H2A.X) and 53BP1 as result of the DNA damage response can be used as readout for DNA damage.

Cells were transfected with 37.5 nM siRNA targeting GPX1, GPX3 and SOD1 for 96 h in a 96-well format. 6 h before fixation, untransfected cells were treated with 250 nM doxyrubicine, a DNA intercalating agent causing DNA damage, as positive control. Cells were fixed for 2 h in a 50:50 mix of methanol/acetone at -20°C. Following fixation, cells were washed 2x with PBS before incubation in blocking solution (3%

BSA/0.1% Tween20 in PBS) for 1 h at RT or over night at 4°C. Blocking solution is then replenished with 30 µl staining solution, i.e. blocking solution containing 53BP1 (rabbit, H300, Santa Cruz; 1:200 dilution) and γH2A.X (mouse, millipore; 1:400 dilution) antibody. Cells were incubated under constant shaking for 1.5 h at RT. Cells were washed 3x in PBS before adding the secondary fluorescent antibody (Alexa Flour® rabbit and mouse 488 and 594) for 1 h at room temperature. Cells were washed 3x in PBS, replenished with 100 µl PBS and subjected for analysis using a Celomics ArrayScan V^T (Thermo Scientific) and the accompanying Thermo Scientific HCS studio: Cellomics Navigator Version 6.4.4 software.

2.8 Lipid droplet analysis

For basal cytoplasmic lipid droplet analysis, 4000 cells/well were plated in a 96-well format and fixed 48 h later with 80 % ice-cold EtOH over night at -20°C. After fixation, cells were washed 2x with PBS before adding staining solution containing 1:10000 Nile Red (Life Technologies, stock: 1 mg/ml in DMSO) and 1:5000 DAPI (Sigma, stock: 5 mg/ml) in PBS for 15-30 min, RT. Cells were washed 2x with PBS, replenished with 100 µl PBS and subjected for analysis using a Celomics ArrayScan V^T (Thermo Scientific) with associated Thermo Scientific HCS studio: Cellomics Navigator Version 6.4.4 software.

2.9 Nucleic acid manipulations

2.9.1 Extraction of total RNA

Total RNA was extracted from cells using an RNeasy Mini Kit (Qiagen) according to the manufacturer's instructions for extraction of animal cells. Cells were lysed with RLT buffer and disrupted by centrifugation in shredder columns (QIAshredder, Qiagen). The obtained RNA was eluted in 20-40 µl nuclease-free water (Ambion) and RNA concentration was measured using a NanoDrop spectrophotometer (ThermoFisher Scientific). RNA was stored at -80ºC.

2.9.2 Complementary DNA synthesis

Total RNA was used to generate its complementary DNA (cDNA) with SuperScript II reverse transcriptase, Oligo dT_{12-18} and RNaseOUT (Invitrogen). Reverse transcription was performed according to the first-strand cDNA synthesis protocol (Invitrogen). Briefly, 1 µg RNA was mixed with 1 µl of 10 mM dNTPs (Invitrogen), 1 µl Oligo dT_{12-18} primer (500 µg/ml; Invitrogen) and nuclease-free water (Ambion) up to a total volume of 12 µl. This mix was heated for 5 min at 65ºC and then cooled for 5 min on ice before adding 8 µl RT reaction mix (Invitrogen) to each sample. Reactions were thoroughly mixed and incubated at 42ºC for 1.5h.

RT reaction mix

4 µl	5x first strand buffer
2 µl	DTT (0.1 M)
1 µl	RNAseOUT (40 units/µl)
1 µl	SuperScript II reverse transcriptase (200 units/µl)

Finally, cDNA was diluted to a final concentration of 10 ng/µl with nuclease-free water (Ambion).

2.9.3 Quantitative real time qPCR (RT-qPCR)

Quantitative real time PCR (RT-qPCR) is based on a PCR, where the amplified product is measured after each cycle by a fluorescence detector for amplification (7900HT Fast Real-Time PCR System, Applied Biosystems). Here, the SYBR Green I dye (Platinum® SYBR® Green qPCR SuperMix-UDG with ROX, Invitrogen) was used as fluorphore, which binds to double-stranded DNA during the elongation phase. To avoid unspecific fluorophore binding, each run included a standard melting curve programme (90ºC-65ºC) and a dissociation curve was produced (SDS2.3 software) as reference for internal quality control. A dissociation curve plots the ratio of fluorescence intensity and temperature over time for each PCR product analysed. The more identical products present, the more the curve ascends until it reaches a peak. This peak indicates the maximal dissociation ratio within the melting curve.

RT-qPCRs were performed on 96-well plates and each reaction mix included

12.5 µl	Platinum® SYBR® Green qPCR SuperMix-UDG with ROX
2.5 µl	QuantiTect Primer (10 pmol/µl; Quiagen)
10 µl	cDNA (10 ng/µl)

Table 2.4 gives a full list of qPCR primers used in this study.

RT-qPCR analysis is based on the number of PCR cycles that are needed to accumulate a certain threshold of fluorescence, the so-called cycle threshold (C_T) obtained for a sample. The C_T value is proportional to the logarithm of initial amount of the mRNA/cDNA of the gene of interest in a sample. To compare relative RNA levels of a gene of interest among different samples, determination of RNA levels of the housekeeping gene *ACTB* (ecodes β-actin) was included in each set of RT-qPCRs for normalisation purposes. The difference in cell cycle numbers, ΔC_T, were compared to each other (Livak and Schmittgen, 2001).

RT-qPCR conditions

50°C	2 min	
95°C	5 min	
95°C	15 sec	} 40x
60°C	1 min	

Table 2.4: Qiagen QuantiTect Primer used in this study

Gene symbol	Protein	Catalogue number
ACTB	b-Actin	QT01680476
BAX	Bcl-2-associated X proteine	QT00031192
CAT	Catalase	QT00079674
CDKN1A	p21/WAF1/CIP1	QT00062090
CDKN1B	p27/Kip1	QT00998445
CPT1A	Carnitine palmitoyltransferase IA	QT00082236
CPT1B	Carnitine palmitoyltransferase IB	QT00057036
FOXO1	Forkhead box transcription factor of the O class 1	QT00044247
FOXO3	Forkhead box transcription factor of the O class 3	QT00031941
FOXO4	Forkhead box transcription factor of the O class 4	QT00029141
G6PD	Glucose-6-phosphate dehydrogenase	QT00071596
GCLC	Glutamate-cysteine ligase catalytic subunit	QT00037310
GLS	Glutaminase	QT00019397
GPX1	Glutathione peroxidase 1	QT00203392
GPX2	Glutathione peroxidase 2	QT00200039
GPX3	Glutathione peroxidase 3	QT00062279
GPX4	Glutathione peroxidase 4	QT00067165
GPX5	Glutathione peroxidase 5	QT00044744
GPX6	Glutathione peroxidase 6	QT01677088
GPX7	Glutathione peroxidase 7	QT00009492
GPX8	Glutathione peroxidase 8	QT00032347
GSR	Glutathione reductase	QT00038325
GSS	Glutathione synthetase	QT00014413
MYC		QT00035406
NFE2L2	Nuclear respiratory factor 2, NRF2	QT00027384
PDHK1	Pyruvate dehydrogenase kinase 1	QT00069636
PMAIP1/ NOXA1	Phorbol-12-myristate-13-acetate-induced protein 1	QT00074438
PPARGC1B	PGC1B	QT00081865
PRDX2	Peroxiredoxin 6	QT00000098
PUMA/BBC3	53 upregulated modulator of apoptosis (PUMA) or Bcl-2-binding component 3 (BBC3)	QT00082859
RAD51		QT00072688
SCAP	SREBP cleavage activating protein	QT00197764
SCD	Stearoyl-CoA desaturase-1	QT01669521
SEPSECS	O-phosphoseryl-tRNA(Sec) selenium transferase	QT00048342
SLC1A5	Solute carrier family 1 (neutral amino acid transporter), member 5	QT00083909
SLC7A11	solute carrier family 7 (anionic amino acid transporter light chain, xc- system), member 11	QT00002674
SLC7A9	Solute carrier family 7 (cationic amino acid transporter, y+ system), member 9	QT00057778
SOD1	Cu/Zn superoxide dismutase	QT01671551
SOD2	Mn superoxide dismutase	QT01008693
TFAM	Mitochondrial transcription factor A	QT00012782
TOMM20	Translocase of outer mitochondrial membrane 20 homolog (yeast)	QT00088914
TP53	p53	QT00060235
VEGFA	Vascular endothelial growth factor A	QT01682072
XRCC6	Ku70	QT00036064

Note: Lyophilised qPCR primers were resuspended in 1.1 ml TE (pH 8.0) to obtain 10x stock dilutions.

2.9.4 Single-nucleotide polymorphism (SNP) analysis of part of chromosome 3p

Genomic DNA was extracted using a DNeasy Blood and Tissue Kit (Quiagen) according to the manufacturers protocol. DNA concentrations were measured using a NanoDrop spectrophotometer (ThermoFisher Scientific). 250 ng/ml DNA were subjected to a targeted PCR with the following commercially available SNP primers (Invitrogen):

D3S2450, D3S4420, D3S2947E, D3S4351, D3S1317,
D3S1351, D3S1259 D3S1211, D3S1581, D3S36

To each sample DNA, 8 µl PCR reaction mix and nuclease-free water to a final volume of 25 µl was added.

PCR reaction mix

2.5 µl	10x Buffer
0.2 µl	dNTPs (2.5mM each)
0.1 µl	primer pair (200µM)
5 µl	reagent Q (comes with Taq polimerase; Quiagen)
0.2 µl	Taq polymerase (Quiagen)

PCR conditions

94°C	5 min	
94°C	1 min	⎫
55°C	1 min	⎬ 35x
72°C	1 min	⎭
72°C	10 min	
4°C	∞	

The PCR product was cleaned up using a QIAquick PCR Purification kit following the manufacturer's guidelines.

For the sequencing reaction, to 4 µl of the cleaned PCR product 8 µl BigDye® Terminator (BDT, provided by the LRI Equipment Park), 1 µl sequencing primer (20 µM) and 7 µl ddH_2O was added.

Sequencing conditions

96°C	5 min	
96°C	1 min	⎫
50°C	1 min	⎬ 35x
60°C	1 min	⎭
4°C	∞	

The obtained results were analysed using GeneMapper software 5 (Applied Biosystems).

2.10 Protein manipulations

2.10.1 Protein quantification using Sulforhodamine B (SRB) assay

To determine cellular protein content as means of normalisation where cell number readout was not possible, sulforhodamine B staining was performed. This method was adapted from (Vichai and Kirtikara, 2006) and was mainly performed on a 96-well format. Supernatant/media was aspirated from cells before adding ice-cold 10 % tri-chloro-acetic acid (TCA in milliQ H_2O) in PBS for fixation for ≥1 h at 4ºC. Cells were washed 2x with 100 µl/well ddH_2O and air-dried over night at RT. The following day, 50 µl/well of a 0.4 % Sulforhodamine B in 1 % acetic acid solution was added and incubated for 30 min at RT constantly shaking. Cells were washed 2x in 1 % acetic acid and dried completely before adding 100 µl/well 10 mM TRIS (pH 8) for 15 min at RT constantly shaking to re-solubilise the protein-bound Sulforhodamine B. Luninescence at 530, 565 and 690 nm was measured using a SpectraMax 190 plate reader (Molecular Devices, Sunnyvale, CA, USA) and SoftMax Pro software. Note: a cell-free, media only –containing well was always included in order to determine background SRB levels. For cell mass determination, the following calculation was performed:

λ_{570} - λ_{690} (background of respective well) - average protein background

2.10.2 Protein quantification using Bradford assay

In order to load equal amounts of protein samples on SDS-polyacrylamide gels, protein concentrations were determined using Bradford reagent (Bio-Rad Protein Assay). BSA was used to generate a standard curve (0, 2, 4, 6, 8, 10, 12, 14 µl BSA (0.025 µg/µl) + 250 µl Bradford reagent, respectively, for 0, 0.4, 0.8, 1.2, 1.6, 2.0, 2.4, 2.8 µg/µl BSA). Bradford reagent was diluted 1:5 in ddH_2O and 250 µl were added per well to 10 µl 1:5 protein sample dilution (in ddH_2O). After 5 min incubation constantly shaking at RT, the absorbance at $\lambda = 595$ nm was measured on a SpectraMax 190 plate reader using the SoftMax Pro software (Molecular devices).

2.10.3 Preparation of cell lysates for immunoblots

Medium was aspirated and cells were washed 2x with cold PBS prior to lysis with 100-200 µl cold TNET buffer supplemented with protease (Complete, EDTA free, Roche) and phosphatase (PhosStop, Roche) inhibitors and DTT. After incubation on ice for 20 min constantly shaking, cells were scraped using cell scraper (Sarstedt; Newton, NC USA) and collect cell lysates were centrifuged at 13000 rpm for 10 min at 4°C. Supernatants were carefully transferred into new tubes. Protein lysates were stored at -80°C until further use.

TNET lysis buffer pH7.5

1 %	NP-40
20 mM	Tris-HCL (pH 7.5)
137 mM	NaCl
10 %	Glycerol
2 mM	EGTA
1 mM	DDT

NuPage loading dye (4x) was added to 10-15 µg protein lysates for protein denaturing. TNET buffer was used to equalise total volumes of cell lysates used for separation on sodium dodecyl sulphate (SDS)-gels. The mixture was vortexed followed by a 10 min incubation period at 70°C.

NuPage Loading Dye

8 %	SDS
200 mM	TRIS Base
40 %	Glycerol
0.01 g/l	Bromphenol Blue
2 %	β-Mercaptoethanol
1 mM	DDT

2.10.4 Sodium dodecyl sulphate (SDS) –PAGE

SDS-page is a common method used to analyse cellular protein contents. This technique allows separation of proteins based on their molecular weight. The detergent SDS is not only used to denature the proteins but it also imparts a uniform charge to them. Therefore, proteins will separate solely based on size and not charge. In this study, only pre-cast 4-12 % Novex®- NuPage TRIS-glycine SDS-page gradient gels (Invitrogen) were used in Bio-Rad electrophoresis chamber systems.

The following running buffers were used:

20x NuPAGE® MOPS Running Buffer
pH 7.7 (Novex/leife technologies, NP0001)

50 mM	MOPS
50 mM	TRIS Base
0.1 %	SDS
1 mM	EDTA

20x NuPAGE® MES Running Buffer
pH 7.3 (Novex/life technologies, NP0002)

50 mM	MES
50 mM	TRIS Base
0.1 %	SDS
1 mM	EDTA

The pre-stained full-range protein marker RPN800E (Amersham) was used as molecular size standard to determine approximate protein sizes. Protein separation was performed at 150 V for ± 90 min.

2.10.5 Westerm Blotting

Immunoblotting is a commonly used method to transfer proteins separated by denaturing gel electrophoresis onto a membrane. SDS gradient gels obtaind in 2.10.4 were transfered onto an Immobilon-P membrane (Merck Millipore) using an electrophoretic transfer cell (Bio-Rad). Briefly, PVDF membranes were activated by a quick rinse in methanol followed by two quick washes with transfer buffer. All other components for the blot were equilibrated in transfer buffer while preparing the sandwich. The transfer was carried out at 250 mA for 120 min, Membranes were blocked in 5% milk/TBS for 0.5-1 h at RT constantly shaking to prevent unspecific binding of antibodies to membranes. Incubation with primary antibody (1:1000 dilution in 3% BSA/Azide/Tris buffered saline/Tween20 (TBST)) occurred over night at 4°C constantly shaking. The following day the primary antibody solution was removed and membranes were washed 2x 5 min in 5 % milk/TBST and 3x 5 min in 0.1 % TBST constantly shaking. Then, secondary antibody conjugated to horseradish-peroxidase (HRP) (1:2000 dilution in 5 % milk/TBST) was added for 45 min at RT under constant shaking. Visualisation of protein bands occurred by chemiluminescence using an Amersham ECL detection kit (GE Healthcare) on Medical X-ray films (Hyperfilm, GE Healthcare), which were developed using an automatic X-ray film processor (JP-33, *JPI* Healthcare Solutions, Planview, NY, USA).
Composition of used buffers are listed below:

Transfer Buffer

250 mM	Glycine
25 mM	TRIS Base
10 %	Methanol

TRIS-buffered saline (TBS), pH 7.4

137 mM	NaCl
25 mM	TRIS Base

TBST, pH 7.4 – wash buffer

500 ml	TBS
0.1 %	Tween 20

Blocking solution

5 %	Semi-skimmed milk powder
500 ml	TBS
0.1 %	Tween20

Western blot stripping buffer, pH 2.5

1 M	Glycine
2 %	SDS
to adjust pH	HCl, conc.

Table 2.5 lists all antibodies used in this study.

Table 2.5: Antibodies used in this study

Primary Antibody	Host	Predicted size [kDa]	Clone	Cat No	Manufacturer
53BP1	Rabbit	220	H300	Sc-22760	Santa Cruz
ACC	Rabbit	280		3662	Cell Signalling
ACLY	Rabbit	120		4332S	Cell Signalling
AKT	Rabbit	60		9272	Cell Signalling
BCL-2	Mouse	26			
BrdU	Mouse				BD Bioscience
c-Myc	Mouse	57-65	9E10 ♯21	M4439	Sigma-Aldrich
CDK2	Rabbit	33	78B2	2546	Cell Signalling
CDK6	Mouse	36	DCS83	3136	Cell Signalling
Cyclin A	Rabbit	54	H-432	Sc-751	Santa Cruz
Cyclin D1	Mouse	36		Sc-20044	Santa Cruz
ERK1/2	Rabbit	42/44		9102	Cell Signalling
FASN	Mouse	265	23	610962	BD Bioscience
GPX1	Rabbit	22	C8C4	3286	Cell Signalling
GSK3α/β	Mouse	47/51		368662	Calbiochem
HA.11 – HA-tag	Mouse		16B12	MMS-101P	Covance
HIF-1α	Mouse	120	54/HIF1α	610959	BD Bioscience
HIF-2α	Rabbit	120		NB100-122	Novus
LAMINA/C	Mouse	~70	636	Sc-7292	Santa Cruz
MEK1/2	Rabbit	45		9122	Cell Signalling
MitoProfile® Total OXPHOS human WB antibody cocktail	Mouse	I – 18, II – 29, III – 48, IV – 22, V - 54		ab110411	Abcam
mTOR	Rabbit	289		2972	Cell Signalling
p16		16	JC8		CRUK in house
p21/WAF1/CIP1	Rabbit	21		Sc-397	Santa Cruz
p27/Kip1	Mouse	27		610241	BD Transduction lab
p53	Mouse	53	DO-7	610984	Dako
pACC (S79)	Rabbit	280		3661S	Cell Signalling
pACLY (S455)	Rabbit	120		4331	Cell Signalling
pAKT (S473)	Rabbit	60		9271S	Cell Signalling
pAKT (T308)	Rabbit	60		9275	Cell Signalling
PARP	Rabbit	116 (FL) / 89 (cleaved)		9542	Cell Signalling
pERK1/2 (T202/Y204)	Mouse	42/44	E10	9106	Cell Signalling
pGSK3α/β (S21/9)	Rabbit	47/51	S21/9	9331	Cell Signalling
pHistone H2A.X (S139)	Mouse	15		05-636	Merck Millipore
pP38 (T180/Y182)		38			
PPARγ	Mouse	55	E-8	Sc-7273	Santa Cruz
pRb (S780)	Goat	107/140		Sc-12901	Santa Cruz
pS6 (S235/236)	Rabbit	32		2211	Cell Signalling
pS6 (S240/244)	Rabbit	32		2215	Cell Signalling
PTEN	Rabbit	54		9552	Cell Signalling
Rb	Rabbit	107/140	C-15	Sc-050	Santa Cruz
S6 Ribosomal protein	Rabbit	64	5G10	2217	Cell Signalling
SOD1	Mouse	18	71G8	4266S	Cell Signalling
SOD2	Rabbit	25		SOD-110	Stressgen
SREBP1	Mouse	125, 70	2A4	557036	BD PharMingen
SREBP2	Mouse	120	1C6	557037	BD PharMingen
TOMM20	Rabbit	20		Sc-11415	Santa Cruz
β-Actin-HRP	Mouse	45	AC-15	A3854	Sigma-Aldrich

Secondary Antibody	Host	Cat No	Manufacturer
ECL™ Anti-mouse IgG-HRP	Sheep	NA931V	GE Healthcare
ECL™ Anti-rabbit IgG-HRP	Donkey	NA934V	GE Healthcare
Alexa Fluor® 488 anti-rabbit- IgG	Donkey	A21206	Life Technologies
Alexa Fluor® 594 anti-mouse- IgG	Goat	A11005	Life Technologies

2.11 Metabolic Manipulations

2.11.1 Measurements of Oxygen Consumption Rate (OCR) and Extracellular Acidification Rate (ECAR)

Oxygen consumption and lactate secretion are physiological symptoms that go with active cellular metabolism, more specifically, the ratio is an indicator of how glycolytic or respiratory cells are. The Seahorse Bioscience Extracellular Flux (XF) Analyser (Seahorse Bioscience, Massachusetts, USA) is a valuable tool to evaluate cellular oxygen consumption rates (OCRs) and extracellular acidification rates (ECARs) the latter of which are supposed to correlate with lactate secretion.

Cells were plated on 96-well XF Cell Culture Microplates (seahorse Bioscience) in 80 µL culture medium the day before assaying. Appropriate plating cell numbers need to be determined beforehand, as these are crucial for successful analysis. Cells were seeded so that they were 100 % confluent at time of analysis. Note also, that the XF sensor cartridge (Seahorse Bioscience) needs to be hydrated in 200 µl/well XF Calibrant solution (pH 7.4) (Seahorse Bioscience) over night at 37°C in a CO_2-free incubator (Seahorse Bioscience). The next day, assay medium was freshly prepared by supplementation of plain XF Assay Medium (Seahorse Bioscience) with the necessary nutrients. This medium was also used to prepare 10x drug concentrations and was distributed to the appropriate injection ports on the XF sensor cartridge for injection during the assay. The sensor cartridge was then placed into the XF Analyser for calibration. In the meantime, cells were washed carefully in assay medium, replenished with the appropriate amount of this and incubated at 37°C for ≥ 30 min in the CO_2-free incubator to deacidify the medium. Following calibration, the XF Cell Culture Microplate was inserted into the XF analyser for flux analysis. Compositions for the respective assay media used for the different assays together with the respective treatments are listed in Table 2.6, and a standard flux analysis protocol is depicted in Table 2.7.

Table 2.6: Media composition and drug concentrations for OCR/ECAR measurements

Assay	Glycolysis	Respiratory capacity	β-Oxidation vs. Glycolysis	β-Oxidation
Medium	XF assay medium modified DMEM (no Glucose, 2 mM Glutamax; Part no: 102352-000)			Krebs-Henseleit Buffer (KHB) (111 mM NaCl, 4.7 mM KCl, 2 mM $MgSO_4$, 1.2 mM Na_2HPO_4)
Supplements	25 mM Glucose		10 mM Glucose	2.5 mM Glucose
	10 mM Sodiumpyruvate		1 mM Sodium pyruvate	0.5 mM Carnitine
Added drugs (in order)	25 mM Glucose	1.3 µM Oligomycin	50 µM Etomoxir	100 µM Sodium palmitate
	1.3 µM Oligomycin	0.4 µM FCCP	25 mM Glucose	50 µM Etomoxir
	50 mM 2-DG			

Table 2.7: Standard Seahorse Bioanalyser protocol for 3 injections

Protocol Steps		
Command	**Time (min)**	Port
Calibrate	0.00	
Equilibrate		
Mix	3.00	
Wait	1.00	
Measure	4.00	
Mix	3.00	
Wait	1.00	
Measure	4.00	
Mix	3.00	
Wait	1.00	
Measure	4.00	
Mix	3.00	
Wait	1.00	
Measure	4.00	
Inject		A
Mix	3.00	
Wait	3.00	
Measure	4.00	
Mix	3.00	
Wait	1.00	
Measure	4.00	
Mix	3.00	
Wait	1.00	
Measure	4.00	
Inject		B
Mix	3.00	
Wait	3.00	
Measure	4.00	
Mix	3.00	
Wait	1.00	
Measure	4.00	
Mix	3.00	
Wait	1.00	
Measure	4.00	
Inject		C
Mix	3.00	
Wait	3.00	
Measure	4.00	
Mix	3.00	
Wait	1.00	
Measure	4.00	
Mix	3.00	
Wait	1.00	
Measure	4.00	
EndProtocol		

2.11.2 Measurement of intracellular glutathione levels

To determine basal intracellular gluthathion in ccRCC cells and in HK-2 cells, a Gluthathione Fluorometric Assay Kit (BioVision, Cat. No. K264-100) was employed according to the manufacturer's guidelines. In brief, quick handling and keeping the samples cold/on ice as much as possible is essential. Cells were plated on 10 cm tissue culture dishes and shock-frozen on dry ice 48 h later for lysis. Cells were stored at -80°C until processed. Following collection of the lysed cells via a cell scraper and further mechanical disruption using a 21 G syringe, cell lysates were quickly transferred to pre-prepared perchloric acid (PCA) and vortexed to obtain a homogenous mixture. After 5 min on ice, emulsions were centrifuged at 4°C for 2 min at 13000 rpm, to collect the supernatant. Ice-cold 6 N KOH was added in a 1:2 ratio to the PCA-preserved sample, incubated for 5 min on ice and spun down for 2 min at 13000 rpm at 4°C. A 6^{th} of each sample supernatant was transferred to a 96-well plate for (a) reduced glutathione (GSH), (b) oxidised GSSG and (c) total glutathione detection. To detect GSSG, samples were first pretreated with 10 µl GSH quencher for 10 min at RT and then with 10 µl reducing agent to destroy any excessive quencher and convert GSSG to GSH. The latter treatment applies also for determination of total glutathione. In parallel a GSH, GSSG and GSH+GSSG standard was prepared the same way including a reagent only containing background control. To start the reaction, 10 µl o-phthalaldehyde (OPA) was added and mixed well. After ~40 min incubation at RT, OPA fluorescence (Ex/Em = 340/420 nm) was detected using a PHERAstarPlus-plate reader (BMG Labtech).

To calculate GSH amountst, the background was subtracted, the standard curves were plotted (RFU vs. GSH standard) and the sample values were applied to the standard curves to obtain glutathione amounts.

For being able to compare across samples, GSH, GSSG and total glutathione levels were normalised to total protein concentrations used in the assay. Protein concentrations were determined using Bradford protein quantification assay.

2.11.3 Measurement of GPX activity

To determine how GPX activity compares between ccRCC and HK-2 cells, GPX activity was measured using a Glutathione Peroxidase Assay Kit (Abcam, ab102530) according to the manufacturer's guidelines. Briefly, cells were plated on 10 cm tissue culture dishes and harvested 48 h later by shock-freezing on dry ice. Cells were further mechanically disrupted by passing several times through 21G syringes before centrifugation at 10000 rpm for 15 min at 4°C, to collect the supernatant. 25 µl of each sample was transferred to a well on a 96-well plate (in duplicates) including a positive (purified GPX) and a negative (reagents only) control and volume was brought to 50 µl with Assay buffer). A standard curve was prepared as displayed in Table 2.8, and NADPH autoflourescence was measured (Ex/Em = 340/420 nm).

Table 2.8: NADPH standard curve

ml NADPH standard (1 mM)	nmol/well NADPH standard	µl assay buffer
0	0	100
20	20	80
40	40	60
60	60	40
80	80	20
100	100	0
120	120	0

Reaction Mix per well

33 µl Assay buffer
3 µl NADPH solution (40mM)
2 µl Glutathione reductase solution
2 µl GSH solution

40 µl reaction mix was added to each sample containing well. The reaction was started with addition of 10 µl Cumene Hydroperoxide following 15 min incubation. Changes in NADPH conversion were recorded manually every minute for 20 min using an Envision plate reader. GPX activity was calculated as follows:

$$\text{GPX activity} = \frac{\text{NADPH decrease over time}}{\Delta \text{ time [min]} \times \text{pretreated sample volume added into the reaction well [ml]}} \times \text{sample dilution} = \text{nmol/min/ml} = \text{mU/ml}$$

With one unit being defined as amount of enzyme needed to cease the oxidation of 1 µmol of NADPH to NAD^+ per minute under assay kit conditions at 25°C.

For being able to compare across samples, the obtained GPX activity values were normalised to total protein concentrations used in the assay. Protein concentrations were determined using Bradford protein quantification assay.

2.12 Data analysis

2.12.1 Analysis of quantitative experiments

Data are usually presented as mean values and the error bars represent either the standard deviation (SD) or standard error of the mean (SEM) as described in the figure legend. All quantitative data was analysed and graphed up using GraphPad Prism 6.0 (GraphPad software). Drug dose response curves were generated using the "log(inhibitor) vs. response – variable slope (four parameters)" analysis and IC50 values were extracted from the accompanied table of XY coordinates. For statistical analysis, when the different ccRCC cell line behaviours were compared to HK-2 cell behaviour, 2-way ANOVA analysis with Dunnett multiple comparison testing was carried out. The same is true for time courses or some dose response curves, when different time points were compared to t_0 or vehicle control treatment. Indicated p-values (or asterisks) were obtained as stated in the respective figure legends and are corrected for multiple comparison testing. Only p-values ≤ 0.05 were considered to be statistically significant with *, $p \leq 0.05$; **, $p \leq 0.01$; ***, $p \leq 0.005$; ****, $p \leq 0.001$.

2.12.2 Analysis of ccRCC TCGA dataset

TCGA kidney renal cell carcinoma data were downloaded from the cBioPortal website (http://www.cbioportal.org/public-portal/), via Bioconductor's "cgdsr" package (Jacobsen, 2013). Processed RNA-seq expression signals (kirc_tcga_rna_seq_v2_mrna) and clinical data (kirc_tcga_rna_seq_v2_mrna) were gathered for a selection of genes (GPX1, GPX3, SOD1, GLS, GCLC, GCLM, GSS, GSR, G6PD, SLC1A5, SLC7A9 and SLC7A11).

Single gene survival analysis

For each selected gene, expression across patient samples were categorised into high, medium and low expression groups based on 1/3 and 2/3 quantiles. Kaplan-Meier survival curves were plotted for the resulting groups. The effect of expression on overall survival was then assessed using a Cox proportional hazard model from the Biocoductor package "survival".

Chapter 3: Metabolic characterisation of a panel of ccRCC cell lines and pVHL-isogenic cell line pairs

3.1 Introduction

ccRCC is characterised by high intratumoural heterogeneity (Gerlinger et al., 2012a). Furthermore, as described above, sporadic and hereditary ccRCC is characterised by a heterogeneous loss of DNA fragments on the short arm of chromosome 3, which harbours *VHL* amongst others. The gene product of this gene, pVHL encodes an E3 ubiquitin ligase whose most prominent target is the α-subunit of the heterodimeric HIF transcription factor (Maxwell et al., 1999). HIF orchestrates a metabolic switch from oxidative respiration to anaerobic glycolysis and stimulates vascularisation in response to hypoxic stress. ccRCC cells are presenting a pseudo-hypoxic state, in which HIF is constitutively active despite the presence of ample oxygen levels, leading to a highly glycolytic phenotype of this cancer subtype (Figure 1.5).
Apart from *VHL*, other adjacent genes are lost in the course of ccRCC tumourigenesis, many of which are involved in metabolic processes. In a systems-biology approach, it has been found that ccRCC metabolism is distinct from that of other cancer types and that ccRCC cells have highly compromised nucleotide, inositol and glycerol(phospho)lipid metabolism (Gatto et al., 2014).
To fully appreciate the heterogeneity of ccRCC, for the studies described in the following, a cell line panel of 12 ccRCC cell lines and one non-tumourigenc kidney epithelial cell line, HK-2, was assembled. This panel comprises eight cell lines that have endogenously lost functional pVHL (RCC4, UMRC2, A498, 786-O, 769-P, CAKI2, UMRC3 and A704) and four cell lines that still express endogenous pVHL (TK10, CAKI1, ACHN and UO31).

In order to study pVHL function in the context of ccRCC, a selection of isogenic ccRCC cell lines was obtained from the laboratory of Prof. William Kaelin (Dana-Farber Cancer Institute, Boston, MA). These cell lines had been generated by introducing a wild type *VHL* allele (pBABE-puro-HA-VHL) into different established ccRCC cell lines that lack endogenous functional pVHL. As control, parental cells were transfected with the empty vector backbone (EV). Five isogenic cell line pairs, namely RCC4 EV, RCC4 VHL, UMRC2 EV, UMRC2 VHL, A498 EV, A498 VHL, 786-O EV, 786-O VHL, 769-P EV and 769-P VHL, were obtained to carry out a functional siRNA

screen to identify metabolic enzymes that show synthetic lethal interactions with pVHL (see Chapter 4). In this section, both the parental cell lines as well as the isogenic cell line pairs will be examined for their HIF-expression patter, respiratory and glycolytic profile as well as specific nutrient dependencies.

3.2 LOH of chromosome 3p fractions is common in ccRCC cell lines

Fractional LOH of chromosome 3p is a common characteristic of ccRCC cells. In order to establish the LOH pattern within the cell line panel, the 12 ccRCC cell lines were analysed for single-nucleotide polymorphisms (SNP) along the short arm of chromosome 3 from 3p26.1 to 3p13 spanning ~70.5Mb (Figure 3.1A). All of the cancer cell lines that are known to have lost functional pVHL were found to have only one copy of all the SNP markers tested (LOH of 3p26.1 to 3p13). Surprisingly, ACHN, known to express functional pVHL, showed the very same pattern (Figure 3.1B). In this case, LOH of chromosome 3p must not be accompanied by *VHL* mutation on the other allele, leaving one functional *VHL* copy for transcription. In contrast, all other cell lines known to express functional pVHL (HK-2, TK10, CAKI1 and UO31) were found to have a patchy SNP pattern towards the distal part of the 3p chromosome arm, with some stretches being scored as heterozygous (Figure 3.1B). Interestingly, the non-tumourigenic HK-2 cells but also positive blood sample controls (Ctr. I and Ctr. II) are not fully heterozygous for the whole 3p chromosome, but show LOH towards the proximal centromere stretch.

A

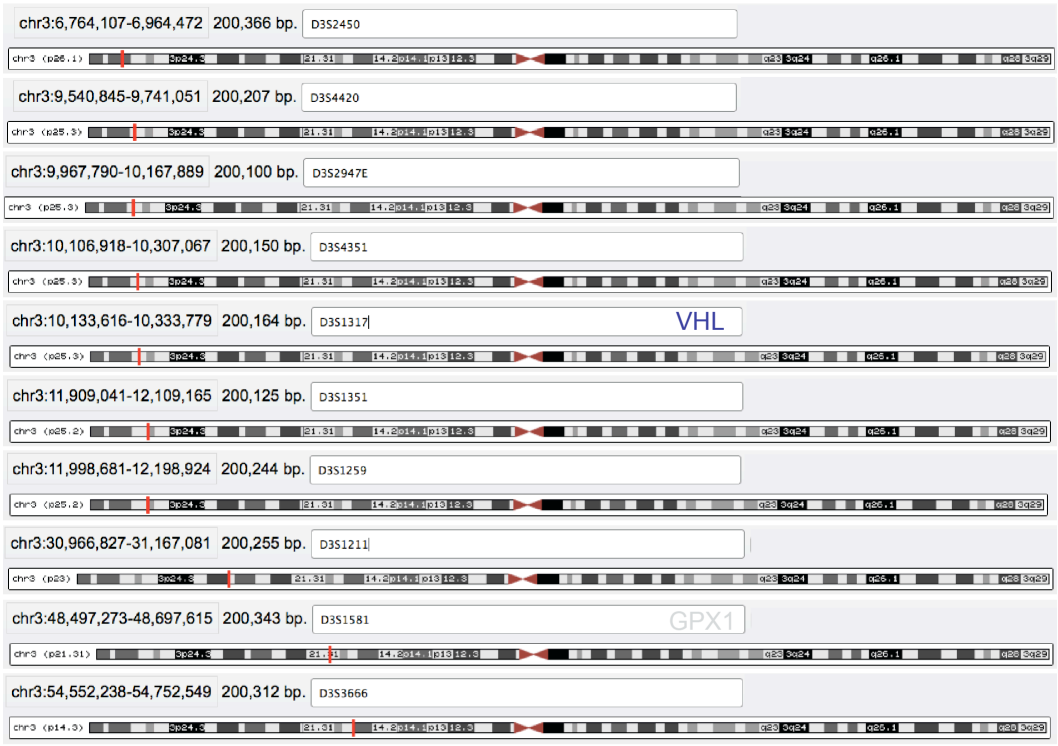

B

	D3S2450 3p26.1	D3S4420 3p25.3	D3S2947E 3p25.3	D3S4351 3p25.3	D3S1317 3p25.3	D3S1351 3p25.2	D3S1259 3p25.2	D3S1211 3p23	D3S1581 3p21.31	D3S3666 3p14.3
Ctr. I										
Ctr. II		UD								
RCC4										
UMRC2										
A498										
786-O										
769-P										
CAKI2										
UMRC3										
A704										
TK10										
CAKI1										
UO31										
ACHN										
HK-2										

HET LOH

Figure 3.1: Heterozygous loss of a substantial stretch of chromosome 3p is common in ccRCC cells.

(A) List of single-nucleotide polymorphism (SNP) markers tested on the ccRCC cell line panel to examine loss of heterozygosity (LOH) along the indicated stretch of chromosome 3p. *VHL*, commonly lost in ccRCC lies within marker D3S1317. (B) Summary of SNP array analysis on genomic DNA of ccRCC and HK-2 cells. Ctr. I and Ctr. II are blood DNA samples from healthy patients, which were kindly provided by Andrew Rowan, Translational Cancer Theapeutics, CRUK LRI. Blue cells indicate LOH, red cells indicate heterozygosity (HET); UD, undetermined.

3.3 Profiling of ccRCC cells for HIF stabilisation and hypoxia tolerance

3.3.1 ccRCC cell lines express either both HIF-α isoforms or only HIF-2α

As pVHL is a negative regulator of the transcription factor HIF, basal HIF expression and transcriptional activity was examined in the ccRCC cell lines. ccRCC cell lines that have lost functional pVHL clearly show higher basal levels of HIF-α protein expression compared to cells that express functional pVHL (Figure 3.2A). A498 cells were found to express a truncated form of HIF-1α protein. This truncated form has recently been described and shown to lack the domains encoded by exons 2-6, resulting in a ΔHIF-1α isoform with reduced tumour suppressor function (Shen et al., 2011). Furthermore, in 786-O and 769-P cells, no expression of HIF-1α was detectable. Interestingly, only cell lines that show stabilisation of HIF-1α also display increased levels of pyruvate dehydrogenase kinase 1 (PDHK1) mRNA (Figure 3.2B), an established HIF-1α transcriptional target (Kim et al., 2006). A498, 786-O, 769-P and all cell lines expressing functional pVHL show low levels of PDHK1 mRNA (Fig. 3.2B). Non-tumourigenic HK-2 cells show similar basal HIF-1α protein levels as pVHL-null ccRCC cells and moderate expression of PDHK1. Levels of HIF-2α were low in these cells (Figure 3.2B).

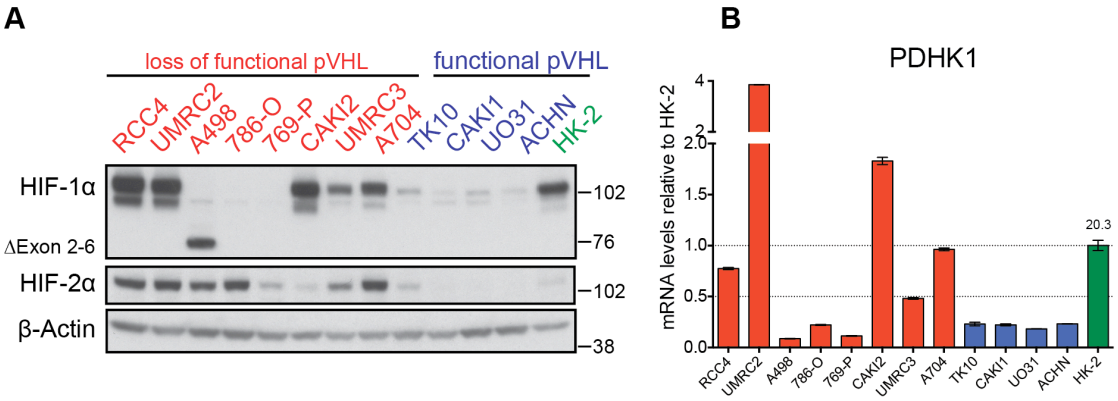

Figure 3.2: ccRCC cells express different levels of HIF-1α and HIF-2α
(A) The indicated ccRCC cell lines and HK-2 cells were analysed for basal HIF-1α and HIF-2α protein expression. β-Actin serves as loading control. (B) HIF-1α activity was assessed by measuring mRNA abundances for its downstream target pyruvate dehydrogenase kinase 1 (PDHK1). Bar graphs depict average of duplicate measurements normalised to ACTB and relative to HK-2 ± SD. Number above HK-2 bar represents average ΔC_T value for comparison.

With regard to the isogenic cell line pairs, all pVHL-null cell lines showed the same pattern of HIF-α isoform expression as the parental cell lines (Figure 3.3). In contrast, the pVHL-expressing cells show a substantial reduction in HIF-α expression. This was especially prominent for HIF-2α in RCC4, A498 and 786-O cells. Moreover, detection of exogenous pVHL showed strong overexpression in RCC4 and A498 cells, while 786-O and 769-P cells show moderate expression. Only weak expression of pVHL could be detected in UMRC2 cells. 786-O and 769-P cells seem to express pVHL at endogenous levels (Figure 3.3A).

As expected, expression of the HIF target gene vascular endothelial growth factor A (VEGFA) is modulated in a pVHL-dependent manner, while expression of PDHK1 was modulated only in the HIF-1α expressing cell lines RCC4 and UMRC2 (Figure 3.3B).

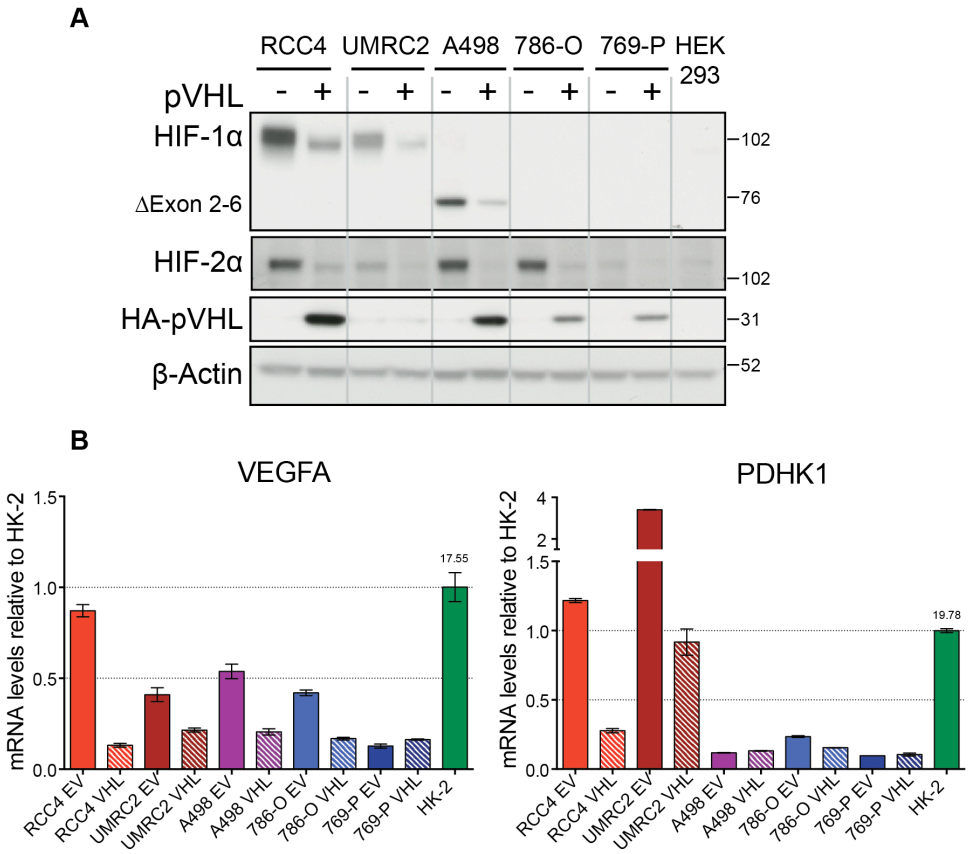

Figure 3.3: Exogenous pVHL represses HIF-α stabilisation and activity

(A) Basal HIF-1α, HIF-2α and HA-tagged pVHL expression in isogenic cell line pairs. HEK293 cells were used as positive control. (B) HIF activity was assessed by measuring mRNA abundances for its downstream targets pyruvate dehydrogenase kinase 1 (PDHK1) and vascular endothelial growth factor A (VEGFA). Bar graphs depict average of duplicate measurements normalised to ACTB and relative to HK-2 ± SD. Number above HK-2 bar represents average ΔC_T value for comparison.

3.3.2 MG-132, DMOG and hypoxia stabilise HIF-α protein in VHL reconstituted cell lines

In order to evaluate the capacity of stabilising HIF-α isoforms in pVHL expressing versus pVHL deficient ccRCC cells, cells were treated with the proteasome inhibitor MG-132 to prevent proteasomal degradation of HIF-α. MG-231 treatment resulted in substantial HIF-1α and HIF-2α accumulation both in all pVHL expressing and lacking cell line pairs, although HIF-α levels were higher in cells lacking pVHL (Figure 3.4B). 769-P cells express very low levels of HIF-2α, which was increased following MG-132 treatment. The observation that proteasome inhibition also resulted in accumulation of HIF-α protein in pVHL-null cells, hints to the existence of degradation systems other than the pVHL-mediated regulation.

A more specific way of examining HIF-α stabilisation is achieved by inhibiting the activity of the negative regulators of HIF-α, the PHDs, using the competitive inhibitor dimethyloxallyl glycine (DMOG). The isogenic cell line pairs as well as CAKI2, CAKI1, TK10, UO3 and HK-2 cells were treated with DMOG and analysed for HIF-α accumulation. DMOG treatment was as efficient in inducing HIF-α accumulation as MG-132 treatment in all cell lines tested (Figure 3.4C). Contrary to MG-132, DMOG only increased HIF-1α levels in pVHL containing RCC4 and UMRC2 cells, confirming the specificity of the treatment. HK-2 cells were found to have a quite large HIF-1α pool, and DMOG treatment increased HIF-1α protein levels even above the levels of RCC4 cells, which display the largest amount of HIF-1α protein among the cancer cell lines (Figure 3.4C). DMOG treatment in pVHL expressing cells results in HIF-2α levels similar to those in untreated EV cells without causing any additional increase in cells lacking pVHL (Figure 3.4C).

Finally, isogenic cell lines together with HK-2 cells were subjected to oxygen deprivation for short (6 h) and long (24 h) term in order to mimic the actual HIF activating environment and to assess HIF-α accumulation. In pVHL-expressing cells, HIF-1α and HIF-2α protein levels were increased after 6 h exposure to 0.1% oxygen but declined to almost basal levels after 24 h of oxygen deprivation (Figure 3.4D). This transient induction could indicate the possibility of adaptation to long-term hypoxia exposure. While RCC4 and A498 EV cells maintained their basal HIF-1α and HIF-2α levels upon short and long term oxygen deprivation, 786-O EV cells showed a reduction

of HIF-2α protein after 24 h in hypoxia. Moreover, UMRC2 EV cells seemed to gradually lose both HIF-1α and HIF-2α expression over time in hypoxia, again suggesting adaptation mechanisms. Interestingly, the non-tumourigenic HK-2 cells strongly upregulated both HIF-1α and HIF-2α in hypoxia and maintained these high levels over at least 24 h of oxygen deprivation. No induction of HIF-1α or HIF-2α protein could be detected in 769-P cells (Figure 3.4D).

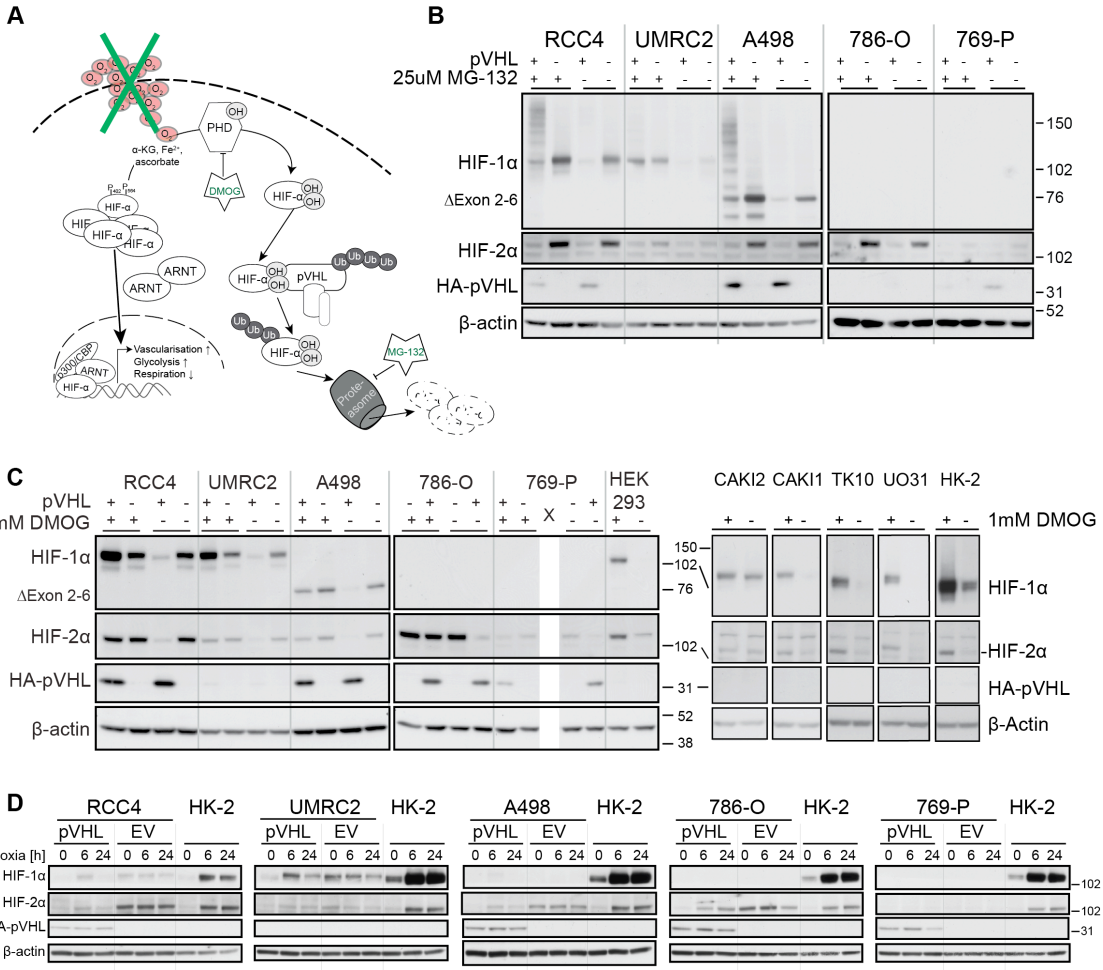

Figure 3.4: HIF-α stabilisation in isogenic ccRCC cells upon treatment with MG-132 and DMOG

(A) Schematic depicting HIF signalling and degradation and highlighting some ways of interfering with the pathway to stabilise HIF protein. (B) HIF-α protein leves and pVHL in pVHL-isogenic ccRCC cell line pairs upon treatment with 25 µM MG-132, a proteasome inhibitor, for 2 h. (C) HIF-α and pVHL protein levels in ccRCC isogenic cell lines, CAKI2, CAKI1, TK10, UO31 and HK-2 cells upon treatment with the PHD competitive inhibitor DMOG (1 mM) for 4 h. (D) HIF-α and pVHL protein levels upon short (6 h) and long (24 h) term incubation in 0.1% oxygen. (B-D) β-actin serves as loading control.

Taken these data together, pVHL-reconstituted cells showed the expected regulation of the HIF-α isoforms. pVHL-expression resulted in lower basal expression of HIF-1α and

HIF-2α protein but this negative effect could be reversed by treatment with MG-132 or DMOG. Moreover, these cell lines also showed induction of HIF-α in hypoxia. The non-tumourigenic HK-2 cells, surprisingly, showed substantial basal HIF-1α accumulation, which was enhanced in hypoxia and maintained over longer oxygen deprivation.

3.3.3 ccRCC cells are more sensitive to 0.1% than 0.5% oxygen conditions independent of pVHL expression

To assess the tolerance of the isogenic ccRCC cell lines as well as HK-2, TK10 and CAKI1 cells towards oxygen deprivation, cell proliferation was monitored over five days in oxygen-deprived conditions. Supply with 0.5% and 0.1% oxygen were compared to normoxia (21% oxygen). For the first 2-3 days, proliferation of most of the cancer cell line pairs and HK-2 cells did not differ much between the different oxygen conditions (Figure 3.5A). Around day 3-4, proliferation rates dropped significantly in 0.5% oxygen for all but the 769-P cell line pairs as well as for TK10 cells. Surprisingly, RCC4 and UMRC2 cells expressing pVHL had slightly higher proliferation rates in normoxic conditions than their pVHL-lacking counterparts. Only A498 pVHL-null cells outgrew their pVHL-expressing partners. Notably, in hypoxia, the respective pairs had similar growth kinetics. The 786-O and 769-P cell line pairs showed very similar growh rates in both normoxic and hypoxic conditions (Figure 3.5A).

Decreasing the oxygen supply even further to 0.1% significantly reduced cell proliferation from day 2 onwards in all cell lines (Figure 3.5B). The respective cell line pairs showed similar growth rates, although RCC4 and 769-P pVHL-expressing cells grew faster than their pVHL-deficient partners.

In summary, ccRCC cells were relatively tolerant towards oxygen deprivation to a level of 0.5% for several days. However, levels below this oxygen concentration seemed to be stressful for the cells and resulted in ~50% growth inhibition. Furthermore, previous observations could be confirmed that showed that, despite slowing down tumour growth *in vivo*, re-expression of pVHL does not inhibit ccRCC cell proliferation *in vitro* (Chen et al., 1995, Iliopoulos et al., 1995).

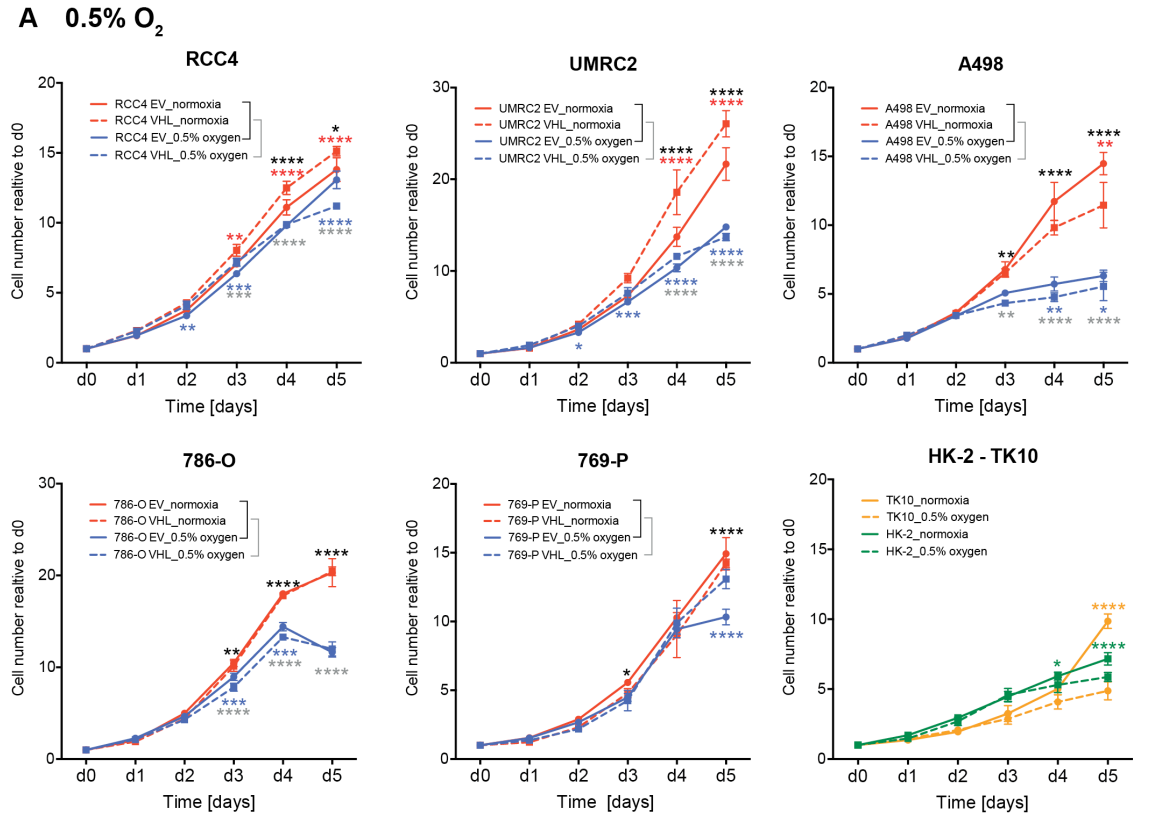
A 0.5% O2
RCC4
RCC4 EV_normoxia
RCC4 VHL_normoxia
RCC4 EV_0.5% oxygen
RCC4 VHL_0.5% oxygen
UMRC2
UMRC2 EV_normoxia
UMRC2 VHL_normoxia
UMRC2 EV_0.5% oxygen
UMRC2 VHL_0.5% oxygen
A498
A498 EV_normoxia
A498 VHL_normoxia
A498 EV_0.5% oxygen
A498 VHL_0.5% oxygen
786-O
786-O EV_normoxia
786-O VHL_normoxia
786-O EV_0.5% oxygen
786-O VHL_0.5% oxygen
769-P
769-P EV_normoxia
769-P VHL_normoxia
769-P EV_0.5% oxygen
769-P VHL_0.5% oxygen
HK-2 - TK10
TK10_normoxia
TK10_0.5% oxygen
HK-2_normoxia
HK-2_0.5% oxygen
Cell number realtive to d0
Time [days]
d0 d1 d2 d3 d4 d5

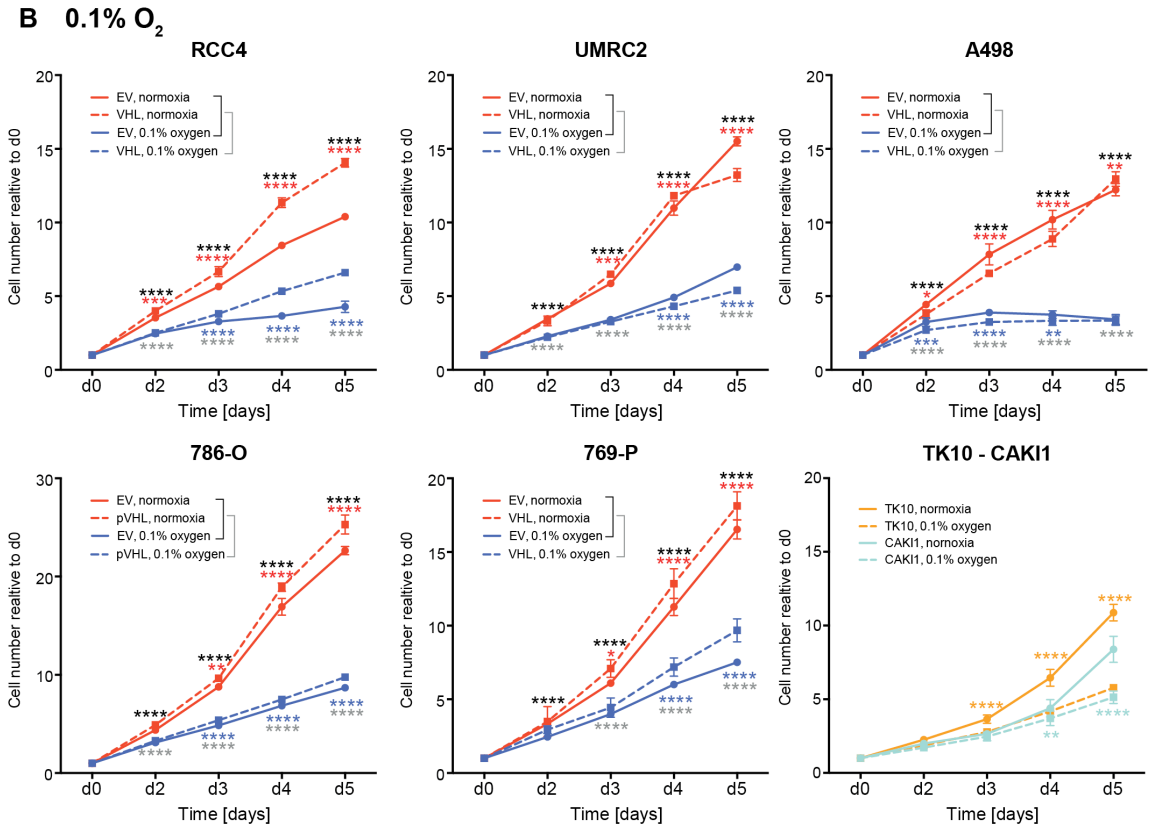
B 0.1% O2
RCC4
EV, normoxia
VHL, normoxia
EV, 0.1% oxygen
VHL, 0.1% oxygen
UMRC2
EV, normoxia
VHL, normoxia
EV, 0.1% oxygen
VHL, 0.1% oxygen
A498
EV, normoxia
VHL, normoxia
EV, 0.1% oxygen
VHL, 0.1% oxygen
786-O
EV, normoxia
pVHL, normoxia
EV, 0.1% oxygen
pVHL, 0.1% oxygen
769-P
EV, normoxia
VHL, normoxia
EV, 0.1% oxygen
VHL, 0.1% oxygen
TK10 - CAKI1
TK10, normoxia
TK10, 0.1% oxygen
CAKI1, normoxia
CAKI1, 0.1% oxygen
Cell number realtive to d0
Time [days]
d0 d2 d3 d4 d5

Figure 3.5: Proliferation rates of isogenic ccRCC cell line pairs under hypoxic conditions
The 5 isogenic cell lines as well as TK10, CAKI1 and HK-2 cells were plated in a 96-well format. The next day, one half of the cells were placed in a regular incubator, the other half was placed in a hypoxia chamber with (A) 0.5% or (B) 0.1% oxygen supply. Parallel plates of cells were fixed every 24 h over a time course of 5 days. Graphs represent average endpoint cell numbers of 4 wells (A) / 8 wells (B) ± SD. Red / blue asterisks indicate statistically significant differences in proliferation under normoxic / hypoxic conditions when pVHL expressing cells were compared to pVHL-null cells. Black / grey asterisks indicate statistically significant cell number differences in pVHL-null / pVHL-expressing cells when survival was compared in normoxia vs hypoxia (2-way ANOVA analysis with Bonferroni multiple comparison testing; *, $p \leq 0.05$; ****, $p \leq 0.001$).

3.4 Profiling of ccRCC cell lines for nutrient utilisation

3.4.1 ccRCC cells are highly glycolytic

Due to a constitutively active HIF pathway, ccRCC cells are known to be highly glycolytic. To examine how variable the different ccRCC cell lines are in this respect and if there is a HIF-α isoform-specific pattern or a difference between pVHL expressing cell lines compared to pVHL-null cells, cells were analysed for their glycolytic profile using a Metabolic Flux Analyzer (Seahorse Biosciences). This instrument measures simultaneously oxygen consumption rates (OCR) and extracellular acidification rates (ECAR) in real time, thereby providing a readout for mitochondrial respiration and cellular proton secretion. Proton secretion is likely to be an indicator of the export of lactate produced from glucose through glycolysis (Figure 3.6A). After measurement of basal ECAR, cells were subsequently treated with glucose to stimulate glycolysis, the ATP synthase inhibitor Oligomycin to determine the maximal glycolytic capacity and with 2-deoxyglucose (2-DG) to inhibit glycolysis (Figure 3.6B).

The slowest proliferating cell line of the panel, A704, showed the highest basal glycolytic rate when compared to the average basal ECAR. 786-O, UMRC3, CAKI1 and UO31 cells were significantly more glycolytic than average, while 769-P and A704 cells were significantly less glycolytic (Figure 3.6D). None of the cancer cell lines showed a glycolytic capacity or a glycolytic reserve that was above average.

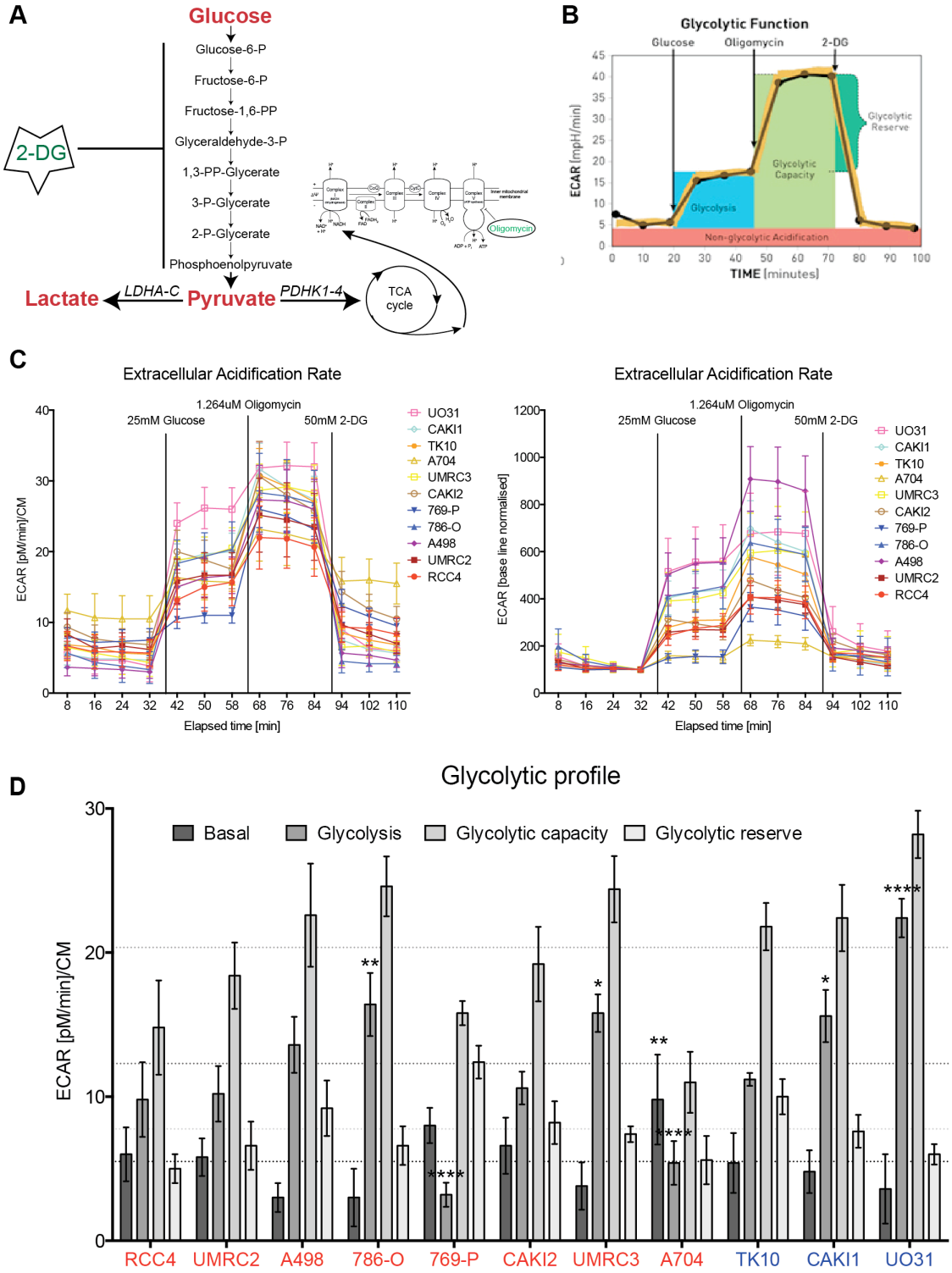

Figure 3.6: ccRCC cells are highly glycolytic

(A) Flow diagram illustrating the several intermediates that glucose (a 6-carbon unit) is subsequently converted to, ultimately resulting in pyruvate (a 3-carbon unit). Pyruvate can either be shuttled to the mitochondria to enter the TCA cycle for mitochondrial respiration, or it can be converted to lactate by lactate dehydrogenase (LDH) when oxygen levels are low (hypoxia). Lactate secretion results in extracellular acidification due to the symport of protons. (B) Schematic illustrating the ECAR profile that can be obtained when cells are sequentially treated with glucose (stimulates glycolysis), the ATP synthase inhibitor Oligomycin (to determine maximal glycolytic capacity) and 2-deoxyglucose (2-DG, an inhibitor

of glycolysis). This schematic was obtained with permission from the Seahorse Bioscience website. (C) Using a Seahorse XF^{e}96 Bioanalyzer, the extracellular acidification rate (ECAR) of the different ccRCC cells was determined. Cells were plated in a 96-well plate format the day before analysis in full growth medium. For analysis, growth medium was replaced with assay medium containing 25mM glucose, 2mM Glutamax and 10mM sodium pyruvate. Cells were placed into the instrument and basal ECAR was determined. Subsequently, glucose, Oligomycin and 2-DG were added. Graphs represent average of at least 5 wells normalised either to cell mass (CM, left hand graph) or to the last basal rate (right hand graph) ± SD. (D) Bar graph summarising, apart from average basal ECAR rates, also average glycolytic rate, maximal glycolytic capacity and the glycolytic reserve ± SD. These rates were calculated according to (B) from last rates for each treatment in (C). Asterisks indicate statistical difference of the respective rate for a given cell line compared to the general average for this rate (dotted lines in respective colour shading) (2-way ANOVA with Dunnett multiple testing analysis; * $p \leq 0.05$).

3.4.2 ccRCC cells have high respiratory capacity

The mitochondrial respiratory capacity was determined using a Seahorse Bioanalyzer. For this, upon measuring basal OCR levels, ccRCC and HK-2 cells were subsequently treated with Oligomycin and FCCP. Oligomycin inhibits ATP synthase and, in this case, serves to measure ATP-production. FCCP leads to proton leakage and disruption of the mitochondrial membrane potential along the electron transport chain (ETC) and allows measurement of the maximal cellular respiratory capacity (Figure 3.7A-B).

Surprisingly, only RCC4, UMRC2, A704 and UO31 cells showed significantly lower basal respiration compared to HK-2 cells, while all other cell lines showed comparative or even significantly higher basal respiration; 769-P and TK10 cells being an example of the latter. 769-P and TK10 cells also had the highest respiratory capacity, although all but UMRC2, UMRC3 and UO31 cells showed significantly higher respiratory capacity than HK-2 cells (Figure 3.7D). Hence, the spare respiratory capacity of HK-2 cells is very limited and apart from CAKI2, UMRC3 and UO31 much higher in the cancer cells. Interestingly, ATP production resulting from this respiratory pattern seemed to be similar in ccRCC and HK-2 cells. Only 769-P and TK10 cells displayed significantly higher and A704 cells significantly lower ATP production than HK-2 cells (Figure 3.7D).

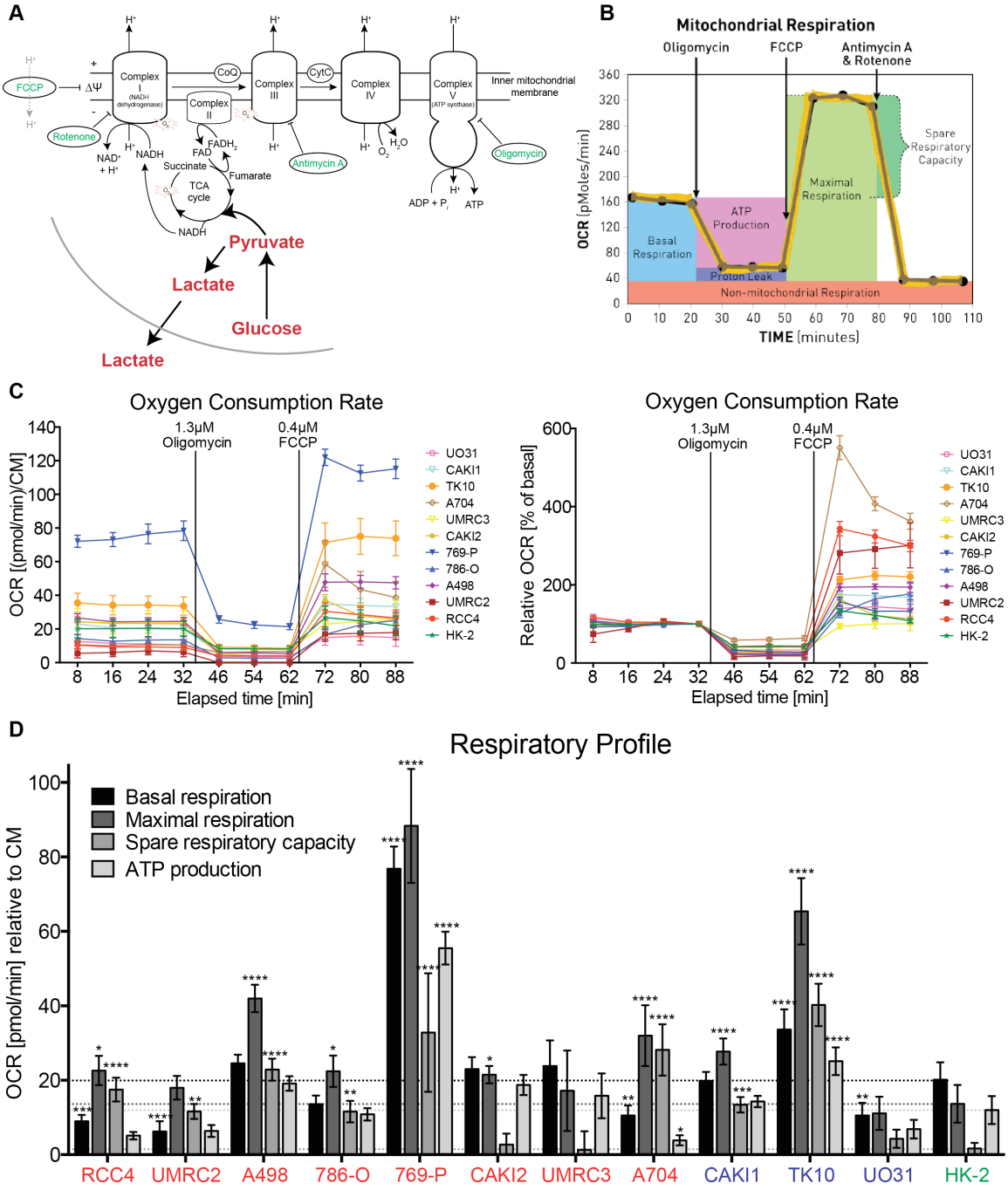

Figure 3.7: ccRCC cells have a higher respiratory capacity than HK-2 cells

(A) Schematic illustrating the different components of the mitochondrial electron transport chain (ETC). The ETC is fuelled with electrons from NADH and $FADH_2$, which are generated through subsequent oxidation of glucose-derived pyruvate in the TCA cycle. Oxygen functions as an electron acceptor within the ETC. When oxygen concentrations are low (hypoxia), pyruvate can be alternatively converted into lactate, which is secreted from the cell. (B) Schematic illustrating the oxygen consumption rate (OCR) profile that can be obtained when treating cells with the ATP synthase inhibitor Oligomycin, the uncoupler FCCP and the mitochondrial poisons Antimycin A (complex III inhibitor) and Rotenone (complex I inhibitor). This schematic was obtained with permission from the Seahorse Bioscience website. (C) Using a Seahorse XF^e96 Bioanalyzer, OCR levels of ccRCC and HK-2 cells were determined. Cells were plated the day before analysis in full growth medium. For analysis, growth medium was replaced with assay medium containing 25mM glucose, 2mM Glutamax and 10mM sodium pyruvate. After determination of basal OCR, Oligomycin and FCCP were added subsequently to the cells

and changes in OCR were recorded. Graphs summarise mean measurements ± SD of at least 5 replicate wells normalised to cell mass (CM, left hand graph) or the last basal rate (left hand graph) and are representative of at least 3 independent experiments. (D) Bar graph summarising average basal respiration, maximal and spare respiratory capacity, as well as ATP production ± SD. These were calculated according to (B) from last rates for each treatment in (C). Asterisks indicate statistical difference of the respective rate compared to HK-2 cells (dotted lines in respective colour shading) (2-way ANOVA with Dunnett multiple testing analysis; * $p \leq 0.05$).

Assessment of mitochondrial OxPhos complexes revealed that, although all ccRCC cell lines expressed similar levels of complex III and V, expression of complex I and IV was more heterogeneous (Figure 3.8). 769-P cells consistently expressed the highest levels of all complexes, potentially explaining their high OCR. RCC4 cells expressed very low levels of complexes I and IV, while CAKI2 and UMRC3 cells express relatively low levels of complex IV (Figure 3.8). pVHL-expressing cell lines, including HK-2 cells, expressed on average lower levels of complex I compared to pVHL-null cells. At the same time, pVHL cells expressed higher levels of c-MYC compared to cell lines that lost functional pVHL. TOMM20, a mitochondrial transmembrane protein transporter, was used to evaluate differences in mitochondrial mass across the cell line panel and revealed that pVHL-null cells have presumably in average more mitochondrial mass (with exception of A704 cells) than pVHL-expressing cells (Figure 3.8). Expression of TOMM20 correlated, at least to some extend, with PGC1-α protein levels, a transcriptional regulator involved in mitochondrial biogenesis (Scarpulla, 2011), while it inversely correlated with c-MYC expression (Figure 3.8), another driver of mitochondrial biogenesis (Li et al., 2005, Zhang et al., 2007, Kim et al., 2008).

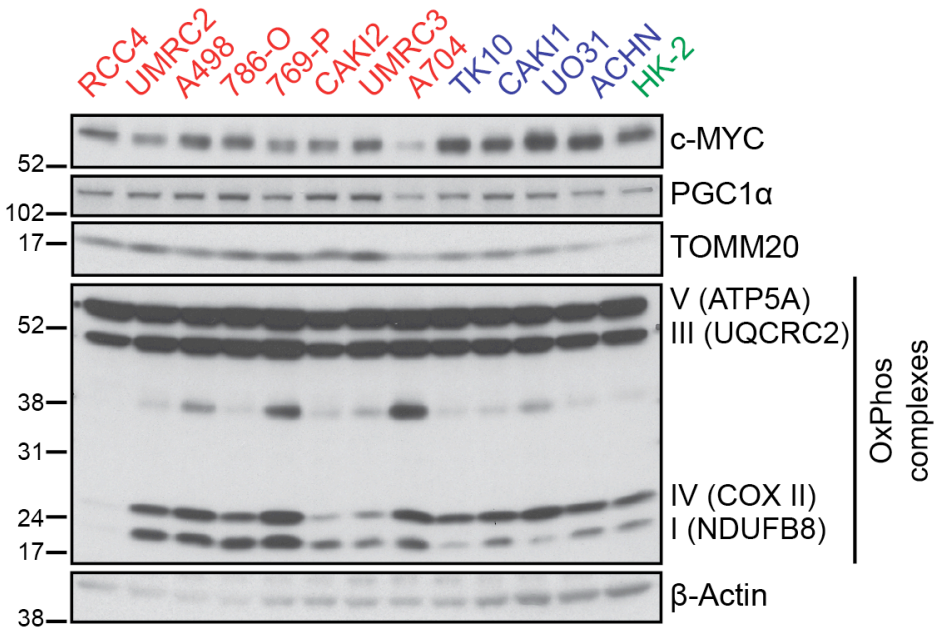

Figure 3.8: pVHL-null cells have lower c-MYC but higher PGC1α and TOMM20 protein levels

Cells were plated in a 6-well plate format and lysed 48 h later for protein extraction. Whole protein lysates were analysed for representative subunits of the different electron transport chain complexes (OxPhos) as well as for PGC1α and c-MYC, transcription factors known to drive mitochondrial biogenesis and TOMM20, an indicator for mitochondrial mass. β-Actin serves as loading control.

Next, respiration in the five isogenic cell line pairs was evaluated using the same technique. Figure 3.9A shows representative respiration profiles for the isogenic cell lines. Interestingly, only the RCC4 isogenic cell line pair showed a significant difference in basal respiration, maximal and spare respiratory capacity although the resulting ATP production seemed to be similar. All other ccRCC cell line pairs seemed to have comparative respiratory properties (Figure 3.9B).

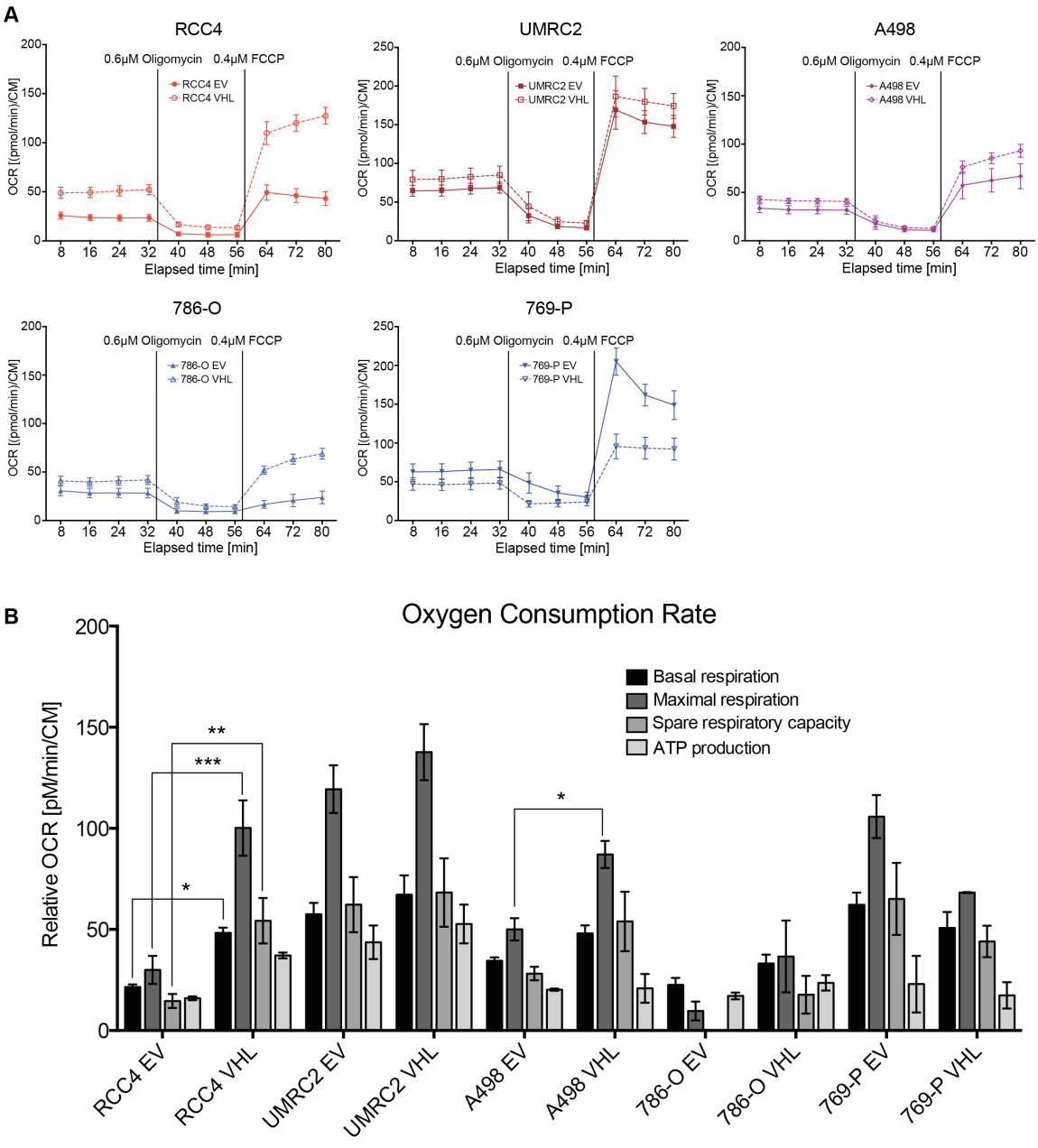

Figure 3.9: pVHL-null ccRCC cells tend to have a higher respiratory capacity than their pVHL-reconstituted counterparts

Using a Seahorse XF^{e}96 Bioanalyzer, mitochondrial respiration rates (OCR) were determined for the 5 isogenic cell lines. Cells were plated the day before analysing in full growth medium. For analysis, growth medium was replaced with assay medium containing 25 mM glucose, 2 mM Glutamax and 10 mM sodium pyruvate. Subsequently, Oligomycin and FCCP were added. (A) Representative graphs summarise average of at least 5 wells ± SD normalised to cell mass (CM). (B) Bar graph summarising average basal respiration, maximal and spare respiratory capacity, as well as ATP production ± SD. These rates were calculated from the last rates for each treatment in (A) of 3 independent experiments. Asterisks indicate statistical difference of the respective rate between the isogenic cell line pairs (2-way ANOVA with Bonferroni multiple testing analysis; * $p \leq 0.05$).

It has been proposed that HIF-1α regulates mitochondrial biogenesis in pVHL-deficient renal carcinoma cells by inhibition of c-MYC transcriptional activity (Zhang et al.,

2007). When comparing mRNA expression levels, only pVHL-expressing RCC4 and 786-O cells showed a small increase in PGC1β, TFAM and TOMM20 mRNA compared to their respective *VHL*-deficient counterpart (Figure 3.10). In contrast, UMRC2, A498 and 769-P showed no *VHL*-dependent variation in expression of these factors. These mRNA data do not unambiguously reflect what could be seen on protein levels (Figure 3.8).

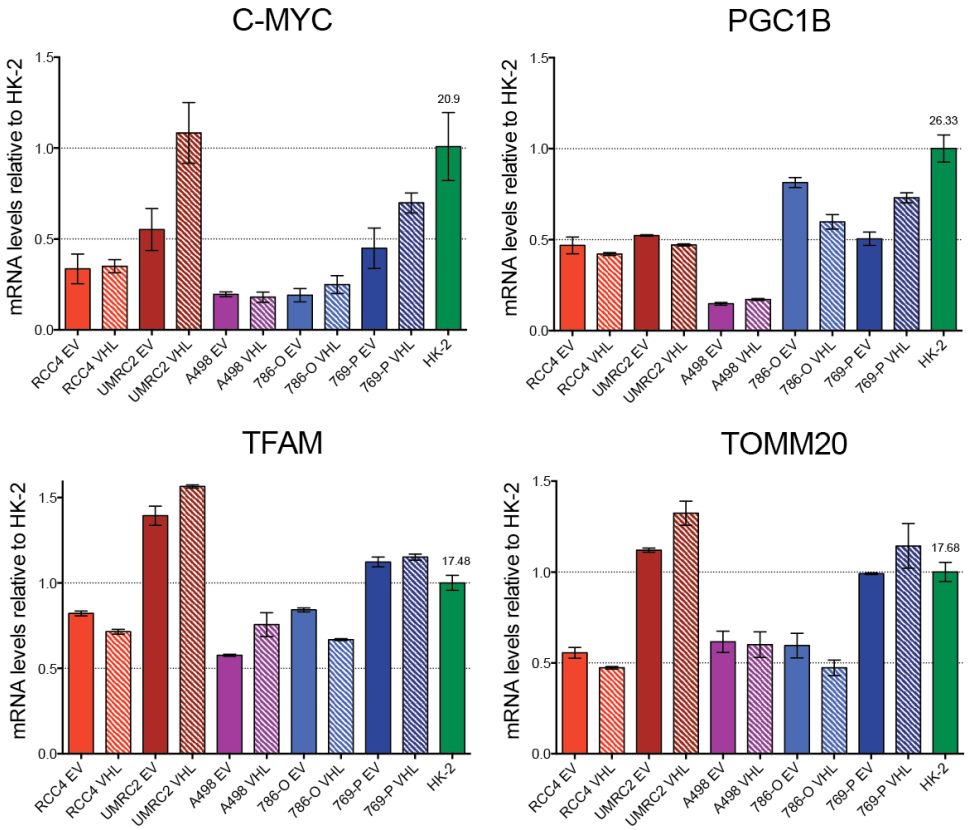

Figure 3.10: pVHL-null cells show similar mRNA levels of mitochondrial biogenesis driver
Cells were plated in a 6-well plate format and lysed 48 h later for total RNA extraction. RNA was reverse transcribed and cDNA was analysed for the abundance of c-MYC, PGC1β and TFAM, transcription factors driving mitochondrial biogenesis, and the mitochondrial amino acid transporter TOMM20 by RT-qPCR. Bars represent average of duplicate measurements normalised to ACTB and data are displayed relative to mRNA levels in HK-2 cells. Error bars indicate SD. Number above the HK-2 bar indicates average ΔC_T value for comparison.

3.4.3 ccRCC cells depend on glucose and glutamine for proliferation but not on pyruvate

Glucose is one of the main nutrients used for energy production, both via glycolysis and via mitochondrial oxidative metabolism. Pyruvate, the canonical substrate that feeds into the TCA cycle, is the end product of glycolysis. However, glutamine is another

substrate that can feed into the TCA cycle after it is converted into glutamate and subsequently α-ketoglutarate (α-KG) (Figure 3.11A). Moreover, glucose and glutamine also act as carbon sources for the synthesis of macromolecules. To delineate which of these three nutrients, glucose, pyruvate and glutamine, serves as preferred energy and carbon source in ccRCC cells, cell proliferation was monitored in an IncuCyte life cell imaging system under nutrient deprived conditions. Cells were supplied with medium lacking glucose, pyruvate or glutamine or combinations thereof. It should be noted that HK-2 cells were grown in DMEM rather than their generic growth medium KSFM. This might explain the apparent differences in growth between full medium and nutrient depleted medium (Fig. 3.11B). As can be appreciated from Figure 3.11C-G, all ccRCC cells, independent of pVHL expression, were severely sensitive to glucose withdrawal. Moreover, deprivation of glutamine caused an even more dramatic reduction in proliferation. In contrast, lack of pyruvate did hardly affect any of the ccRCC cell lines. Another interesting observation was the fact that, in the nutrient deprived situation, all cell lines displayed an initial growth burst over the first 24-48 h, even exceeding the proliferation rate of cells grown in full medium. This could be an overcompensation effect, potentially mediated by the induction of autophagy, which might be initially beneficial but is detrimental in the long run because cell intrinsic resources get depleted.

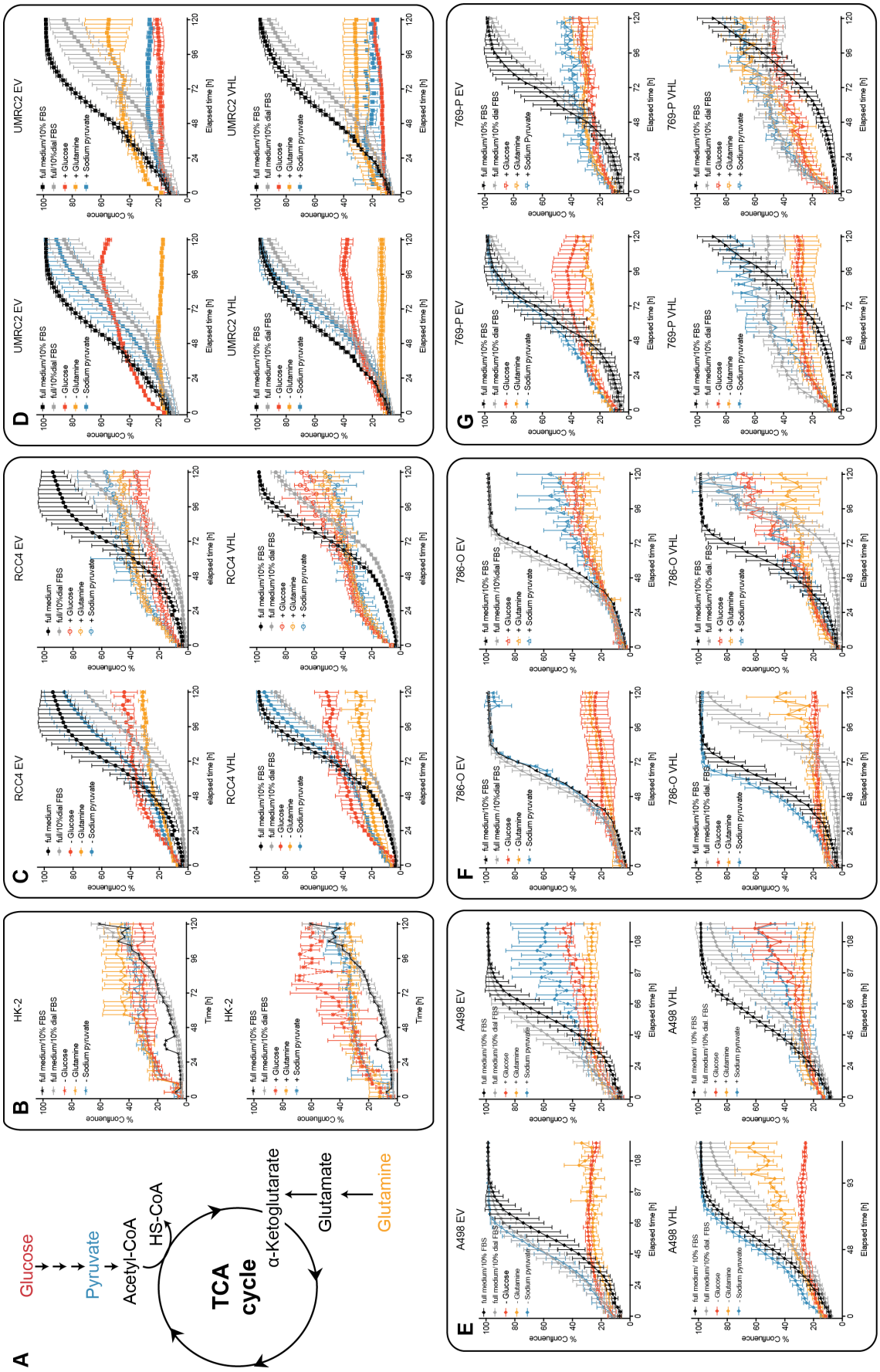
A
Glucose
Pyruvate
Acetyl-CoA
HS-CoA
TCA cycle
α-Ketoglutarate
Glutamate
Glutamine
B
HK-2
C
RCC4 EV
RCC4 VHL
D
UMRC2 EV
UMRC2 VHL
E
A498 EV
A498 VHL
F
786-O EV
786-O VHL
G
769-P EV
769-P VHL
% Confluence
Elapsed time [h]
Time [h]

Figure 3.11: ccRCC cells are dependent on glucose and glutamine for proliferation but not pyruvate

(A) Schematic depicting the main nutrients, glucose and glutamine (and the intermediate pyruvate) for energy production via glycolysis, mitochondrial respiration or glutaminolysis, respectively. (B-G) 2000 cells/well of the 5 isogenic ccRCC cell lines and HK-2 cells were plated in standard culture medium in a 96-well format. The next day, cells were transferred into medium containing 10 % dialysed FBS and either glucose, glutamine or sodium pyruvate (respective right hand panel) or a combination of glutamine and sodium pyruvate ('- glucose' condition), glucose and sodium pyruvate ('- glutamine' condition) or glutamine and glucose ('- sodium pyruvate' condition) (respective left hand panels). Plates were placed in an IncuCyte live cell imager and monitored for proliferation every 3 h for 5 days. Graphs represent average confluence measurement of 3 wells ± SD for each time point recorded.

3.5 Profiling of ccRCC cell lines for growth factor dependencies

3.5.1 Serum starvation has a stronger anti-proliferative effect on pVHL-expressing ccRCC cells with lost HIF-1α

Seen that ccRCC cells are heavily dependent on glucose and glutamine supply, it was considered whether they are also dependent on constant growth factor supply and whether presence or absence of functional pVHL affect growth factor dependency. To examine this, the isogenic cell line pairs together with HK-2 cells were monitored in an IncuCyte life cell imaging system for growth kinetics in growth medium containing 1% or 10% FCS. The growth curves depicted in Figure 3.12 show that only in the RCC4 and 769-P isogenic cell line pairs, cells expressing pVHL were growth inhibited compared to their matched EV cell line. Moreover, while proliferation of 786-O EV, UMRC2 and A498 EV cells was not affected by serum deprivation, both RCC4 cell lines, 769-P EV and HK-2 cells exhibited a strong reduction in their proliferation rate when serum starved (Figure 3.12).

Interestingly, RCC4 and UMRC2 cells, which both express HIF-1α and HIF-2α, did not show significant difference in serum dependency between cells lacking functional pVHL and those in which the protein had been re-expressed. In contrast, in the 786-O and 769-P isogenic cell line pairs, both expressing only the HIF-2α isoform, slow down of proliferation upon serum starvation occured in a pVHL-dependent manner (Figure 3.12). This suggests that these cells require serum-derived growth factors when HIF-2α is inhibited by the re-expression of pVHL.

Of note: HK-2 cells are normally maintained in serum-free keratinocyte medium supplemented with recombinant EGF and bovine pituitary gland extract. For this analysis, HK-2 cells were transferred into DMEM supplemented with 10% or 1% FCS.

The observation that ccRCC cell lines were on the whole only inhibited in their proliferation over the 5 day time course but did not significantly arrest and die, suggests that they can sustain an efficient autocrine signalling system for self-preservation.

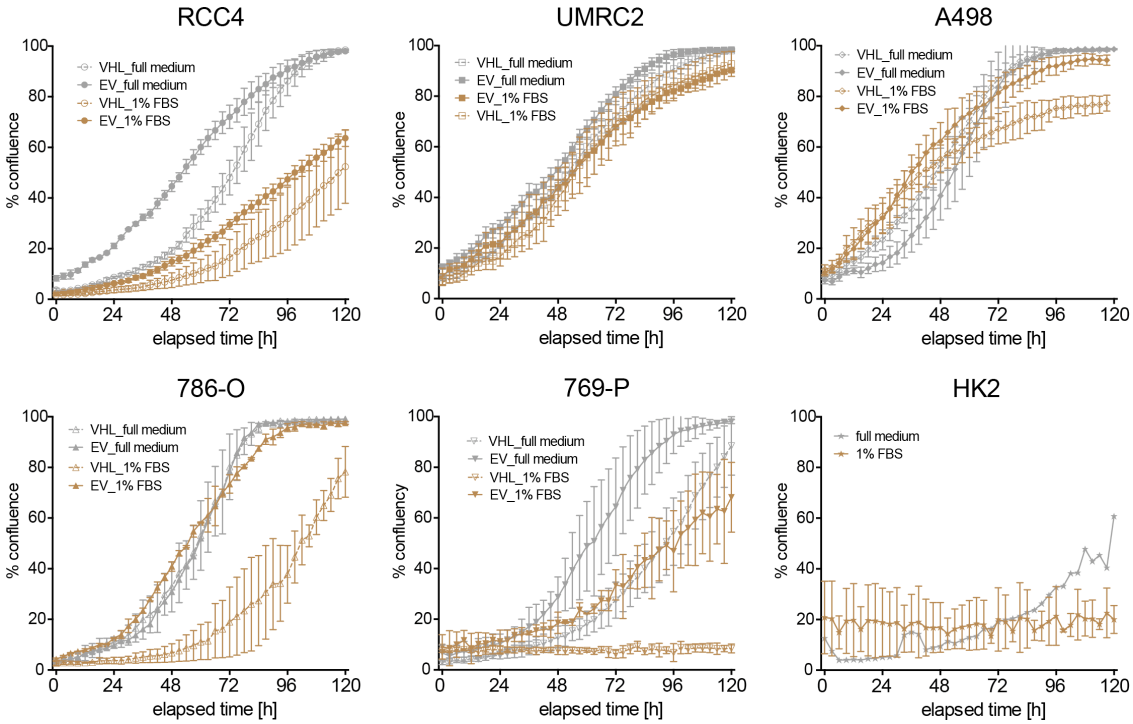

Figure 3.12: pVHL-expressing ccRCC cells with lost HIF-1α expression are more sensitive to serum withdrawal than their counterparts

2000 cells/well of the 5 isogenic cell lines and HK-2 cells were plated in standard culture medium in a 96-well format. The next day, the culture medium was replaced with 200 µl/well freshly prepared culture medium supplemented with either 10 % or 1 % FBS. Plates were placed in an IncuCyte life cell imaging system and monitored for proliferation every 3 h for 5 days. Graphs represent average confluence measurement of 3 wells (except for HK-2 cells, full medium one well only) ± SD for each time point recorded.

3.5.2 ccRCC cells show heterogeneous basal PI3K/AKT and MAPK protein expression and activation patterns

Most cancer cells have deregulated growth factor signalling leading to uninhibited cell growth and proliferation. To assess whether the observed growth inhibition upon serum starvation is due to differential growth factor signalling, ccRCC cell lines were analysed for expression of components of the PI3K/AKT and MAP kinase pathway. Only the RCC4 and 769-P isogenic cell line pairs showed a difference in AKT, mTOR and S6 protein expression or phosphorylation. While pVHL seemed to repress AKT/mTOR/S6 pathway activity in RCC4 cells, this pathway was inhibited in 769-P cells by the absence of pVHL (Figure 3.13B). Furthermore, 786-O cells do not express PTEN and, hence, showed strong AKT activation (Figure 3.13B). Also, it seems as if phospho-GSK3α is generally higher in pVHL-expressing cells (Figure 3.13B).

Comparison of AKT and MAPK pathway activity amongst all ccRCC cell lines revealed that despite normal PTEN expression, A498 and the non–tumourigenic HK-2 cells closely followed 786-O cells in their levels of AKT phosphorylation (Figure 3.13C). Furthermore, although all ccRCC and HK-2 cells showed similar amounts of ERK2 expression and activation, levels of (phospho-)ERK1 were heterogeneous: 786-O, 769-P and CAKI1 cells showed low levels of phospho-ERK1, while they were above average in A498, CAKI2 and UO31 cells (Figure 3.13C).

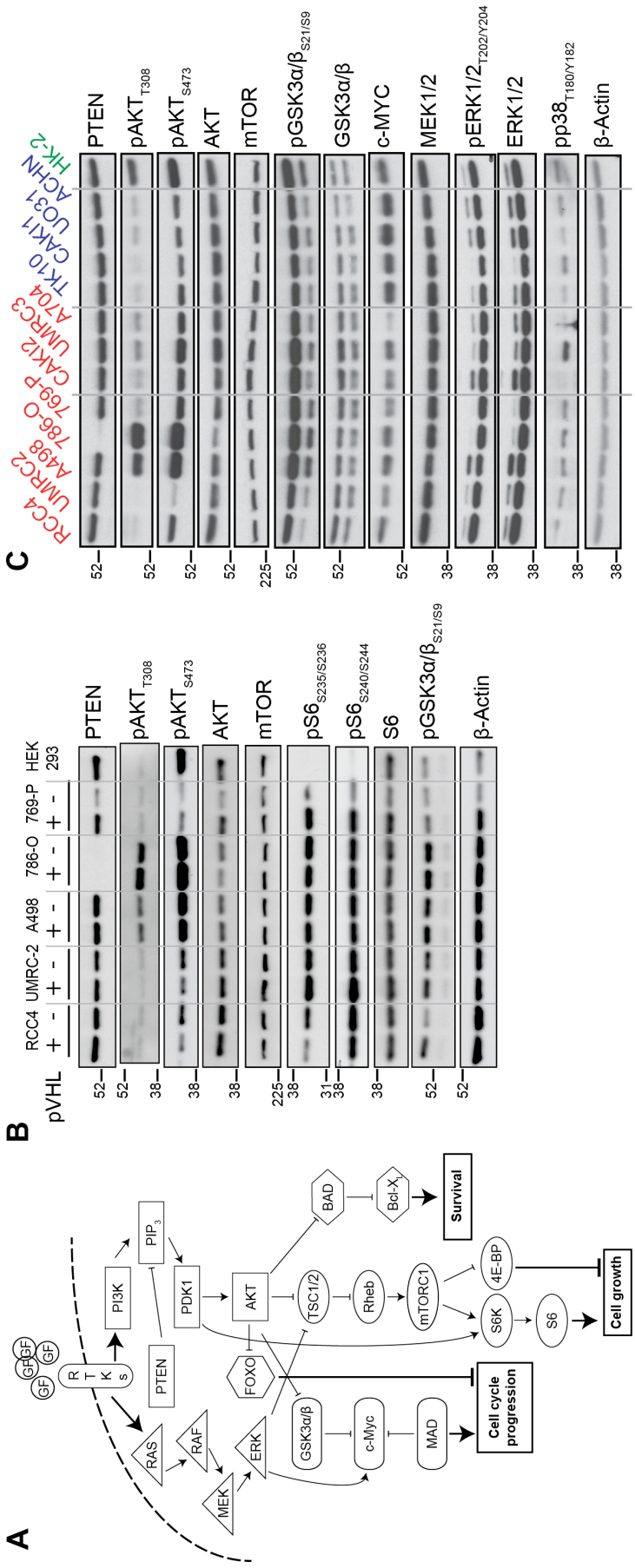
A
RTKs
GF
GRGF
PI3K
PIP3
PDK1
PTEN
AKT
RAS
RAF
MEK
ERK
FOXO
GSK3α/β
c-Myc
MAD
TSC1/2
Rheb
mTORC1
S6K
4E-BP
S6
BAD
Bcl-XL
Survival
Cell cycle progression
Cell growth
B
pVHL
RCC4 UMRC-2 A498 786-O 769-P HEK 293
PTEN
pAKT T308
pAKT S473
AKT
mTOR
pS6 S235/S236
pS6 S240/S244
S6
pGSK3α/β S21/S9
β-Actin
C
RCC4 UMRC2 A498 786-O 769-P UMRC3 A704 TK10 CAKI1 UO31 ACHN HK-2
PTEN
pAKT T308
pAKT S473
AKT
mTOR
pGSK3α/β S21/S9
GSK3α/β
c-MYC
MEK1/2
pERK1/2 T202/Y204
ERK1/2
pp38 T180/Y182
β-Actin

Figure 3.13: ccRCC cells only show minor pVHL-dependent differences in the activation state of signalling pathways but show substantial cell line heterogeneity

(A) Schematic of receptor tyrosine kinase (RTK) downstream signalling to promote cell growth, proliferation and survival. The PI3K/AKT cascade leads to cell cycle progression via inhibition of GSK3 resulting in the stabilisation and activation of c-MYC. Activation of the mTOR pathway by AKT induces protein translation, ribosomal biogenesis and cell growth, while inhibition of pro-apoptotic BCL2 proteins promotes cell survival. RTKs also activate the ERK/MAP kinase cascade via RAS to stimulate cell growth and proliferation via positively regulating the mTOR pathway and c-MYC respectively. (B) The 5 isogenic cell lines and HEK293 were analysed for the indicated proteins and phospho-sites to examine basal protein expression and phosphorylation status. β-Actin serves as loading control. (C) The parental ccRCC cell lines and HK-2 cells were analysed for the indicated proteins and phospho-sites to examine basal protein expression and activation status. β-Actin serves as loading control. pVHL-expressing cell lines are marked in blue while *VHL* deficient cell lines are marked in red.

3.6 Profiling ccRCC cell lines for lipid utilisation

3.6.1 ccRCC cells only partially rely on exogenous lipid supply

Despite growth factors, serum also contains the lipid fraction cells can source from if needed. To distinguish whether growth inhibition upon serum starvation is due to limiting growth factors or if it is rather caused by a limitation in lipid supply, ccRCC and HK-2 cells were monitored for 5 days for their proliferation rates in an IncuCyte live imaging system in growth medium containing lipid depleted serum (LDS). As can be seen from Figure 3.14, the respective cell line pairs have distinct growth patterns. What all of them but UMRC2 cells have in common, though, is the initial growth spurt within the first 24-48 h in which cells in LDS outgrew cells in conventional FCS that was also observed when cells were glucose or glutamine starved. In 786-O and 769-P cells (both express only HIF-2α) lacking pVHL this growth spurt seemed to be even more extreme than in pVHL-reconstituted cells. The RCC4, UMRC2 and 769-P isogenic pairs shared a similar pattern in that cells lacking pVHL expression, after the initial growth spurt, adapted the same growth rate in LDS as pVHL-null cells had in conventional FCS; the respective pVHL-null cells reduced their growth rate by ~50%. UMRC2 cells do not seem to be limited in their proliferation by lack of external lipid and lipoprotein supply independent of their pVHL status and neither do A498 pVHL-null cells. A498 pVHL-expressing cells proliferated even faster in lipid deficient serum as compared to full serum. Both 786-O cell lines had inhibited growth rates without external lipid supply, whereby pVHL-expressing cells were more impaired than pVHL-

null cells. Interestingly, HK-2 cells seemed to have a growth advantage in lipid-deprived medium as they proliferated almost twice as fast as cells in full serum.

Taken together, it seems as if RCC4, 786-O and 769-P cells rely to some extent on extrinsic lipid supply as they grew slower under lipid-starved conditions, while UMRC2 cells are lipid self-sufficient. Contrary, A498 and HK-2 cells prefered a lipid-free environment for enhanced growth. Furthermore, all cells showed an initial growth burst over the first 24-48 h independent of pVHL expression.

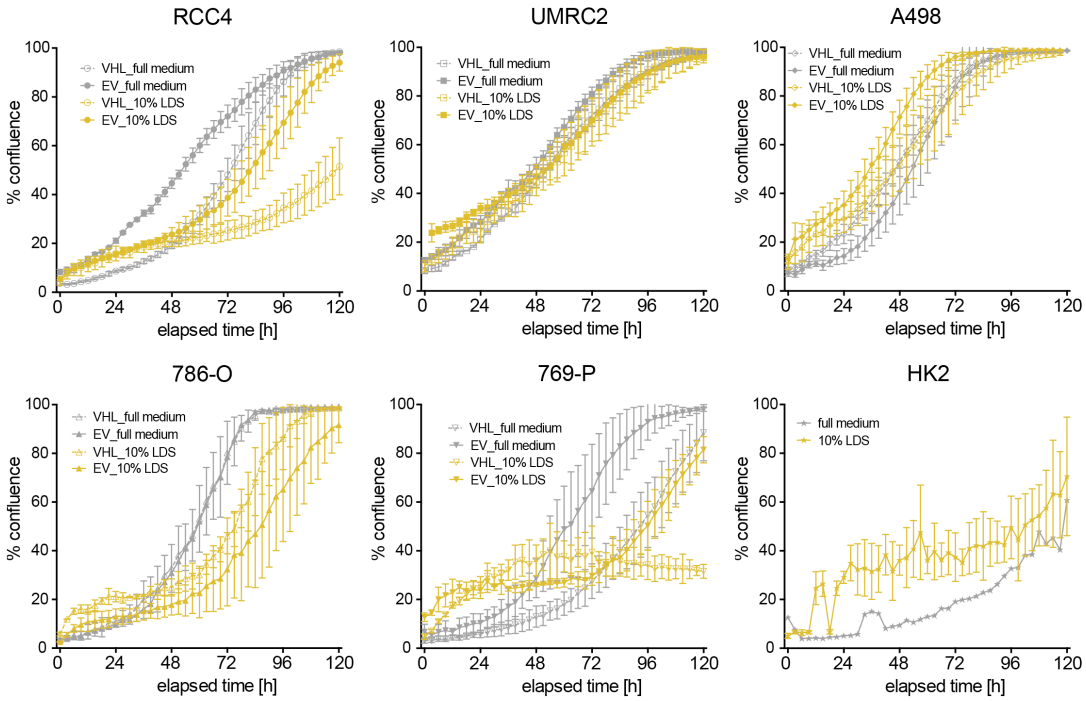

Figure 3.14: ccRCC cells are partially dependent on external lipid supply
2000 cells/well of the 5 isogenic cell lines and HK-2 cells were plated in standard culture medium in a 96-well format. The next day, the culture medium was replaced with 200 µl/well freshly prepared full growth medium containing either 10 % regular FCS or 10 % lipid depleted FCS (LDS). Plates were placed in an IncuCyte live cell imaging system and monitored for proliferation every 3 h for 5 days. Graphs represent average confluence measurement of 3 wells (except for HK-2 cells, full medium one well only) ± SD for each time point recorded.

3.6.2 Expression of *de novo* lipid synthesis enzymes negatively correlate with the proliferation pattern seen under lipid deprived conditions

In lipid depleted growth medium, RCC4, A498 and 769-P cells lacking pVHL had higher proliferation rates than their pVHL-expressing counterparts. Contrary, 786-O pVHL-expressing cells showed more proliferation than their pVHL deficient partners in these conditions. Cancer cells have been shown to reactivate *de novo* lipid synthesis even in the presence of ample exogenous lipid supply and present increased expression

of enzymes involved in lipid synthesis such as ATP citrate lyase (ACLY), acetyl-coA carboxylase (ACC) and fatty acid synthase (FASN) (Medes et al., 1953, Menendez and Lupu, 2007, Yahagi et al., 2005, Yoon et al., 2007). To see if there is any correlation between tolerance towards limited lipid supply and intrinsic *de novo* lipid synthesis, ccRCC cells were examined for their basal lipid synthesis enzyme expression. Moreover, expression of SREBP1 and SREBP2 were also established. SREBPs are important for cellular lipid homeostasis. There are two SREBP isoforms, SREBP1 and SREBP2. While SREBP1 mainly regulates genes involved in *de novo* fatty acid synthesis, SREBP2 regulates genes involved in cholesterol biosynthesis (Brown and Goldstein, 1997) (Figure 3.15A).

What can be taken from Figure 3.15B is that tolerance towards limiting lipid concentration seems to correlate with expression of *de novo* lipid biosynthesis enzymes. UMRC2 cells showed high levels of SREBP1, SREBP2, ACC and FASN expression, while A498 cells displayed high levels of ACLY phosphorylation, which increases the activity of this enzyme. Although expression of lipid biosynthesis enzymes does not directly translate into lipid synthesis rates, this observation suggests that cells with higher basal rate of *de novo* lipid synthesis could be protected from variations in extrinsic variations in lipid supply. There was also some *VHL*-dependent regulation. SREBP1 protein levels as well as downstream targets ACC, FASN and ACLY were higher in UMRC2, A498 and 769-P cells expressing pVHL compared to their pVHL-deficient counterparts (Figure 3.15B). However, this did not correlate with the sensitivity of the cells towards lipid deprivation. No obvious pVHL-dependent difference could be seen on mRNA level for the desaturase SCD, although levels were slightly lower in the ccRCC cells compared to the HK-2 cells; UMRC2 cells form an exception (Figure 3.15C).

The parental cell lines showed similar expression patterns as the isogenic cell lines. ccRCC cell lines that maintain functional pVHL expression displayed on average higher levels of FASN and ACLY but also higher phospho-ACC than pVHL-deficient ccRCC cell lines (Figure 3.15D). Interestingly, HK-2 cells, which showed enhanced proliferation in delipidated growth medium, expressed comparatively low basal levels of SREBP1 but relatively high levels of PPARγ, FASN and ACC protein when cultured in standard growth medium (Figure 3.15D).

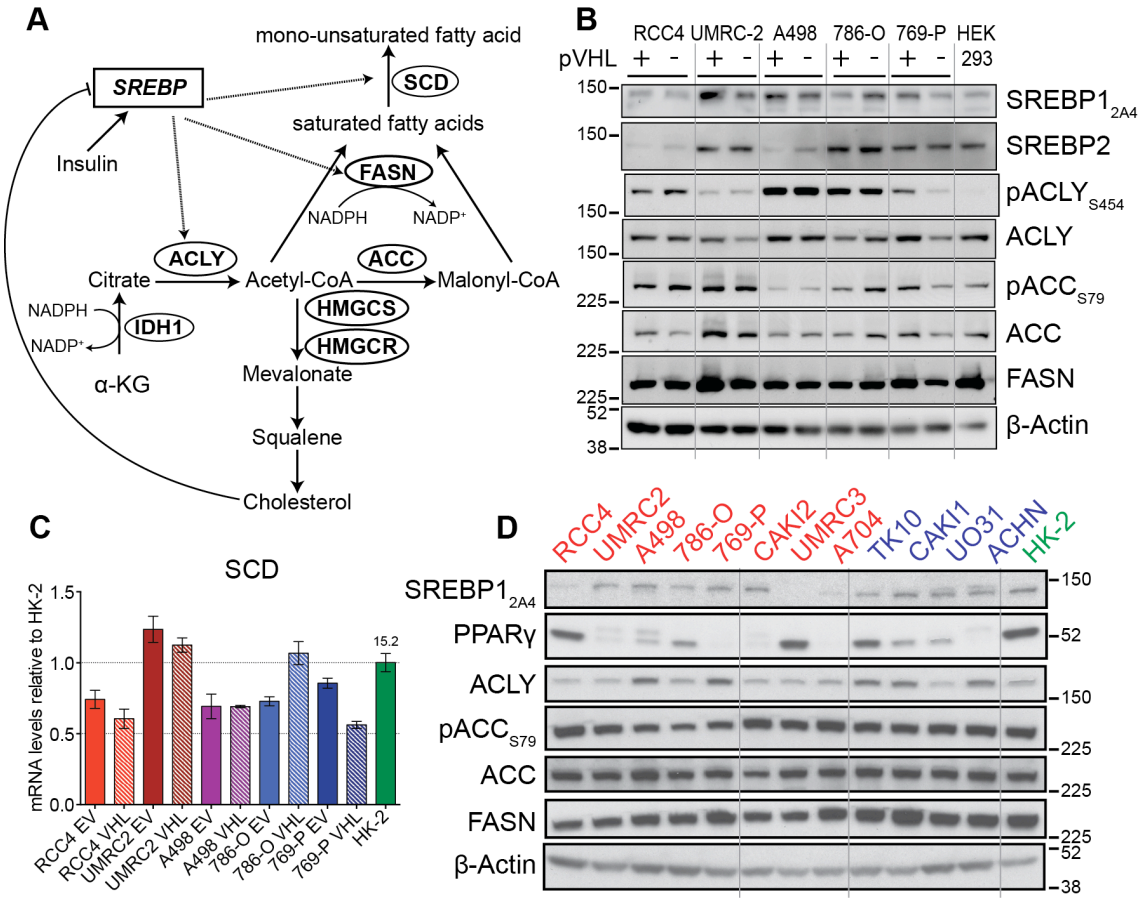

Figure 3.15: Expression of fatty acid biosynthesis enzymes in ccRCC cell lines

(A) Schematic of fatty acid and cholesterol biosynthesis: An acetyl-group is split from citrate and is conjungated to CoA by ATP citrate lyase (ACLY) and can then be used for fatty acid or cholesterol biosynthesis. Conversion of acetyl-CoA to malonyl-CoA by acetyl-CoA carboxylase (ACC) produces the substrate for fatty acid synthase (FASN), which condenses acetyl-CoA and malonyl-CoA to form the growing acyl-chain. Steroyl-CoA desaturase (SCD) introduces a double carbon bond in saturated fatty acids to generate mono-unsaturated fatty acids. Transcription factors of the sterol element binding protein family (SREBPs) are the main transcriptional regulators of *de novo* lipid biosynthesis. (B) The 5 isogenic cell lines and HEK293 cells were plated in standard culture medium and whole cell lysates were analysed for the indicated proteins and phospho-sites to assess protein expression and activity levels. β-actin serves as loading control. (C) The 5 isogenic cell lines and HK-2 cells were plated in standard culture medium. Total mRNA was reverse transcribed and generated cDNA was analysed for mRNA abundance for SCD via RT-qPCR. Bar graphs represent average of 2 replicate measurements normalised to ACTB ± SD and data are displayed relative to HK-2 mRNA levels. Number above HK-2 bar represents average ΔC_T value for comparison. (D) The parental ccRCC and HK-2 cells were plated in standard culture medium and whole cell lysates were analysed for the indicated proteins and phospho-sites to assess protein expression and activity levels. β-actin serves as loading control.

3.6.3 Isogenic ccRCC cells are sensitive to Bezafibrate treatment in a pVHL-specific manner

Having seen that ccRCC cells show varying sensitivity to lipid withdrawal, it was considered whether treatment with the peroxisome proliferator-activated receptor α (PPARα) agonist Bezafibrate would also modulate this effect. The transcription factor

PPARα is activated when cellular/organismal energy levels drop, e.g. under prolonged starvation. PPARα positively regulates genes involved in fatty acid transport, binding and activation as well as genes involved in peroxisomal and mitochondrial β-oxidation and ketogenesis (Buzzai et al., 2005).

Under full serum conditions, there was a tendency of cells expressing pVHL and both HIF-α isoforms (RCC4, UMRC2 and A498 to some extend) to show higher sensitivity towards Bezafibrate treatment than their pVHL-deficient counter parts. However, the reverse was observed for cell lines expressing only the HIF-2α isoform (especially 769-P). HK-2 cells were tolerant towards all drug concentrations tested (Figure 3.16A).

Under lipid-depleted conditions, all cells were dramatically more sensitive towards Bezafibrate treatment, with HK-2 and UMRC2 pVHL-expressing cells showing the highest sensitivity (Figure 3.16B), suggesting PPARα hyperactivity causing more problems than it solves in ccRCC cells, but especially in the non-tumourigenic HK-2 cells, under lipid deprivation.

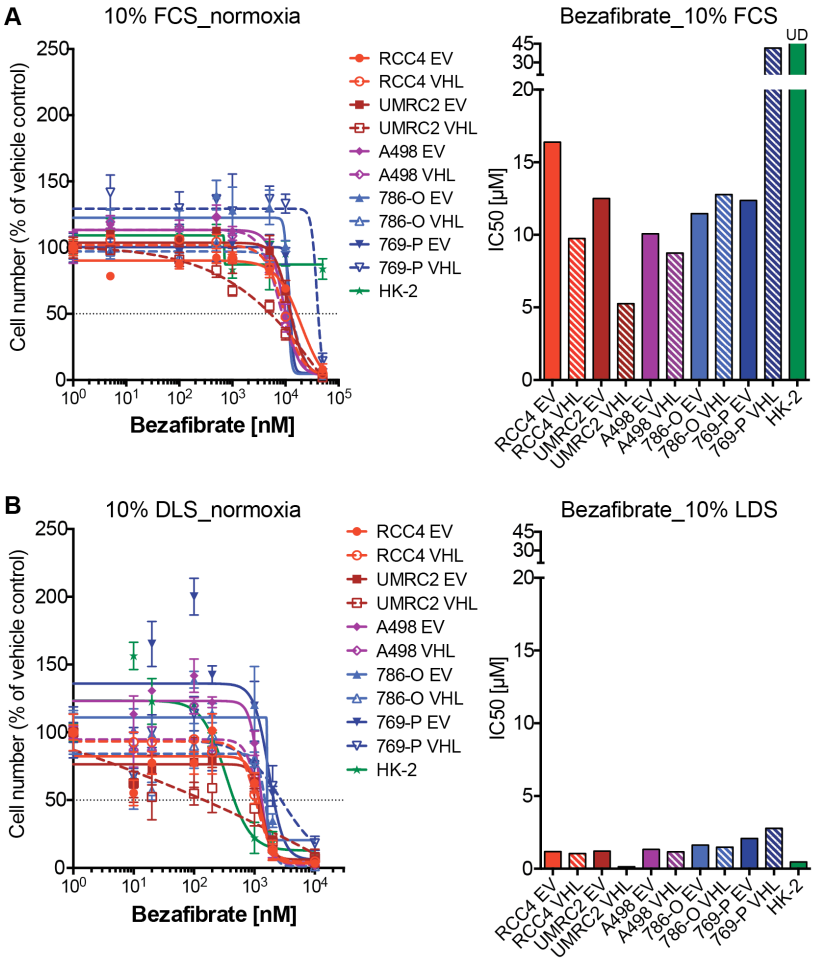

C

R^2	10% FBS	10% DLS
RCC4 EV	0.9429	0.8093
RCC4 VHL	0.9771	0.961
UMRC2 EV	0.9392	0.8526
UMRC2 VHL	0.9794	0.7373
A498 EV	0.9651	0.9408
A498 VHL	0.959	0.8961
786-O EV	0.8845	0.8561
786-O VHL	0.9824	0.7744
769-P EV	0.9506	0.6608
769-P VHL	0.8396	0.7021
HK-2	0.5808	0.9129

Figure 3.16: Dose response of the PPARα agonist Bezafibrate under full serum or lipid-depleted conditions

2000 cells/well of the 5 isogenic cell lines and HK-2 cells were plated in standard culture medium in a 96-well format. The next day, cells were transferred into medium supplemented with either (A) 10% regular FCS or (B) 10% lipid depleted FCS (LDS) and the indicated concentrations of Bezafibrate and incubated for 72 h. Dose response curves (left-hand panel) were modelled in Graphpad Prism 6 to measured endpoint cell numbers (average values obtained from 3 different wells ± SD). Bar graphs (center panel) represent Bezafibrate IC50 values extracted from dose-response curves. (C) Table summarising R^2 values of goodness-of-fit for the modelled dose-response curve to the collected data points.

3.6.4 Isogenic cells differ in their levels of lipid droplet content

ccRCC obtained its name from the observation that ccRCC cells appear clear under the microscope due to deposition of glycogen, phospholipids and neutral lipids, particularly cholesterol esters, in the cytoplasm (Gebhard et al., 1987). To investigate if reintroduction of functional pVHL affects the accumulation of lipid droplets, isogenic ccRCC cell lines were analysed for intracellular lipid droplets (LDs). The most obvious observation was that UMRC2 and A498 cells had the highest cellular LD density, whereby 769-P and CAKI1 cells had the lowest. Furthermore, all isogenic cell line pairs but 769-P cells also displayed differential LD accumulation. However, while in RCC4 and 769-P cells the LD density was higher in the pVHL-null cells, in the UMRC2 and A498 pairs it was higher in the pVHL-expressing cells (Figure 3.17B top graph). Compared to their counterparts, RCC4 and 769-P pVHL-null cells did not only have less but also smaller LDs, while UMRC2 pVHL-expressing cells had larger LDs. In A498 and 769-P cells, LDs were similar in size independent of pVHL-status (Figure 3.17B center and bottom graph).

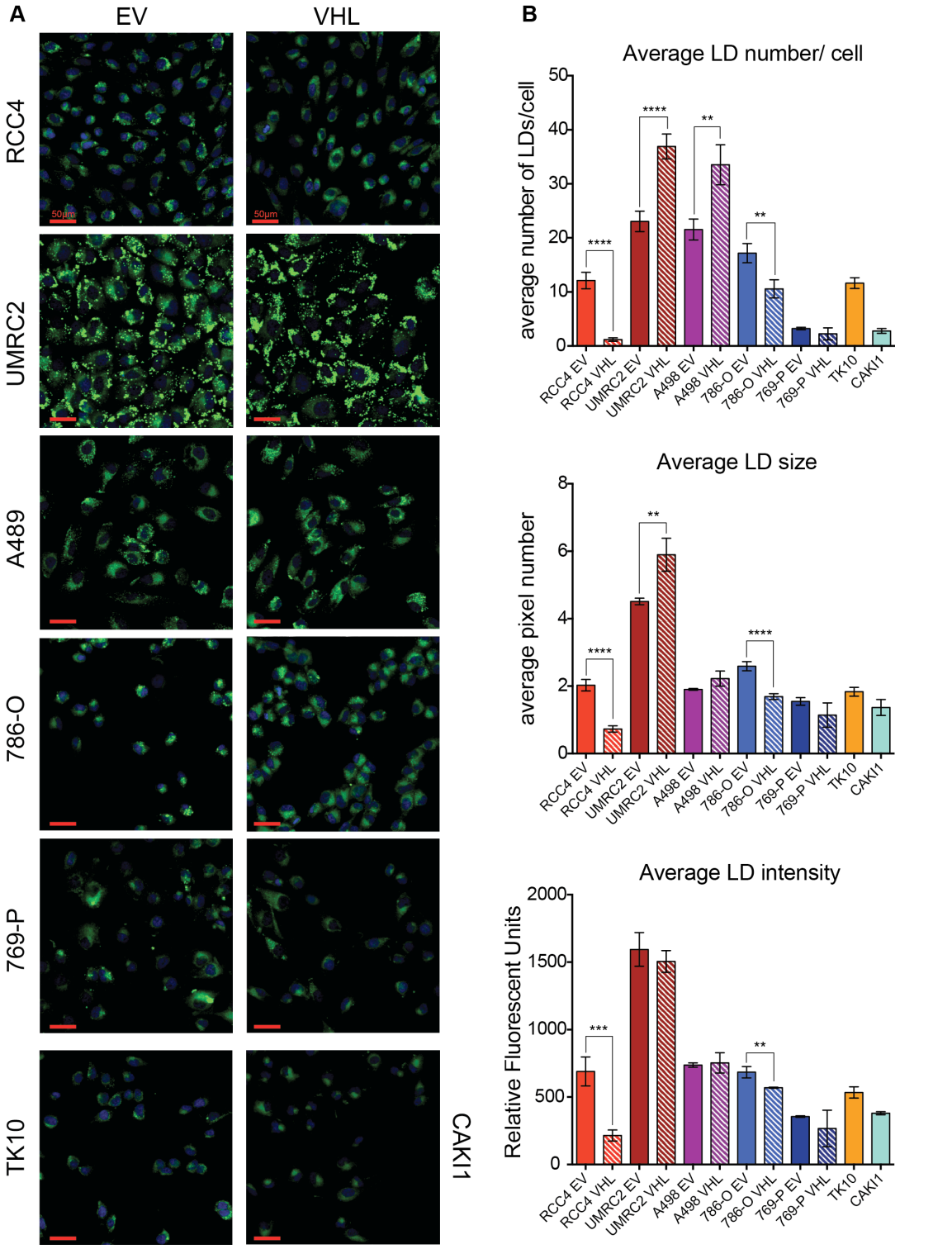

Figure 3.17: Isogenic ccRCC pairs differ in their cytoplasmic lipid droplet accumulation

The five isogenic cell lines were analysed for basal lipid droplet properties under standard growth conditions. (A) Representative images of ccRCC isogenic, TK10 and CAKI1 cells, grown in standard culture medium in a 96-well format, stained for lipid droplets (LDs) with the lipophilic dye Nile Red (green pseudo colour) and chromatin with DAPI (blue pseudo colour). Scale bar, 50 µm. (B) Quantification of LD number, size and intensity per cell. Bar graphs represent average of at least duplicate wells ± SD. Asterisks indicate statistical difference of LD number, size and intensity in the isogenic ccRCC pairs (multiple t-test, Holm-Sidak method, *, $p \leq 0.05$).

3.6.5 Palmitate addition lowers ECAR, which can be restored by Etomoxir treatment

As was shown before, both nutrient starvation as well as lipid depletion resulted in an initial growth spurt of the ccRCC cells. One explanation would be, that due to the large amount of stored lipids, ccRCC cells could mobilise these lipid stores for energy generation via β-oxidation. β-oxidation takes place in the mitochondria or peroxisomes and is a gradual breakdown of fatty acids (FAs) to yield acetyl-CoA, which serves as substrate for the TCA cycle and subsequent ATP generation via oxidative phosphorylation. Cellular FAs first need to be activated by carnitine palmitoyl-transferase 1 (CPT1), which attaches a carnitine moiety that is needed for the shuttling of acetyl-chains to the mitochondria. Once in the mitochondria, CPT2 removes the carnitine moiety and releases the FA to the β-oxidation cascade (Figure 3.18A).

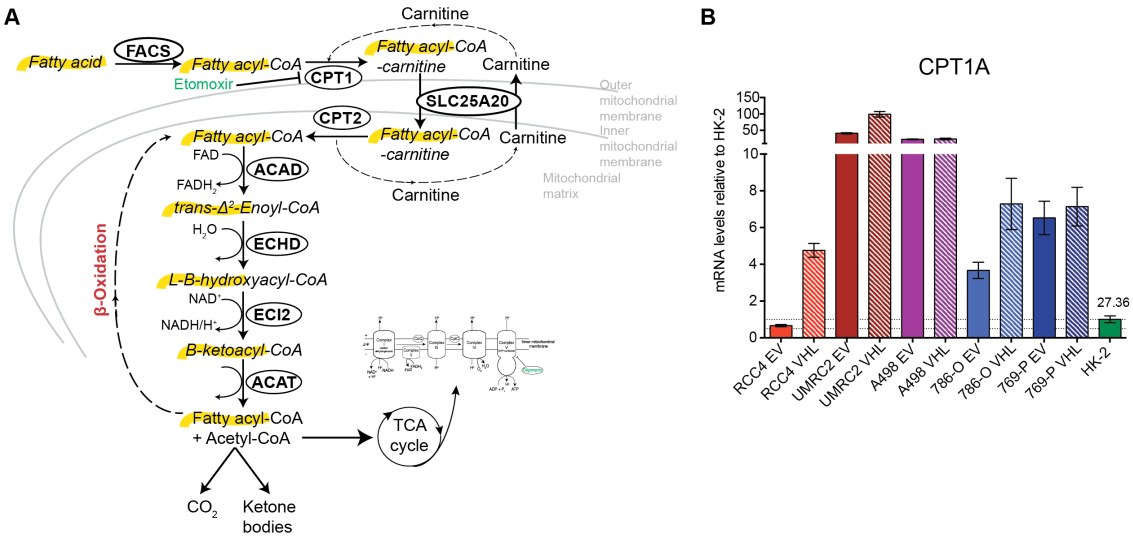

Figure 3.18: ccRCC cells express much higher CPT1A mRNA levels than HK-2 cells
(A) Schematic illustrating β-oxidation initiation via carnitine-coupled shuttling of fatty acids into the mitochondrial matrix and the subsequent catabolic degradation cascade. (B) The 5 isogenic cell lines and HK-2 cells were plated in standard culture medium. Total mRNA was reverse transcribed and generated cDNA was analysed for mRNA abundance for CPT1A via RT-qPCR. Bar graph represents average of 2 replicate measurements normalised to ACTB ± SD and data are displayed relative to HK-2 mRNA levels. Number above HK-2 bar represents average ΔC_T value for comparison.

In ccRCC cells, CPT1A mRNA levels are highly upregulated compared to HK-2 cells. Furthermore, at least in RCC4, UMRC2 and 786-O pVHL-expressing cells, expression of CPT1A mRNA was almost twice as high as in their pVHL-null counterparts (Figure 3.18B), indicating increased β-oxidation activity with pVHL expression in these cells.

To verify this initial observation, in an initial experiment, the ccRCC isogenic cell lines were assessed for their capacity to use lipids as fuel source using a Seahorse Bioscience Analyzer. OCR and ECAR were measured upon injection of palmitate to stimulate β-oxidation followed by treatment with Etomoxir, an inhibitor of CPT1 and thereby β-oxidation. Surprisingly, no increase in OCR upon injection of palmitate could be observed in any of the isogenic ccRCC cells (Figure 3.19A,C), but a clear decrease in ECAR rates in all but A498 and 786-O pVHL-expressing and CAKI1 cells (Figure 3.19B,C). Although addition of palmitate did not increase mitochondrial respiration, it seemed to drive conversion of pyruvate into lactate as opposed to shuttling it into the mitochondria for subsequent respiration. This phenotype was reversed upon addition of Etomoxir, which led to a significant decrease in OCR in most of the cell lines (Figure 3.19A,C) accompanied by an increase in ECAR rates in most of the cell lines to higher or lesser extent, except for the A498 isogenic cell line pair, CAKI1 and HK-2 cells (Figure 3.19B,C). The fact that palmitate did not stimulate OCR in these cells could indicate that either the amount added was too low or that these cells already have sufficient FA supply to carry out β-oxidation, possibly through utilisation of lipids stored within lipid droplets, so that a potential effect could be masked.

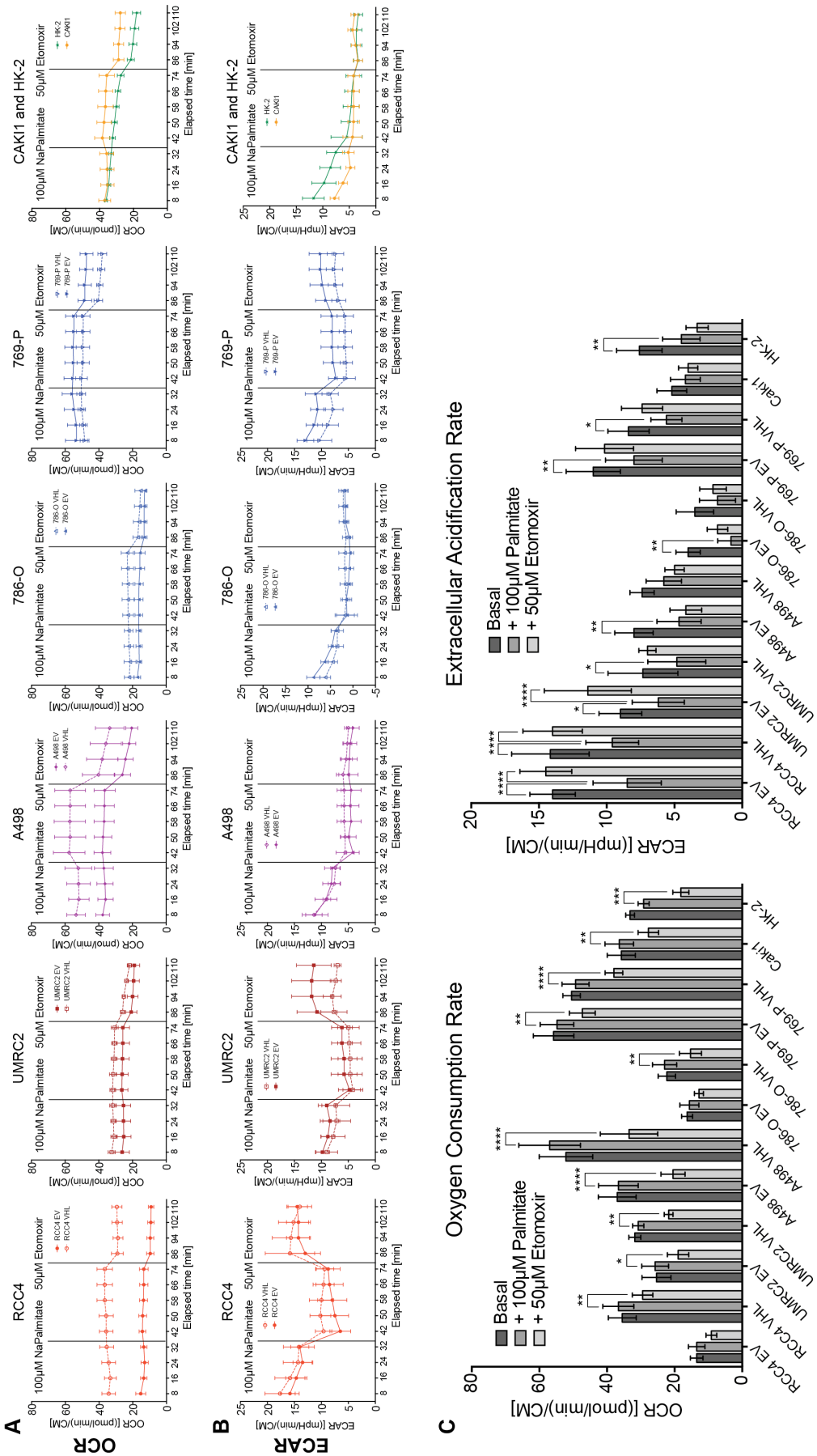
A
OCR
RCC4
A498
786-O
769-P
CAKI1 and HK-2
UMRC2
100μM NaPalmitate
50μM Etomoxir
OCR [(pmol/min)/CM]
Elapsed time [min]
B
ECAR
ECAR [(mpH/min)/CM]
C
Oxygen Consumption Rate
Extracellular Acidification Rate
Basal
+ 100μM Palmitate
+ 50μM Etomoxir
RCC4 EV
RCC4 VHL
UMRC2 EV
UMRC2 VHL
A498 EV
A498 VHL
786-O EV
786-O VHL
769-P EV
769-P VHL
Caki1
HK-2

Figure 3.19: Palmitate addition decreases ECAR in ccRCCs, which can be reversed through Etomoxir treatment

(A-B) OCR and ECAR determination following palmitate and Etomoxir addition using an XF^{e}96 Seahorse Bioanalyzer. Cells were plated the day before analysing in full growth medium. For analysis, growth medium was replaced with Krebs-Henseleit assay medium containing 2.5 mM glucose and 0.5 mM carnitine. Subsequently, sodium-palmitate to stimulate β-oxidation and Etomoxir, a β-oxidation inhibitor, were added at the indicated time points. Graphs represent (A) average OCR and (B) average ECAR measurements of at least 5 wells normalised to cell mass (CM) ± SD. (C) Bar graph summarising average rates from last measurement for each treatment in (A) and (B). Asterisks indicate statistical difference between basal OCR/ECAR levels and those resulting from addition of palmitate and differences that result from addition of Etomoxir following palmitate treatment (2-way ANOVA with Bonferroni multiple testing analysis; *, $p \leq 0.05$).

3.6.6 ccRCC cells are sensitive to CPT1A but not CPT1B ablation, while either supports HK-2 cell proliferation

As Etomoxir was significantly affecting OCR in ccRCC cells, the longer-term effects of Etomoxir treatment on cell viability were examined. Increasing doses of Etomoxir had hardly any effect on cell survival in ccRCC cells but had a negative effect on HK-2 cells (Figure 3.20A). This suggests that over a longer period β-oxidation might be dispensible in ccRCC cells but not in HK-2 cells. As this result was quite unexpected, inhibition of β-oxidation was also investigated by silencing the expression of the two CPT1 isoforms CPT1A (liver) and CPT1B (muscle) using siRNA. Surprisingly, RNAi-mediated ablation of either CPT1 isoform resulted in the opposite effect as the one seen following Etomoxir treatment: CPT1 depletion procured a growth advantage to HK-2 cells compared to the ccRCC cells (Figure 3.20B). Furthermore, while CPT1A silencing had in average a negative effect on ccRCC cell numbers compared to control silencing, siCPT1B had hardly any effect (Figure 3.20B). Taking into accaount that ccRCC cells showed high CPT1A mRNA levels in comparison to HK-2 cells (Figure 3.18B), there is the possibility that ccRCC cells express and rely mainly on CPT1A in contrast to HK-2 cells. However, the high tolerance of ccRCC cells to Etomoxir suggest that further experiments are needed to establish the importance of β-oxidation for energy supply and cell survival in ccRCC cells.

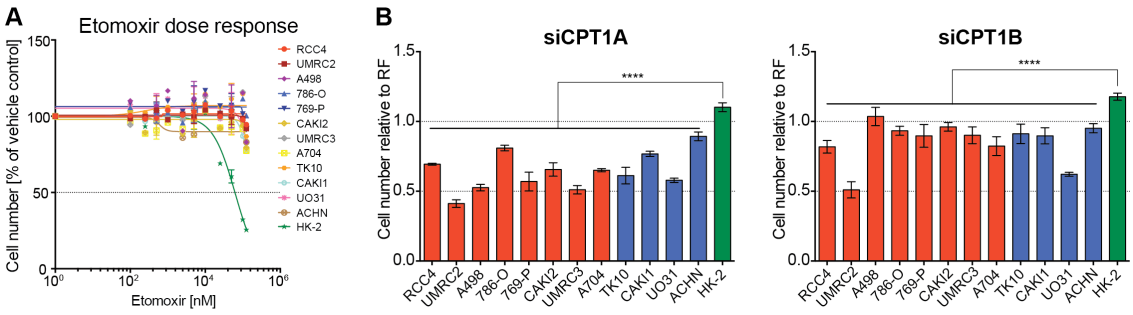

Figure 3.20: ccRCC cells are resistant to Etomoxir treatment, but ablation of either CPT1A or CPT1B has a negative effect on ccRCC compared to HK-2 cell viability

(A) 2000 cells/well of the indicated ccRCC and HK-2 cell lines were plated in standard culture medium in a 96-well format. The next day, full growth medium supplemented with Etomoxir was added to yield the indicated concentratins. Cells were incubated for 72 h. Dose response curves were modelled in Graphpad Prism 6 to measured endpoint cell numbers (average values obtained from 3 different wells ± SD). (B) 2000 cells/well of the indicated ccRCC cell lines and HK-2 cells were reverse transfected with siRNA SMARTpools targeting CPT1A or CPT1B in a 96-well format for 96 h. Bar graphs represent average of 3 wells and are normalised to the negative RISC-free (RF) control. Error bars represent SD. Asterisks indicate statistical difference in endpoint cell number between ccRCC cell lines and HK-2 cells (2-way ANOVA with Dunnett multiple testing analysis; ****, $p \leq 0.001$).

3.7 Discussion

Otto Warburg defined cancer as a metabolic disease (Warburg, 1956b, Warburg, 1956a), a statement, which is likely to be more relevant for ccRCC than for many other cancer types. ccRCC cells have constitutively active HIF expression and activity (Figure 3.2-3.4), and are highly glycolytic (Figure 3.6). Moreover, these cells require both glucose and glutamine as nutrients and show substantial growth retardation when deprived of these nutrients (Figure 3.11). Intriguingly, ccRCC cells also have a high respiratory capacity (Figure 3.7) and their mitochondrial metabolism cannot only be fuelled with glucose-derived pyruvate but also with fatty acids via β-oxidation, suggesting that they utilise several metabolic pathways to facilitate their growth.

What became clear from the metabolic characterisation that was undertaken in this study is that ccRCC can tolerate most of the tested metabolic insults. ccRCC cells continue to proliferate under serum starvation (Figure 3.12), in lipid-deprived conditions (Figure 3.14) or under almost anoxic experimental conditions (Figure 3.5) for several days. Hence, this cancer type must have developed a highly dynamic metabolic network that can quickly adapt to different metabolic conditions. But, crucially, ccRCC cells displayed less tolerance to nutrient stress conditions as depletion of glucose or glutamine was highly detrimental to cancer cell proliferation and survival

(Figure 3.11). These findings suggest that pathways integral to glucose and glutamine utilisation and metabolism are essential for ccRCC growth. And this could be considered an Achilles heel in ccRCC. Dietary restriction of these nutrients is not feasible, thus targeting essential components of these pathways could have potent anti-cancer activity in ccRCC.

It is likely that these cells can satisfy at least some of their energy demand through β-oxidation, fuelled by the large amounts of lipids stored in their cytoplasm; as ccRCCs are histochemically defined by the presence of lipid droplets (Gebhard et al., 1987). Interestingly, apart from the liver, the kidney cortex is the only other site within the mammalian body where gluconeogenesis (GNG) can take place. GNG is the process of generating glucose from non-carbohydrate structures such as pyruvate, lactate, glycerol, but also fatty acids in times of fasting. GNG is an energy consuming process and is often connected with ketosis, a state where the main energy source is liver-derived ketone bodies, consisting of acetoacetate and β-hydroxybutyrate. It is thus possible that ccRCC cells could utilise GNG to convert lipid-derived carbon into glucose to provide riboses for DNA synthesis. Also, ccRCC cells could mobilise stored glycogen to replenish the glucose pool. However, these potential alternative mechanisms cannot support ccRCC cell survival after long-term glucose withdrawal. Further analysis will be necessary to gain deeper insight in lipid droplet contribution to ccRCC proliferation.

One possibility to identify specific metabolic dependencies in different cancer types is provided by a systems biology approach that models all possible metabolic reactions within a cancer cells. Using this approach, it has been found recently that ccRCC displays a unique metabolic network that is associated with LOH of chromosome 3p. Moreover, nucleotide, one-carbon, and glycerophospholipid metabolism was found to be severely compromised in ccRCC cells (Gatto et al., 2014). As glucose is the main precursor of the synthesis of nucleotides, limiting glucose levels would impair nucleotide generation to a critical point in ccRCC cells, thereby inhibiting cell proliferation. Also, glucose could be feeding the serine biosynthesis pathway. Serine has recently been found to be essential for breast cancer carcinogenesis (Maddocks et al., 2013) as serine-depletion induced oxidative stress, particularly in p53-deficient cells.

It is now well appreciated that, apart from glucose, glutamine is an essential nutrient for cancer cells, as glutamine depletion is detrimental for many cancer cells including ccRCC cells (Fuchs and Bode, 2006, Gordan et al., 2007a, Yuneva et al., 2007, Vander Heiden et al., 2011). However, the discrete mechanism of glutamine-dependent survival is not clearly defined and is under examination by several research groups. Glutamine is the most abundant amino acid in the cellular microenvironment (DeBerardinis and Cheng, 2010). Its uses stretch from energy production as substrate for the TCA cycle to contributing nitrogen for nucleotide synthesis and to being a component of glutathione, the most abundant non-enzymatic cellular anti-oxidant. As glutamine is a non-essential amino acid, i.e. can be produced by the cell, the question arises why ccRCC cells depend on external glutamine supply. As with other cancer types, ccRCC cells have been found to have enhanced levels of c-MYC expression, which drives cell cycle progression and mitochondrial biogenesis (Gordan et al., 2007a, Tang et al., 2009). One possibility is that ccRCC cells depend on glutamine for nucleotide biosynthesis to maintain cell proliferation.

So far, it has been shown that ccRCC cells, although growth inhibited, maintained some level of proliferation even after serum depletion (Figure 3.12), suggesting efficient production of autocrine growth factors. Indeed, Franovic and colleagues showed that HIF-2α expression allows autonomous growth of cancer cells *in vivo* and *in vitro* by activation of epidermal growth factor receptor (EGFR) and insulin-like growth factor receptor type I (IGF1R) signalling (Franovic et al., 2009). However, this observation was specific for HIF-2α and not observed with the HIF-1α isoform. In accordance with this observation, results from the isogenic cell line panel showed that HIF-2α -expressing ccRCC cells were less able to tolerate serum starvation than their pVHL-null counterparts (Figure 3.12), suggesting that HIF-2α induces autocrine growth factor signalling to maintain proliferation even under exogenous growth factor withdrawal.

Overall, the pVHL-isogenic models employed in this study proved to modulate HIF expression and response to oxygen deprivation in a VHL-dependent fashion, as expected (Figure 3.4 and 3.5). Furthermore, pVHL expression was shown to enhance

the respiratory capacity of cells (Figure 3.9) while other metabolic tracts such as adaptation to nutrient and lipid deprivation were unaffected by the presence or absence of pVHL (Figure 3.12 and 3.14), reinforcing the possibility that only a limited amount of the typical metabolic characteristics of ccRCC may depend on pVHL expression. Besides pVHL expression, the presence of different HIF-α isoforms also influences metabolic characteristics, as sensitivity to serum starvation is decreased in HIF-2α only expressing ccRCC cells (Figure 3.12).

To elucidate the extend by which pVHL or the different HIF-α isoforms condition metabolic vulnerabilities within the core glucose, amino acid and fatty acid metabolism, the isogenic ccRCC cells were subjected to a customised metabolic RNAi screen, which is described in the next chapter.

Chapter 4: Unbiased functional metabolic siRNA screen to determine VHL-synthetic lethality in ccRCC

4.1 Introduction

4.1.1 Synthetic lethality

Two genes/proteins are synthetic lethal, when loss of either of them individually has no effect on cell viability, while simultaneous loss of both leads to cell death (Kaelin, 2005). In order to maintain viability despite the possibility of genetic loss of a functional gene either due to the accumulation of random mutations or exposure to genotoxic environmental stress, organisms employ compensatory mechanisms to balance genetic variations. Compensation may occur in form of another protein of the same or a related family that can carry out the same function as the lost gene, or another pathway stepping in leading to the same net result/phenotype through a different system.

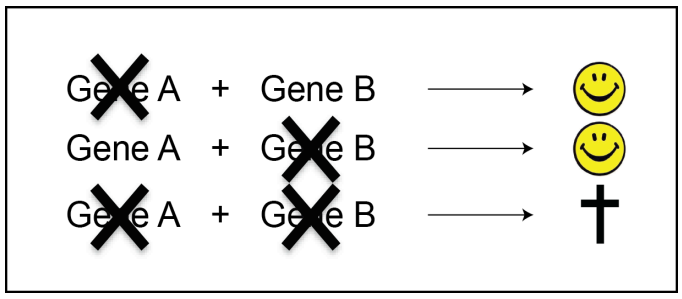

Figure 4.1: Principle of synthetic lethality
Loss of either Gene A or Gene B on its own does not affect cell survival. However, loss of both genes simultaneously is detrimental for the cell.

Exploring synthetic lethality within the context of a specific genetic makeup can elucidate compensatory relationships with other gene products, cellular pathways or biochemical processes. In case the gene/protein of interest is frequently mutated or lost and involved in a disease syndrome, identified (compensatory) relationships can then be exploited for treatment through developing drugs that disrupt this link.

Investigating synthetically lethal relationships between activated proto-oncogenes or mutations in tumour suppressors using genetic screens is an effective approach in cancer research. This strategy can identify essential processes that are required for the survival of cancer cells with a given genetic background. Synthetic lethal targets can provide novel therapeutic windows for drug development. Targeting synthetic lethal processes should not affect cells without the mutation and therefore result in less harmful side effects than those caused by classical chemotherapies.

4.1.2 The concept and mechanism of RNA interference

RNA interference (RNAi) mediated by either micro RNA (miRNA) or small interfering RNA (siRNA) is an important, evolutionary conserved cellular mechanism to regulate gene expression post transcriptionally on messenger RNA (mRNA) levels. Furthermore, RNAi plays an important role for the immune response against invading parasitic nucleic acids such as viruses and transposons.

miRNAs are cell endogenous RNA molecules and are directly transcribed as pre-miRNA stem-loop structures in the nucleus. In contrast, siRNAs are exogenously-derived double stranded RNA (dsRNA) fragments that can originate for example from retroviruses. Once these dsRNAs are in the cytoplasm, they are recognised by the endoribonuclease Dicer, which cleaves them into short dsRNA fragments of 20-25 base pairs in length with a two-nucleotide 3' overhang on each end (Preall et al., 2006, Vermeulen et al., 2005). Dicer also facilitates the activation of the RNA-induced silencing complex (RISC). This muliprotein complex incorporates one strand of the miRNA or siRNA dsRNA fragments, the so-called 'guide strand' while the other so-called 'passenger strand' is degraded. Distinction of guide and passenger strand is performed by the RISC's catalytically active RNase Argonaute and is based on the thermodynamic stability of the 5' end (Preall et al., 2006). The incorporated guide strand serves as template for the recognition of complementary mRNA, which, upon binding to the RISC complex, gets degraded by Argonaute resulting in decreasing levels of this mRNA species (Figure 4.2). At least for short-lived proteins, reduced mRNA levels will ultimately result in decreased protein levels.

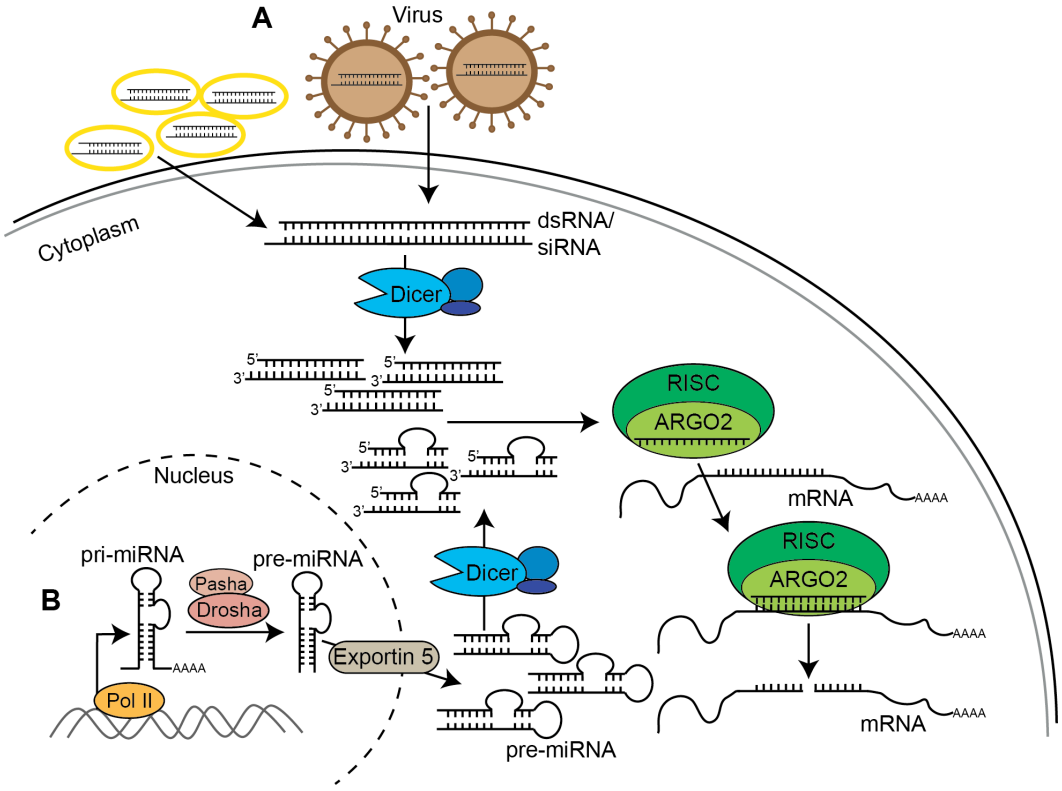

Figure 4.2: Mechanism of RNA interference (RNAi)
Schematic overview of the RNAi mechanism: (A) When extracellular small interfering RNA (siRNA) or double stranded RNA (dsRNA) from e.g. viruses enters a cell, it is recognised by the cytoplasmic endoribonuclease Dicer, which cleaves them into short dsRNA fragments (20-25 bp long with 2 nt 3' overhang), ready to be further processed by the RNA-induced silencing complex (RISC). One strand of these dsRNA fragments (guide strand) is incorporated into RISC and serves as template for recognition of complementary mRNA. Upon successful matching of mRNA and RISC incorporated guide strand, the mRNA is degraded by RISC's RNase Argonaute (ARGO2). The same Dicer-/RISC-dependent RNAi mechanism takes effect for endogenously generated micro RNAs (miRNAs). (B) miRNAs are transcribed directly from the genome by RNA polimerase II (Pol II) as primary miRNA (pri-miRNA), which is further processed by the RNase complex Pasha/Drosha. The resulting precursor miRNAs (pre-miRNAs) are actively shuttled from the nucleus to the cytoplasm via Exportin 5. Once in the cytoplasm, pre-miRNAs are cleaved by Dicer and lead to RISC-mediated mRNA degradation.

4.1.3 The pVHL-isogenic ccRCC cell system to study synthetic lethality

We used the five isogenic cell line pairs RCC4, UMRC2, A498, 786-O and 769-P received from William Kaelin's laboratory that were characterised in the previous Chapter to carry out a functional siRNA screen to identify metabolic enzymes that show synthetic lethal interactions with pVHL. A similar approach targeting a small subset of the human kinome has already been performed successfully in the Kaelin laboratory, where two of these isogenic cell line pairs, RCC4 and 786-O, were transfected with an shRNA library targeting 88 kinases (Bommi-Reddy et al., 2008). In this study, CDK6,

MET and MEK1 were identified as potential synthetic lethal interactors of pVHL as shRNA-mediated silencing of these proteins resulted in preferential killing of the RCC4 and 786-O pVHL-null cells compared to their pVHL-reconstituted counterparts. In the case of CDK6, the shRNA-mediated effect on killing in $pVHL^{-/-}$ cells could be confirmed with a small-molecule Cdk4/6 inhibitor, suggesting that novel VHL-specific therapeutic targets can be identified using RNAi screens in ccRCC (Bommi-Reddy et al., 2008).

This chapter will describe a customised functional metabolic screen, whose primary aim was the identification of novel metabolic genes that are synthetic lethal with pVHL in a panel of the five pVHL-isogenic ccRCC cell line pairs: RCC4, UMRC2, A498, 786-O and 769-P ± *VHL* respectively.

4.2 Screen Optimisation

Based on previous experience, the efficiency of siRNA transfection using different transfection reagents (TR) can show large variations between different cell lines. To determine optimal transfection efficiency while minimising cell toxicity, a series of optimisation experiments was performed in collaboration with Dr. Ming Jiang in the LRI High Throughput Screening (HTS) facility.

4.2.1 Optimisation of duration of siRNA-mediated gene silencing

Determining the timing of the screen was straightforward and based on the nature of the screen as well as previous experience. siRNA-mediated gene knockdown (KD) occurs quickly after transfection. It is likely that the target mRNA gets depleted within the first 24 h post-transfection and, depending on the stability of the targeted protein, protein depletion should be achieved after approx. 48-72 h. At the same time, siRNA-mediated KD is only transient as siRNA is not very stable and gets depleted with every cell duplication. Therefore, the siRNA-mediated effect is diminishing over time and untransfected cells could outgrow the cultures if the assay continues for too long. For the screen shown here, cells were incubated for 96 h post-transfection to ensure efficient

target depletion and detect potential detrimental effects on proliferation and survival of the transfected cells.

4.2.2 Starting cell number

As readout for the screen, measurement of cell viability at the endpoint of the experiment 96 h post transfection was chosen. Cell number was determined using an Acumen® $^{e}X^{3}$ laser-scanning microplate cytometer (TTP Lab Tech Ltd.), which detects DAPI-stained nuclei. In order to detect a good dynamic range of effects on cell number, optimisation of initial cell plating densities was performed. Cells were plated to ensure exponential growth during the experiment to detect maximal effects of gene silencing on proliferation without reaching confluence at the end of the assay as this affects accurate discrimination of individual nuclei and could result in skewed data. At the same time, sufficient cell numbers had to be reached to reliably detect small differences in cell number.

As the different cell lines have specific growth kinetics, different cell numbers of the isogenic cell line pairs were plated on 96-well plates and cell proliferation was monitored using an IncuCyte™ kinetic live-cell imaging system (Essen BioScience). The growth curves over 4 days depicted in Figure 4.3 show that all ccRCC cell lines are highly proliferative and duplicate approx. every 36 h. As already seen from the cell characterisation, ectopic expression of pVHL does not negatively affect cell proliferation in the isogenic cell line pairs *in vitro*.

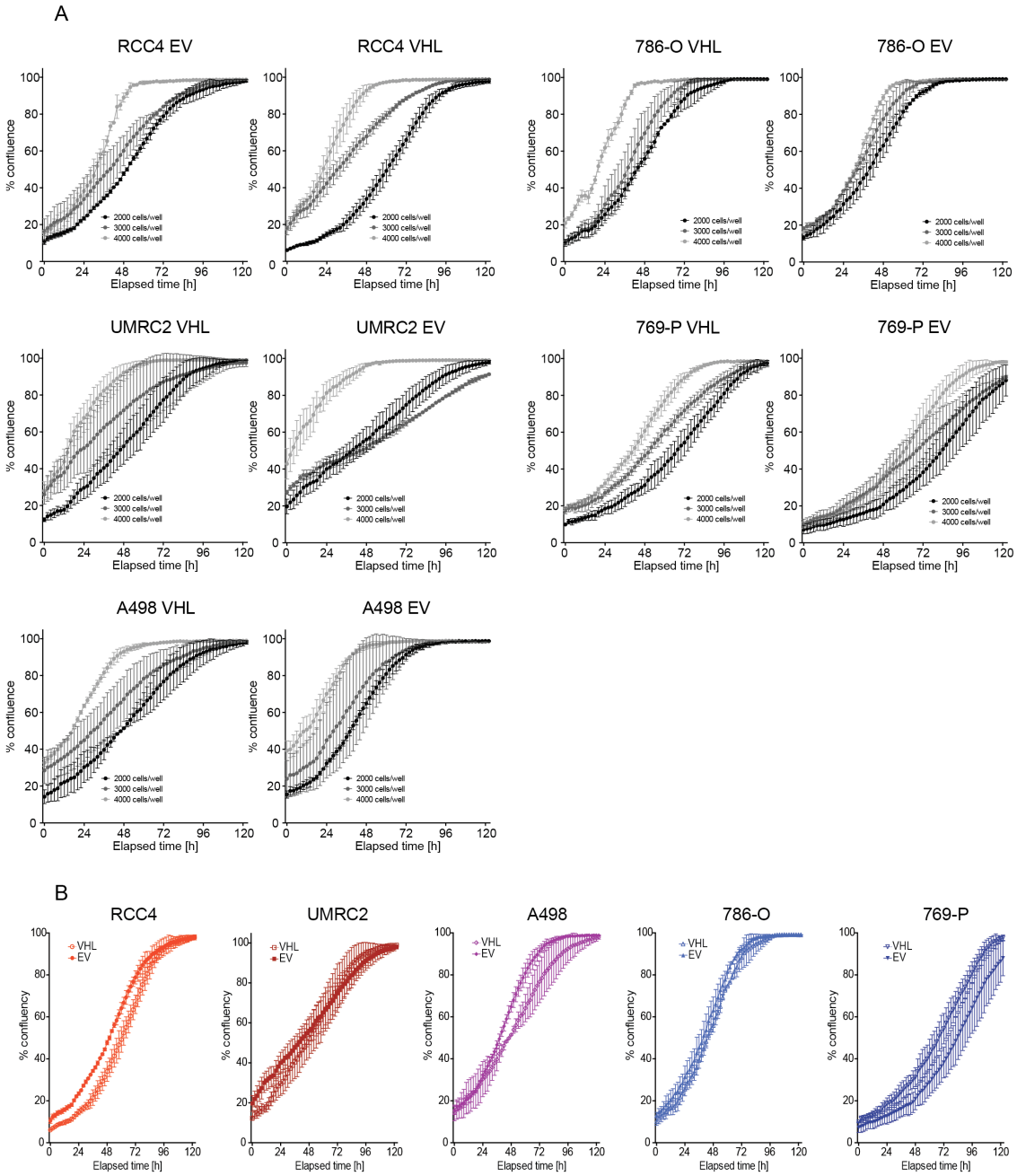

Figure 4.3: Growth kinetcs of isogenic ccRCC cell line pairs

(A) The 5 isogenic cell line paires were plated at a density of 2000 (black), 3000 (dark grey) or 4000 (light grey) cells/well in a 96-well plate format. Cells were monitored in an IncuCyte live cell imaging system. Data acquisition occurred every 2 h. (B) Growth curve comparison of the respective isogenic cell line pairs for the plating density of 2000 cells/well extracted from (A) that was chosen for the screen and subsequent experiments. Data points show mean of duplicate wells ± SD.

The live-cell imaging results could be confirmed with a time course cell mass assay. Tested were starting cell numbers between 1000 and 8000 cells/well on a 96-well plate format. Also this assay narrowed down the suitable plating densities to 2000 or 4000

cells/well. In this range, all cell lines were close to confluence but still exhibit exponential growth on day 4 when left untreated (Figure 4.4).

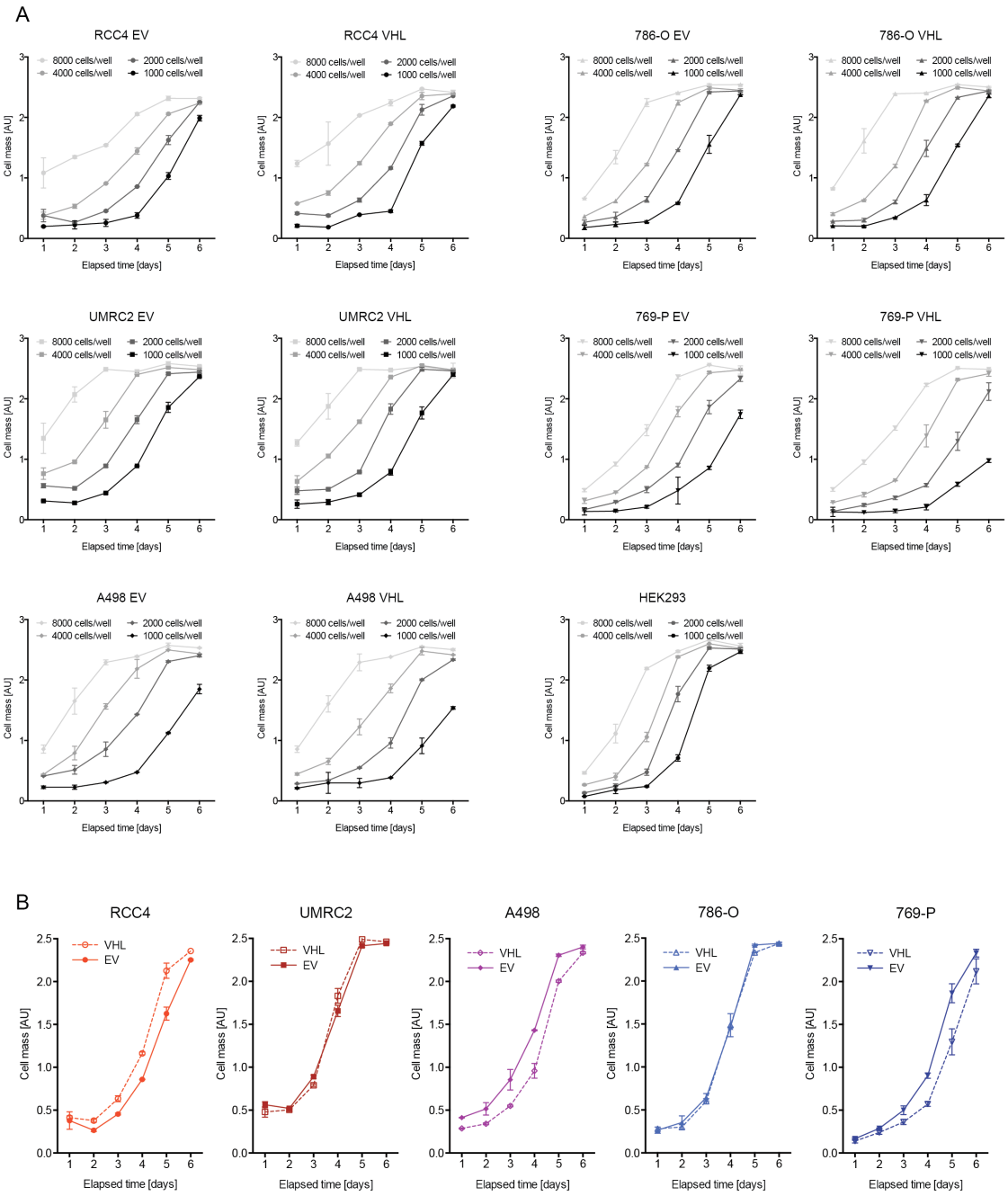

Figure 4.4: Cell mass-based growth kinetcs of isogenic ccRCC cell line pairs
(A) The 5 isogenic cell line pairs as well as HEK 293 cells were plated at at a density of 1000 (black), 2000 (dark grey), 4000 (lighter grey) or 8000 (light grey) cells/well in a 96-well plate format. Cells were fixed with 10 % TCA every 24 h and cellular protein content was subsequently measured using a sulforhodamine B protein assay. (B) Growth curve comparison of the respective isogenic cell line pairs for the plating density of 2000 cells/well extracted from (A), which was chosen as starting cell number for the screen and subsequent experiments. Data points show mean of triplicate wells ± SD.

4.2.3 Optimisation of transfection reagent

siRNA is delivered to the cells using a lipid-based transfection reagent (TR), which forms micelles enclosing the siRNA-containing solution to be delivered in its centre. This liposome-like structure fuses with the cell membrane and discharges its cargo into the cytoplasm. There are many different TRs on the market and a suitable TR had to be identified that would deliver siRNA efficiently and ideally to all cell lines while having the least toxic effect. In collaboration with the LRI High throughput Screening Service, 23 different TRs were tested in two concentrations (0.1 µl and 0.3 µl per 100 µl transfection reaction volume) to transfect the cell lines with an siRNA SMARTpool against the non-essential nuclear envelope protein Lamin A/C (Elbashir et al., 2001, Thaker et al., 2010) in a 96-well format. 48 h post transfection, cells were analysed for Lamin A/C expression measuring immunofluorescence (IF) intensities and for endpoint cell numbers by counting DAPI-positive nuclei.

Figure 4.5 holds the transfection results for the isogenic UMRC2 and 769-P cell lines. For completion, Figure 4.6 shows the transfection reagent results for parental A498 and 786-O cells, which were analysed in the contest of another screen the HTS facility performed, as well as the transfection results for the non-tumourigenic renal epithelial HK-2 cell line. Finally, Figure 4.7 summarises the transfection results for each cell line with the ten most promising TRs.

Across the ccRCC cell lines tested, 0.1 µl DharmaFect2, DharmaFect3, DharmaFect4 or Lullaby showed the most promising results. Compared to non-transfected cells, transfection with these reagents reduced Lamin A/C intensity considerably and had no major effect on cell viability (Figure 4.5 - 4.7).

Based on the results of this optimisation, DharmaFect2 (Dh2) was chosen for the screen as it showed good knockdown efficiency and low toxicity across the cell line panel (Figure 4.7).

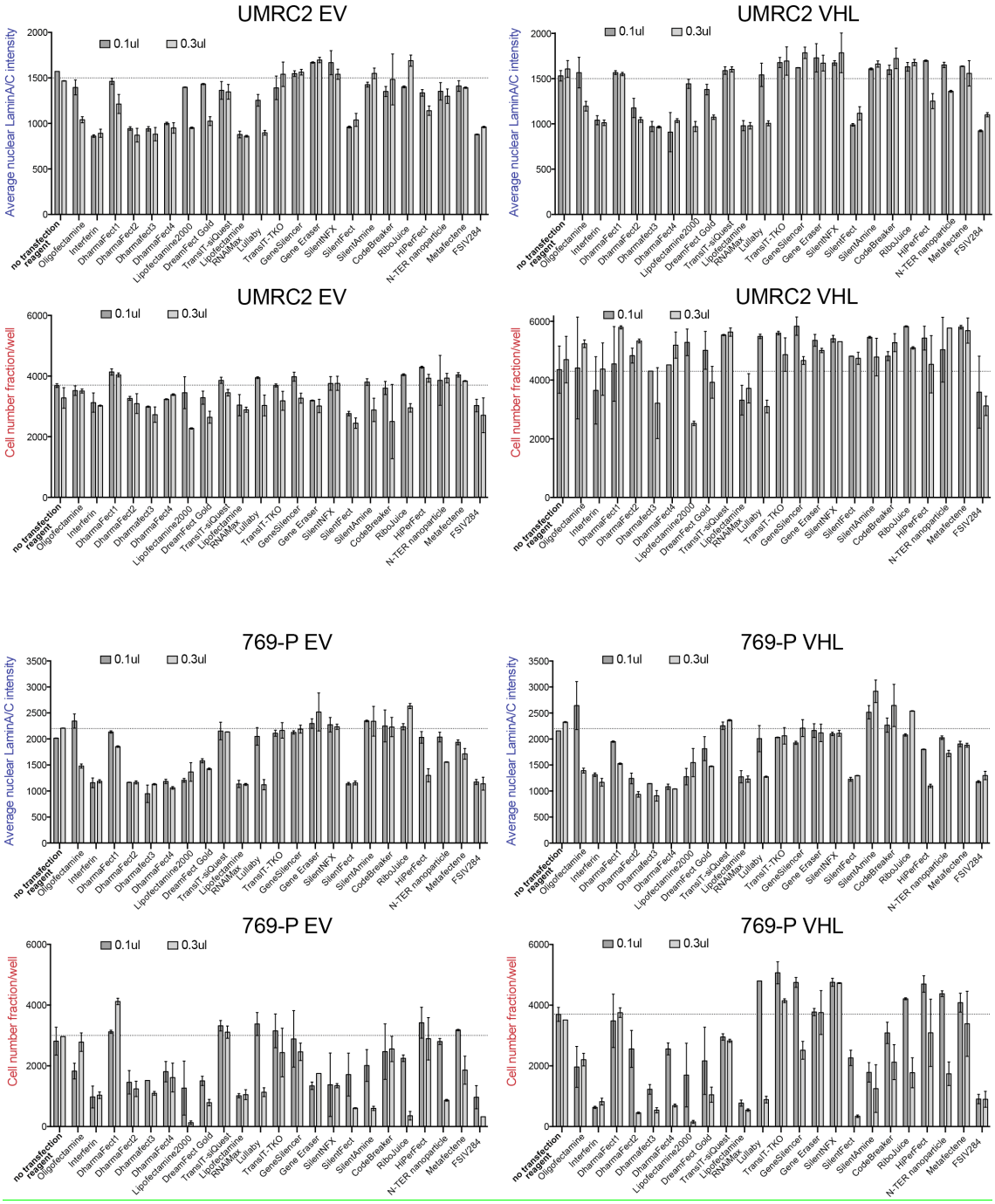

Figure 4.5: Screening of transfection reagents I

4000 cells/well of the *VHL*-isogenic UMRC2 and 769-P cell line pairs were reverse transfected in duplicates with 37.5 nM siRNA SMARTpool against the non-essential nuclear envelope protein Lamin A/C using a panel of 23 different transfection reagents in a 96-well plate format. Upon fixation 48 h post transfection, cells were stained for Lamin A/C and DAPI and analysed for lamin A/C immuno-flourescence intensity (upper panel) and cell number (lower panel) using a Cellomix® ArrayScan® VTI HCS Reader (Thermo Scientific). Bars represent mean of duplicate wells ± SD. Note: The cell number data represent the analysed fraction of cells that were analysed for Lamin A/B intensity. These fractions are representative for the whole well. These experiments were performed by Ming Jiang from the High Throughput Screening facility at the LRI.

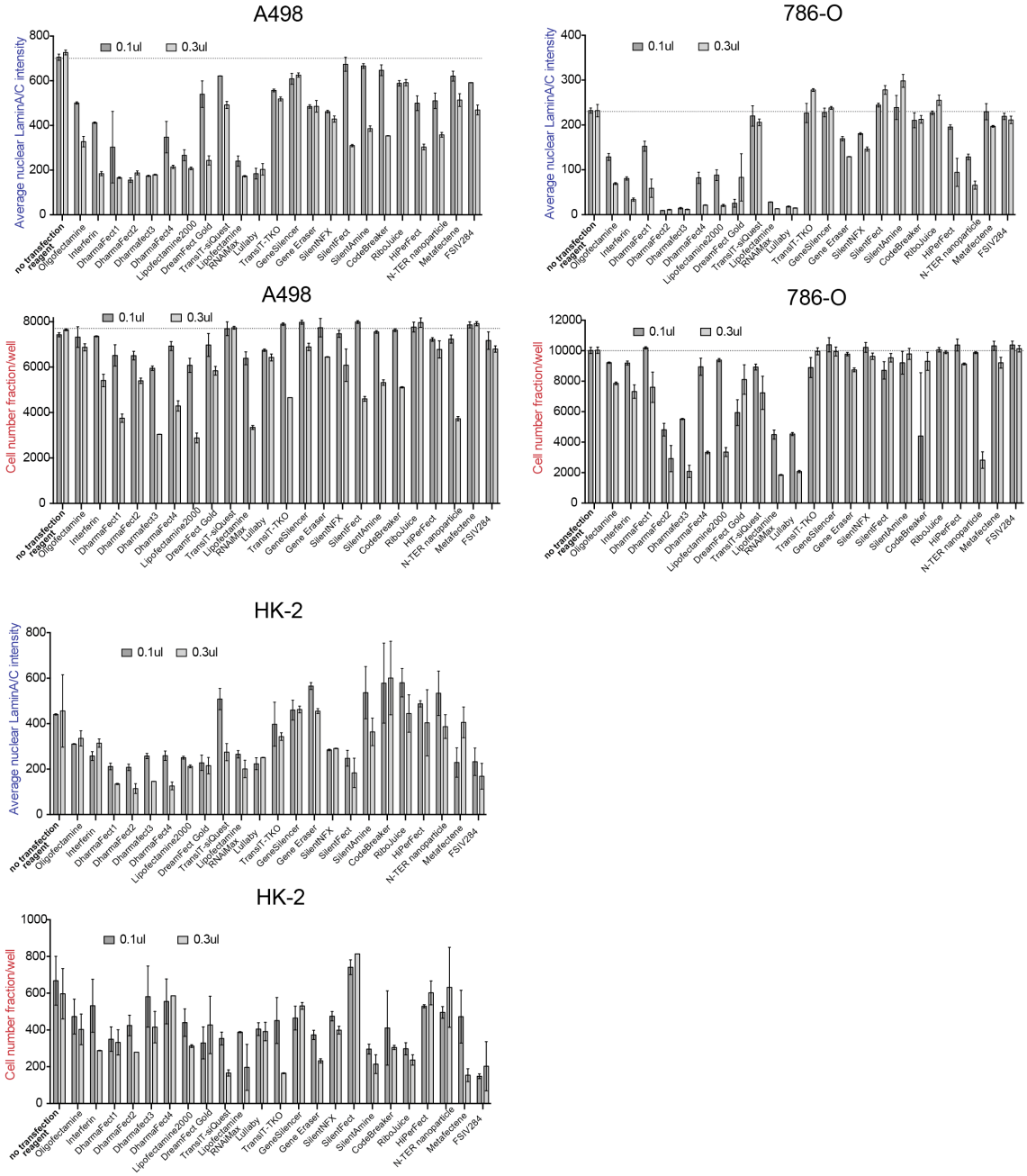

Figure 4.6: Screening of transfection reagents II

4000 cells/well of parental A498 and 769-P as well as the non-tumourigenic HK-2 cells were reverse transfected in duplicates with 37.5 nM siRNA SMARTpool against the non-essential nuclear envelope protein Lamin A/C using a panel of 23 different transfection reagents in a 96-well plate format. Upon fixation 48 h post transfection, cells were stained for Lamin A/C and DAPI and analysed for lamin A/C immuno flourescence intensity (upper panel) and cell number (lower panel) using a Cellomix® ArrayScan® VTI HCS Reader (Thermo Scientific). Bars represent mean of duplicate wells ± SD. Note: The cell number data represent the analysed fraction of cells that were analysed for Lamin A/B intensity. These fractions are representative for the whole well. These experiments were performed by Ming Jiang from the High Throughput Screening facility at the LRI.

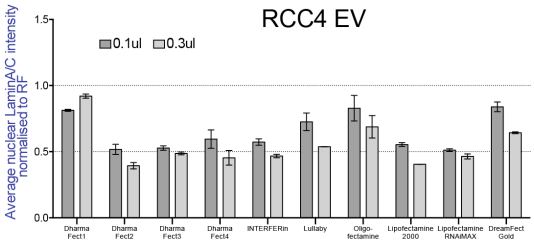
RCC4 EV
0.1ul
0.3ul
Average nuclear LaminA/C intensity normalised to RF
1.5
1.0
0.5
0.0
Dharma Fect1
Dharma Fect2
Dharma Fect3
Dharma Fect4
INTERFERin
Lullaby
Oligo-fectamine
Lipofectamine 2000
Lipofectamine RNAiMAX
DreamFect Gold

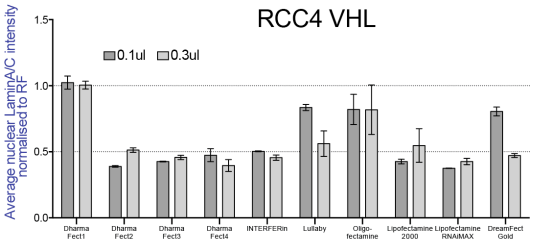
RCC4 VHL
0.1ul
0.3ul
Average nuclear LaminA/C intensity normalised to RF
1.5
1.0
0.5
0.0
Dharma Fect1
Dharma Fect2
Dharma Fect3
Dharma Fect4
INTERFERin
Lullaby
Oligo-fectamine
Lipofectamine 2000
Lipofectamine RNAiMAX
DreamFect Gold

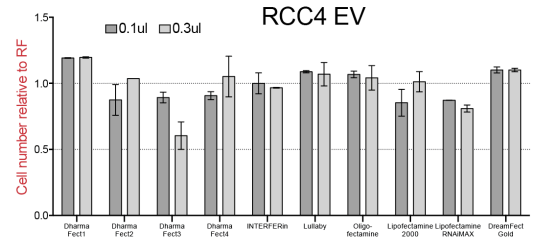
RCC4 EV
0.1ul
0.3ul
Cell number relative to RF
1.5
1.0
0.5
0.0
Dharma Fect1
Dharma Fect2
Dharma Fect3
Dharma Fect4
INTERFERin
Lullaby
Oligo-fectamine
Lipofectamine 2000
Lipofectamine RNAiMAX
DreamFect Gold

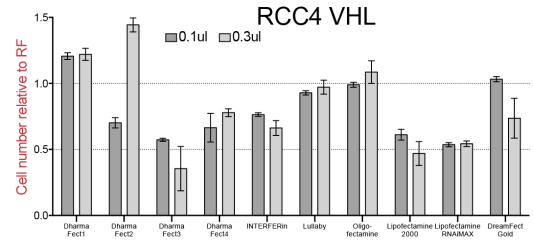
RCC4 VHL
0.1ul
0.3ul
Cell number relative to RF
1.5
1.0
0.5
0.0
Dharma Fect1
Dharma Fect2
Dharma Fect3
Dharma Fect4
INTERFERin
Lullaby
Oligo-fectamine
Lipofectamine 2000
Lipofectamine RNAiMAX
DreamFect Gold

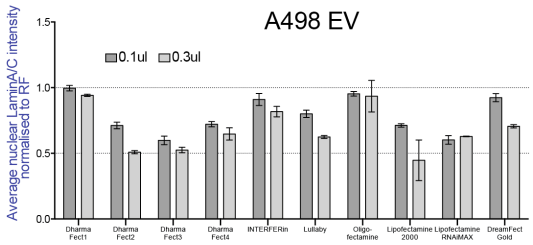
A498 EV
0.1ul
0.3ul
Average nuclear LaminA/C intensity normalised to RF
1.5
1.0
0.5
0.0
Dharma Fect1
Dharma Fect2
Dharma Fect3
Dharma Fect4
INTERFERin
Lullaby
Oligo-fectamine
Lipofectamine 2000
Lipofectamine RNAiMAX
DreamFect Gold

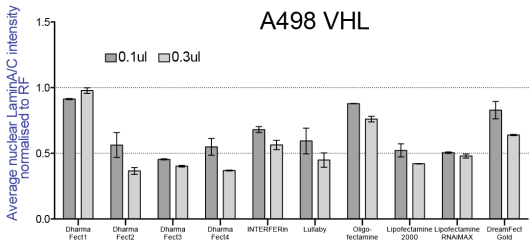
A498 VHL
0.1ul
0.3ul
Average nuclear LaminA/C intensity normalised to RF
1.5
1.0
0.5
0.0
Dharma Fect1
Dharma Fect2
Dharma Fect3
Dharma Fect4
INTERFERin
Lullaby
Oligo-fectamine
Lipofectamine 2000
Lipofectamine RNAiMAX
DreamFect Gold

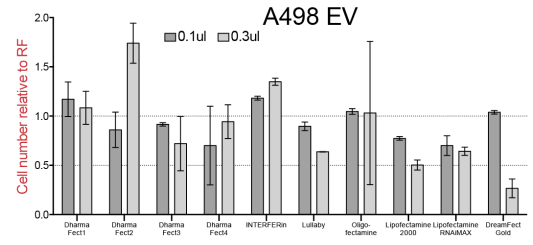
A498 EV
0.1ul
0.3ul
Cell number relative to RF
2.0
1.5
1.0
0.5
0.0
Dharma Fect1
Dharma Fect2
Dharma Fect3
Dharma Fect4
INTERFERin
Lullaby
Oligo-fectamine
Lipofectamine 2000
Lipofectamine RNAiMAX
DreamFect Gold

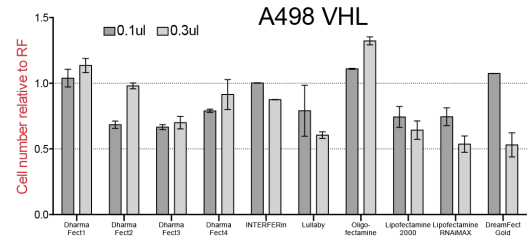
A498 VHL
0.1ul
0.3ul
Cell number relative to RF
1.5
1.0
0.5
0.0
Dharma Fect1
Dharma Fect2
Dharma Fect3
Dharma Fect4
INTERFERin
Lullaby
Oligo-fectamine
Lipofectamine 2000
Lipofectamine RNAiMAX
DreamFect Gold

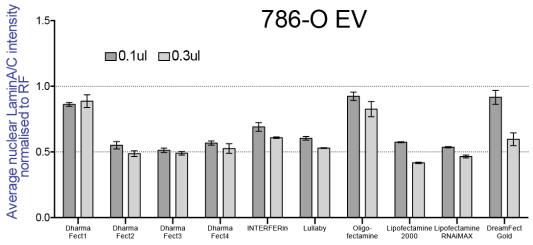
786-O EV
0.1ul
0.3ul
Average nuclear LaminA/C intensity normalised to RF
1.5
1.0
0.5
0.0
Dharma Fect1
Dharma Fect2
Dharma Fect3
Dharma Fect4
INTERFERin
Lullaby
Oligo-fectamine
Lipofectamine 2000
Lipofectamine RNAiMAX
DreamFect Gold

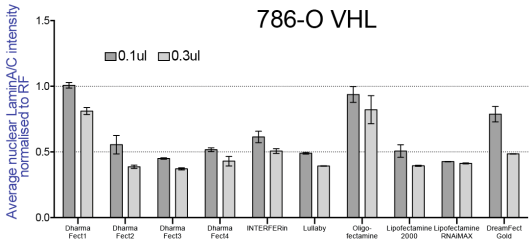
786-O VHL
0.1ul
0.3ul
Average nuclear LaminA/C intensity normalised to RF
1.5
1.0
0.5
0.0
Dharma Fect1
Dharma Fect2
Dharma Fect3
Dharma Fect4
INTERFERin
Lullaby
Oligo-fectamine
Lipofectamine 2000
Lipofectamine RNAiMAX
DreamFect Gold

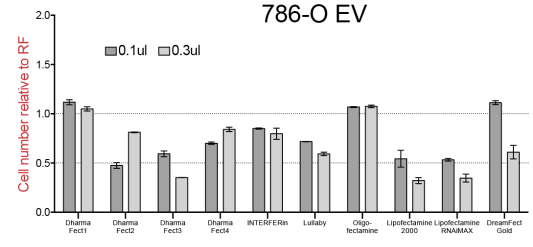
786-O EV
0.1ul
0.3ul
Cell number relative to RF
2.0
1.5
1.0
0.5
0.0
Dharma Fect1
Dharma Fect2
Dharma Fect3
Dharma Fect4
INTERFERin
Lullaby
Oligo-fectamine
Lipofectamine 2000
Lipofectamine RNAiMAX
DreamFect Gold

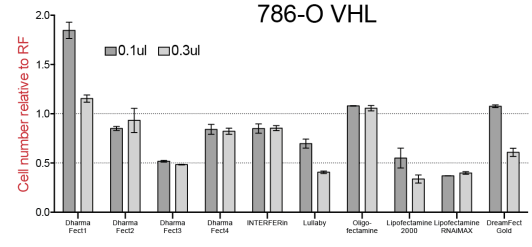
786-O VHL
0.1ul
0.3ul
Cell number relative to RF
2.0
1.5
1.0
0.5
0.0
Dharma Fect1
Dharma Fect2
Dharma Fect3
Dharma Fect4
INTERFERin
Lullaby
Oligo-fectamine
Lipofectamine 2000
Lipofectamine RNAiMAX
DreamFect Gold

Figure 4.7: Screening of transfection reagents III
4000 cells/well of the 5 *VHL*-isogenic ccRCC cell line pairs were reverse transfected with 37.5 nM siRNA SMARTpool against the non-essential nuclear envelope protein Lamin A/C using the ten most promising transfection reagents from the panel tested (see Figure 4.5 & 4.6) in a 96-well plate format. Upon fixation 48 h post transfection, cells were stained for Lamin A/C and DAPI and analysed for lamin A/C immuno flourescence intensity (respective upper panel) and cell number (respective lower panel) using a Cellomix® ArrayScan® VTI HCS Reader (Thermo Scientific). Bars represent mean of duplicate wells ± SD. Note: The cell number data represent the analysed fraction of cells that were analysed for Lamin A/B intensity. These fractions are representative for the whole well. These experiments were performed by Ming Jiang from the High Throughput Screening facility at the LRI.

4.2.4 Optimisation of transfection controls

Defining suitable controls is very important to obtain reliable results from an siRNA screen. There are two sorts of controls: a) Negative controls that give information about the baseline cellular response to the transfection procedure. Ideally, these should have almost no effect on cell viability and can be used for normalisation. b) Positive controls that should cause significant cell death and that can be used an indicator for transfection efficiency. As negative controls, siRNAs that are either non homologous to the human genome (siControl 1-4 (siC1-4) and siOTP1-4) or are chemically modified so that they are not recognised by the RISC complex (RISC-free, RF) were used. As positive controls, siRNAs targeting the polyubiquitin precursor ubiquitin B (UBB) or the mitotic regulator polo-like-kinase 1 (PLK1) were chosen. Both proteins are vital in human cells and their ablation results in substantial cell death by apoptosis. Furthermore, cells were treated with the transfection reagent Dh2 alone. Figure 4.8 illustrates the responses of the different cell lines to the individual negative control-siRNAs (siC1 - siC4 and siOTP1 - siOTP4) as well as to the positive control-siRNA (siUBB SMARTpool). Although only the siC1-4 and siOTP1-4 pools were used in the screen and subsequent experiments, this experiment shows the effect that the individual control sequences have in the different cell lines. All negative control-siRNAs had some negative effect on cell viability. However the different siOTP sequences showed only a minor reduction in cell number compared to the different siC1-4 sequences (Figure 4.8). As will be shown in further experiments, pooling the individual siC1-4 and siOTP1-4 sequences diminishes the negative effect on cell number. As expected, silencing of UBB resulted in a > 90% loss of cell viability in all cell lines.

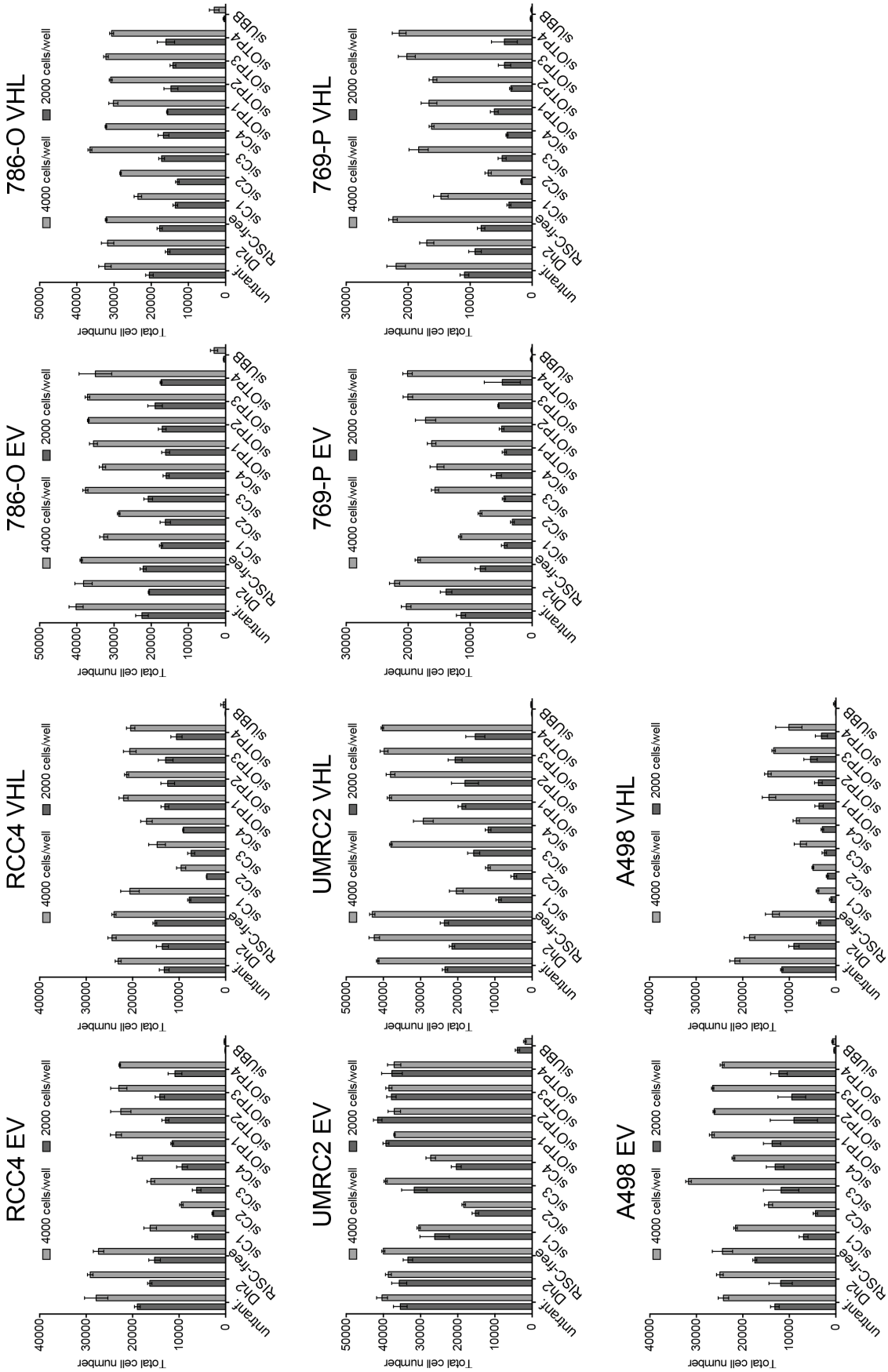
786-O VHL
769-P VHL
786-O EV
769-P EV
RCC4 VHL
UMRC2 VHL
A498 VHL
RCC4 EV
UMRC2 EV
A498 EV
4000 cells/well
2000 cells/well
Total cell number
untranf.
Dh2
RISC-free
siC1
siC2
siC3
siC4
siOTP1
siOTP2
siOTP3
siOTP4
siUBB

Figure 4.8: Effect of positive and negative siRNA transfection controls on ccRCC cells
2000 or 4000 cells/well of the 5 *VHL*-isogenic ccRCC cell lines were reverse transfected with 37.5 nM of the individual negative control-siRNA sequences and the siRNA SMARTpool against UBB using 0.1 µl of DharmaFect2 transfection reagent in a 96-well format. Cells were fixed 96 h post transfection, DAPI stained and analysed for cell number using an Acumen laser scanning microplate cytometer. Bars represent mean of triplicate wells ± SD.

4.2.5 Pilot screen

Having optimised assay duration, transfection conditions, initial plating density and transfection controls, a mini pilot screen was performed. In this test screen, siRNAs targeting 4 metabolic genes that were predicted thought to have differential effect on the 5 pVHL-isogenic ccRCC cell line pairs were used in addition to positive and negative control siRNAs. These genes were monocarbxylate transporter 4 (MCT4 or SLC16A3) (Gerlinger et al., 2012b), c-MYC (Gordan et al., 2007b) as well as the HIF-targets pyruvate dehydrogenase kinase 1 (PDHK1) and malic enzyme 1 (ME1) Also, this experiment was used to finalise the seeding density for the screen. 2-3 independent experiments were performed using two different batches of cells at different passage numbers to examine the consistency and reproducibility of transfection efficiency in the 5 isogenic cell line pairs. Reassuringly, the variability between the different experiments was relatively low, with the positive controls siUBB and siPLK1 consistently leaving only about 10 % viable cells after 96 h of transfection (Figure 4.9). The isogenic cell line pairs showed similar behaviour towards the negative controls, although the effect differed between different cell lines. With regard to the 4 target genes tested, a reduction in cell numbers was observed across the cell line panel (Figure 4.9). However, none of these genes showed an obvious differential effect between pVHL-expressing and pVHL-null cells.

In hindsight, it would have been wise to include one of the kinases (MET, MEK1 and particularly CDK6) that were positively identified to have a pVHL-differential effect in the shRNA screen carried out by Bommi-Reddy and colleagues (Bommi-Reddy et al., 2008). Inclusion of these kinases could have helped to make a better judgement of what range a differential effect on cell number between the isogenic cell line pairs can be expected.

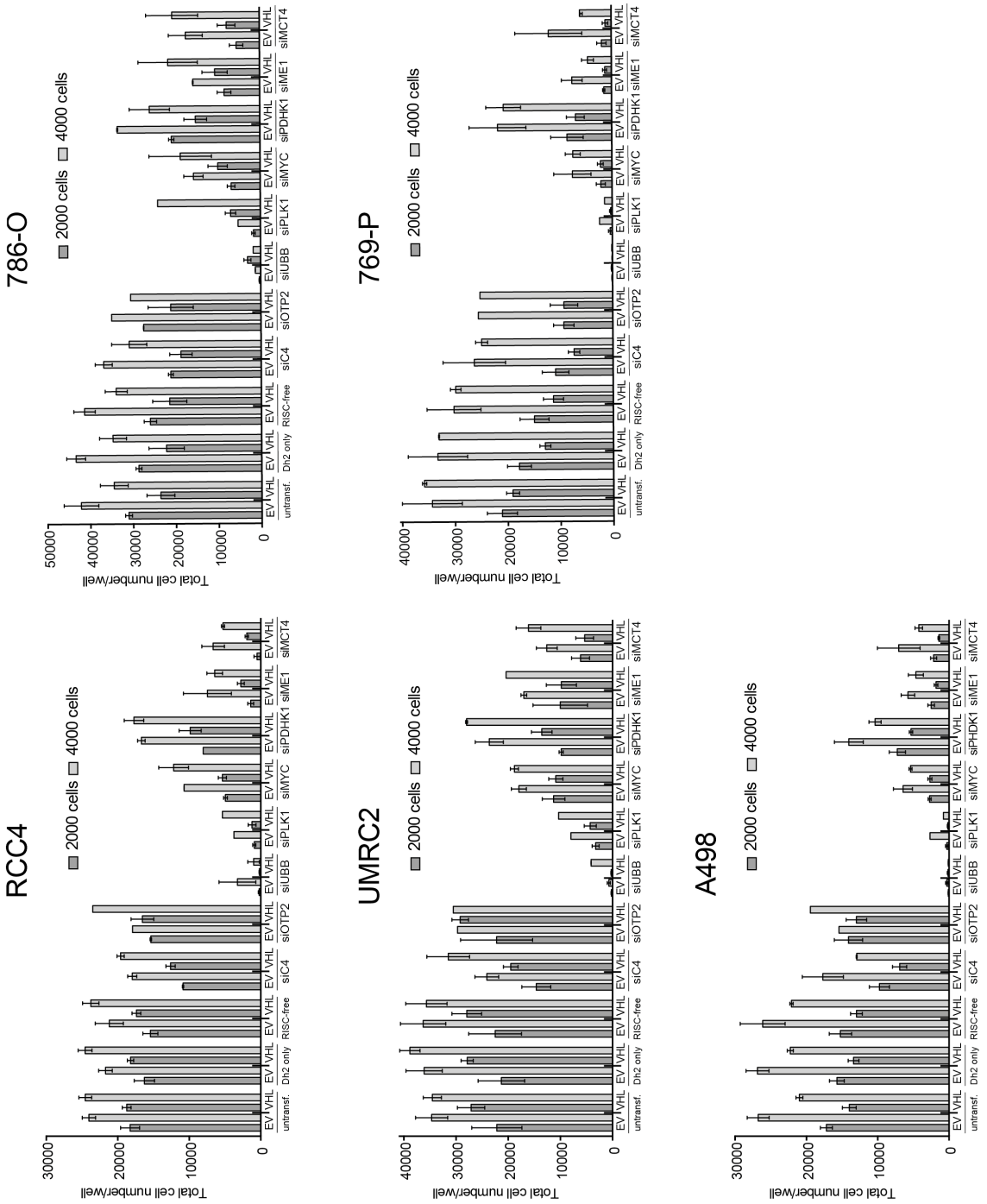
786-O
769-P
RCC4
UMRC2
A498
2000 cells
4000 cells
Total cell number/well
untransf.
Dh2 only
RISC-free
siC4
siOTP2
siUBB
siPLK1
siMYC
siPDHK1
siME1
siMCT4
EV
VHL

Figure 4.9: Summary of pilot screen
2000 or 4000 cells/well of the 5 *VHL*-isogenic ccRCC cell line pairs were reverse transfected with 37.5 nM siRNA SMARTpools targeting the indicated genes in a 96-well format. Cells were fixed 96 h post transfection, DAPI stained and analysed for cell number using an Acumen laser scanning microplate cytometer. Bars represent mean cell numbers of 3 independent experiments in triplicate wells each for 2000 cells/well seeding density and 2 independent experiments with triplicate wells each for 4000 cells/well seeding density with SEM as error bar. 2-way ANOVA (with Bonferroni multiple testing analysis) did not reveal any differential proliferation effect between pVHL-expressing and pVHL-null ccRCC cells for the four genes tested: c-MYC, PDHK1, ME1 and MCT4. Note: The different experiments were performed a) with different freezing batches and b) at different cell passages.

4.3 Functional metabolic siRNA screen of five pVHL-isogenic ccRCC cell line pairs

4.3.1 Screen setup and execution

In order to explore novel metabolic dependencies and regulations that are essential for cancer cell growth and survival, an siRNA library targeting 240 metabolic enzymes, regulators and nutrient transporters involved in central carbon metabolism was designed (Figure 4.10A) by a former postdoc in the lab, Dr Claudio Santos. This customised siRNA library was purchased from Dharmacon and the siRNA SMARTpools and controls are distributed over three 96-well plates. The plate layout is depicted in Figure 4.10B. The screen was performed in the 5 *VHL*-isogenic ccRCC cell lines in triplicate, resulting in a total of 90 assay plates that were processed in two batches. A detailed protocol for the screen execution can be found in Chapter 2: Materials and Methods. Figure 4.10C illustrates the screening process in a flow diagram.

A

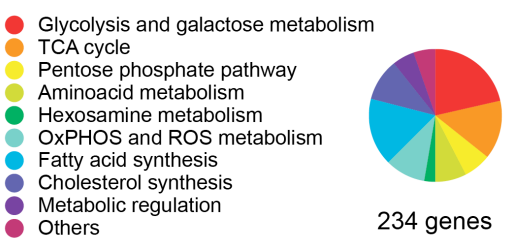

B

PLATE #1

	1	2	3	4	5	6	7	8	9	10	11	12
A	RISC-free	Control 1-4	HK1	HK-2	GCK	PKLR	PKM2	PC	PDHA1	PDHA2	PDHB	DLD
B	OTP1-4	PLK1	DLAT	ACACA	LDHA	LDHB	LDHC	CS	ACLY	G6PD	FASN	CHKA
C	Control 1-4	UBB	CHKB	HMGCS1	HMGCS2	HMGCR	SLC2A4	SLC2A1	SREBF1	SREBF2	PRKAA1	PRKAA2
D	OTP1-4	RIS-free	HIF1A	AKT1	AKT2	SKT3	ILVBL	PHGDH	MDH1	MDH2	GPD1	GPD2
E	Control 1-4	PLK1	PRPS1	PRPS2	PPAT	UMPS	SLC1A5	SLC7A5	PFKL	GAPDH	GAPDS	PGK1
F	RISC-free	UBB	PGK2	ENO1	IDH1	IDH2	OGDH	SDHA	SDHB	SDHC	SDHD	FH
G	UBB	RISC-free	CHPT1	MVK	PMVK	MVD	FDPS	GGPS1	LSS	DHCR7	PRKAG2	PRKAG3
H	OTP1-4	PLK1	PRKAB1	PRKAB2	PRKAG1	EPAS1	MT-ND1	MT-ND2	MT-ND3	MT-ND4	MT-ND5	MT-ND6

PLATE #2

	1	2	3	4	5	6	7	8	9	10	11	12
A	RISC-free	Control 1-4	GALK1	GALK2	GALT	PGM1	PGM3	GLUD1	GLUD2	HK3	GPI	PFKM
B	OTP1-4	PLK1	PFKP	PFKFB1	PFKFB2	PFKFB3	PFKFB4	ALDOA	ALDOB	ALDOC	TPI1	PGAM4
C	Control 1-4	UBB	PGAM1	PGAM2	BPGM	ENO2	ENO3	LDHAL6A	LDHAL6B	PDK3	PDK4	PPM2C
D	OTP1-4	RIS-free	PDP2	ACO1	ACO2	LOC441996	IDH3A	IDH3B	IDH3G	DLST	LOC283398	SUCLG2
E	Control 1-4	PLK1	SUCLG1	SUCLA2	GOT1	GOT2	SLC25A11	GPD1L	ME3	GLUL	GPT	GPT2
F	RISC-free	UBB	DDO	AGXT	AGXT2	PSAT1	CAD	ODC1	SHMT1	SHMT2	TKT	TKTL1
G	UBB	RISC-free	DKFZP434L1717	PGLS	H6PD	PGD	RPIA	PRPS1L1	GPAM	AGPAT1	AGPAT2	DKFZP586M1819
H	OTP1-4	PLK1	UNQ1849	AGPAT3	AGPAT4	PPAP2A	PPAP2C	PPAP2B	PCYT1A	PCYT1B	PLD1	PLD2

PLATE #3

	1	2	3	4	5	6	7	8	9	10	11	12
A	RISC-free	Control 1-4	ACAS2L	ACAS2	ACACB	MT	THEDC1	FLJ20604	ELOVL6	SCD	SCD5	ACAT1
B	OTP1-4	PLK1	ACAT2	AACS	IDI1	IDI2	FDFT1	SQLE	CYP51A1	NSDHL	HSD17B7	EBP
C	Control 1-4	UBB	SC5DL	DHCR24	SOD1	SOD2	SOD3	CAT	GPX6	GPX1	GPX2	GPX3
D	OTP1-4	RIS-free	GPX4	GPX5	GPX7	SCO2	ATPIF1	COX4I1	COX4I2	COX5A	C12ORF5	OXCT1
E	Control 1-4	PLK1	OXCT2	SLC16A7	SLC16A3	SLC16A8	SLC16A4	TALDO1	RPE	GFPT1	GFPT2	GNPNAT1
F	RISC-free	UBB	UAP1	OGT	PGM1	PGM3	WBSCR14	SLC25A10	ME1	ME2	GLS	GLS2
G	UBB	RISC-free	PIK3CA	MYLCD	Control1-4	Control1-4	no siRNA	IRS1	Control1-4	Control1-4	no siRNA	PTEN
H	OTP1-4	PLK1	MYC	RPTOR	RICTOR	SLC16A1	SLC25A1	PDK1	PDK2	CPT1A	CPT1B	AKT pooled

C

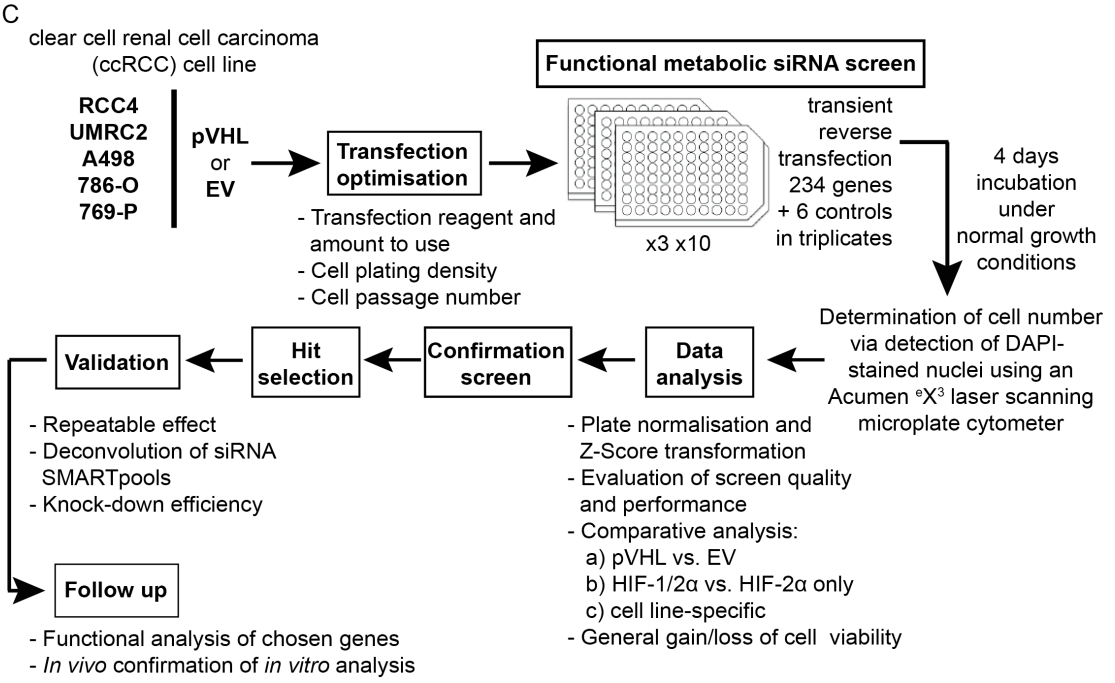

Figure 4.10: Screen Setup

(A) Overview of processes and relative distriburtion of the 240 genes targeted with the customised Dharmacon siGenome siRNA library. (B) Plate layout of the custom siRNA library. The 240 SMARTpools are distributed over three 96-well plates. Each plate additionally includes 16 wells with positive (blue) and negative (red) controls. (C) Flow diagram of the screening process performed in this study.

4.3.2 Normalisation of primary screen data

Comparison of data from different cell lines requires normalisation of raw screen results to exclude bias. This initial data analysis was performed by Dr. Rebecca Saunders (LRI High Throughput Screening Service) using the cellHTS2 software package (Bioconductor) (Boutros et al., 2006). Raw cell number values were first centred to the respective plate median including only the sample wells while excluding the 16 control wells. The plate median was chosen over the plate mean as the screen comprises of only a relatively small number of genes targeted and the latter would be more sensitive to outliers. Subsequently, a Z-Score transformation was applied to the plate-normalised cell numbers for each cell line. A Z-Score represents the number of standard deviations (SDs) that a given individual measurement differs from the population mean. In this screen, the Z-Score was calculated using the median absolute deviation (MAD) of the population. A Z-Score$_{(MAD)}$ value close to 0 indicates that the given measurement is very similar to the median of the population, a negative Z-Score value indicates a loss in cell number while a positive Z-Score$_{(MAD)}$ represents a gain in cell number compared to the population median. Z-Score$_{(MAD)}$ values $\leq$ -1.7 and $\geq$ 1.7 are considered to indicate significant effects on cell number compared to the population median. These Z-Score$_{(MAD)}$ values were used to define hits in the course of the screen data analysis.

4.3.3 Evaluation of screen quality

Following normalisation, the screen quality was evaluated. First, the plate medians of the individual replicates were compared to each other on a plate-by-plate basis using Spearman Rank Correlation to check for reproducibility of the effect within the experiment. The boxplots in Figure 4.11 illustrate the raw and Z-Score$_{(MAD)}$-transformed cell number value distributions (excluding positive and negative controls) for each plate and replicate for each of the ten cell lines. The associated table depicts the range of the calculated Spearman Rank Factors for each cell line and plate. A Spearman Rank Factor $\geq$ 0.65 is considered to indicate good correlation while smaller values are considered to indicate low or no correlation. The box plots and the Spearman Rank

Factors shown in Figure 4.11 indicate that reproducibility was good for the A498 and 769-P isogenic pairs, but only moderate for the other three cell line pairs.

Based on the relatively low Spearman Rank Factor for UMRC2 EV and RCC4 VHL, the screen was repeated for these two cell lines. The reproducibility of all 3 plates increased for RCC4 VHL (termed RCC4 VHL II from here onwards) but only of plate ♯1 for the UMRC2 EV cell line (further referred at as UMRC2 EV II) (Figure 4.11 bottom). For all further analyses, these repeat experiments were included as additional replicates.

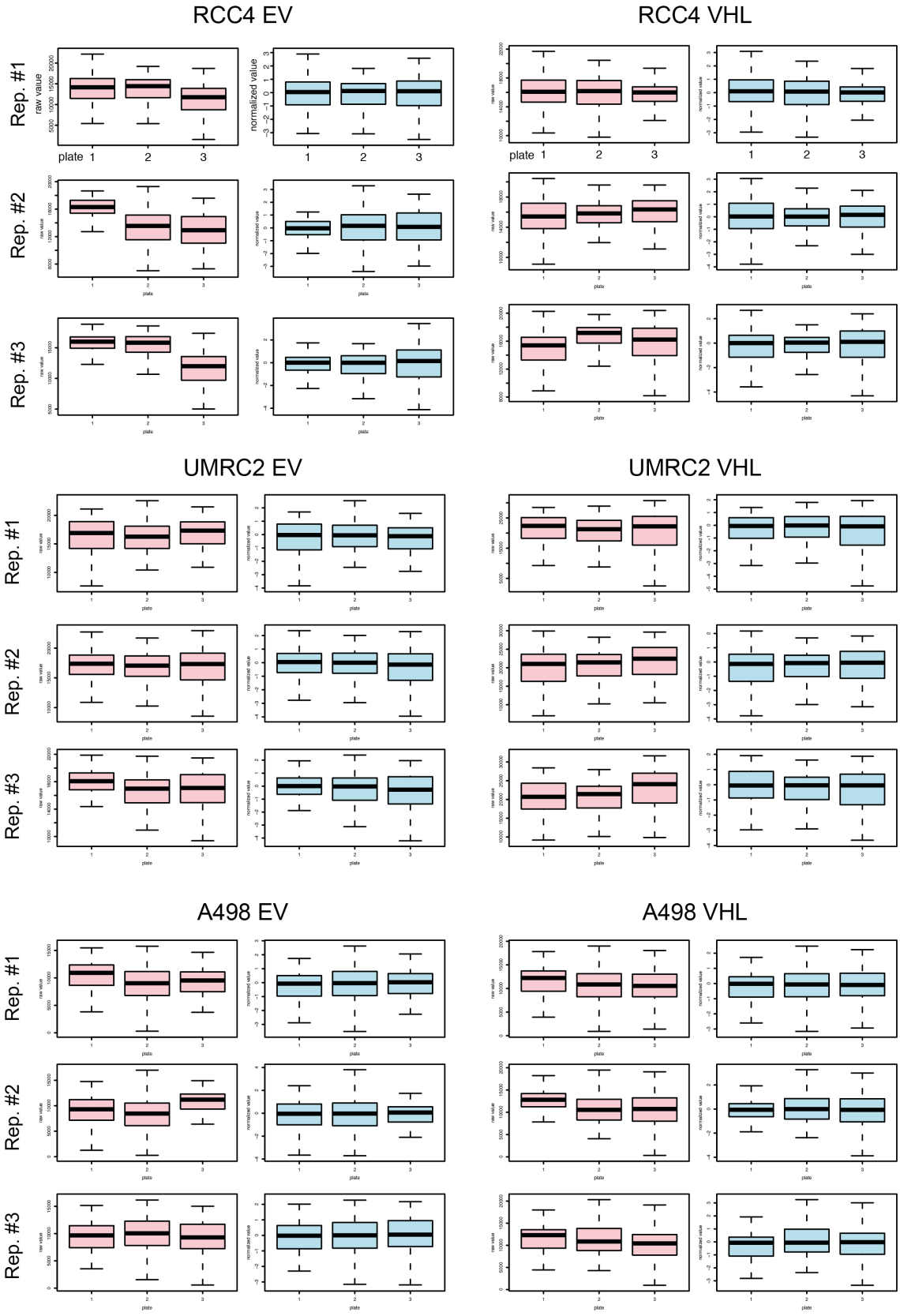
RCC4 EV
RCC4 VHL
UMRC2 EV
UMRC2 VHL
A498 EV
A498 VHL
Rep. #1
Rep. #2
Rep. #3
raw value
normalized value
plate

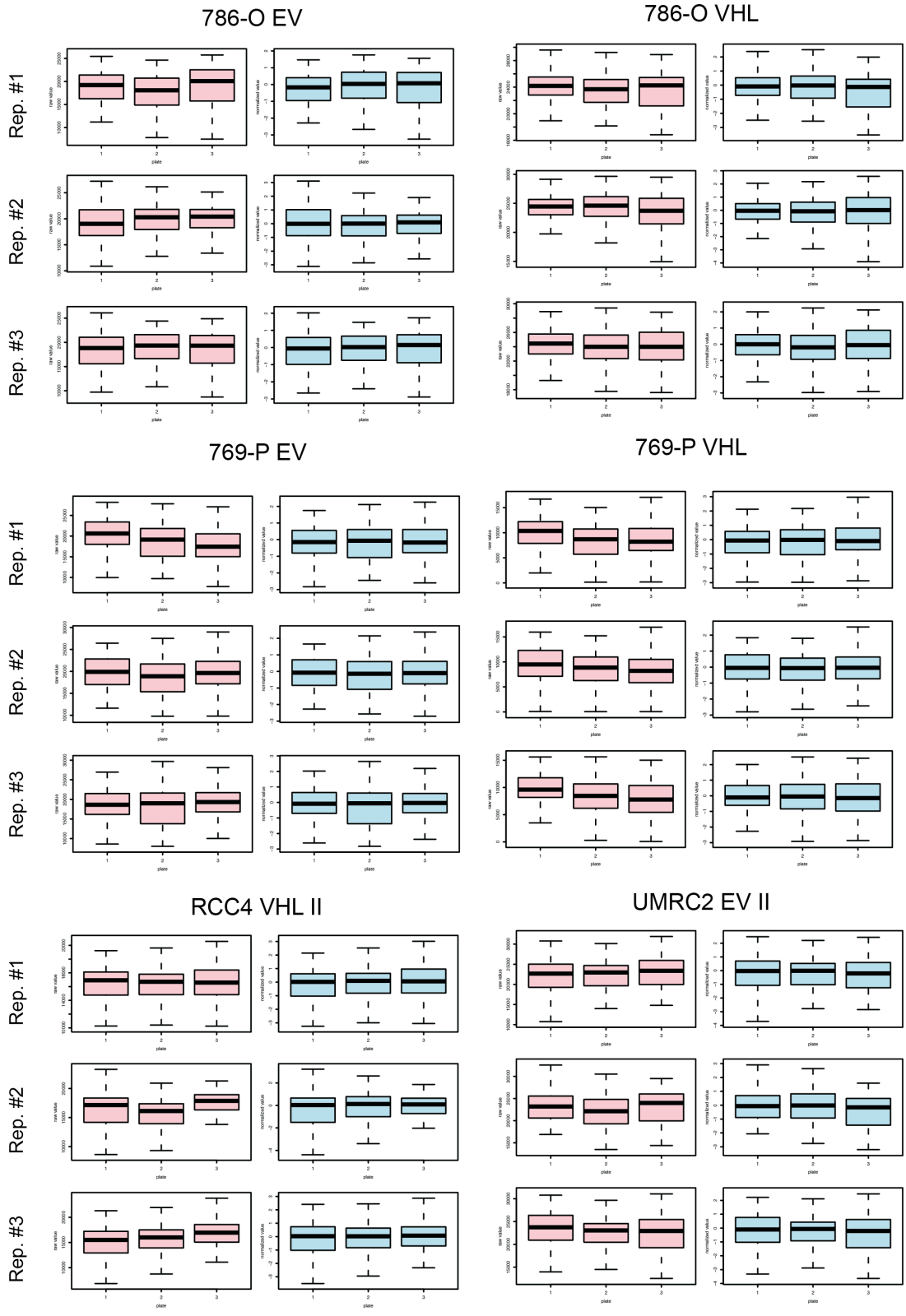

Range of Spearman Rank Correlation for replicates

	RCC4 EV	RCC4 VHL	RCC4 VHL II	UMRC2 EV	UMRC2 EV II	UMRC2 VHL	A498 EV	A498 VHL	786-O EV	786-O VHL	769-P EV	769-P VHL
plate #1	0.55 - 0.73	**0.76 - 0.83**	**0.73 - 0.81**	0.05 - 0.61	**0.66 - 0.77**	**0.8 - 0.86**	**0.81 - 0.85**	**0.7 - 0.89**	0.62 - 0.69	0.42 - 0.47	**0.85 - 0.88**	**0.83 - 0.86**
plate #2	**0.72 - 0.86**	0.64 - 0.74	**0.78 - 0.81**	0.61 - 0.67	0.59 - 0.64	**0.78 - 0.85**	**0.82 - 0.91**	**0.84 - 0.87**	**0.77 - 0.8**	0.55 - 0.77	**0.87 - 0.9**	**0.83 - 0.89**
plate #3	**0.81 - 0.84**	0.61 - 0.68	**0.66 - 0.9**	**0.65 - 0.77**	0.56 - 0.69	0.44 - 0.69	**0.86 - 0.93**	**0.87 - 0.91**	0.58 - 0.69	0.55 - 0.8	**0.84 - 0.89**	**0.7 - 0.78**

Figure 4.11: Overview of raw and Z-Score$_{(MAD)}$-normalised cell number values for each of the three replicates and plates

Boxplots represent the range of median raw (pink, respective left-hand panel) and Z-Score$_{(MAD)}$-normalised (blue, respective right-hand panel) sample cell numbers for each of the three plates for the screened cell lines. Error bars indicate cell number range. The table at the bottom of the figure summarises range of Spearman Correlation Factors obtained for each cell line when each of the three replicates of one plate was compared to each other replicate (comparison of normalised data). Values ≥ 0.7 are considered to represent good correlation and with that good reproducibility. Note: RCC4 VHL and UMRC2 EV cells were re-screened and the results were included in this Figure (RCC4 VHL II and UMRC2 EV II) and subsequent analyses.

Next, performance of positive and negative controls was evaluated. As can be seen from the graphs in Figure 4.12, the individual values for each control cluster together for most of the cell lines, indicating that variability in transfection efficiency was low. Also, apart from 786-O VHL and the RCC4 cell line pair, negative controls separated well away from the positive controls, indicating achievement of a good dynamic range in response to RNAi.

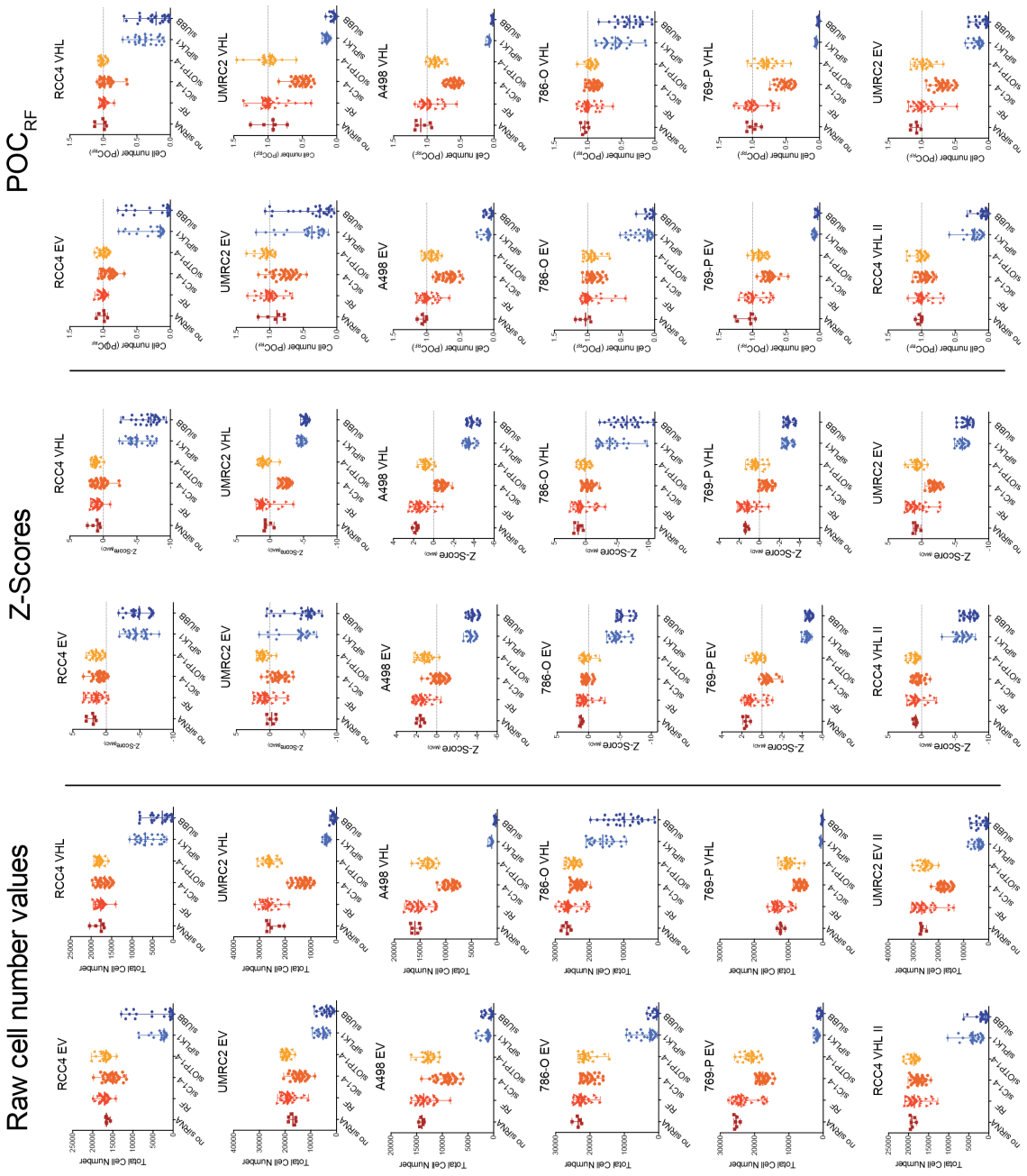

Figure 4.12: Performance of negative and positive controls in the screen

The scatterplots show raw, Z-Score$_{(MAD)}$-transformed and RISC-free-normalised (POC_{RF}) cell number values for all individual control wells, their median ± range. Controls from all plates are pooled. In most cases, positive controls (blue) separate well away from negative controls (red/orange/yellow). Note: RCC4 EV and UMRC2 VHL have twice as many data points as the repeated screen values were integrated in this analysis.

Finally, Figure 4.13 gives an overview of the variability of the individual replicates across the three screen plates for each cell line (excluding controls), while the histograms in Figure 4.14 show the distribution of the overall cell number Z-Scores$_{(MAD)}$ (including controls) for the individual cell lines.

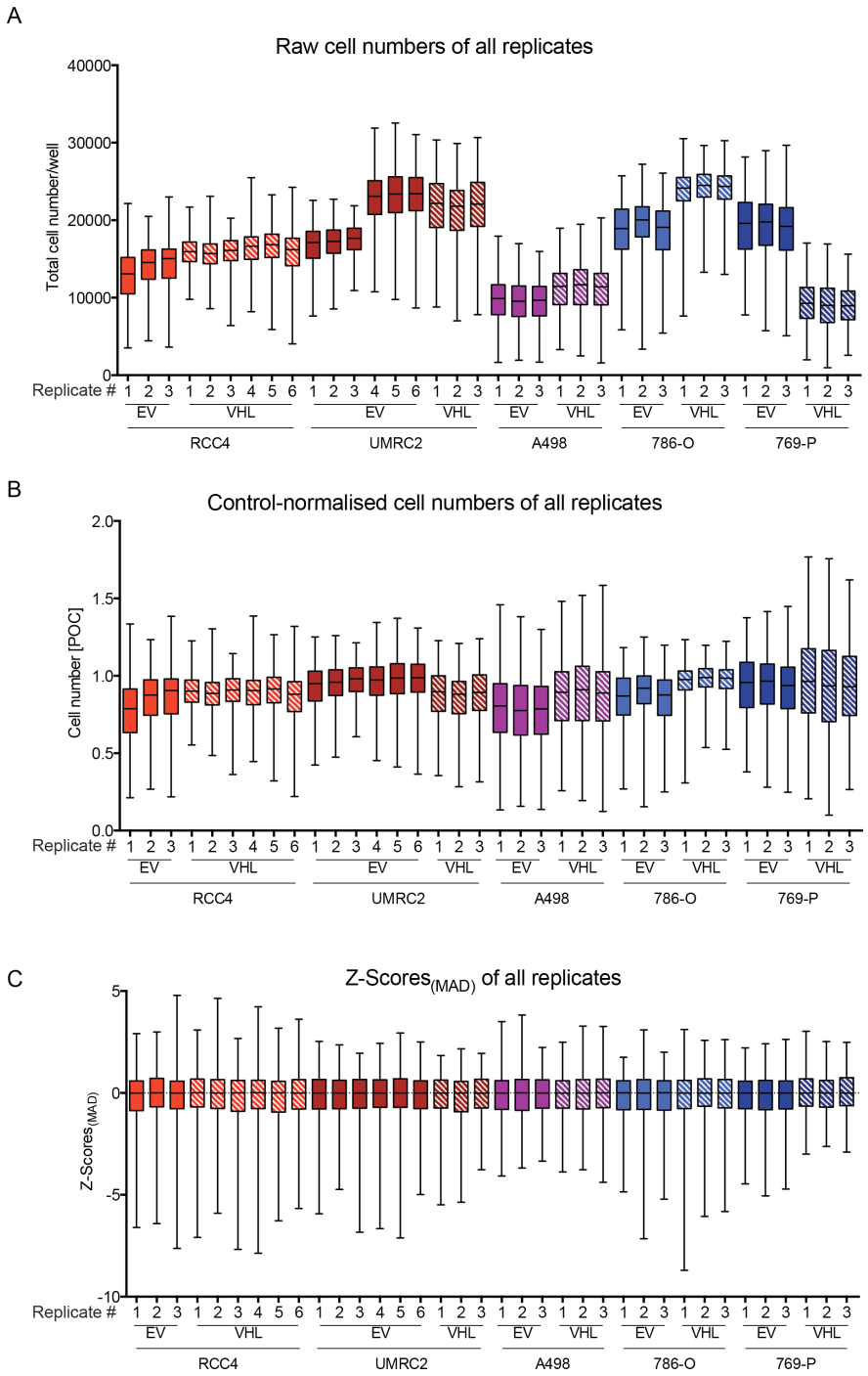

Figure 4.13: Profiles of individual replicates for isogenic ccRCC cell lines screened

Box plots represent raw (A), control-normalised (% of control, POC) (B) or Z-Score$_{(MAD)}$-transformed (C) cell number values excluding positive and negative controls.

786-O VHL
786-O EV
769-P VHL
769-P EV
UMRC2 EV II
RCC4 VHL II
RCC4 VHL
RCC4 EV
UMRC2 VHL
UMRC2 EV
A498 VHL
A498 EV
Frequency
Z-Score

Figure 4.14: Overview of Z-Score$_{(MAD)}$-distribution for the individual ccRCC cell lines
All replicate Z-Score$_{(MAD)}$ values for each cell line were used for the Z-Score$_{(MAD)}$ distribution analysis including positive and negative controls. Histograms were generated with GraphPad Prism 6.

In conclusion, evaluation of the screen quality implied the involvement of some technical issues during the screen execution process and it was advised to be cautious when interpreting the results. As a result, high stringency was applied during data analysis and the effects of potential hits were confirmed by independent validation experiments.

4.3.4 Analysis of screen results

Unsupervised clustering analysis was performed with the median Z-Scores$_{(MAD)}$ values (excluding controls) to see how the cell lines and genes tested relate to each other. The dendrogram in Figure 4.15 shows that the cell lines clustered as isogenic pairs rather than according to pVHL-status. Noticeably, UMRC2 cells clustered away from the other ccRCC cell line pairs, potentially as these cells are described as having polygonal rather than epithelial cell morphology (according to ATCC tissue bank). The siRNAs separated into two main clusters: cluster I comprises of siRNAs that have a negative effect on cell number. Sub-cluster IA contains siRNAs with the most detrimental effect across most cell lines. Cluster II consists of siRNAs that enhance cell viability with sub-cluster IIB having the strongest positive effect across most cell lines (Figure 4.15).

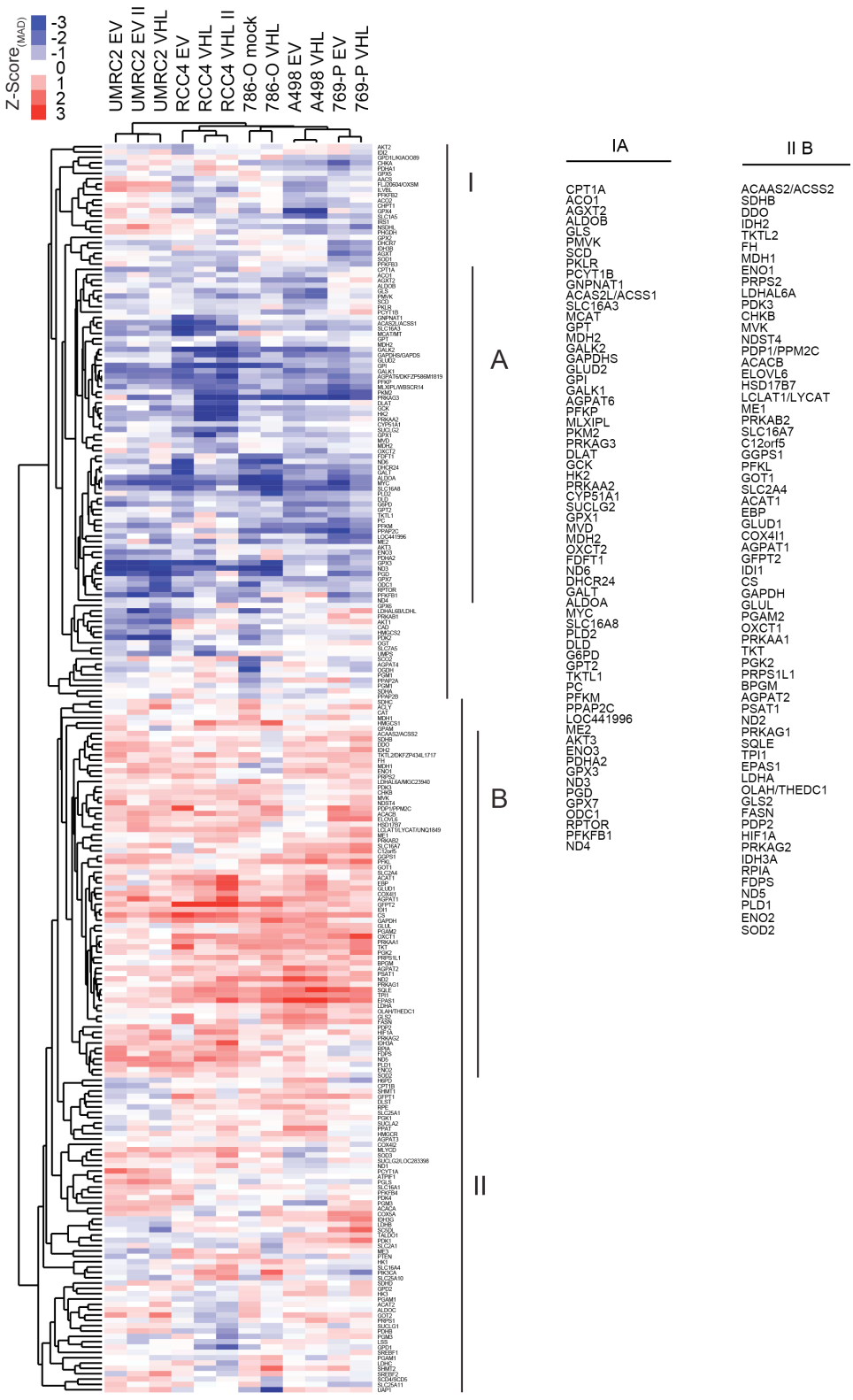

Figure 4.15: Unsupervised hierarchical cluster analysis of siRNA screen data

The median Z-Scores$_{(MAD)}$ of the three replicates for each cell line were subjected to an unsupervised clustering analysis using Cluster 3.0 and Java TreeView 1.1.6r2 software applications. The resulting heatmap revealed two main clusters: cluster IA, comprised of genes that had a negative effect on cell viability for most cell lines, while cluster IIB comprised of genes that had a positive effect on cell proliferation.

siRNAs that clustered in IA target genes within the glycolytic pathway (*ALDOA/B*, *GPI*, *PKM2*, *HK2*, *PFKM*, *ENO3*, *PFKFB1*, *PKLR*), the TCA cycle (*ACO1*, *MDH2*, *DLAT*, *SUCLG2*, *DLD*) and triacyl-glyceride / fatty acid and cholesterol biosynthesis (*AGPAT6*, *PPAP2C*, *SCD*, *MCAT*, *PMVK*, *CYP51A1*, *MVD*, *FDFT1*, *DHCR24*). Furthermore, this cluster also harbours siRNAs targeting members of the glutathione peroxidase (GPX) family (*GPX1*, *GPX3* and *GPX7*), subunits of the mitochondrial NADH dehydrogenase, which constitutes Complex I of the electron transport chain (ETC) (*MT-ND3*, *MT-ND4* and *MT-ND6*) and the transcription factor (TF) c-MYC (Figure 4.15).

Interestingly, sub-cluster IIB showed a similar representation of pathways affected as seen for sub-cluster IA. This may indicate that knocking down different isoforms of the same enzyme or ablating different enzymes within the same pathway can either result in loss of viability or enhanced cell survival/proliferation. In the glycolytic pathway, knocking down ENO1, ENO2, GAPDH or PFKL lead to cell number increase. The depletion of some proteins in the cholesterol biosynthesis pathway (MVK, HSD17B7, GGPS1, ACAT1, IDI1, SQLE, FDPS) also seemed to have an overall positive effect on cell numbers. Within the TCA cycle, it was siRNA against *SDHB*, *IDH2*, *IDH3B*, *FH*, *PDK3*, *CS*, *PDP1* and *PDP2* that seemrd to increase cell numbers. This cluster also included two other components of Complex I of the ETC, namely MT-ND2 and MT-ND5 as well as two isoforms of the HIF-α subunit, HIF-1α and HIF-2α/EPAS (Figure 4.15).

With regard to genes that had a general positive or negative effect on ccRCC cell viability, disturbance of glycolysis, the TCA cycle and triacyl-glyceride / fatty acid / cholesterol biosynthesis seemed to be the most effective.

4.3.5 Comparative analysis to detect *VHL*-synthetic lethality

To detect *VHL*-synthetic lethal genes, two approaches were taken. Firstly, a cell line specific approach for which the Z-Score$_{(MAD)}$-transformed data of the five isogenic cell line pairs were compared to each other individually. Correlation graphs for the isogenic cell line pairs are displayed in Figure 4.16. Tables listing genes that passed the threshold of Z-Score$_{(MAD)} \leq$ -1.7 are shown in Figure 4. 17 in ranked order.

A498 and 769-P isogenic cell line pairs showed good correlation ($R^2_{A498} = 0.87$ and $R^2_{769\text{-}P} = 0.72$) (Figure 4.16), indicating that reintroduction of a wt *VHL* gene has no major effect on their sensitivity towards ablation of metabolic genes. Nevertheless, some siRNAs showed differential effects depending on VHL status in these cells. In particular, A498-EV cells were sensitive to ablation of GAPDHS, TKTL1 and DHCR24, while A498-VHL cells showed reduced proliferation after silencing of *GLS*, *AGXT2*, *ME2* and *PKM2*. For 769-P-EV cells, silencing of *c-MYC*, *CHLA*, *AGXT*, *PGD*, *PFKM*, *PFKFB1*, *PC*, *AGPAT6*, *GALK2*, *GALT*, *DHCR7*, *G6PD* or *PFKP* had a strong negative effect on cell proliferation, while NSDHL and SLC25A10 were essential to 769-P-VHL cells (Figure 4.17). An effect was called differential when a significant reduction in cell number was observed in one cell line for each pair, while the effect in the isogenic counterpart was either not significant or the difference between the two effects was ≥ 0.2.

The RCC4, UMRC2 and 786-O cell line pairs diverged in their response to RNAi-mediated gene silencing as their R^2 correlation values were low (Figure 4.16). However, these pairs did not show many *VHL*-dependent differential effects. In the case of RCC4, which displayed the strongest diversity, pVHL-null cells were sensitive to depletion of GALT, ND6, DHCR24, GNPNAT1, PFKFB1, PGD, ALDOA and GPX4. RCC4 pVHL-expressing cells showed reduced cell numbers after silencing of *HK2*, *PRKAA2*, *GCK*, *PRKAG3*, *GAPDHS*, *DLAT*, *PKM2* and *MLXIPL*. UMRC2 cells lacking pVHL were sensitive to depletion of PFKFB1 and ENO3, while UMRC2 pVHL-expressing cells required ODC1, GPX7, PRKAB1, GCK, ME2 and IDH3G. Finally, for 786-O cells, silencing of *PGM1*, *ODC1*, *CAD*, *AGPAT4*, *OGDH*, *DHCR24*, *ME2*, *UMPS*, *GAPDHS* and *PFKFB1* negatively affected proliferation only for pVHL-null cells, while depletion of UAP1, PLD2, GALT, GALK2 and PC reduced proliferation of pVHL-expressing cells (Figure 4.17).

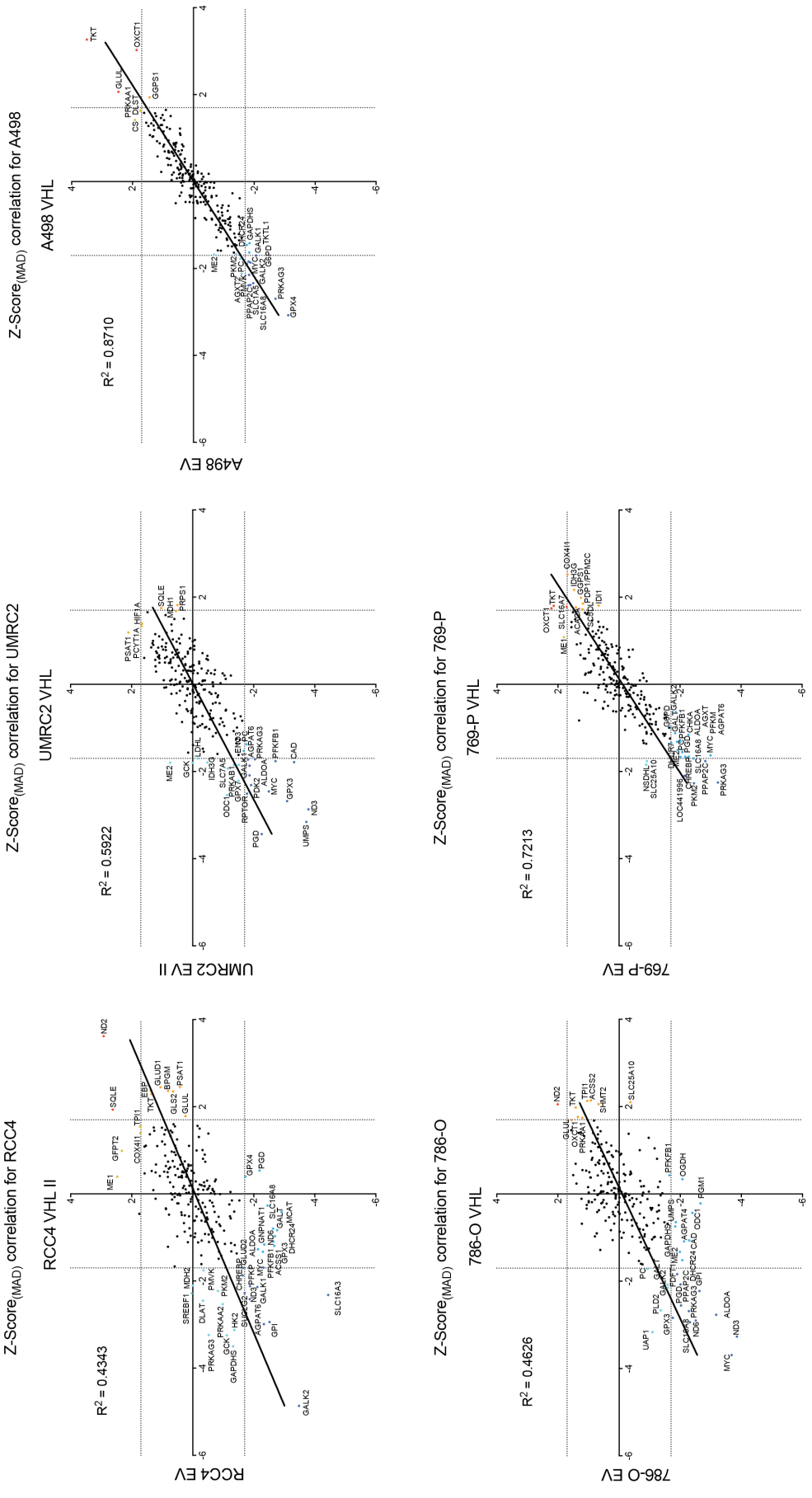
Z-Score(MAD) correlation for A498
A498 VHL
A498 EV
R2 = 0.8710
Z-Score(MAD) correlation for UMRC2
UMRC2 VHL
UMRC2 EV II
R2 = 0.5922
Z-Score(MAD) correlation for 769-P
769-P VHL
769-P EV
R2 = 0.7213
Z-Score(MAD) correlation for RCC4
RCC4 VHL II
RCC4 EV
R2 = 0.4343
Z-Score(MAD) correlation for 786-O
786-O VHL
786-O EV
R2 = 0.4626

Figure 4.16: Correlation of Z-Scores$_{(MAD)}$ for each of the 5 isogenic ccRCC cell line pairs
Median Z-Scores$_{(MAD)}$ of the three replicates for each cell line pair were plotted against each other and a Spearman Correlation analysis was performed. R^2 values for each cell line pair correlation is given. A cut-off of Z-Score$_{(MAD)} \leq -1.7$ and ≥ 1.7 was set to define genes having a significant reduction in cell number. Highlighted in blue are genes that when silenced resulted in loss of viability; highlighted in orange are siRNA-targeted genes that resulted in a cell number gain according to the set cut-off.

A small number of siRNAs showed a selective effect in more than one isogenic cell line pair. Depletion of DHCR24 for example had a strong negative effect on viability of RCC4, A498 and 786-O pVHL-null cells but not in their pVHL-expressing counterparts. Similar effects were observed for PFKFB1 in RCC4, UMRC2, 786-O and 769-P pVHL-null cell lines. Some siRNAs, such as siME2, had a specific negative effect in the UMRC2 and A498 *VHL*-reconstituted cell lines but also in 786-O pVHL-null cells and in both 769-P cell lines (Figure 4.17). In these cases, genes were not considered as differential hits.

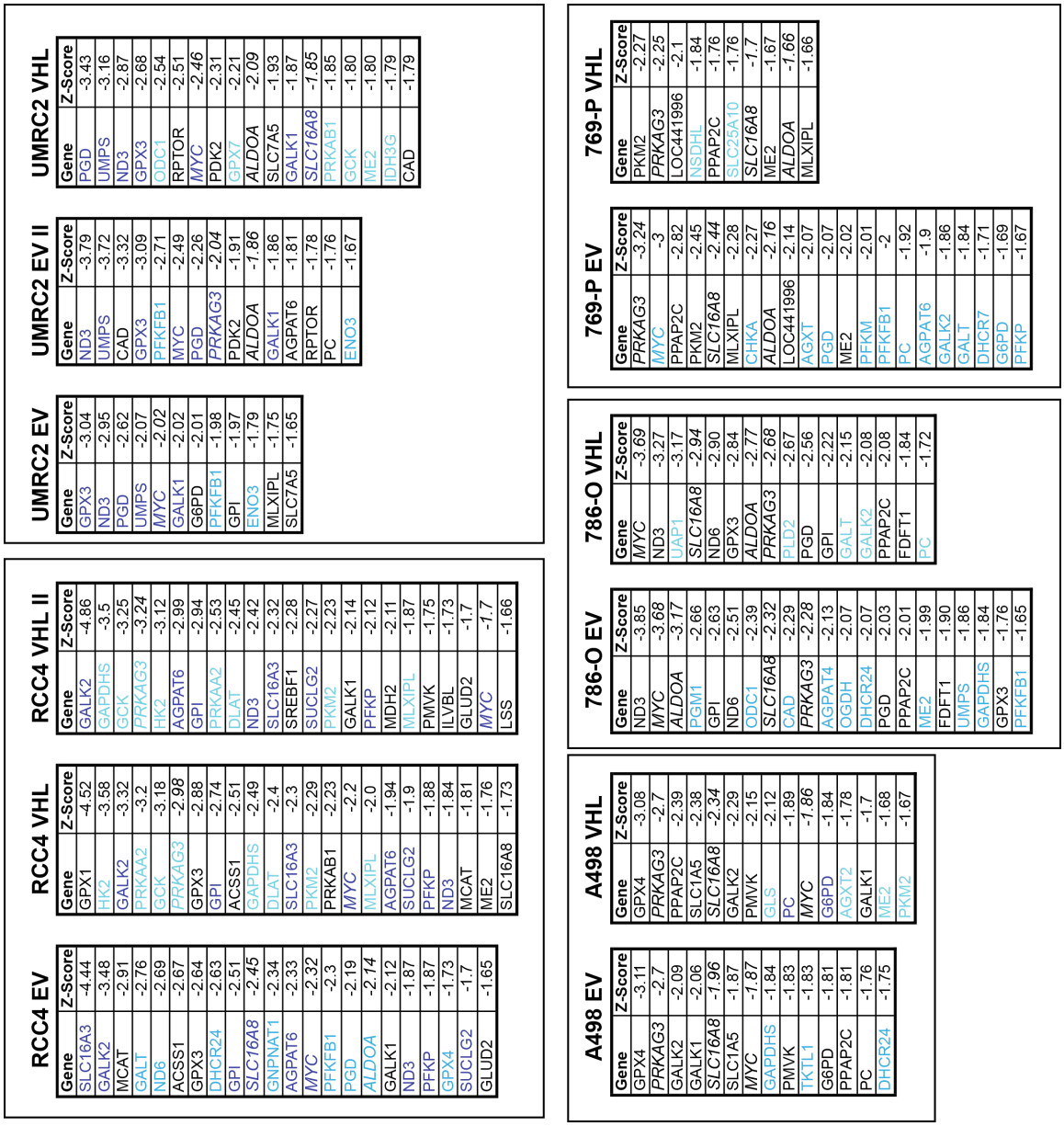

RCC4 EV	
Gene	Z-Score
SLC16A3	-4.44
GALK2	-3.48
MCAT	-2.91
GALT	-2.76
ND6	-2.69
ACSS1	-2.67
GPX3	-2.64
DHCR24	-2.63
GPI	-2.51
SLC16A8	*-2.45*
GNPNAT1	-2.34
AGPAT6	-2.33
MYC	*-2.32*
PFKFB1	-2.3
PGD	-2.19
ALDOA	*-2.14*
GALK1	-2.12
ND3	-1.87
PFKP	-1.87
GPX4	-1.73
SUCLG2	-1.7
GLUD2	-1.65

RCC4 VHL	
Gene	Z-Score
GPX1	-4.52
HK2	-3.58
GALK2	-3.32
PRKAA2	-3.2
GCK	-3.18
PRKAG3	*-2.98*
GPX3	-2.88
GPI	-2.74
ACSS1	-2.51
GAPDHS	-2.49
DLAT	-2.4
SLC16A3	-2.3
PKM2	-2.29
PRKAB1	-2.23
MYC	*-2.2*
MLXIPL	-2.0
AGPAT6	-1.94
SUCLG2	-1.9
PFKP	-1.88
ND3	-1.84
MCAT	-1.81
ME2	-1.76
SLC16A8	-1.73

RCC4 VHL II	
Gene	Z-Score
GALK2	-4.86
GAPDHS	-3.5
GCK	-3.25
PRKAG3	*-3.24*
HK2	-3.12
AGPAT6	-2.99
GPI	-2.94
PRKAA2	-2.53
DLAT	-2.45
ND3	-2.42
SLC16A3	-2.32
SREBF1	-2.28
SUCLG2	-2.27
PKM2	-2.23
GALK1	-2.14
PFKP	-2.12
MDH2	-2.11
MLXIPL	-1.87
PMVK	-1.75
ILVBL	-1.73
GLUD2	-1.7
MYC	*-1.7*
LSS	-1.66

A498 EV	
Gene	Z-Score
GPX4	-3.11
PRKAG3	*-2.7*
GALK2	-2.09
GALK1	-2.06
SLC16A8	*-1.96*
SLC1A5	-1.87
MYC	*-1.87*
GAPDHS	-1.84
PMVK	-1.83
TKTL1	-1.83
G6PD	-1.81
PPAP2C	-1.81
PC	-1.76
DHCR24	-1.75

A498 VHL	
Gene	Z-Score
GPX4	-3.08
PRKAG3	*-2.7*
PPAP2C	-2.39
SLC1A5	-2.38
SLC16A8	*-2.34*
GALK2	-2.29
PMVK	-2.15
GLS	-2.12
PC	-1.89
MYC	*-1.86*
G6PD	-1.84
AGXT2	-1.78
GALK1	-1.7
ME2	-1.68
PKM2	-1.67

UMRC2 EV	
Gene	Z-Score
GPX3	-3.04
ND3	-2.95
PGD	-2.62
UMPS	-2.07
MYC	*-2.02*
GALK1	-2.02
G6PD	-2.01
PFKFB1	-1.98
GPI	-1.97
ENO3	-1.79
MLXIPL	-1.75
SLC7A5	-1.65

UMRC2 EV II	
Gene	Z-Score
ND3	-3.79
UMPS	-3.72
CAD	-3.32
GPX3	-3.09
PFKFB1	-2.71
MYC	-2.49
PGD	-2.26
PRKAG3	*-2.04*
PDK2	-1.91
ALDOA	*-1.86*
GALK1	-1.86
AGPAT6	-1.81
RPTOR	-1.78
PC	-1.76
ENO3	-1.67

UMRC2 VHL	
Gene	Z-Score
PGD	-3.43
UMPS	-3.16
ND3	-2.87
GPX3	-2.68
ODC1	-2.54
RPTOR	-2.51
MYC	*-2.46*
PDK2	-2.31
GPX7	-2.21
ALDOA	*-2.09*
SLC7A5	-1.93
GALK1	-1.87
SLC16A8	*-1.85*
PRKAB1	-1.85
GCK	-1.80
ME2	-1.80
IDH3G	-1.79
CAD	-1.79

786-O EV	
Gene	Z-Score
ND3	-3.85
MYC	*-3.68*
ALDOA	*-3.17*
PGM1	-2.66
GPI	-2.63
ND6	-2.51
ODC1	-2.39
SLC16A8	*-2.32*
CAD	-2.29
PRKAG3	*-2.28*
AGPAT4	-2.13
OGDH	-2.07
DHCR24	-2.07
PGD	-2.03
PPAP2C	-2.01
ME2	-1.99
FDFT1	-1.90
UMPS	-1.86
GAPDHS	-1.84
GPX3	-1.76
PFKFB1	-1.65

786-O VHL	
Gene	Z-Score
MYC	*-3.69*
ND3	-3.27
UAP1	-3.17
SLC16A8	*-2.94*
ND6	-2.90
GPX3	-2.84
ALDOA	*-2.77*
PRKAG3	*-2.68*
PLD2	-2.67
PGD	-2.56
GPI	-2.22
GALT	-2.15
GALK2	-2.08
PPAP2C	-2.08
FDFT1	-1.84
PC	-1.72

769-P EV	
Gene	Z-Score
PRKAG3	*-3.24*
MYC	*-3*
PPAP2C	-2.82
PKM2	-2.45
SLC16A8	*-2.44*
MLXIPL	-2.28
CHKA	-2.27
ALDOA	*-2.16*
LOC441996	-2.14
AGXT	-2.07
PGD	-2.07
ME2	-2.02
PFKM	-2.01
PFKFB1	-2
PC	-1.92
AGPAT6	-1.9
GALK2	-1.86
GALT	-1.84
DHCR7	-1.71
G6PD	-1.69
PFKP	-1.67

769-P VHL	
Gene	Z-Score
PKM2	-2.27
PRKAG3	*-2.25*
LOC441996	-2.1
NSDHL	-1.84
PPAP2C	-1.76
SLC25A10	-1.76
SLC16A8	*-1.7*
ME2	-1.67
ALDOA	*-1.66*
MLXIPL	-1.66

Figure 4.17: Summary of cell line-specific siRNAs with negative effect on cell viability
Tables summarising siRNA-targeted genes that showed cell number loss with Z-Score$_{(MAD)}$ ≤ -1.7. Highlighted in bright blue are genes that when silenced have a significant negative effect exclusively in the EV or in the VHL cell line of the respective isogenic cell line pairs, Highlighted in dark blue are genes that have overlapping negative effects in the repeated RCC4 VHL and UMRC2 EV sample sets. Knockdown of c-MYC, SLC16A8 and PRKAG3 (italic labelling) are detrimental for most of the cell lines tested.

As second approach, data from all five pVHL-null cell lines and all five *VHL*-reconstituted cell lines were pooled and their median Z-Scores$_{(MAD)}$ were compared in order to investigate potential global *VHL*-dependent effects on ccRCC cell survival (Figure 4.18). Surprisingly, the list of siRNAs negatively regulating ccRCC cell viability was relatively short. siRNA-mediated gene silencing showed a consistent selective negative effect on cell number only for six genes, namely *PGD*, *ALDOA*, *PFKFB1*, *GALK1*, *GPI* and *AGPAT6* in pVHL-null ccRCC cells. In contrast, siRNAs targeting *PKM2*, *ME2* and *MLXIPL*, were identified to have a selective detrimental effect on pVHL-reconstituted cell lines.

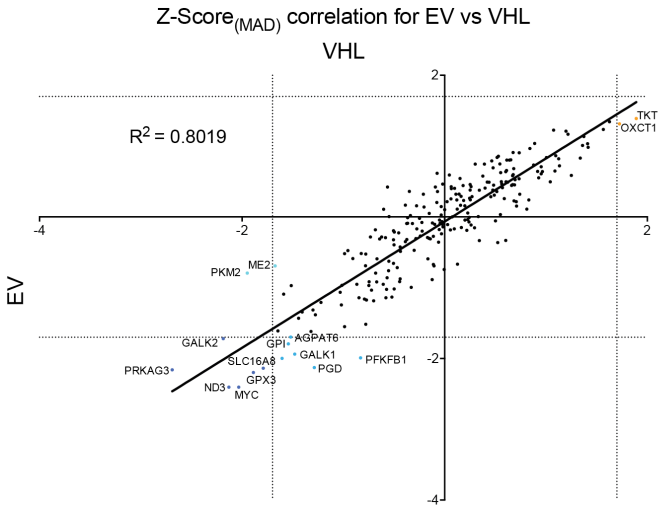

EV

Gene	Z-Score
ND3	-2.41
MYC	-2.41
GPX3	-2.20
PRKAG3	-2.16
SLC16A8	-2.14
PGD	-2.13
ALDOA	-2.00
PFKFB1	-1.99
GALK1	-1.94
GPI	-1.79
GALK2	-1.72
AGPAT6	-1.70

VHL

Gene	Z-Score
PRKAG3	-2.69
GALK2	-2.19
ND3	-2.13
MYC	-2.03
PKM2	-1.95
GPX3	-1.89
SLC16A8	-1.79
ME2	-1.67
MLXIPL	-1.65

Figure 4.18: Correlation of Z-Scores$_{(MAD)}$ with respect to pVHL-status
Median Z-Score$_{(MAD)}$ from all pVHL-null and all *VHL*-reconstituted cell lines were plotted against each other. Highlighted in blue are genes that when silenced resulted in loss of viability; highlighted in orange are siRNA-targeted genes that resulted in a cell number gain according to the set cut-off (Z-Score$_{(MAD)} \leq$ -1.7). The associated tables list siRNAs that had a strong global negative effect on either EV or VHL cells. Highlighted in bright blue / turquoise are EV / VHL specific genes.

4.3.6 Comparative analysis to detect HIF-α isoform-specific correlations

As the screened cell line panel consists of cell lines showing variations in HIF-α isoform expression, the screen data was also analysed with regard to correlation of cell number loss with HIF-α status. RCC4 and UMRC2 cells express both HIF-1α and HIF-2α, while 786-O and 769-P express only HIF-2α. A498 cells were excluded from this analysis as they express only a truncated form of HIF-1α and HIF-2α (see Figure 3.3).

Median cell number Z-Scores$_{(MAD)}$ of RCC4 and UMRC2 pVHL-null cells were pooled and plotted against the median cell number Z-Scores$_{(MAD)}$ of 786-O and 769-P pVHL-null cells (Figure 4.19). A differential hit was defined as showing a significant reduction in cell number (Z-Score$_{(MAD)}$ ≤ -1.7) in one condition (HIF-1/2α) but not in the other (HIF-2α). A substantial number of siRNAs showed HIF-2α-specific cell number loss without affect HIF-1/2α-expressing cells. These siRNAs targeted PRKAG3, PPAP2C, SLC16A8, ME2, MLXPL, DHCR24, GALK2, CHKA, LOC441996, GALT, ND6 and ODC1. In contrast, only five genes seemd to be essential for HIF-1/2α expressing cell lines: *GPX3*, *UMPS*, *GALK1*, *AGPAT6* and *ENO3*.

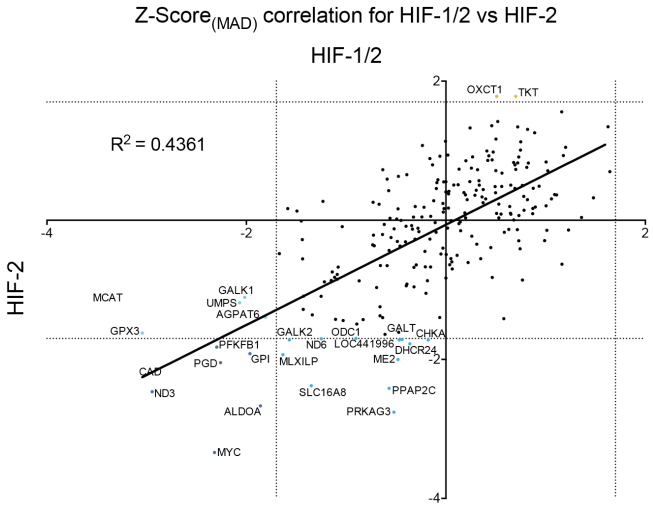

HIF-1/2

Gene	Z-Score
GPX3	-3.04
ND3	-2.95
MYC	-2.32
PFKFB1	-2.30
PGD	-2.26
UMPS	-2.07
GALK1	-2.02
GPI	-1.97
ALDOA	-1.86
AGPAT6	-1.81
ENO3	-1.67

HIF-2

Gene	Z-Score
MYC	-3.34
PRKAG3	-2.76
ALDOA	-2.67
ND3	-2.47
PPAP2C	-2.42
SLC16A8	-2.38
PGD	-2.05
ME2	-2.00
MLXIPL	-1.93
GPI	-1.92
PFKFB1	-1.82
DHCR24	-1.78
GALK2	-1.72
CHKA	-1.72
LOC441996	-1.72
GALT	-1.72
ND6	-1.70
ODC1	-1.70

Figure 4.19: Correlation of Z-Scores$_{(MAD)}$ with respect to HIF-α-isoform expression
Replicate Z-Scores$_{(MAD)}$ of RCC4 and UMRC2 pVHL-null cells were pooled for the HIF-1/2α set and replicate Z-Scores$_{(MAD)}$ of 786-O and 769-P cells were pooled for the HIF-2α set. The respective medians were plotted against each other. Highlighted in blue are genes that when silenced resulted in loss of viability; highlighted in orange are siRNA-targeted genes that resulted in a cell number gain according to the set cut-off (Z-Score$_{(MAD)}$ ≤ -1.7). The associated tables list siRNas that had a strong negative effect (Z-Score ≤ -1.7) on either HIF-1/2α- or HIF-2α-expressing cells. Highlighted in turquoise / bright blue are HIF-1/2α- / HIF-2α-specific genes.

Several of the genes that came up in this differential analysis had been previously identified in the other pVHL-comparative analyses (Figure 4.16 - 4.18). None of the siRNAs identified as differential killers, affected exclusively pVHL-null cells and only the siRNA pool targeting the muscle-specific isoform of pyruvate kinase, PKM2, which catalyses the final step in glycolysis, effectively killed only pVHL-harbouring cells making it a pVHL-specific hit (Figure 4.20). HIF-2α-expressing cells seemed to be

particular sensitive to siRNA-mediated gene silencing as targeting *CHKA*, *DHCR24*, *GALT*, *LOC441996*, *ND6*, *ODC1* and *PPAP2C* turned out to be detrimental for this cell population. Ablation of the glycolytic enzyme enolase 3 (ENO3) and the pentose phosphate pathway enzyme UMPS on the other hand were detrimental specifically for HIF-1/2α-expressing cells (Figure 4.20). Finally, all four pools were sensitive to depletion of the transcription factor c-MYC and the Complex I component MT-ND3 making these siRNAs the over all strongest killers.

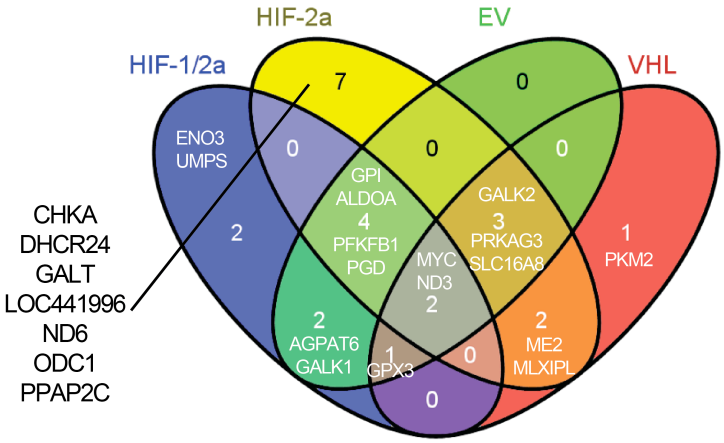

Figure 4.20: Overlap of negative Z-Score$_{(MAD)}$ when comparing pVHL- and HIF-α-isoform-specific hits
Venn diagram visualising the overlap or distinctiveness of siRNAs targeting the indicated genes that have strong negative effects in one or more of the analysed pooled populations. Illustration was produced using the online tool venny (http://bioinfogp.cnb.csic.es/tools/venny/index.html).

4.3.7 Validation screen of selected genes

To test the validity and reproducibility of the differential targets identified in the screen, a series of validation experiments was performed. Table 4.1 summarises the genes tested for knockdown and the results obtained. Due to the smaller number of siRNAs used for this validation screen, it was not feasible to perform a Z-Score analysis. Thus, cell numbers after siRNA-mediated gene silencing were normalised to the respective negative control (RISC-free). The cut-off for strong negative effects was set stringently to ≤ 0.5 % of control (POC_{RF}). The overall effects of gene silencing in these validation experiments were much stronger compared to the initial screen. Silencing of many of the genes tested decreased cell numbers substantially in most of the cell lines (Table 4.1).

Gene	RCC4		UMRC2		A498		786-O		769-P	
	EV	VHL	EV	VHL	EV	VHL	EV	VHL	EV	VHL
ACO1	0.48	0.62	0.52	0.68	0.24	0.32	0.22	0.47	0.67	0.71
ACO2	0.64	0.50	0.86	0.86	0.31	0.29	0.71	0.75	0.47	0.60
AGPAT4	0.20	0.47	0.53	0.57	0.51	0.54	0.19	0.26	0.30	0.54
AKT1	0.50	0.63	0.32	0.46	0.43	0.52	0.51	0.79	0.53	0.56
AKT2	0.43	0.37	0.42	0.58	0.40	0.48	0.25	0.28	0.39	0.39
ALDOA	0.60	0.53	0.61	0.76	0.60	0.43	0.31	0.33	0.49	0.47
ALDOB	0.58	0.60	0.83	0.64	0.44	0.49	0.42	0.52	0.88	0.78
CAD	0.59	0.62	0.62	0.64	0.64	0.63	0.48	0.54	0.90	0.91
CHKA	0.30	0.53	0.57	0.91	0.67	0.61	0.48	0.56	0.13	0.41
CHPT1	0.20	0.25	0.16	0.57	0.25	0.36	0.03	0.14	0.21	0.30
CPT1A	0.59	0.46	0.53	0.58	0.50	0.52	0.64	0.69	0.70	0.71
DHCR24	0.14	0.15	0.27	0.26	0.11	0.09	0.08	0.15	0.09	0.08
DHCR7	0.57	0.38	0.52	0.48	0.66	0.54	0.99	0.56	0.28	0.28
FDFT1	0.63	0.73	0.84	0.95	0.74	0.89	0.51	0.50	0.69	0.60
G6PD	0.61	0.75	0.77	0.81	0.40	0.34	0.64	0.76	0.61	0.74
GALK1	0.76	0.61	0.64	0.66	0.45	0.30	0.72	0.71	0.71	0.65
GALK2	0.60	0.48	0.73	0.84	0.44	0.28	0.34	0.50	0.59	0.72
GALT	0.20	0.39	0.49	0.51	0.56	0.73	0.33	0.29	0.12	0.33
GLS	0.48	0.41	0.53	0.76	0.27	0.29	0.32	0.49	0.39	0.45
GLS2	0.49	0.80	0.69	0.76	0.62	0.71	0.46	0.59	0.08	0.37
GLUL	0.62	0.77	0.58	0.75	0.97	0.96	0.74	1.07	0.52	0.69
GPI	0.11	0.12	0.10	0.07	0.13	0.15	0.07	0.12	0.07	0.13
GPX1	0.34	0.15	0.46	0.68	0.44	0.49	0.32	0.35	0.29	0.29
GPX3	0.21	0.32	0.32	0.24	0.40	0.43	0.32	0.34	0.22	0.29
GPX4	0.51	0.23	0.81	0.88	0.09	0.17	0.02	0.65	0.38	0.37
HMGCS2	0.20	0.20	0.22	0.15	0.22	0.33	0.09	0.30	0.13	0.08
IDH3B	0.25	0.50	0.59	0.61	0.66	0.74	0.60	0.31	0.20	0.33
ILVBL	0.21	0.29	0.61	0.84	0.45	0.46	0.42	0.49	0.52	0.44
LOC441996	0.73	0.69	0.71	0.67	0.54	0.60	0.12	0.18	0.30	0.53
MCAT	0.23	0.40	0.38	0.58	0.66	0.73	0.51	0.60	0.35	0.48
MDH2	0.48	0.48	0.50	0.64	0.51	0.56	0.45	0.53	0.51	0.51
ME1	0.25	0.24	0.43	0.42	0.33	0.36	0.29	0.45	0.45	0.56
ME2	0.50	0.59	0.84	0.77	0.48	0.34	0.22	0.25	0.42	0.28
MVD	0.53	0.48	0.46	0.56	0.37	0.34	0.58	0.58	0.38	0.51
MYC	0.58	0.47	0.64	0.54	0.34	0.28	0.18	0.45	0.39	0.35
NSDHL	0.43	0.58	0.61	0.84	0.62	0.40	0.57	0.34	0.22	0.36
OGDH	0.88	0.73	0.72	0.82	0.84	0.91	0.65	0.71	0.83	0.78
OGT	0.51	0.71	0.39	0.63	0.54	0.60	0.61	0.66	0.43	0.45
OXCT1	0.56	0.93	0.75	1.15	1.04	1.32	1.05	0.70	0.96	0.98
OXCT2	0.35	0.27	0.72	0.71	0.27	0.27	0.46	0.36	0.45	0.39
PFKFB1	0.54	0.74	0.81	0.85	1.03	1.21	0.54	0.55	0.74	0.84
PFKM	0.40	0.78	0.60	0.96	0.72	0.87	0.60	0.63	0.45	0.57
PGM1	0.45	0.60	0.34	0.82	0.82	0.98	0.21	0.10	0.35	0.46
PKLR	0.63	0.51	0.43	0.59	0.33	0.44	0.39	0.65	0.52	0.67
PKM2	0.39	0.21	0.69	0.95	0.41	0.59	0.42	0.53	0.25	0.25
PMVK	0.10	0.18	0.08	0.09	0.05	0.06	0.07	0.08	0.04	0.08
PPAP2A	0.33	0.44	0.34	0.54	0.61	0.69	0.56	0.52	0.59	0.64
PPAP2C	0.12	0.26	0.35	0.46	0.15	0.25	0.33	0.17	0.13	0.19
PRKAB1	0.63	0.57	0.63	0.53	0.63	0.66	0.59	0.64	0.81	0.84
PRKAG3	0.17	0.14	0.15	0.13	0.07	0.08	0.10	0.10	0.09	0.12
PTEN	0.86	0.89	0.76	0.94	0.85	0.74	0.86	0.79	0.77	0.81
SCD	0.27	0.30	0.25	0.62	0.62	0.53	0.13	0.37	0.51	0.52
SDHC	0.37	0.45	0.53	0.61	0.19	0.23	0.28	0.56	0.55	0.62
SLC16A8	0.36	0.28	0.64	0.63	0.49	0.51	0.28	0.32	0.34	0.29
SLC1A5	0.88	0.88	0.92	1.08	0.54	0.33	0.65	0.60	0.78	0.75
SLC25A10	0.83	0.82	0.79	0.90	0.72	0.64	0.72	0.86	0.76	0.60
SOD1	0.14	0.12	0.58	0.46	0.52	0.44	0.52	0.15	0.12	0.19
SREBF1	0.55	0.26	0.72	0.89	0.88	0.79	0.39	0.63	0.63	0.58
TKT	0.67	0.55	0.64	0.92	1.31	1.14	1.02	0.95	1.06	1.03
TKTL1	0.73	0.82	0.83	0.95	0.57	0.40	0.60	0.79	0.64	0.61
UMPS	0.44	0.47	0.39	0.33	0.72	0.71	0.37	0.45	0.66	0.56

POC_{RF} 0.00 0.20 0.40 0.60 0.80 1.00 1.20 1.40 1.60 1.80

Table 4.1 Summary heat-map of validation screen

Gene ablation effects from the screen were re-evaluated in a secondary validation screen. Heat map represents RISC-free (RF)-normalised endpoint cell numbers (POC_{RF}) for the individual isogenic cell line pairs obtained following 4 days siRNA treatment on a 96-well plate format.

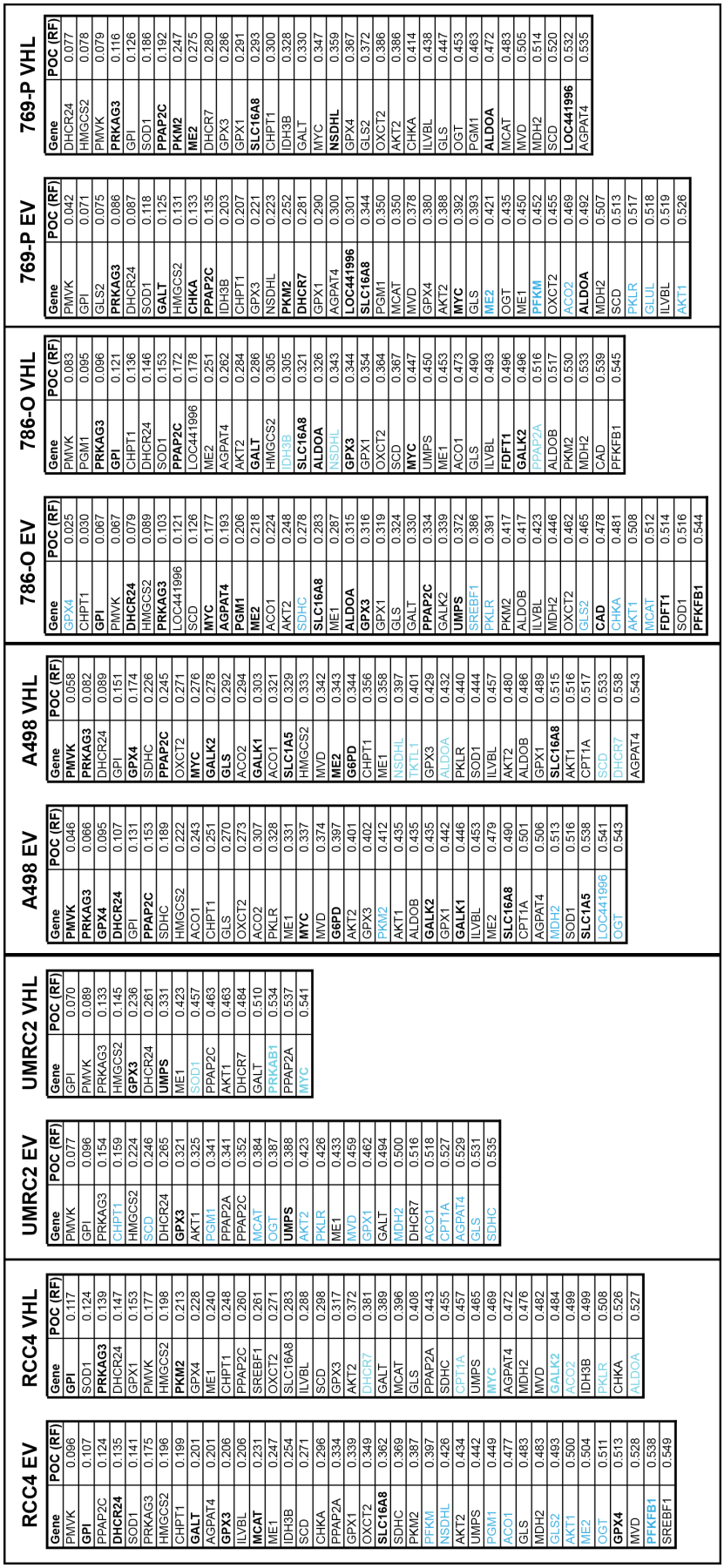

RCC4 EV	
Gene	POC (RF)
PMVK	0.096
GPI	0.107
PPAP2C	0.124
DHCR24	0.135
SOD1	0.141
PRKAG3	0.175
HMGCS2	0.196
CHPT1	0.199
GALT	0.201
AGPAT4	0.201
GPX3	0.206
ILVBL	0.206
MCAT	0.231
ME1	0.247
IDH3B	0.254
SCD	0.271
CHKA	0.296
PPAP2A	0.334
GPX1	0.339
OXCT2	0.349
SLC16A8	0.362
SDHC	0.369
PKM2	0.387
PFKM	0.397
NSDHL	0.426
AKT2	0.434
UMPS	0.442
PGM1	0.449
ACO1	0.477
GLS	0.483
MDH2	0.483
GLS2	0.493
AKT1	0.500
ME2	0.504
OGT	0.511
GPX4	0.513
MVD	0.528
PFKFB1	0.538
SREBF1	0.549

RCC4 VHL	
Gene	POC (RF)
GPI	0.117
SOD1	0.124
PRKAG3	0.139
DHCR24	0.147
GPX1	0.153
PMVK	0.177
HMGCS2	0.198
PKM2	0.213
GPX4	0.228
ME1	0.240
CHPT1	0.248
PPAP2C	0.260
SREBF1	0.261
OXCT2	0.271
SLC16A8	0.283
ILVBL	0.288
SCD	0.298
GPX3	0.317
AKT2	0.372
DHCR7	0.381
GALT	0.389
MCAT	0.396
GLS	0.408
PPAP2A	0.443
SDHC	0.455
CPT1A	0.457
UMPS	0.465
MYC	0.469
AGPAT4	0.472
MDH2	0.476
MVD	0.482
GALK2	0.484
ACO2	0.499
IDH3B	0.499
PKLR	0.508
CHKA	0.526
ALDOA	0.527

UMRC2 EV	
Gene	POC (RF)
PMVK	0.077
GPI	0.096
PRKAG3	0.154
CHPT1	0.159
HMGCS2	0.159
SCD	0.246
DHCR24	0.265
GPX3	0.321
AKT1	0.325
PGM1	0.341
PPAP2A	0.341
PPAP2C	0.352
MCAT	0.384
OGT	0.387
UMPS	0.388
AKT2	0.423
PKLR	0.426
ME1	0.433
MVD	0.459
GPX1	0.462
GALT	0.494
MDH2	0.500
DHCR7	0.516
ACO1	0.518
CPT1A	0.527
AGPAT4	0.529
GLS	0.531
SDHC	0.535

UMRC2 VHL	
Gene	POC (RF)
GPI	0.070
PMVK	0.089
PRKAG3	0.133
HMGCS2	0.145
GPX3	0.236
DHCR24	0.261
UMPS	0.331
ME1	0.423
SOD1	0.457
PPAP2C	0.463
AKT1	0.463
DHCR7	0.484
GALT	0.510
PRKAB1	0.534
PPAP2A	0.537
MYC	0.541

A498 EV	
Gene	POC (RF)
PMVK	0.046
PRKAG3	0.066
GPX4	0.095
DHCR24	0.107
GPI	0.131
PPAP2C	0.153
SDHC	0.189
HMGCS2	0.222
ACO1	0.243
CHPT1	0.251
GLS	0.270
OXCT2	0.273
ACO2	0.307
PKLR	0.328
ME1	0.331
MYC	0.337
MVD	0.374
G6PD	0.397
AKT2	0.401
GPX3	0.402
PKM2	0.412
AKT1	0.435
ALDOB	0.435
GALK2	0.435
GPX1	0.442
GALK1	0.446
ILVBL	0.453
ME2	0.479
SLC16A8	0.490
CPT1A	0.501
AGPAT4	0.506
MDH2	0.513
SOD1	0.516
SLC1A5	0.538
LOC441996	0.541
OGT	0.543

A498 VHL	
Gene	POC (RF)
PMVK	0.058
PRKAG3	0.082
DHCR24	0.089
GPI	0.151
GPX4	0.174
SDHC	0.226
PPAP2C	0.245
OXCT2	0.271
MYC	0.276
GALK2	0.278
GLS	0.292
ACO2	0.294
GALK1	0.303
ACO1	0.321
SLC1A5	0.329
HMGCS2	0.333
MVD	0.342
ME2	0.343
G6PD	0.344
CHPT1	0.356
ME1	0.358
NSDHL	0.397
TKTL1	0.401
GPX3	0.429
ALDOA	0.432
PKLR	0.440
SOD1	0.444
ILVBL	0.457
AKT2	0.480
ALDOB	0.486
GPX1	0.489
SLC16A8	0.515
AKT1	0.516
CPT1A	0.517
SCD	0.533
DHCR7	0.538
AGPAT4	0.543

786-O EV	
Gene	POC (RF)
GPX4	0.025
CHPT1	0.030
GPI	0.067
PMVK	0.067
DHCR24	0.079
HMGCS2	0.089
PRKAG3	0.103
LOC441996	0.121
SCD	0.126
MYC	0.177
AGPAT4	0.193
PGM1	0.206
ME2	0.218
ACO1	0.224
AKT2	0.248
SDHC	0.278
SLC16A8	0.283
ME1	0.287
ALDOA	0.315
GPX3	0.316
GPX1	0.319
GLS	0.324
GALT	0.330
PPAP2C	0.334
GALK2	0.339
UMPS	0.372
SREBF1	0.386
PKLR	0.391
PKM2	0.417
ALDOB	0.417
ILVBL	0.423
MDH2	0.446
OXCT2	0.462
GLS2	0.465
CAD	0.478
CHKA	0.481
AKT1	0.508
MCAT	0.512
FDFT1	0.514
SOD1	0.516
PFKFB1	0.544

786-O VHL	
Gene	POC (RF)
PMVK	0.083
PGM1	0.095
PRKAG3	0.096
GPI	0.121
CHPT1	0.136
DHCR24	0.146
SOD1	0.153
PPAP2C	0.172
LOC441996	0.178
ME2	0.251
AGPAT4	0.262
AKT2	0.284
GALT	0.286
HMGCS2	0.305
IDH3B	0.305
SLC16A8	0.321
ALDOA	0.326
NSDHL	0.343
GPX3	0.344
GPX1	0.354
OXCT2	0.364
SCD	0.367
MYC	0.447
UMPS	0.450
ME1	0.453
ACO1	0.473
GLS	0.490
ILVBL	0.493
FDFT1	0.496
GALK2	0.496
PPAP2A	0.516
ALDOB	0.517
PKM2	0.530
MDH2	0.533
CAD	0.539
PFKFB1	0.545

769-P EV	
Gene	POC (RF)
PMVK	0.042
GPI	0.071
GLS2	0.075
PRKAG3	0.086
DHCR24	0.087
SOD1	0.118
GALT	0.125
HMGCS2	0.131
CHKA	0.133
PPAP2C	0.135
IDH3B	0.203
CHPT1	0.207
NSDHL	0.223
PKM2	0.252
DHCR7	0.281
GPX1	0.290
AGPAT4	0.300
LOC441996	0.301
SLC16A8	0.344
PGM1	0.350
MCAT	0.350
MVD	0.378
GPX4	0.380
AKT2	0.388
MYC	0.392
GLS	0.393
ME2	0.421
OGT	0.435
ME1	0.450
PFKM	0.452
OXCT2	0.455
ACO2	0.469
ALDOA	0.492
MDH2	0.507
SCD	0.513
PKLR	0.517
GLUL	0.518
ILVBL	0.519
AKT1	0.526

769-P VHL	
Gene	POC (RF)
DHCR24	0.077
HMGCS2	0.078
PMVK	0.079
PRKAG3	0.116
GPI	0.126
SOD1	0.186
PPAP2C	0.192
PKM2	0.247
ME2	0.275
DHCR7	0.280
GPX3	0.286
GPX1	0.291
SLC16A8	0.293
CHPT1	0.300
IDH3B	0.328
GALT	0.330
MYC	0.347
NSDHL	0.359
GPX4	0.367
GLS2	0.372
OXCT2	0.386
AKT2	0.386
CHKA	0.414
ILVBL	0.438
GLS	0.447
OGT	0.453
PGM1	0.463
ALDOA	0.472
MCAT	0.483
MVD	0.505
MDH2	0.514
SCD	0.520
LOC441996	0.532
AGPAT4	0.535

Figure 4.21: Summary of cell line-specific siRNAs with negative effect on cell viability from validation silencing experiments

Tables summarise genes that when knocked down resulted in sever cell number loss with $POC_{RF} \leq 0.5$. Highlighted in bright blue are siRNAs that have a significant negative effect exclusively in EV or VHL cells of the respective isogenic cell line pairs. Marked in bold are siRNAs that reproduce the cell line-specific detrimental effect from the screen.

With respect to pVHL-specific silencing effects, the same approach was taken as for identifying differential effects in the primary screen. The gene ranks ($POC_{RF} \leq 0.5$) for the individual cell lines can be found in Figure 4.21. Surprisingly, although there was an increased amount of siRNAs identified with detrimental outcome on cell number compared to the initial screen, their overlap is limited. *PFKFB1* (6-phosphofructo-2-kinase/fructose-2,6-biphosphatase 1), *PRKAB1* (protein kinase, AMP-activated, beta 1), and *PFKM* (phosphofructokinase, muscle) for example were the only genes that when knocked down maintained their unique negative effect on cell number in RCC4 EV, UMRC2 VHL, and 769-P EV cells, respectively. Apart from those three, many of the siRNAs that scored as cell line specific pVHL-differential did not hold up their negative effects, because in the validation experiment the counterpart became sensitive to the respective gene ablation to a similar extent, hence abolishing the differential effect (Figure 4.21). A similar scenario could be observed for the more global pVHL-differential analysis, where all pVHL-null cell lines were pooled and their mean was compared to the mean of the pooled pVHL-expressing cell lines. Galactokinase 2 (GALK2) was the only gene that when silenced was more detrimental for pVHL-expressing cells (Figure 4.22A).

Analysis to identify specific cell number loss correlation with HIF-α-isoform expression, revealed a much better reproducibility for siRNAs that preferentially affected HIF-2α only expressing cells: siMYC, siME2, siALDOA, siGALK2 and siLOC441996 maintained their effect indicating a strong link between these genes and HIF-2α (Figure 4.22B). Indeed, it is now established that ccRCC cell lines are c-MYC-driven and that HIF-2α directly cooperates with c-MYC to drive at least cell cycle-affecting genes (Gordan et al., 2007a).

A

EV

Gene	POC (RF)
PMVK	0.067
GPI	0.096
PRKAG3	0.103
DHCR24	0.107
PPAP2C	0.153
HMGCS2	0.196
CHPT1	0.199
SCD	0.271
AGPAT4	0.300
GPX3	0.316
GALT	0.330
ME1	0.331
GPX1	0.339
PGM1	0.350
SLC16A8	0.362
SDHC	0.369
GPX4	0.380
MCAT	0.384
MYC	0.392
GLS	0.393
AKT2	0.401
PKM2	0.412
PKLR	0.426
UMPS	0.442
ILVBL	0.453
OXCT2	0.455
MVD	0.459
ACO1	0.477
ME2	0.479
CHKA	0.481
GLS2	0.493
MDH2	0.500
AKT1	0.500
OGT	0.511
SOD1	0.516
LOC441996	0.541

VHL

Gene	POC (RF)
PMVK	0.083
PRKAG3	0.116
GPI	0.121
DHCR24	0.146
SOD1	0.186
HMGCS2	0.198
PPAP2C	0.245
CHPT1	0.300
GPX3	0.317
SLC16A8	0.321
ME2	0.343
GPX1	0.354
OXCT2	0.364
GPX4	0.367
AKT2	0.386
GALT	0.389
NSDHL	0.397
ME1	0.423
MYC	0.447
GLS	0.447
ILVBL	0.457
UMPS	0.465
ALDOA	0.472
DHCR7	0.484
GALK2	0.496
IDH3B	0.499
MVD	0.505
SCD	0.520
PKM2	0.530
MDH2	0.533
AGPAT4	0.535
PPAP2A	0.537

B

HIF-1/2α

Gene	POC (RF)
PMVK	0.086
GPI	**0.102**
PRKAG3	0.165
CHPT1	0.179
DHCR24	0.200
HMGCS2	0.210
PPAP2C	0.238
SCD	0.258
GPX3	0.264
MCAT	0.308
PPAP2A	0.338
ME1	0.340
GALT	0.347
SOD1	0.362
AGPAT4	0.365
PGM1	0.395
GPX1	0.400
ILVBL	0.406
AKT1	0.412
UMPS	0.415
IDH3B	0.422
AKT2	0.429
CHKA	0.435
OGT	0.449
SDHC	0.452
MDH2	0.491
MVD	0.493
ACO1	0.498
PFKM	0.499
SLC16A8	0.500
GLS	0.507
NSDHL	0.518
PKLR	0.526
OXCT2	0.534
PKM2	0.541
DHCR7	0.541

HIF-2α

Gene	POC (RF)
PMVK	0.055
GPI	0.069
DHCR24	0.083
PRKAG3	0.095
HMGCS2	0.110
CHPT1	0.118
GPX4	0.203
LOC441996	0.211
GALT	0.227
PPAP2C	0.235
AGPAT4	0.246
GPX3	0.268
GLS2	0.270
PGM1	0.278
MYC	0.284
GPX1	0.304
CHKA	0.307
SLC16A8	0.314
SOD1	0.317
AKT2	0.318
ME2	0.319
SCD	0.320
PKM2	0.334
GLS	0.358
ME1	0.368
NSDHL	0.397
IDH3B	0.400
ALDOA	0.403
SDHC	0.415
MCAT	0.431
ACO1	0.449
PKLR	0.454
OXCT2	0.459
GALK2	0.466
ILVBL	0.471
MDH2	0.477
MVD	0.479
SREBF1	0.509
UMPS	0.517
AKT1	0.517
OGT	0.522
PFKM	0.527

C

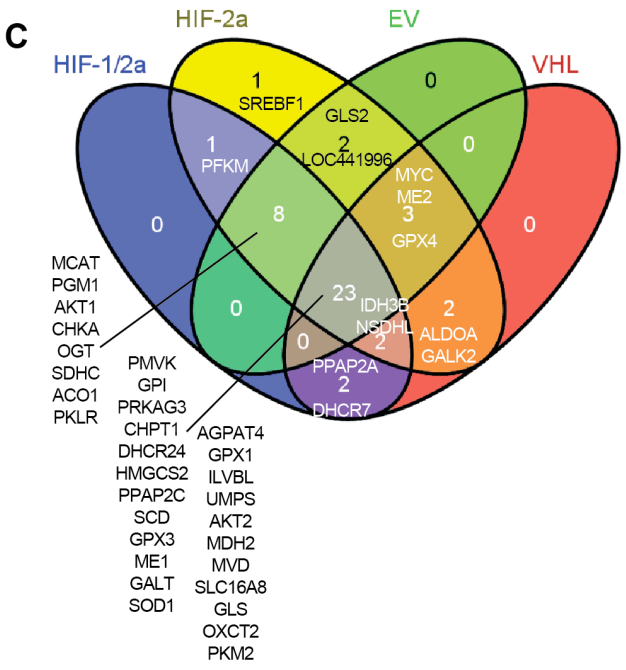

Figure 4.22: Summary of genes with pVHL- or HIF-α isoform-specific effect on cell viability

(A) Tables summarising genes that upon siRNA-mediated silencing resulted in severe cell number loss in a pVHL-specific manner with $POC_{RF} \leq 0.5$. Highlighted in bright blue / turquoisse are genes that have a significant negative effect exclusively in EV / VHL cells. (B) Tables summarising genes that upon siRNA-mediated silencing resulted in severe cell number loss according to HIF-α isoform status $POC_{RF} \leq 0.5$. Highlighted in bright blue / turquoisse are genes that have a significant negative effect exclusively in HIF-1/2α- / HIF-2α only- expressing cells. Marked in bold are genes that reproduce the differential detrimental effect that was seen in the initial screen. (C) Venn-diagram illustrating the overlap or distinctiveness of siRNAs-targets that have strong negative effects in one or more of the analysed pooled populations. Diagram was generated using the online software tool venny (http://bioinfogp.cnb.csic.es/tools/venny/index.html).

Amongst the most detrimental siRNAs across most of the cell lines were those targeting the AMPK subunit PRKAG3, the transcription factor c-MYC, several genes involved in fatty acid, triacyl-glyceride and cholesterol metabolism (*ME1*, *CHPT1*, *PPAP2C*, *HMGCS2*, *PMVK*, *DHCR24*) and genes involved in ROS detoxification (*GPX1*, *GPX3*, *GPX4* and *SOD1*). In addition, the glycolytic enzymes GPI, ALDOA, the lactate transporter SLC16A8, the TCA cycle enzyme ME2 and two AKT isoforms, AKT1 and AKT2 were also identified as being essential for ccRCC cell survival. All of these genes comprised the final gene hit list (Table 4.2). In this case, having the monocarboxylate transporter MCT4 amongst the genes that are essential for ccRCC cell survival served as a positive control, because this gene was previously found in another screen investigating ccRCC disease (Gerlinger et al., 2012b).

Gene	RCC4		UMRC2		A498		786-O		769-P	
	EV	VHL	EV	VHL	EV	VHL	EV	VHL	EV	VHL
ALDOA	0.60	0.53	0.61	0.76	0.60	0.43	0.31	0.33	0.49	0.47
AKT1	0.50	0.63	0.32	0.46	0.43	0.52	0.51	0.79	0.53	0.56
AKT2	0.43	0.37	0.42	0.58	0.40	0.48	0.25	0.28	0.39	0.39
CHPT1	0.20	0.25	0.16	0.57	0.25	0.36	0.03	0.14	0.21	0.30
DHCR24	0.14	0.15	0.27	0.26	0.11	0.09	0.08	0.15	0.09	0.08
GALT	0.20	0.39	0.49	0.51	0.56	0.73	0.33	0.29	0.12	0.33
GLS	0.48	0.41	0.53	0.76	0.27	0.29	0.32	0.49	0.39	0.45
GPI	0.11	0.12	0.10	0.07	0.13	0.15	0.07	0.12	0.07	0.13
GPX1	0.34	0.15	0.46	0.68	0.44	0.49	0.32	0.35	0.29	0.29
GPX3	0.21	0.32	0.32	0.24	0.40	0.43	0.32	0.34	0.22	0.29
GPX4	0.51	0.23	0.81	0.88	0.09	0.17	0.02	0.65	0.38	0.37
HMGCS2	0.20	0.20	0.22	0.15	0.22	0.33	0.09	0.30	0.13	0.08
IDH3B	0.25	0.50	0.59	0.61	0.66	0.74	0.60	0.31	0.20	0.33
ME1	0.25	0.24	0.43	0.42	0.33	0.36	0.29	0.45	0.45	0.56
ME2	0.50	0.59	0.84	0.77	0.48	0.34	0.22	0.25	0.42	0.28
PMVK	0.10	0.18	0.08	0.09	0.05	0.06	0.07	0.08	0.04	0.08
PPAP2C	0.12	0.26	0.35	0.46	0.15	0.25	0.33	0.17	0.13	0.19
PRKAG3	0.17	0.14	0.15	0.13	0.07	0.08	0.10	0.10	0.09	0.12
SCD	0.27	0.30	0.25	0.62	0.62	0.53	0.13	0.37	0.51	0.52
SDHC	0.37	0.45	0.53	0.61	0.19	0.23	0.28	0.56	0.55	0.62
SLC16A8	0.36	0.28	0.64	0.63	0.49	0.51	0.28	0.32	0.34	0.29
SOD1	0.14	0.12	0.58	0.46	0.52	0.44	0.52	0.15	0.12	0.19

POC_{RF} 0.00 0.20 0.40 0.60 0.80 1.00 1.20 1.40 1.60 1.80

Table 4.2 Final Hit list

List extracted from Table 4.1 summarises siRNA-targeted genes that showed strong negative effects on cell proliferation upon silencing in all ccRCC cells tested. Numbers represent obtained POC_{RF} values. Highlighted in red are genes that were chosen for follow-up investigations.

4.4 Screen discussion and follow up

The main objective of the functional genomics approach was to identify pVHL-synthetic lethal metabolic genes that affected ccRCC cell viability. Although some siRNAs were found to have pVHL-dependent effects, these were largely cell line specific and it was not possible to identify solid pVHL-synthetic lethal genes that affected all ccRCC cell lines (Figure 4.16 – 4.18). The differential effects seen in individual cell lines, predominantly in the RCC4 cell line pair, were neither substantial nor exclusive in that all cell lines that showed a differential effect showed it in the same direction. In addition, many of the tested differential hits were either not reproducible or inconsistent when trying to validate them further (Figure 4.21 and 4.22).

One of the reasons for not being able to identify strong differential gene effects might be due to the high variability between the individual replicates observed in the screen (Figure 4.11). This internal variability might mask potential real differential effects between cell lines. Indeed, in the subsequent smaller validation screen, variability between technical replicates was minimal and the number of hit genes increased. Unfortunately, no siRNAs could be identified within the validation screen that had a substantial differential effect on cell viability. This might result from the high cut off threshold, which was set to ≤ 50 % of RISC-free control silencing (POC_{RF}), but the aim was to identify genes whose ablation had a strong biological impact. Unfortunately, we missed to include the top hit kinases, MET, MEK1 and particularly CDK6, that were identified as potential synthetic lethal interactors of pVHL in the shRNA screen carried out by Bommy-Reddy and colleagues (Bommi-Reddy et al., 2008) and which would have provided us with a positive control for our pVHL-differential hit analysis.

Also, we cannot discount that differential hits common to all cell line pairs could have been identified if the readout of the screen would have been changed i.e. if tested for changes in migration or invasion or if a metabolic readout such as redox-flux would have been chosen.

Aside from potential technical issues and high cut off thresholds, it cannot be excluded that the screen itself was not ideal to detect pVHL-synergistic genes. Although ccRCCs show a prominent metabolic phenotype, which was shown to distinguish them from

other cancer types (Gatto et al., 2014), the metabolic screen library the isogenic cell lines were subjected to is relatively small, with only 240 target genes. The library could potentially be expanded to encompass more metabolic genes relevant for *VHL*-synthetic lethality in the ccRCC-specific context. Subjecting the ccRCC cell lines to a whole genome screen might have yielded more results.

Furthermore, as mentioned in the introduction, there is increasing evidence, that ccRCCs are highly heterogeneous and acquire subclonal genetic alterations during tumour progression (Gerlinger et al., 2012a, Martinez et al., 2013). To accommodate this heterogeneity, a panel of 5 isogenic pairs was used for screening. Although the cell lines have some commonalities such as a high glycolytic phenotype (Figure 3.6), high respiratory capacity (Figure 3.7) and show high sensitivity to glutamine and glucose withdrawal (Figure 3.11) when compared to non-tumourigenc HK-2 cells, these commonalities varied somewhat amongst the different ccRCC cell lines and could be the consequence of their distinct genetic backgrounds (for more details, see catalogue of somatic mutations in cancer (COSMIC; http://cancer.sanger.ac.uk/cancergenome/projects/cell_lines/)). This genetic heterogeneity may make it difficult to identify common ccRCC-synthetic lethal relationships, which could be validated *in vivo*.

Identification of genes that decreased cell numbers in a HIF-α isoform specific manner yielded a small number of genes that were predominantly HIF-2α specific. No convincing genes were found to have a more pronounced effect in cells expressing both HIF-α isoforms (Figure 4.19). Amongst the HIF-2α-specific genes was c-MYC, which is in line with reports of HIF-2α:c-MYC cooperation for induction of a transcriptional programme that drives cell proliferation in hypoxia (Gordan et al., 2007a, Gordan et al., 2007b). With regard to the other genes, *LOC441996*, *ME2*, *ALDOA* and *GALK2*, although silencing of these showed higher cell number loss in HIF-2α-expressing cells, their ablation *per se* had a strong negative effect on the whole cell line panel (Figure 4.20 and 4.22). Hence, the relevance of this specificity is not clear but their increased importance in HIF-2α driven tumours might be able to be resolved more easily in longer-term assays where differences would be larger.

A final conclusion that can be made from the siRNA screen is that although *VHL* loss/mutation is unequivocally an early and important event in ccRCC initiation and growth (Gerlinger et al., 2012a), the subsequent alterations that take place as a consequence of HIF loss mean that re-addition of functional pVHL alone is able to change the respiratory capacity of the cells for example but would be unable to rewire the subtle metabolic differences that have developed in each of the tumours which the cell lines were derived from.

As the screen revealed a promising number of genes, whose depletion resulted in convincing and reproducible negative effects on cell number in most, if not all, ccRCC cell line pairs (Table 4.2), it was decided to focus on this set of genes for further investigations. Furthermore, by comparison with the non-tumourigenic HK-2 renal epithelial cell line, cancer-specific effects might be identifiable.

A promising lead for further investigation in ccRCC appeared to be within the ROS detoxification system, with a special focus on the glutathione peroxidase family, as silencing of several members of this family (GPX1, GPX3, GPX4, GPX7) repeatedly came up as particularly detrimental for the ccRCC cell lines tested while having little or no effect in the non-tumourigenic renal epithelial HK-2 cells as will be shown in the following.

Chapter 5: The glutathione redox system is essential for ccRCC cell survival

5.1 Introduction

5.1.1 Adaptable redox balance is essential for cancer cell proliferation and survival

Cellular redox homeostasis is maintained by the balance between the generation and elimination of reactive oxygen species (ROS). ROS species are constantly generated as by-products in metabolic processes whenever electron leakage occurs and electrons are transferred to an oxygen atom instead of a carbon or a phosphate molecule. Processes that can produce oxygen radicals include the mitochondrial electron transport chain (ETC) and endoplasmic reticulum (ER) stress (Santos et al., 2009, Higa and Chevet, 2012) (Figure 5.1). In addition, active enzyme-catalysed ROS production occurs through the function of specific metabolic enzymes, such as cytochrome P450 (CYP450) (Hanukoglu, 2006), lipoxygenase (LOX), cyclooxygenase (COX) as well as NADPH oxidase (NOX, membrane-bound), xanthine oxidase (XO) and nitric oxide synthase (NOS) (Keisari et al., 1983, Los et al., 1995) (Figure 5.1). ROS species include hydrogen peroxide (H_2O_2), the superoxide anion (O_2^-), the very reactive hydroxyl radical ($OH^\bullet$, generated from H_2O_2 in the presence of Fe^{2+} through a Fenton reaction), organic hydroperoxides (ROOH) and highly reactive alcoxy and peroxy radicals ($RO^\bullet$, $ROO^\bullet$). Due to dynamic changes in ROS species present in the cellular milieu and the lack of tools to detect and quantitatively measure these changes, ROS is often used to summarise H_2O_2 and O_2^- only. Sequestering these ROS species are various endogenous antioxidants such as glutathione (GSH), thioredoxin (TRX) and NADPH (provides the reducing equivalents for regeneration of these antioxidants), as well as dietary antioxidant compounds, which can be supplemented exogenously, such as vitamin C (ascorbate), vitamin E (tocopherol family), β-carotene (a carotenoid) and the non-metal selemnium (Se). These antioxidants harbour intrinsic redox capacity in either thiol groups (GSH and TRX) or in their, sometimes multiple, double bonds (vitamin C and E, β-carotene) and are less substrate-specific than endogenous ROS-detoxifying enzymes like superoxide dismutase (SOD), catalase (CAT, predominantly in peroxisomes), glutathione peroxidase (GPX), glutathione transferase (GST), glutaredoxin (GRX), and peroxiredoxin (PRX). Some of these enzymes use GSH as co-substrate (Figure 5.1).

SODs are the only enzymes that can convert highly reactive O_2^- into less reactive H_2O_2, which can then be converted to water by CAT, GPXs and other enzymes. There are three SOD isoforms: mitochondrial MnSOD/SOD2 and cytoplasmic and extracellular Cu/ZnSOD (SOD1 and SOD3 respectively) covering the main cellular compartments of O_2^- generation (Figure 5.1).

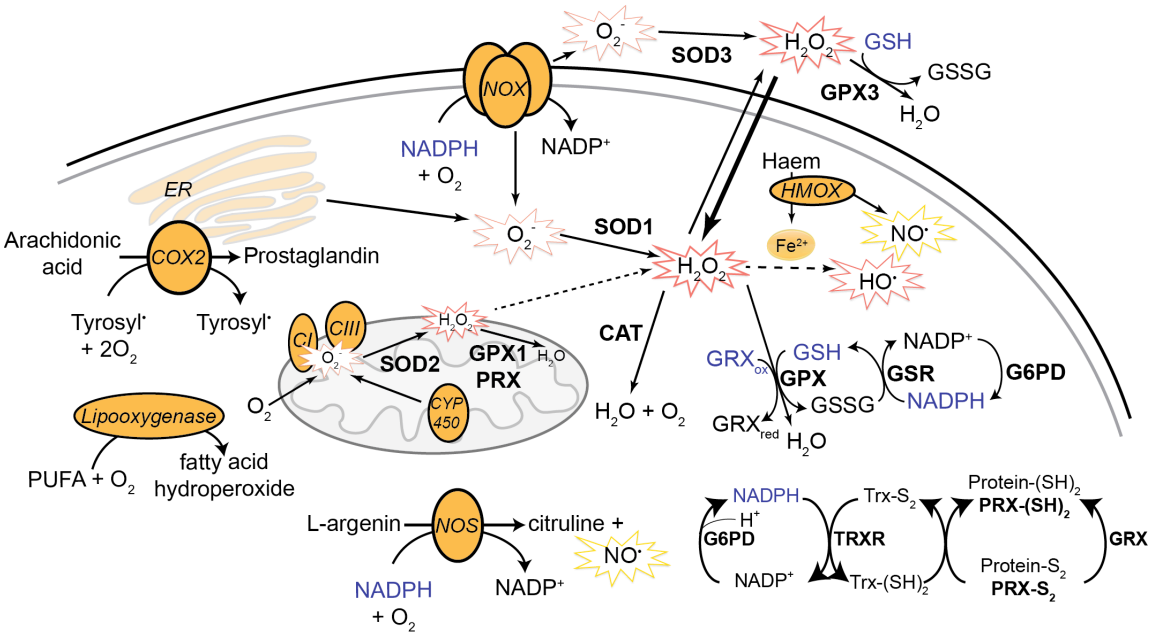

Figure 5.1: Cellular enzymatic ROS generation and detoxification systems
Reactive oxygen species (ROS) are usually generated as by-products from the electron transport chain at complex I and III (CI, CIII) or the endoplasmic reticulum (ER). But ROS can also be actively generated by enzymes such as nitric oxide synthase (NOS), NADPH oxidases (NOX), cyclooxygenase 2 (COX2) or heme oxygenase (HMOX). Opposed to these ROS generating enzymes are ROS scavenging enzymes (bold labelling) such as superoxide dismutases (SODs) that convert O_2^- to H_2O_2, which is further converted to water by catalase (CAT), glutathione peroxidases (GPXs), thioredoxins (TRXs) and peroxyredoxins (PRXs). GSH, reduced glutathione; GSSG, oxidised glutathione; GSR, glutathione reductase; TRXR, thioredoxin reductase. Highlighted in orange are ROS producers; highlighted in blue are non-enzymatic antioxidants and co-substrates for redox-active enzymes, which are highlighted in bold lettering.

The master regulator of antioxidant response to oxidative stress is the ubiquitously expressed transcription factor nuclear factor erythroid 2-related factor 2 (NRF2). Under normal conditions, NRF2 is bound to Kelch-like ECH-associated protein 1 (KEAP1) restraining it to the cytoplasm. Furthermore, KEAP1, a BTB-containing protein acts as an adaptor for cullin 3 (CUL3) binding, which, together with the E3 ubiquitin ligase RING-box protein 1 (RBX1), form a BCR E3 ubiquitin ligase complex. This E3 ubiquitin ligase complex polyubiquitinates NRF2, thereby marking it for proteasomal

degradation. In response to oxidative stress, KEAP1 gets oxidised and the binding to NRF2 is lost, enabling NRF2 translocation to the nucleus where it activates the transcription of its downstream targets (Taguchi et al., 2011). NRF2 drives the expression of the two subunits of γ-glutamylcysteine synthetase (γ-GCL): GCLC (catalytic subunit) and GCLM (modifying subunit). γ-GCL is the rate-limiting enzyme in GSH production. NRF2 also controls the supply of cysteine by controlling the expression of the cystine/glutamate antiporter solute carrier family 7 member 11 (SLC7A11 or XCT) (Sasaki et al., 2002). Cysteine is the rate-limiting substrate not only for GSH production, but also for the generation of selenocysteine, a special amino acid incorporated in the catalytic centre of several enzymes, including some involved in ROS scavenging (e.g. GPXs and TRX reductase (TRXR)). In addition, NRF2 positively regulates NADPH-producing enzymes such as malic enzyme 1 (ME1), glucose-6-phosphate dehydrogenase (G6PD) and isocitrate dehydrogenase (IDH) (Mitsuishi et al., 2012). Other NRF2 targets include TXNRD1, PRDX1 (Kim et al., 2007), GPX2, and several GSTs, heme oxygenase (decycling) 1 (HMOX1), components of the ferritin complex (ferritin light chain (FTL) and ferritin heavy chain (FTH)) (Chorley et al., 2012) and NAD(P)H quinone oxidoreductase 1 (NQO1).

Other important transcriptional regulators of antioxidant proteins are forkhead transcription factors of the O subgroup (FOXOs). In mammals, there are four FOXO isoforms: FOXO1, FOXO3, FOXO4 and FOXO6. FOXOs are regulated through phosphorylation by AKT, which causes their exclusion from the nucleus and subsequent proteasomal degradation. Although most FOXO target genes are predominantly associated with cell cycle arrest and apoptosis (van der Horst and Burgering, 2007), FOXO3 and FOXO4 are involved in ROS detoxification, as they regulate the expression of SOD2, CAT and sestrin 3 (Kops et al., 2002a, Nogueira et al., 2008, Ferber et al., 2012).

The tumour suppressor TP53 (p53), which is best known for its checkpoint activity in the cell cycle transition from G1 to S-phase is furthermore involved in cellular redox metabolism. p53 responds to DNA damage through activation by ataxia telangiectasia mutated (ATM) and ataxia telangiectasia and Rad3-related protein (ATR) by stalling the

cell cycle through upregulation of the inhibitory protein p21. p21 binds to and inhibits the cyclin dependent kinase 2 (CDK2), leading to arrest of the cell cycle in G1 and providing time for DNA repair mechanisms to be activated. If the damage exceeds beyond repair, p53 is able to induce either senescence or apoptosis to remove the faulty cell from the system. This is accomplished, amongst other mechanisms, by enhancing ROS production through induction of p53-induced gene 3 (PIG3) (Polyak et al., 1997), mitochondrial proline dehydrogenase (PRODH) (Rivera and Maxwell, 2005), BAX, PUMA (Liu et al., 2005) and p66SHC (Trinei et al., 2002) and by downregulation of aldehyde dehydrogenase 4 (ALDH4) (Yoon et al., 2004), SOD2 and GPX1 (Johnson et al., 1996, Drane et al., 2001). At the same time, p53 has the capacity of inducing a ROS-elimination programme by positively regulating GPX1 and SOD2 (Hussain et al., 2004, Tan et al., 1999) and inhibiting COX2 (Subbaramaiah et al., 1999) and NOS2 (Ambs et al., 1998, Forrester et al., 1996). Hence, in the context of ROS, p53 acts as a double–edged sword (Figure 5.2).

Despite the prevalent notion that ROS are 'all bad' and that their accumulation will result in severe and irreversible damage of DNA, proteins and lipids, eventually causing cell death (Figure 5.2) and therefore needs to be eliminated or prevented at all costs. However, certain ROS at low to moderate concentrations are important signalling components that act as second messengers reporting back on altered and aberrant metabolic activities and influence signalling cascades to bring about adaptations to maintain the cellular redox balance and homeostasis to guarantee cell survival, proliferation and/or differentiation (Gough and Cotter, 2011) (Figure 5.2). It has been shown that H_2O_2, for example, can activate pro-survival transcription factors such as HIF-1α (Chandel et al., 1998, Chandel et al., 2000a), c-JUN N-terminal kinase 1(JNK1) (Chandel et al., 2000b, Nemoto et al., 2000), nuclear factor κ-light-chain-enhancer of activated B-cells (NF-κB) (Chandel et al., 2000b, Gloire et al., 2006) and p53 (Chandel et al., 2000c) in response to stress (Veal et al., 2007). Moreover, H_2O_2 has been implicated in modulating growth factor, cytokine and mitogen signalling through oxidative alteration of key cysteine residues on signalling molecules, particularly protein tyrosine phosphatases (PTPs) (Tonks, 2005, Xu et al., 2002) such as phosphatase and tensin homologue (PTEN) (Leslie et al., 2003) and MAPK phosphatases, which inhibits

their phosphatase activity and stabilises growth factor signalling (Figure 5.2). Furthermore, overexpression of SOD, CAT, PRXs and GPX1 resulted in depletion of H_2O_2 and negatively interfered with growth factor-mediated proliferation and growth (Shi et al., 2004). Many of these findings were discovered in the context of cancer initiation and survival, highlighting an important role for ROS in tumourigenesis. Cancer cells work at an enhanced metabolic rate in order to meet the high demand of anabolic processes required for fast proliferation, and enhanced ROS production is a by-product of increased metabolic activity. This initial increase in ROS could thereby enhance cell proliferation through increased activation of the PI3K/AKT pathway due to H_2O_2-mediated inactivation of PTEN. At the same time, induction of anti-oxidant mechanisms in cancer cells is needed to prevent excess accumulation of ROS to prevent cellular damage. For example, a recent study by Mitsuishi and colleagues has shown that the PI3K/AKT pathway also leads to nuclear NRF2 accumulation. NRF2 promotes PPP and glutamine metabolism in addition to cytoprotective antioxidant genes (Mitsuishi et al., 2012).

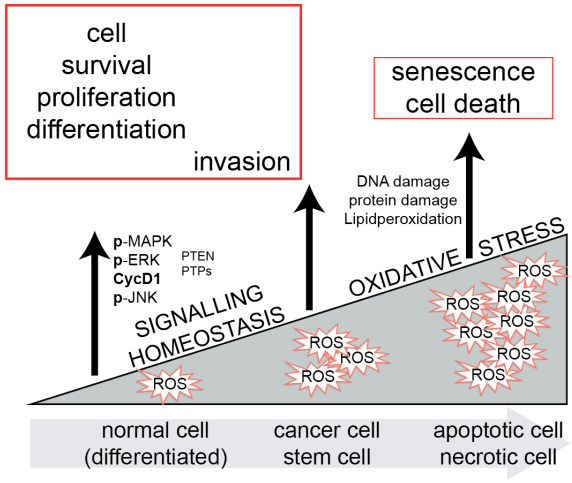

Figure 5.2: Positive or negative effect of ROS on cell survival is concentration dependent
The cell generates and needs a basal level of ROS for homeostasis. ROS are mainly generated as metabolic by-products and their accumulation up to a certain level induces signalling cascades to restore the balance. Once ROS accumulation exceeds another certain threshold, it becomes cytostatic and/or cytotoxic as it can cause severe damage to proteins, lipids and nucleic acids. Cancers found adaptation mechanisms to not only cope with the increased ROS levels that result from high metabolic rates but also to make use of it for their high proliferation rates.

In conclusion, cancer cells seem to have hijacked the cellular ROS scavenging system to maintain and promote proliferation and survive in an unfavourable environment by enhanced ROS accumulation together with upregulated ROS scavenging molecules and enzymes to counteract detrimental macromolecule damage.

5.1.2 GPX gene family and protein synthesis

GPXs are enzymes with the ability of neutralising peroxides such as H_2O_2 or lipid peroxides. In most cases, GSH is used as a co-substrate for the catalytic reaction. In humans, eight GPX isoforms have been identified (GPX1-GPX8) but GPX1-4 are the best studied of the family members. The different isoforms are highly conserved but differ in their expression pattern and substrate specificity, although some overlap.

GPX1 is the most abundant isoform and functions as a homotetramer. It is ubiquitously expressed and can be found in the cytoplasm, mitochondria and peroxisomes. Apart from H_2O_2, GPX1 can also reduce lipid hydroperoxides. GPX1 knockout mice are viable but extremely sensitive to exogenous ROS stimuli (e.g. Paraquat or Diquat treatment) and oxidant-induced injury (de Haan et al., 1998).

GPX2, which also functions as a homotetramer, is mainly expressed in the epithelium of the gastrointestinal tract (Chu et al., 1993). GPX2 knockout mice are also viable.

GPX3, also known as plasma GPX, is the only extracellular GPX isoform. Although GPX3 mRNA can be found in many different tissues, plasma-derived GPX3 is mainly produced in and secreted by the kidney (Avissar et al., 1994, Chu et al., 1992).

GPX4 differs from other GPX proteins in its substrate specificity as it mainly reduces phospholipid hydroperoxides such as tri- or diacylglycerol hydroperoxides (Marinho et al., 1997, Seiler et al., 2008, Toppo et al., 2009). With phospholipids being the main component of biological membranes, GPX4 is located to membranes to protect them from oxidative damage. Unlike the other GPXs, GPX4 is monomeric and, when systemically knocked out in a mouse model, results in embryonic lethality in midgestation (Yant et al., 2003), confirming an essential role for GPX4 in organismal development.

The GPX protein family belongs to a specific class of proteins, namely the selenoproteins. Selenoproteins are relatively rare (only ~25 have been identified so far (Kryukov et al., 2003)) and are characterised by containing a selenocysteine (Sec, U) in their protein sequence. In selenoproteins with enzymatic functions, Sec is localised to the catalytic centre where it catalyses redox reactions. Sec is the rare 21st amino acid and a cysteine (Cys, C) analogue in which the sulphur-containing thiol group is replaced by a selenium-containing selenol group. This alteration lowers both its pKa and its

reduction potential compared to cysteine giving it a distinct antioxidant activity, as it is deprotonated even at physiological pH. Interestingly, incorporation of this special amino acid provides a basis for the unique regulatory mechanism in GPX synthesis. Sec does not have its own genetic code but is encoded as 'UGA' - generally known as STOP codon. Hence, so-called SECIS (Sec insertion sequences) elements, additional regions in the 3' untranslated region (UTR) that form stem-loop structures, are necessary to recruit specific RNA-binding proteins (e.g. SECIS binding protein 2 (SBP2)) that facilitate an event cascade eventually resulting in Sec incorporation (Berry et al., 1991a, Berry et al., 1991b, Copeland et al., 2000, Fagegaltier et al., 2000). Contrary to all other amino acids, there is no Sec pool, as it is too reactive, but it is synthesised on its specific tRNA ($tRNA^{sec}$) just before incorporation into the protein. $tRNA^{sec}$ synthesis occurs in a three-step process: Firstly, $tRNA^{sec}$ becomes aminoacetylated with L-serine by seryl-tRNA synthetase (SerS). This seryl-residue is next converted to O-phosphoseryl-$tRNA^{sec}$ by O-phosphoseryl-$tRNA^{Sec}$ kinase (PSTK). Finally, O-phosphoseryl-$tRNA^{sec}$ is converted to selenocysteinyl-$tRNA^{sec}$ via the action of the Sep (O-phosphoserine) tRNA:Sec (selenocysteine) tRNA synthase (SEPSECS) (Low et al., 1995, Low and Berry, 1996, Tujebajeva et al., 2000, Zavacki et al., 2003).
Selenoprotein production is also dependent on the presence of selenium (Se). With Se being an essential nutrient, dietary Se restriction result in downregulation of selenoprotein mRNA and protein. However, not every selenoprotein is affected to the same extend by a reduction in available Se. There is a hierarchical separation - most likely depending on the importance of the respective selenoprotein. GPX4 and GPX2, for example, rank high and their mRNA is stable even at limiting Se concentrations while GPX1 and GPX3 mRNA, low in rank, get degraded already at moderate Se levels (Lei et al., 1995, Neve, 1995, Bermano et al., 1996, Wingler et al., 1999, Sunde et al., 2009).

5.1.3 GPX1 in tumourigenesis

In the context of cancer, GPX1 is of particular interest. The GPX1 gene contains several oxygen response elements (ORE) (Cowan et al., 1993) as well as binding sites for the tumour suppressor p53 (Hussain et al., 2004) and pro-survival transcription factors,

such as NFκB, AP-1 and SP1 (Abate et al., 1990, Zhou et al., 2001). Furthermore, human GPX1 is located to chromosome 3p21, a region associated with frequent loss of heterozygosity (LOH) in a number of different cancer types including breast, colon, lung, head and neck and kidney cancer (Hardie et al., 2000, Hu and Diamond, 2003, Hu et al., 2004) suggesting a potential tumour suppressive role for GPX1 in humans. In addition, the GPX1 gene is prone to single-nucleotide polymorphisms (SNPs; 38 have been found so far), especially aggregating in the 3' and 5' flanking regions (Foster et al., 2006). Within the protein coding region, there are two consistent SNP sites that are frequently found and alter the protein sequence: (a) leading to variations of in-frame GCG repeats (5, 6 or 7) resulting in varying numbers of alanines at the N-terminus and (b) amino acid 198 exchange (Pro -> Leu) due to a single-nucleotide substitution (CCC -> CTC). Both of these SNPs seem to render GPX1 less sensitive to increasing Se concentrations, at least in breast cancer (Hu et al., 2004) and cardiomyocytes (Jablonska et al., 2004, Lei et al., 2009). There have been several epidemiological studies carried out to link these polymorphisms with risks of breast, lung, prostate and bladder cancer, but no consistent trend towards increased or decreased cancer risk was detected (Ratnasinghe et al., 2000, Duffield-Lillico et al., 2003, Hu and Diamond, 2003, Cebrian et al., 2006, Gresner et al., 2007, Lippman et al., 2009).

Although systemic *GPX1* loss alone did not seem to affect cancer susceptibility in mice, *GPX1/GPX2* double knockout mice developed spontaneous colon/intestinal tumours, most likely due to increased inflammation (Chu et al., 2004). Overexpression of GPX1 has opposing effects on tumour initiation/progression: GPX1 overexpression alone or in combination with SOD2 in MIA PaCa-2 cells (human primary pancreatic adenocarcinoma cells), for example, decreased cancer cell proliferation *in vitro* and *in vivo* (Liu et al., 2004). In contrast, the same approach resulted in enhanced tumour numbers and growth kinetics due to inhibition of apoptotic mechanisms in a mouse skin cancer model (Lu et al., 1997, Kim et al., 2009), hinting to possible tissue-specific susceptibilities.

Taken together, it can be concluded that GPXs are important regulators of cellular and organismal redox balance, which is necessary for normal tissue homeostasis. A deviation from this highly regulated redox state, either mediated through up- or

downregulation of GPXs and consequential decrease or increase of ROS levels, results in the development of disease-associated phenotypes.

5.1.4 Glutathione biosynthesis and recycling

Glutathione is the major endogenous antioxidant produced in the cell. Its production is regulated by NRF2 as many of the enzymes involved in GSH synthesis are. Glutathione is present in relatively high concentrations within the cell, reaching 1-11 mM in the cytoplasm, mitochondria and the nucleus compared to stromal (0.01 mM) or plasma (0.002 mM) concentrations (Carlson and Jones, 1998, Han et al., 2006). Furthermore, liver, kidney and lung contain high levels of glutathione, most likely as these tissues have the highest exposure to toxins. Interestingly, there is evidence for shuttling of glutathione at the organismal level, as glutathione can be transported via the blood stream from the glutathione-producing liver to the GSH-consuming kidney (Anderson and Meister, 1980).
Glutathione occurs in two forms in the cell: as reduced glutathione (GSH) and as oxidised glutathione (GSSG). The ratio of GSH:GSSG is a common indicator of a cell's redox state. During oxidative stress, when GSH is heavily used, more of it is converted into GSSG and the GSH pool becomes more and more exhausted. Although GSH is the predominant form in most of the cellular compartments (GSSG is found in concentrations around 5-50 μM only), this is not the case for the ER. In the ER, where folding and assembly of nascent proteins occur, GSSG provides the necessary environment to favour disulphide bond formation (Hwang et al., 1992).

GSH is a tripeptide formed exclusively in the cytoplasm from L-glutamate, L-cysteine and glycine in a two-step, ATP-dependent, reaction. The first and rate-limiting reaction is the synthesis of γ-glutamylcysteine, which is mediated by γ-GCL under consumption of one ATP molecule. In the second step, monomeric glutathione synthetase (GSS) uses another ATP molecule to add glycine to the C-terminus of γ-glutamylcysteine to form GSH (Figure 5.3). γ-GCL is highly conserved in most eukaryotes and knockout of *GCLC* in mice is embryonic lethal (Dalton et al., 2000, Shi et al., 2000), indicating an essential role for this enzyme during development. In cancer, γ-GCL expression and

activity is often upregulated, most likely in response to enhanced demand for GSH due to enhanced ROS presence.

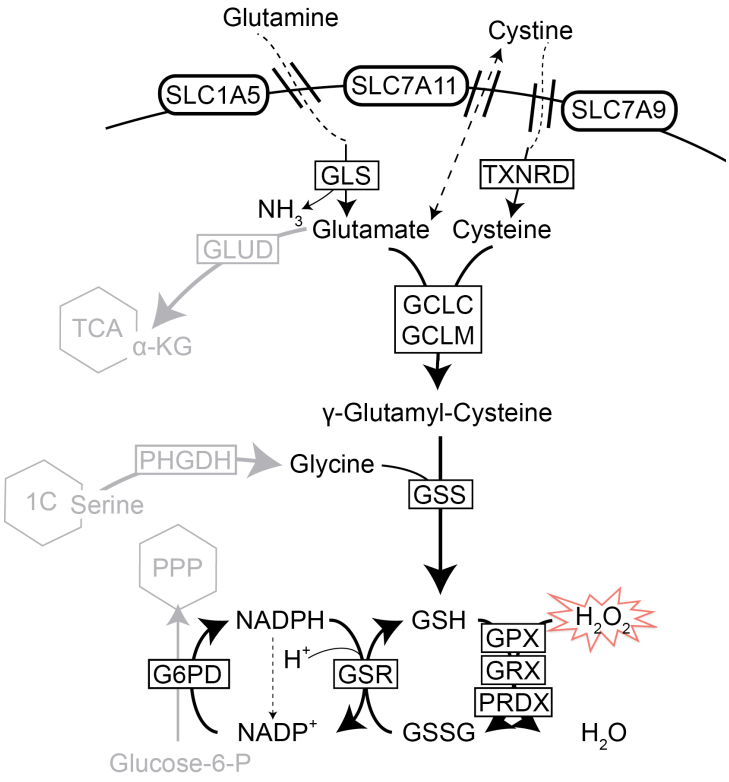

Figure 5.3: Glutathione biosynthesis and recycling
Glutathione (GSH) is synthesised in a three-step process from glutamine, cysteine and glycine. Once inside the cell, glutamine is converted to glutamate by glutaminase (GLS) and cystine is reduced to cysteine by thioredoxin reductase (TXNRD). Glutamate and cysteine are then ligated by γ-glutamylcysteine ligase (GCLC/M). Glutathione synthetase (GSS) adds a glycine to γ-glutamyl-cysteine to form GSH. GSH is a co-substrate for several ROS detoxifying enzymes such as glutathione peroxidase (GPX), glutaredoxin (GRX) and peroxyredoxin (PRDX). Oxidised GSSG can be recycled to reduced GSH by glutathione reductase (GSR), using NADPH as a reducing co-factor. NADPH can be sourced from the PPP, where it is produced by glucose-6-phosphate dehydrogenase (G6PD).

Cysteine is the rate-limiting substrate in GSH production and is reabsorbed from the stroma in the precursor form cystine, an amino acid formed by the covalent binding of two cysteine molecules via a disulphide bond. Cystine is taken up through either SLC7A11 or, especially in kidney tubules, by the cystine transporter SLC7A9 and subsequently reduced to cysteine intracellularly by TRDX or GSH (Figure 5.3). Expression of SLC7A11 and its stabilising cell surface glycoprotein CD44 have both been found to positively influence cancer cell proliferation (Ishimoto et al., 2011, Zhang et al., 2012).

The second amino acid required for GSH synthesis is glutamate, which is taken up as the precursor glutamine by several transporters, including the solute carrier family 1 member 5 (SLC1A5). Once in the cell, glutamine can be hydrolysed to glutamate and ammonia by glutaminase (GLS) (Figure 5.3). There are two isoforms of glutaminase: brain/kidney GLS1 and mitochondrial/liver GLS2. Expression of GLS1 is controlled by the oncogene c-MYC (Gao et al., 2009), while GLS2 is regulated by the tumour

suppressor p53 and has already been implicated to play a role in ROS metabolism (Suzuki et al., 2010).

In the course of reducing ROS, GSH becomes oxidised and dimerises with a second GSH molecule to form GSSG via a disulphide bond. This GSSG can be recycled to two molecules of GSH by glutathione reductase (GSR). GSR activity is dependent on FAD and NADPH, two important cofactors. One source of cytoplasmic NADPH is the pentose phosphate pathway (PPP) (Figure 5.3 and 1.4). Firstly, NADPH is generated through the conversion of glucose-6-phosphate to 6-phosphoglucono-δ-lactone by glucose-6-phosphate dehydrogenase (G6PD). Secondly, two steps further down, 6-phosphogluconate dehydrogenase (6PGD) converts 6-phosphogluconate into ribulose-5-phosphate, generating another NADPH molecule (Figure 1.4). Because of this dependency, GSH maintenance is coupled to the PPP activity.

5.1.5 Drugs perturbing GSH biosynthesis and maintenance

With GSH occupying such a central position in cellular redox regulation, it is not surprising that several nodes of GSH biosynthesis have been targeted for anti-cancer treatment. Figure 5.4 gives an overview of inhibitors and drugs that interfere with glutathione biosynthesis and maintenance. The drug Sulfasalazine targets the cysteine/glutamine antiporter SLC7A11 and has been approved for the treatment of pancreatic and lung cancer (Lo et al., 2010, Guan et al.). The enzyme L-asparaginase depletes glutamine and has been approved for the treatment of leukaemia and pancreatic cancer (Dufour et al., 2012, Pieters et al., 2011). The small molecule 968 (dibenzophenanthridine) and BPTES inhibit glutamine to glutamate conversion through inhibition of GLS and the small molecule 968 was approved to treat lymphoma and breast cancer (Wang et al., 2010, Le et al., 2012). Further down the line, the GCLC inhibitor L-buthionine sulphoximine (BSO) is used in the treatment of ovarian and breast cancer as well as in melanoma treatment (O'Dwyer et al., 1996). Finally, there have been successful attempts to pharmacologically alter the GSH:GSSG ratio (a) by inhibiting G6PD and thus GSH recycling with 6-anicotinamide (6-AN) (approved for

colon cancer treatment (Belfi et al., 1999)) and (b) through the GSSG mimetic NOV-002 (approved for treatment of lung, breast and ovarian cancer (Montero et al., 2012)).

In contrast, augmentation of GSH synthesis can be achieved by providing external supplements. The synthetic small-molecules N-acetyl-L-cysteine (NAC) and L-2-Oxothiazolidine-4-carboxylic acid (OTC) are cysteine derivatives that can fuel GSH production when converted into L-cysteine. NAC is a widely used nutritional supplement (antioxidant) and pharmacological substance used as mucolytic agent, nephron-protective agent and to treat paracetamol overdose amongst others. Another stimulator for GSH production is the soy isoflavone Genistein, which positively regulates γ-GCL and GPX1/GPX2 via activation of NRF1 and NRF2 (Myhrstad et al., 2002, Suzuki et al., 2002, Hernandez-Montes et al., 2006).

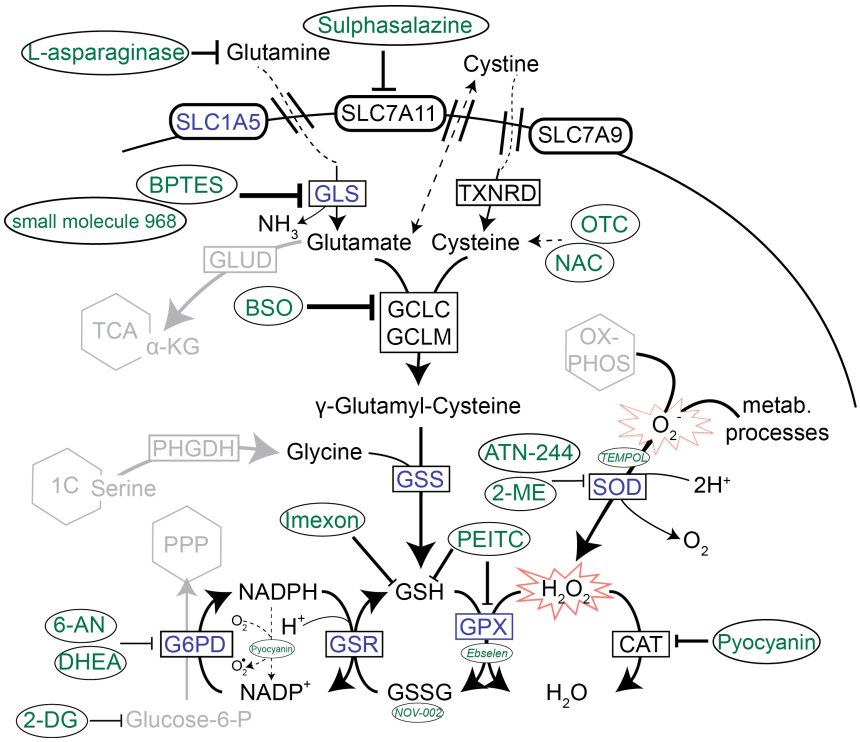

Figure 5.4: Overview of inhibitors and drugs that interfere with glutathione biosynthesis and maintenance

BSO, L-buthionine-S,R-sulfoximine; OTC, L-2-oxothiazolidine-4-carboxylate; NAC, N-acetyl-L-cysteine; 2-ME, 2-methoxyestradiol; PEITEC, phenethyl isothiocyanate; 6-AN, 6-aminonicotinamide; DHEA, dehydroepiandrosterone; 2-DG, 2-deoxy-D-glucose

5.2 Depletion of ROS scavenging enzymes is detrimental for ccRCC proliferation – independent of pVHL-status

As indicated in the previous chapter, analysis of the targeted metabolic screen in ccRCC cells (both the initial and the validation screen) identified several members of the GPX family (GPX1, GPX3, GPX4, GPX7) as well as SOD1 within the top 10% of genes that seemed to be essential for ccRCC cell proliferation (Table 4.1 and 4.2). This predominance of ROS scavenging enzymes amongst all other genes showing detrimental cell number loss when ablated led us to investigating their presumably fundamental role in ccRCC further.

5.2.1 Deconvolution of GPX siRNAs in isogenic ccRCC cell lines

As a second validation step, the SMARTpools for the eight GPX family members were deconvoluted in the RCC4 and 786-O isogenic cell line pairs and the non-malignant HK-2 cells. All eight GPX isoforms were positively deconvoluted as ≥ 2 of the four individual sequences showed a correlative decrease in cell number similar to that of the siRNA pool. Silencing of GPX1, GPX3, GPX4 and GPX7 showed the most negative effect on ccRCC cell viability. Moreover, in many of the cases, this negative effect was cancer-specific as HK-2 cells were hardly affected by depletion of these proteins. This was particularly the case for GPX1, GPX3, GPX6, GPX7 and GPX8. Interestingly, silencing of GPX1, GPX3 and GPX4 resulted in a stronger cell number loss in RCC4 cells compared to 786-O cells, suggesting that depletion of these enzymes could be partially selective for cells expressing both HIF-α isoforms as opposed to cells that have lost HIF-1α expression.

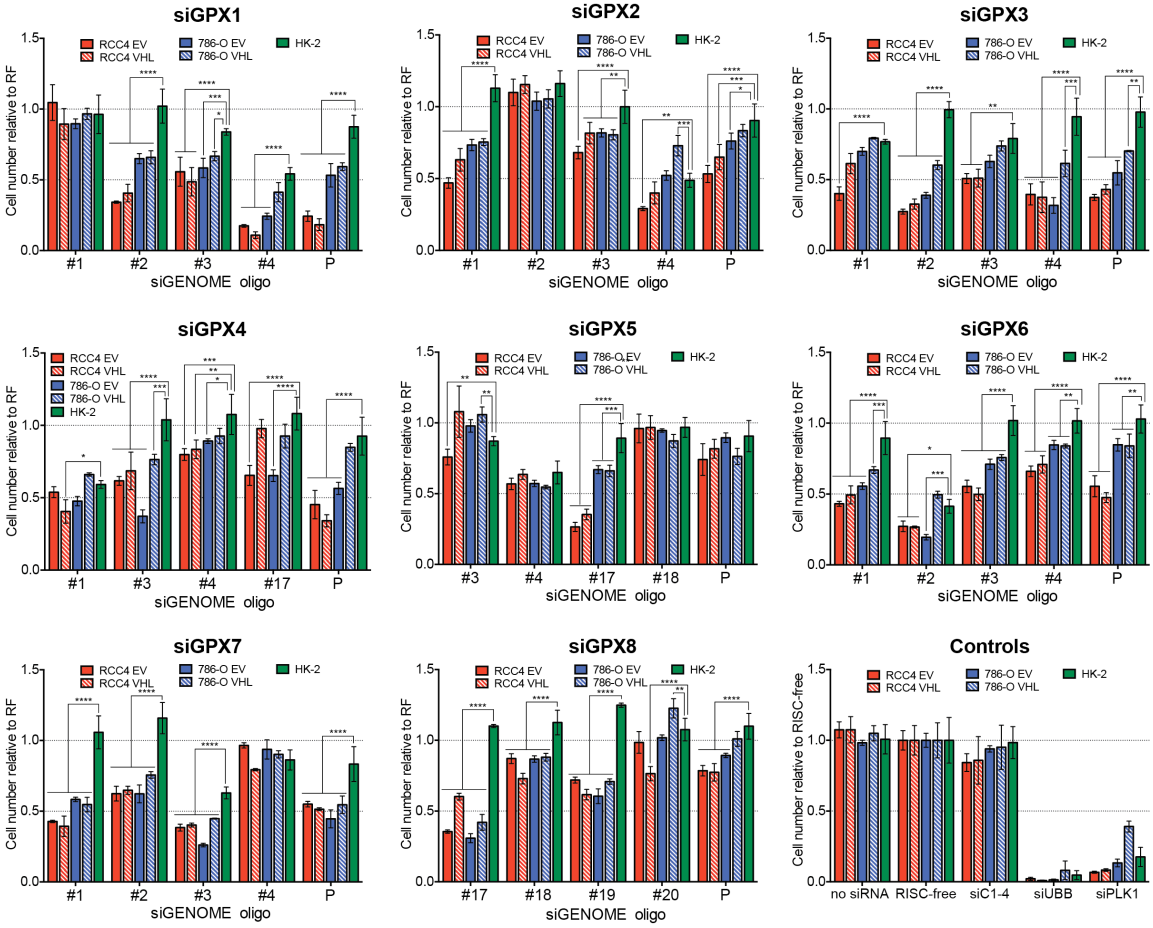

Figure 5.5: Deconvolution of Dharmacon GPX1-8 SMARTpools

The pVHL-isogenic cell line pairs RCC4 and 786-O and HK-2 cells were reverse transfected for 96 h with 37.5 nM of the 4 individual siRNA sequences comprising the SMARTpool in addition to the pool (P) against the 8 GPX isoforms. UBB and PLK1 served as positive and RISC-free (RF) and siC1-4 as negative controls. Bar graphs represent cell number means ± SD of triplicate wells normalised to RF. Significance of differential GPX siRNA effect in ccRCC cells compared to HK-2 cells was assessed by performing a 2-way ANOVA analysis including a Dunnett multiple comparison test (*, $p \leq 0.05$). All 8 SMARTpools deconvoluted successfully with ≥ 2 individual siRNA sequences having a similar (differential) effect as the pool.

5.2.2 Knockdown efficiency of siGPX1-8

Having successfully deconvoluted all eight GPX SMARTpools, knockdown efficiency of each SMARTpool and potential 'cross-reactivity' with any of the other isoforms was assessed. 786-O EV cells were transfected with each of the eight GPX SMARTpools and analysed for mRNA expression 48 h post transfection (Figure 5.6). Silencing of SEPSECS, the third and last enzyme in $tRNA^{sec}$ biosynthesis, was also included.

It seems as if all of the siRNA SMARTpools affected mRNA levels of the other isoforms at least to some extent (Figure 5.6B). Surprisingly, silencing of SEPSECS had

only a minor effect on GPX mRNA levels in general. GPX1, GPX4 and GPX8 mRNA species were the least affected by siRNAs targeting the other isoforms, while GPX2, GPX5, GPX6 and GPX7 mRNA species were the most affected. It seemed, though, that sensitivity of GPX2, GPX5 and GPX7 mRNA to RNAi of the other isoforms correlated with low mRNA abundance, as control transfected 786-O pVHL-null cells had a ΔC_T value ≥ 30 for GPX2, GPX5 and GPX7 (Figure 5.6A). Low basal mRNA levels make the analysis of siRNA knockdown efficiency for these genes less reliable.

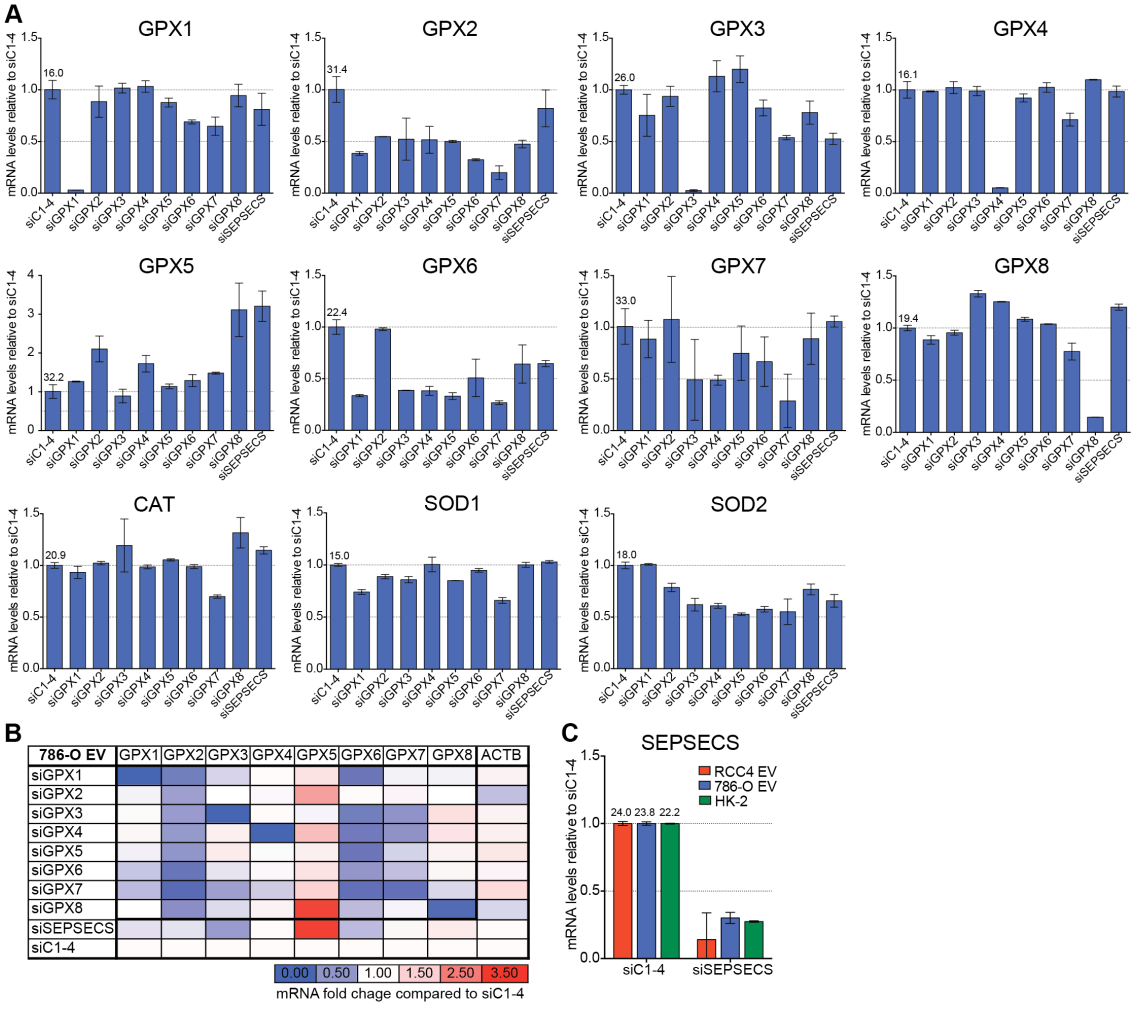

Figure 5.6: siRNA SMARTpools against the individual isoforms show 'cross reactivity' against each other.

(A) 786-O pVHL-null cells were reverse transfected for 48 h with 37.5 nM siRNA against all 8 GPX isoforms and SEPSECS respectively. Total RNA was analysed for mRNA expression of GPX1-8, CAT, SOD1 and SOD2 and SEPSECS using RT-qPCR. Bar graphs represent average ± SD of duplicate measurements normalised to respective ACTB levels and are displayed relative to scramble silencing (siC1-4). Number above siC1-4 bars indicates mean ΔC_T value. (B) Heat map summarising the fold-change differences in mRNA abundance relative to siC1-4 shown as bar graphs in (A). (C) Knockdown efficiency for siSEPSECS relative to siC1-4. Numbers above C1-4 indicate average ΔC_T value for comparison.

As GPX1 and GPX3 are the isoforms most likely to be important for cancer cells, knockdown efficiency of the individual GPX1 and GPX3 siRNA sequences of the SMARTpool and their cross-reactivity with each other was assessed (Figure 5.7). In both RCC4 and 786-O pVHL-null cells, mRNA depletion upon GPX1 and GPX3 silencing was > 90% (Figure 5.7A,B). In HK-2 cells, silencing with the GPX3 SMARTpool was equally effective and resulted in ~90% mRNA depletion (Figure 5.7B). The GPX1 SMARTpool was less efficient on mRNA level with only a 50% knockdown (Figure 5.7A), but efficient depletion of the protein was detected in both RCC4 EV and HK-2 cells (Figure 5.7C). Due to its nature as a secreted protein, monitoring GPX3 on protein level remained unsuccessful with the methods available.

Some GPX1 and GPX3 siRNA sequences showed a mutual effect on the other genes' mRNA levels. Two of the four siRNAs targeting GPX1 also negatively affected GPX3 mRNA levels in 786-O EV cells (Figure 5.7A, right-hand panel); while two of the four siRNAs targeting GPX3 induced GPX1 mRNA expression in RCC4 EV cells (Figure 5.7B, right-hand panel).

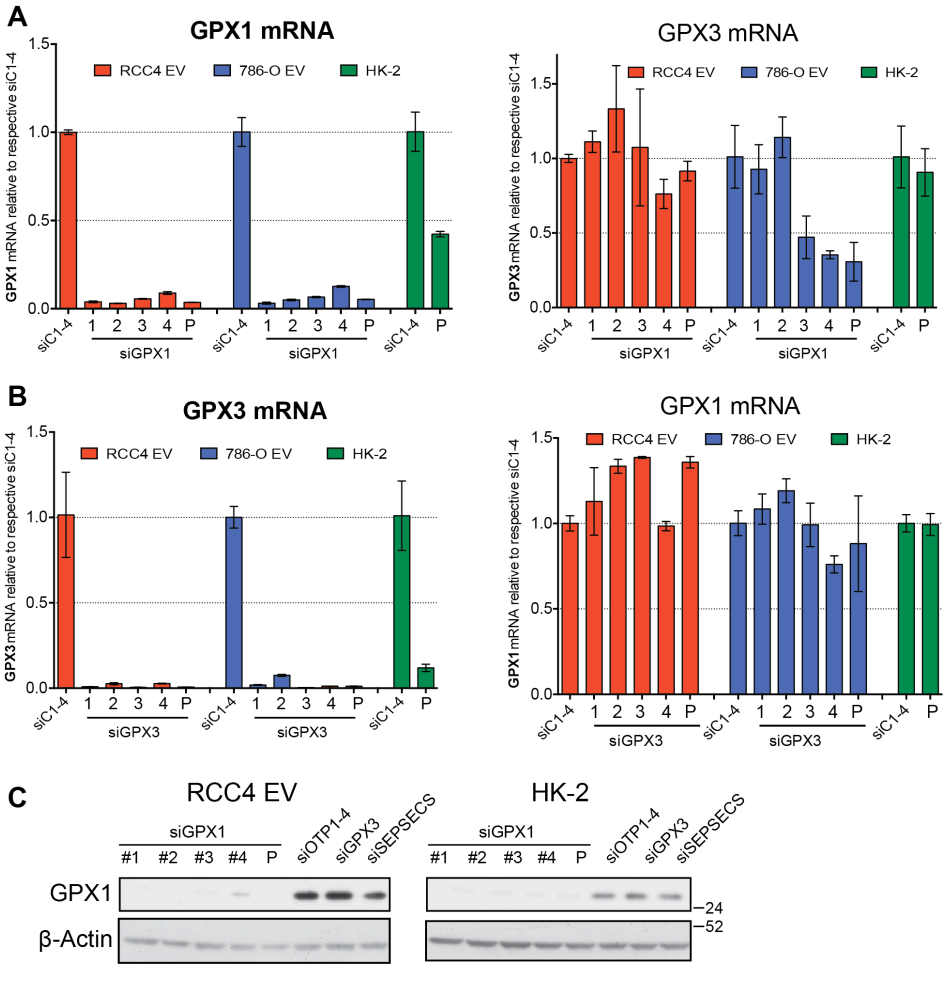

Figure 5.7: GPX1 and GPX3 knockdown is good and efficient
(A-B) RCC4 EV, 786-O EV and HK-2 cells were reverse transfected for 48 h with 37.5 nM of the 4 individual siRNA target sequences (♯1-4) comprising of the SMARTpool and the pool (P) against (A) GPX1 and (B) GPX3. Total RNA abundances for GPX1 and GPX3 were examined using RT-qPCR. Bar graphs represent average of duplicate measurements normalised to respective ACTB levels and are displayed relative to scrambled siRNA (siC1-4). Error bars represent SD. (C) RCC4 EV and HK-2 cells were transfected as above with the deconvoluted siRNA sequences against GPX1. siSEPSECS was included. Whole cell lysates were subjected to SDS/PAGE and were analysed for GPX1 protein expression to check for knockdown efficiency. β-Actin serves as loading control.

5.3 Transfer from *VHL*-isogenic cell line to parental cell lines

As ablation of GPXs did not show pronounced and consistent differential effects between *VHL*-null and -reconstituted cells, it seemed more appropriate to continue the study in the parental RCC4, UMRC2, A498, 786-O and 769-P cell lines. Moreover, for a better representation of the heterogeneity of ccRCCs, all twelve ccRCC cell lines were included for all further investigations.

Reassuringly, GPX knockdown had similar detrimental effects in the parental cell lines and the isogenic cell line pairs (Figure 5.8). Silencing of CAT, SOD1 and SOD2 as well as the ROS-defence master regulator NRF2 was included to cover a broader spectrum of the ROS scavenging system. All ccRCC cell lines were highly sensitive not only to ablation of the different GPXs, but also to silencing of CAT, SOD1, SOD2 and NRF2 (Figure 5.8B). Furthermore, ablation of especially GPX1, GPX3, GPX7 and SOD1 revealed strong cancer-specific effects with HK-2 cells being hardly affected through ablation of any of the proteins tested but NRF2 and TXNRD2 (Figure 5.8).

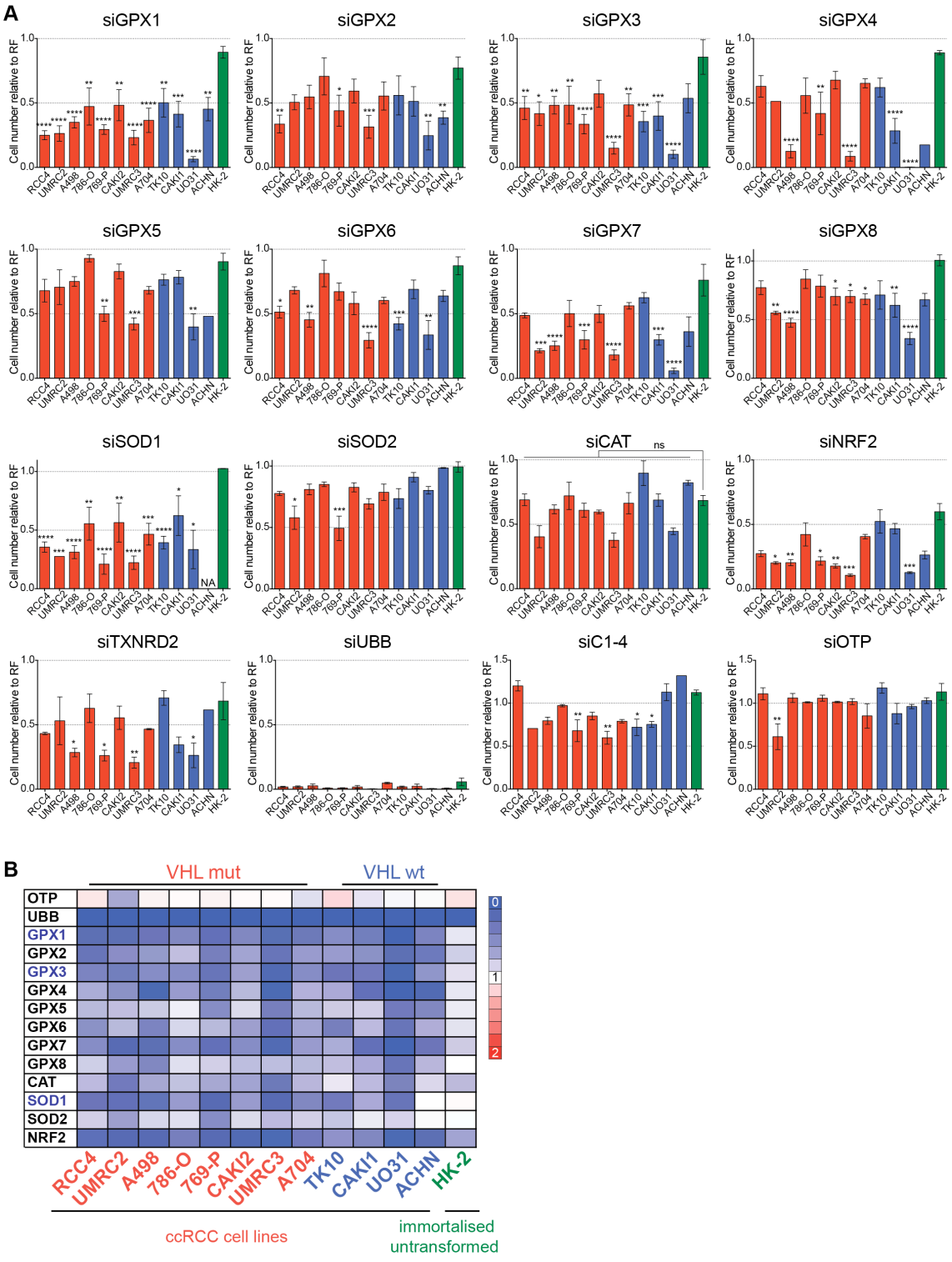

Figure 5.8: Ablation of ROS detoxifying enzymes is detrimental for ccRCC but not for HK-2 cells

(A) Indicated ccRCC cell lines were transfected with 37.5 nM siRNA against the indicated genes for 96 h. Bar graphs represent average endpoint cell numbers relative to RISC-free (RF) of 3 independent experiments performed in triplicates ± SEM. Asterisks indicate ccRCC cell lines with significant cell number loss compared to HK-2 cells upon ablation of the respective protein (2-way ANOVA analysis including Dunnett multiple comparison testing; *, $p \leq 0.05$; ns, not significant). (B) Heat map summarising relative cell number data from (A).

In contrast to the ccRCC cell lines, which are maintained in DMEM, HK-2 cells are maintained in KSFM medium. Hence, the effect of different media on the sensitivity to silencing of components of the anti-oxidant system was addressed in RCC4, 786-O and HK-2 cells. While the observed GPX silencing effect hardly differed in the two different media for RCC4 cells, 786-O cells were more susceptible to cell number loss following ablation of GPXs in DMEM compared to KSFM medium (Figure 5.9). With regard to ablation of GPX1 and GPX3, 786-O cells seemed to encounter a proliferation boost in KSFM compared to DMEM medium (Figure 5.9). HK-2 cells showed higher cell number loss following ablation of only GPX1 and GPX4 in DMEM medium, but as transfection with scrambled siRNA (siC1-4) showed a similar effect, a potential media effect on knockdown efficiency in these cells was neglected (Figure 5.9).

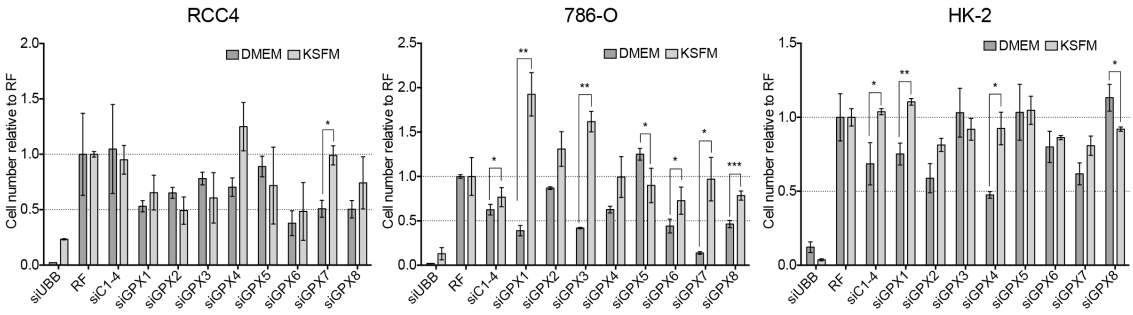

Figure 5.9: Media effect on knockdown efficiency of GPXs is negligible
RCC4, 786-O and HK-2 cells were reverse transfected for 96 h with 37.5 nM siRNA against the 8 GPX isoforms, UBB as positive and C1-4 as negative control in either complete DMEM/10% FBS or KSFM medium. Bar graphs represent cell number means of 3 wells normalised to RISC-free (RF) ± SD. Asterisks indicate significant differences in cell number upon RNAi in the different media (two-tailed paired t-test, *, $p \leq 0.05$).

5.4 GPX1 and GPX3 ablation does not induce apoptosis

To analyse the mechanisms leading to the observed reduction in cell number following ablation of ROS-scavenging enzymes, a subset of cell lines from the cell line panel (RCC4, A498, 769-P, TK10, ACHN and HK-2) was monitored for their growth kinetics in an IncuCyte life cell imaging system. The growth curves depicted in Figure 5.10A indicated that ccRCC cells grew slower rather than underwent cell death upon ablation of GPX1-8. This was particularly obvious by comparison with UBB ablation, which induces apoptosis. Ablation of most GPX isoforms resulted in significant cell number

loss compared to scrambled RNAi, whereby GPX1, GPX3, GPX 7 and SOD1 had the strongest growth inhibitory effects (Figure 5.10B).

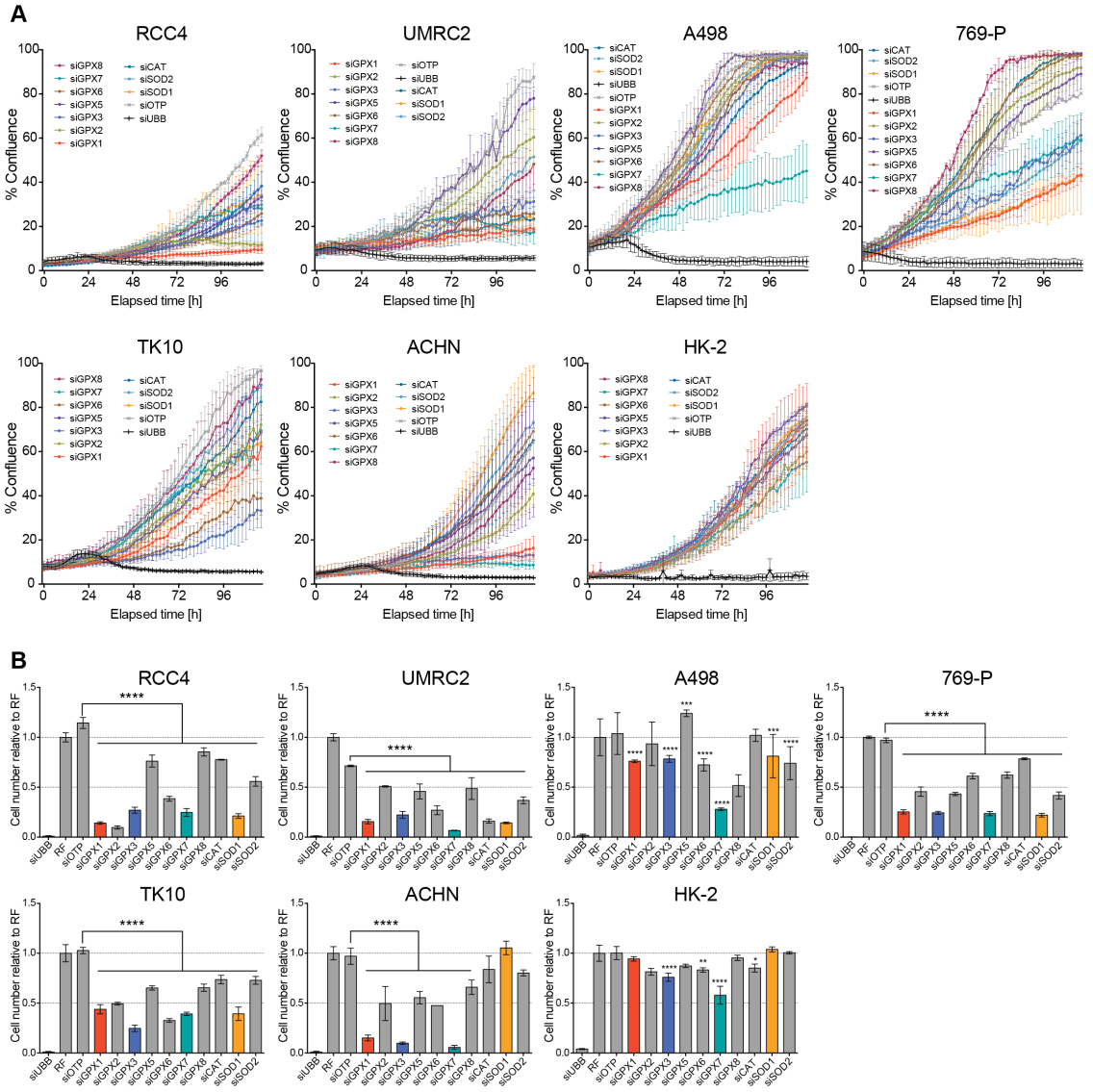

Figure 5.10: Ablation of GPX1, GPX3, GPX7 and SOD1 inhibit ccRCC proliferation

(A) ccRCC and HK-2 cells were reverse transfected with 37.5 nM siRNA against the indicated genes and were monitored for cell proliferation in an IncuCyte live cell imaging system. siUBB serves as positive apoptosis-inducing control, siOTP1-4 as negative control. Curves show average cell proliferation over time generated from confluence measurements every 2 h for 120 h in total of ≥ 2 replicate wells ± SD. (B) Bar graphs represent average endpoint cell numbers of the ≥ 2 wells from (A) normalised to RISC-free (RF) ± SD. Highlighted are genes (GPX1, GPX3, GPX7 and SOD1) that when silenced were particularly detrimental in most ccRCC but not so much in HK-2 cells. Asterisks indicate significant effects on endpoint cell numbers of respective GPX isoform ablation compared to transfection with scrambled siRNA (siOTP) (2-way ANOVA analysis with Dunnett multiple comparison testing, *, $p \leq 0.05$).

Further analysis confirmed the initial observation that GPX ablation was not cytotoxic, as upregulation of any common inducers of the apoptotic process were not obvious. It

was not possible to detect increased caspase3/7 enzymatic activity upon GPX1 or GPX3 knockdown (Figure 5.20A, C) and no accumulation of cleaved poly (ADP-ribose) polymerase (PARP) could be observed (Figure 5.11A). In addition, no changes in B-cell lymphoma 2 (Bcl-2) and Bcl-2 associated X protein (BAX) mRNA could be observed in RCC4 or HK-2 cells (Figure 5.11B). Only expression of the p53 upregulated modulator of apoptosis (PUMA) mRNA seemed to be increased. However, a 2-/3-fold increase in p21 mRNA levels upon ablation of GPX1/GPX3 suggested that the cells were in distress (Figure 5.11B).

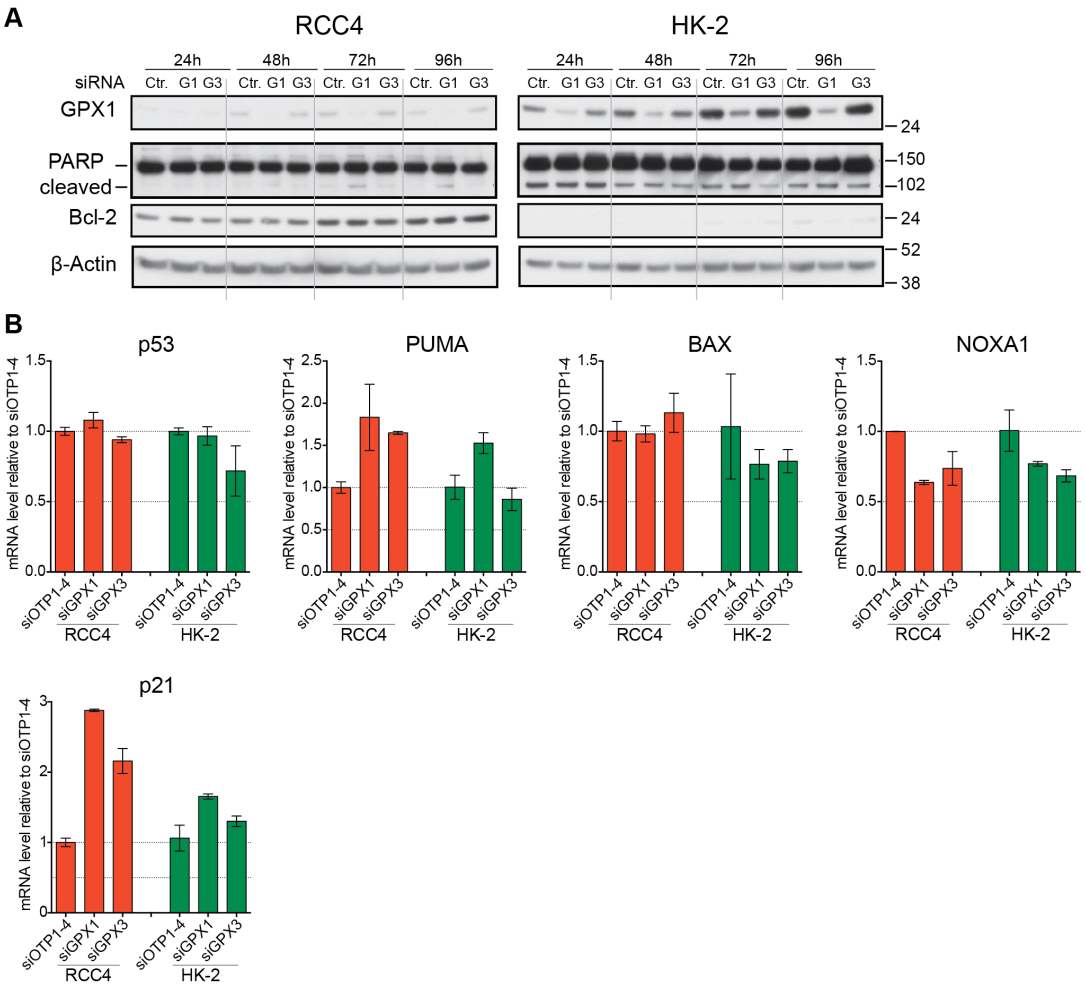

Figure 5.11: GPX1 and GPX3 ablation does not induce apoptosis

(A) RCC4 and HK-2 cells were reverse transfected with siRNA against GPX1 and GPX3 or with scrambled siRNA (siC1-4, Ctr.). Whole cell lysates were prepared 24, 48, 72 and 96h post transfection and analysed for GPX1, (activated, i.e. cleaved) PARP and Bcl-2 protein expression. β-Actin serves as loading control. (B) RCC4 (red) and HK-2 (green) cells were reverse transfected for 48h with siRNA against GPX1 and GPX3. mRNA levels of stress and cell death marker p53, PUMA, BAX, NOXA1 and p21 were determined using RT-qPCR. Bar graphs represent average of duplicate measurements normalised to respective ACTB mRNA levels ± SD and are displayed relative to the respective scramble siRNA (siOTP1-4).

5.5 GPX1 and GPX3 ablation prolong cell cycle duration in RCC4 cells

Depletion of GPX1 and GPX3 resulted in a severe cell number loss compared to control silencing in the different ccRCC cell lines. However, no obvious induction of apoptotic cell death was observed (Figure 5.11). Another route of comparative cell number reduction following 4 days of siRNA treatment could be caused by prolonged cell cycling or cell cycle arrest, leading to reduced proliferation.

RCC4 EV cells were subjected to an 8 h BrdU pulse-chase analysis to assess cell cycle duration following GPX1, GPX3 and SOD1 ablation (Figure 5.12). In contrast to control-silenced cells, where BrdU-positive cells showed a prominent G1-phase peak after 6 h (Figure 5.12A), cells with GPX1, GPX3 and SOD1 knockdown reached this peak with a 2 h delay (Figure 5.12B - D). RCC4 EV cells treated with 1 μM cdk4/6 inhibitor as positive control remained in G1-phase over the experimental duration of 8 h, while vehicle treated cells cycled similarly to control siRNA treated cells (Figure 5.12E - F).

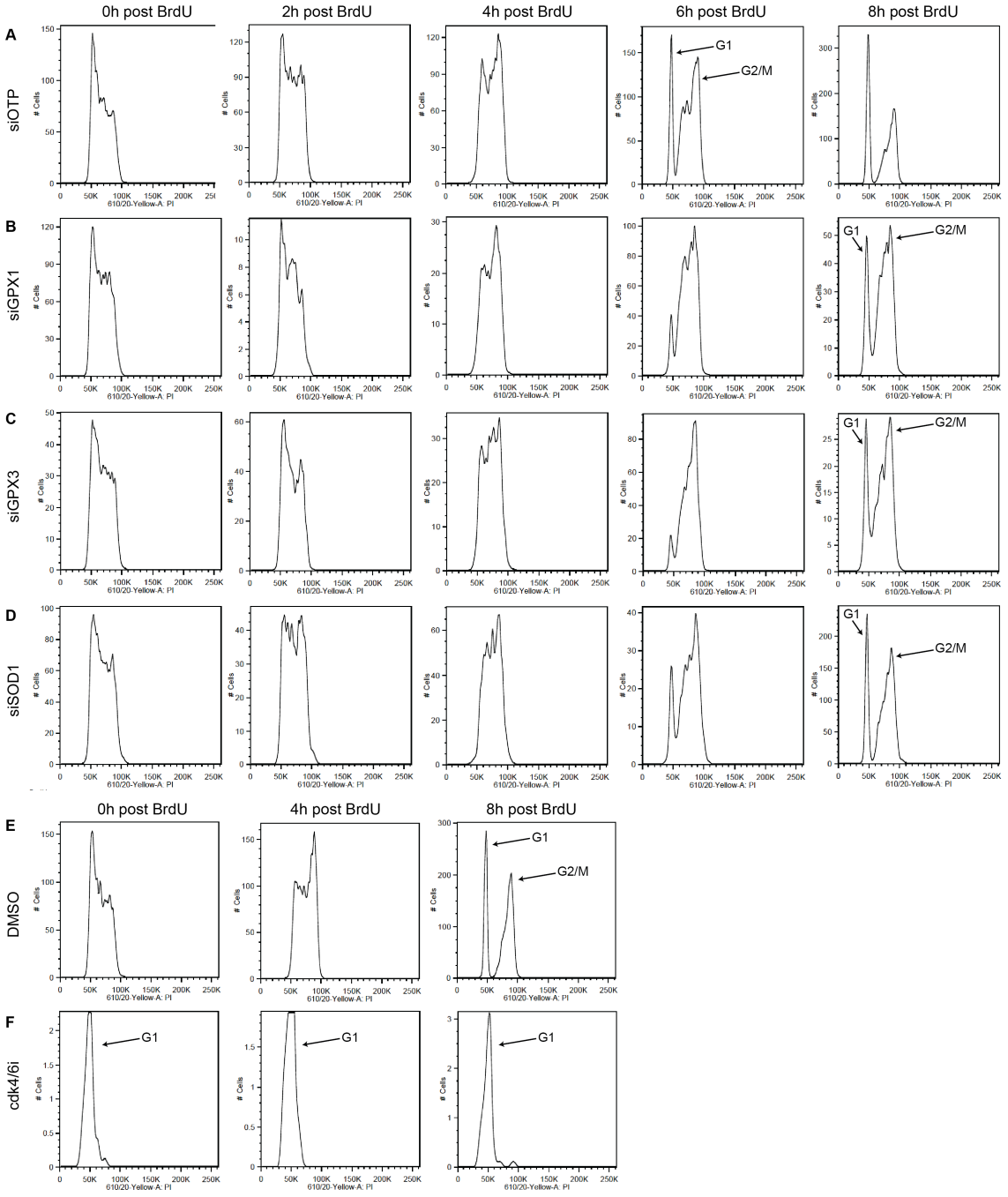

Figure 5.12: Ablation of GPX1, GPX3 and SOD1 results in prolonged cell cycle in RCC4 EV cells

To analyse cell cycle duration 96 h post (A) scrambled (siOTP1-4), (B) GPX1, (C) GPX3 and (D) SOD1 silencing, RCC4 EV cells were pulsed for 15 min with 30 µM BrdU and fixed immediately (0 h), after 2 h, 4 h, 6 h or 8 h. Histograms show PI profile of BrdU-positive RCC4 EV cells. (E) 72 h treatment with (E) 1 µM cdk4/6 inhibitor served as positive control for cell cycle arrest in G1. (F) Vehicle treatment served as negative control for (E).

To assess cell cycle progression over the course of a regular 4 d silencing experiment, changes in cell cycle distribution following siGPX1 and siGPX3 transfection were monitored every 24 h in RCC4 EV cells (Figure 5.13). RNAi in general seemed to have

a cell cycle attenuating effect, as silencing of either GPX1 or GPX3 or scrambled caused an increase in cells in G1-phase and a decrease in cells in S- and G2/M phase over the 4 days (Figure 5.13A). However, GPX1 and GPX3 silencing for 72 h caused a higher increase in G1 or G2/M cell populations compared to scrambled silencing (Figure 5.13B).

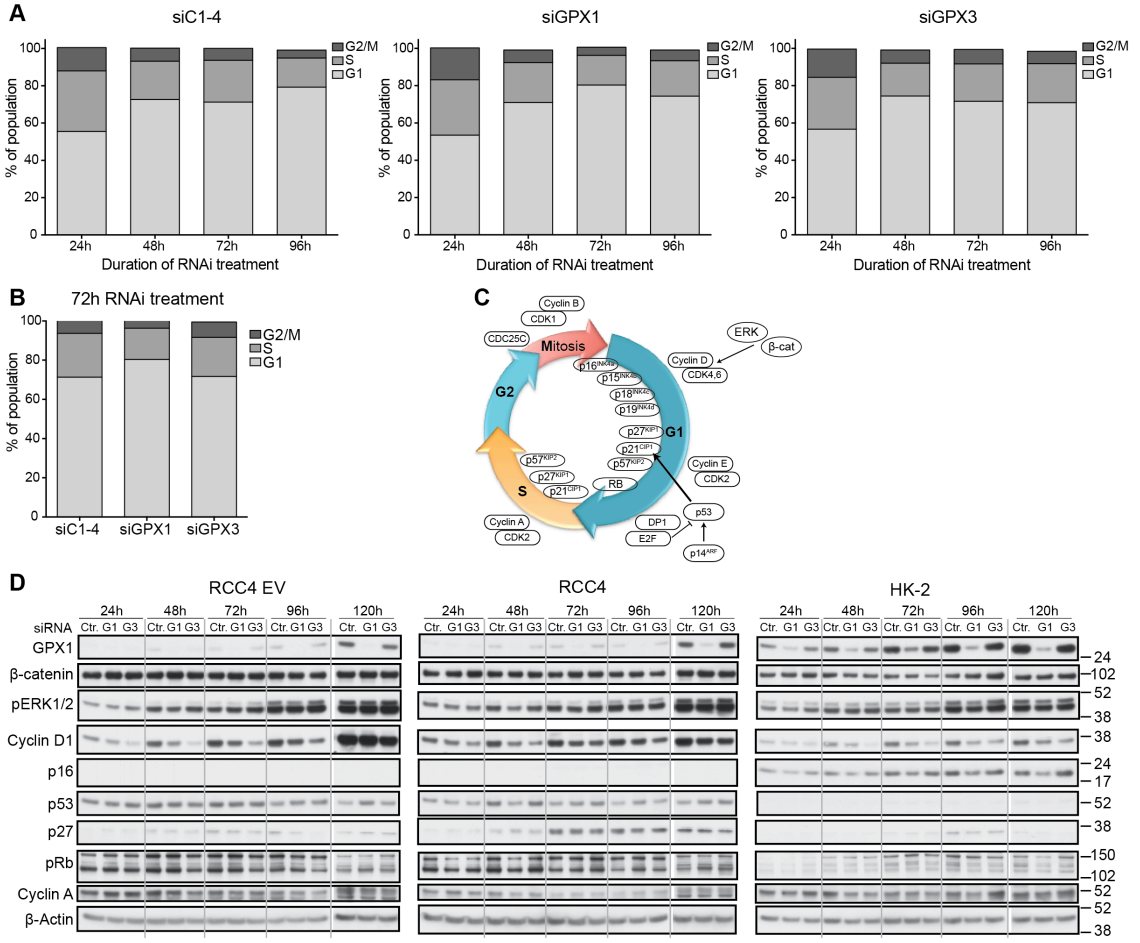

Figure 5.13: GPX1 and GPX3 ablation prolong G1- and G2/M- phase in RCC4 cells

(A-B) RCC4 EV cells were reverse transfected with 37.5 nM siRNA against GPX1 and GPX3. Cells were harvested every 24 h post transfection for 4 d and analysed for cell cycle progression using FACS analysis of incorporated propidium iodide (PI). Stacked bar graphs represent fractionation of analysed cell population in different cell cycle phases at time of fixation. (A) Cell cycle phase progrssion following scrambled (siC1-4), *GPX1* and *GPX3* silencing over time. (B) Cell cycle phase distribution following GPX1 or GPX3 ablation for 72 h (extracted from (A)). siC1-4, negative transfection control. (C) Schematic illustrating the regulating factors behind cell cycle progression. The proteins aligned in the centre are negative regulators of cell cycle progression and inhibit the positive regulators aligned on the outside of the circle in the respective phases of the cell cycle (G1->S->G2->M). The MAP kinase pathway as well as β-catenin can directly influence cell cycle progression by activation of cyclin D, while under cellular stress conditions (e.g. severe DNA damage) p14/ARF activates p53, which activates p21 subsequently, leading to cell cycle arrest in G1. (D) Cells were transfected as in (A-B) and harvested after 24, 48, 72, 96 and 120 h for cell lysis. Whole cell lysates were subjected to SDS/PAGE and analysed for the indicated cell cycle proteins. β-Actin serves as loading control.

RCC4 pVHL-null and HK-2 cells were also analysed for changes in protein expression of key cell cycle regulators over a 5 d period of GPX1 and GPX3 ablation (Figure 5.13D). Over the 5 days, increased levels of cyclin D1 and p27 could be observed in both RCC4 and HK-2 cells; changes in p16 were only present in HK-2 cells. However, cyclin D1 was consistently reduced in cells where GPX1 or GPX3 was ablated (of the two genes, GPX3 had the strongest effect on cyclin D1 repression) compared to control-silenced cells, even in HK-2. Furthermore, p53 and cyclin A protein levels oscillated in synchronisation in RCC4 cells, while in HK-2 cells it was p16 that was synchronised with cyclin A. p16 was undetectable in RCC4 and p53 was beyond detection levels in HK-2 cells (Figure 5.13D).

Taken together, these results indicate that ablation of GPX1 or GPX3 in RCC4 cells causes a delay in cell cycle progression with an extended G1-phase compared to scrambled-silenced cells. This effect seemed to be stronger after silencing of GPX1 compared to GPX3. However, further analysis is necessary to confirm these results.

5.6 Silencing of GPX1 and GPX3 causes a mild DNA damage phenotype

The preliminary cell cycle analyses pointed to a slowing down of cell cycle progression due to a prolonged G1-phase. A common reason for cell cycle stalling is damaged DNA that needs to be repaired before the cell can progress through S-phase and mitosis. Indeed, ccRCC cells show increased basal p21 mRNA levels as compared to HK-2 cells (Figure 5.14A), indicating higher basal stress levels in ccRCC as compared to HK-2 cells. Accumulation of p53 protein was noticed (Figure 5.14B) as well as a 2- and 3-fold increase in p21 mRNA levels following depletion of GPX1 and GPX3 respectively in RCC4 cells (Figure 5.14E). Both observations support the idea for increased DNA damage being causative. Hence, RCC4, 786-O, CAKI1 and HK-2 cells were analysed for DNA damage following knockdown of GPX1, GPX3 and SOD1 by simultaneous detection of immunofluorescence (IF) against γH2.AX and the DNA damage response (DDR) component 53BP1. Quantification of nuclear γH2.AX foci in RCC4 and 786-O cells showed a tendency towards increased foci number upon GPX1, GPX3 or SOD1

ablation compared to control, whereby GPX3 depletion had the strongest effect (Figure 5.14C). CAKI1 and HK-2 cells did not show any alteration from control cells after GPX silencing. 53BP1 accumulates at sites of double strand breaks (DSB) on the DNA and recruits factors involved in DDR of the homologous recombination type (amongst others Ku70:Ku80 and RAD51). An increase in 53BP1 foci could be observed after GPX1 and GPX3 silencing in the cancer cells, but not in HK-2 cells (Figure 5.14D), although the variability between the three replicate experiments was considerable. Surprisingly, RAD51 and Ku70 mRNA levels were not increased in RCC4 cells and in case of HK-2 cells was even reduced by 30% upon GPX1 and GPX3 ablation compared to control (Figure 5.14E). However, an explanation for this discrepancy might be the experimental timing: mRNA levels were examined 48 h post transfection while 53BP1 foci were assessed 96 h post transfection. As 53BP1 accumulation is the first event that recruits RAD51 and Ku70:Ku80, the appropriate detection window of induced RAD51 and Ku70 might have been missed.

In summary, these data suggest that loss of GPX1 and GPX3 result in at least mild DNA damage, quite possibly involving DSBs. These could be caused by ROS accumulation leading to oxidative damage of DNA.

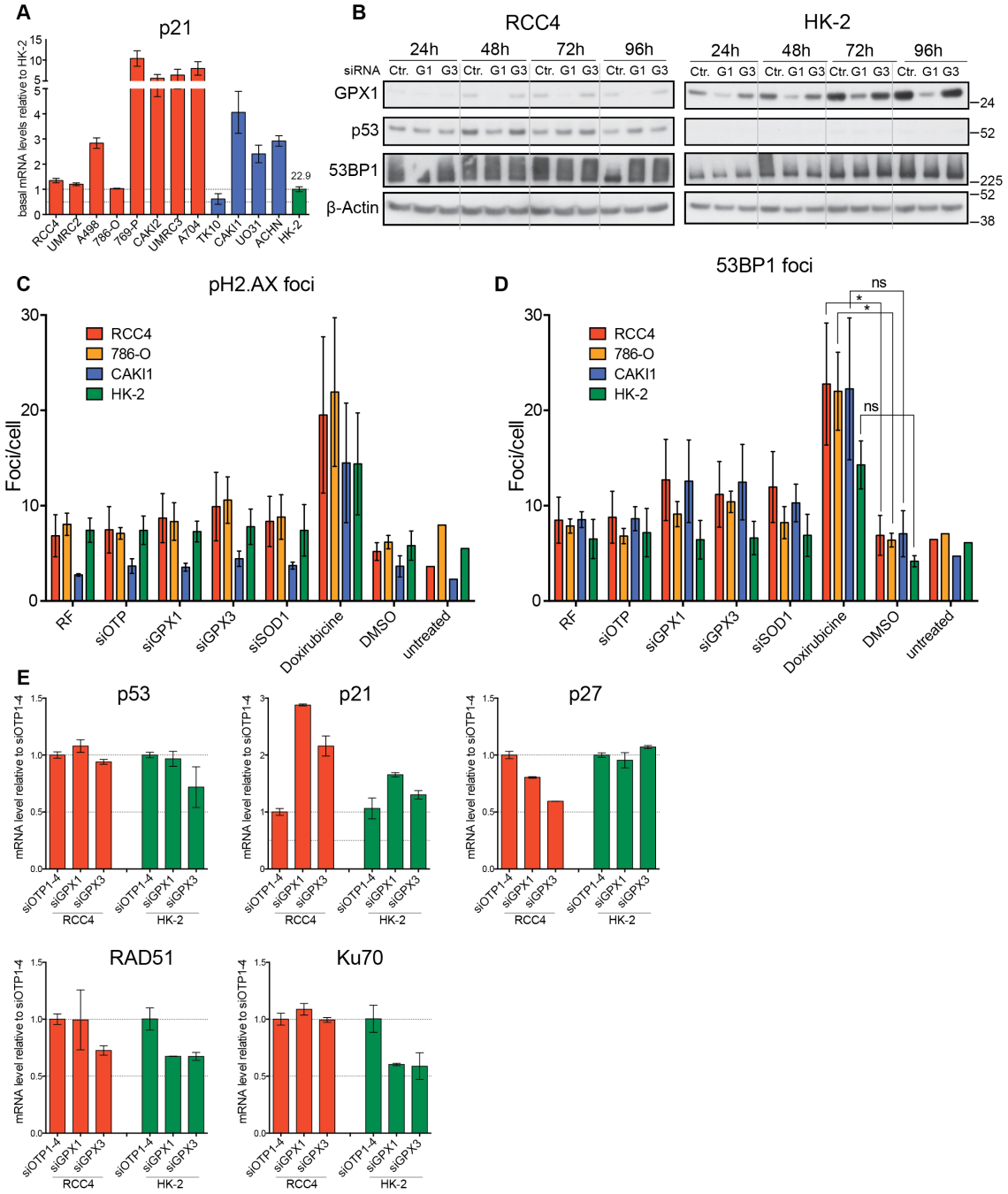

Figure 5.14: Ablation of GPX1, GPX3 and SOD1 induce mild DNA damage

(A) Basal p21 mRNA expression in ccRCC and HK-2 cell lines. Bars represent average of duplicate measurements normalised to respective ACTB mRNA levels and are displayed relative to control silencing (siOTP1-4). Error bars represent SD. Number above HK-2 bar indicates average ΔC_T value for comparison. (B) RCC4 and HK-2 cells were reverse transfected with scrambled (siC1-4, Ctr.), GPX1 (G1) and GPX3 (G3) siRNA for 24, 48, 72 and 96 h before lysis. Whole cell lysates were analysed for GPX1, p53 and 53BP1 protein expression. β-Actin serves as loading control. (C-D) RCC4, 786-O, CAKI1 and HK-2 cells were reverse transfected for 96h with 37.5 nM siRNA targeting GPX1, GPX3 and SOD1.(C) γH2.AX and (D) 53BP1 foci formation was analysed simultaneously using immunofluorescent cytochemistry. Treatment with 250 nM Doxirubicine for 6 h prior to fixation was used as positive control for induction of DNA damage. Bar graphs represent average number of (C) γH2.AX and (D) 53BP1 foci per cell normalised to the respective negative RISC-free (RF) control from 3 independent experiments performed in triplicates. Error bars represent ± SEM. Asterisks indicate significant induction of either

γH2.AX or 53BP1 foci upon GPX1/3 and SOD1 ablation or Doxirubicine treatment compared to control (siOTP or DMSO, respectively) (2-way ANOVA analysis including Dunnett multiple comparison test; *, $p \leq 0.05$; ns, not significant). (E) RCC4 and HK-2 cells were transfected as in (C) and lysed 48h post transfection for total RNA extraction. mRNA abundance of DNA damage response inducers p53, p21, p27 as well as the effectors RAD51 and Ku70 were determined using RT-qPCR. Bar graphs represent average of duplicate C_T measurements normalised to respective ACTB mRNA levels ± SD and are displayed relative to control silencing (siOTP1-4).

5.7 GPX1 and GPX3 silencing positively affects SOD2 expression

The effect of GPX1 and GPX3 silencing on the expression of other components in the main ROS detection system was investigated next in RCC4 and HK-2 cells. Therefore, mRNA levels of SOD1, SOD2, CAT, PRDX6 (a lipidperoxide reducing peroxiredoxin) as well as the ROS defence regulator NRF2 were evaluated (Figure 5.15). Silencing of GPX1 showed a mild downregulation of CAT and PRDX6 mRNA to similar extent in both RCC4 and HK-2 cells (Figure 5.15B). Furthermore, GPX1 loss increases SOD2 mRNA levels ≥ 2-fold in both cell lines (stronger in RCC4 cells) and also induces NRF2 slightly in RCC4 cells. Ablation of GPX3 also caused NRF2 mRNA upregulation in both RCC4 and HK-2 cells while reducing SOD1 and PRDX6 mRNA levels to a similar extend (Figure 5.15B). Interestingly, GPX3 silencing had a major negative effect on SOD2 mRNA levels (50% reduction) in RCC4 but not in HK-2 cells. However, no SOD2 protein reduction could be detected following siGPX3. In contrast, increased levels of SOD2 mRNA following ablation of GPX1 also translated into increased SOD2 protein levels (Figure 5.15C).

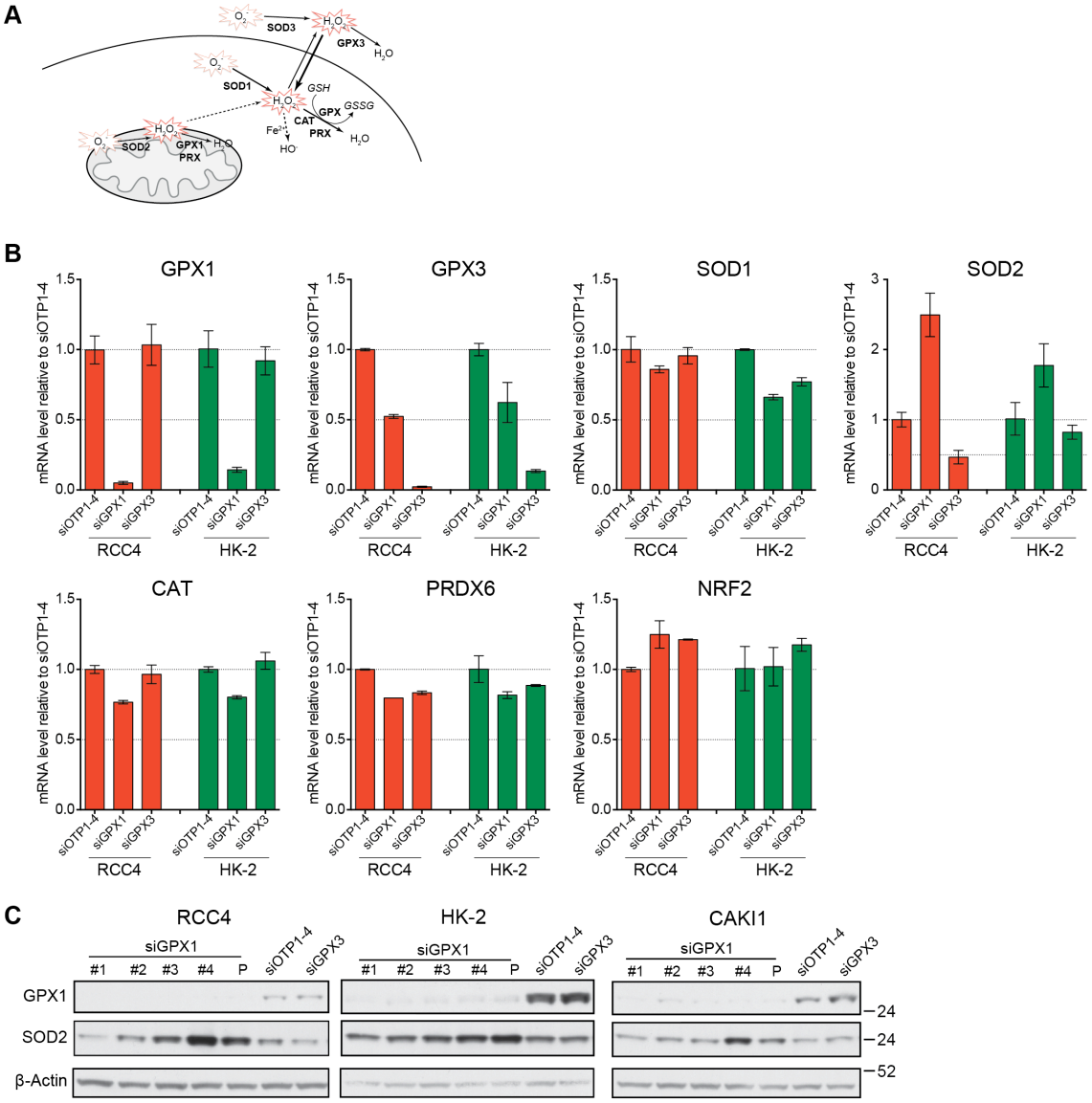

Figure 5.15: GPX1 depletion induces SOD2 mRNA and protein expression.

(A) Schematic illustrating the enzymatic network for ROS detoxification. (B) RCC4 and HK-2 cells were reverse transfected with 37.5 nM siRNA against GPX1 and GPX3 and analysed for mRNA expression of the indicated genes 48 h later. Bar graphs represent average of duplicate C_T measurements normalised to ACTB and relative to the respective scramble control siRNA (siOTP1-4) ± SD. (C) RCC4, CAKI1 and HK-2 cells were reverse transfected with siRNA against GPX1 (SMARTpool, P and deconvoluted: siRNA ♯1-4) or GPX3 (SMARTpool) for 96 h. Whole cell lysates were subjected to SDS/PAGE and analysed for GPX1 and SOD2 protein expression. β-Actin serves as loading control.

5.8 Co-silencing of GPX1 and FOXO4 synergistically slow down cell proliferation

As a stalling of the cell cycle in G1 and upregulation of SOD2 could be observed upon GPX1 ablation, interplay between GPX1 and FOXO factors was considered and further investigated. FOXO factors are known regulators of both cell cycle and ROS metabolism and directly control the expression of SOD2 (van der Horst and Burgering, 2007, Kops et al., 2002a, Kops et al., 2002b, Nogueira et al., 2008, Ferber et al., 2012). RCC4 and HK-2 cells were monitored for their growth kinetics using the IncuCyte life cell imaging system following GPX1, FOXO1, FOXO3 and FOXO4 silencing alone or as combination of GPX1 and one of the three FOXO isoforms respectively (Figure 5.16). In HK-2 cells, ablation of FOXO1, FOXO3 or FOXO4 alone or in combination with GPX1 did not have any significant effect on cell growth (Figure 5.16A, B). In RCC4 cells, knockdown of the individual FOXO isoforms also did not have an effect on proliferation. However, combined silencing of GPX1 and FOXO3 schowed a small, GPX1 and FOXO4 a significant synergistic effect on cell proliferation (Figure 5.16A, B). Furthermore, upregulation of GPX1 and FOXO1 mRNA following FOXO3 ablation in both RCC4 and HK-2 cells was observed, indicating cross-talk between different anti-oxidant control systems (Figure 5.16C). In addition, silencing of FOXO3 or FOXO4 together with GPX1 increased mRNA levels of FOXO1 by approx. 2.5-fold in HK-2 cells, suggesting a compensatory mechanism in these cells. Contrary to RCC4 cells, co-silencing of GPX1 with any of the three FOXO isoforms resulted in a 2- to 3-fold increase in SOD2 mRNA in HK-2 cells (Figure 5.16C). This is surprising, as depletion of FOXO factors should result in a reduced expression of this target gene. However, increased oxidative stress caused by combined depletion of GPX1 and FOXOs could activate SOD2 expression via other pathways.

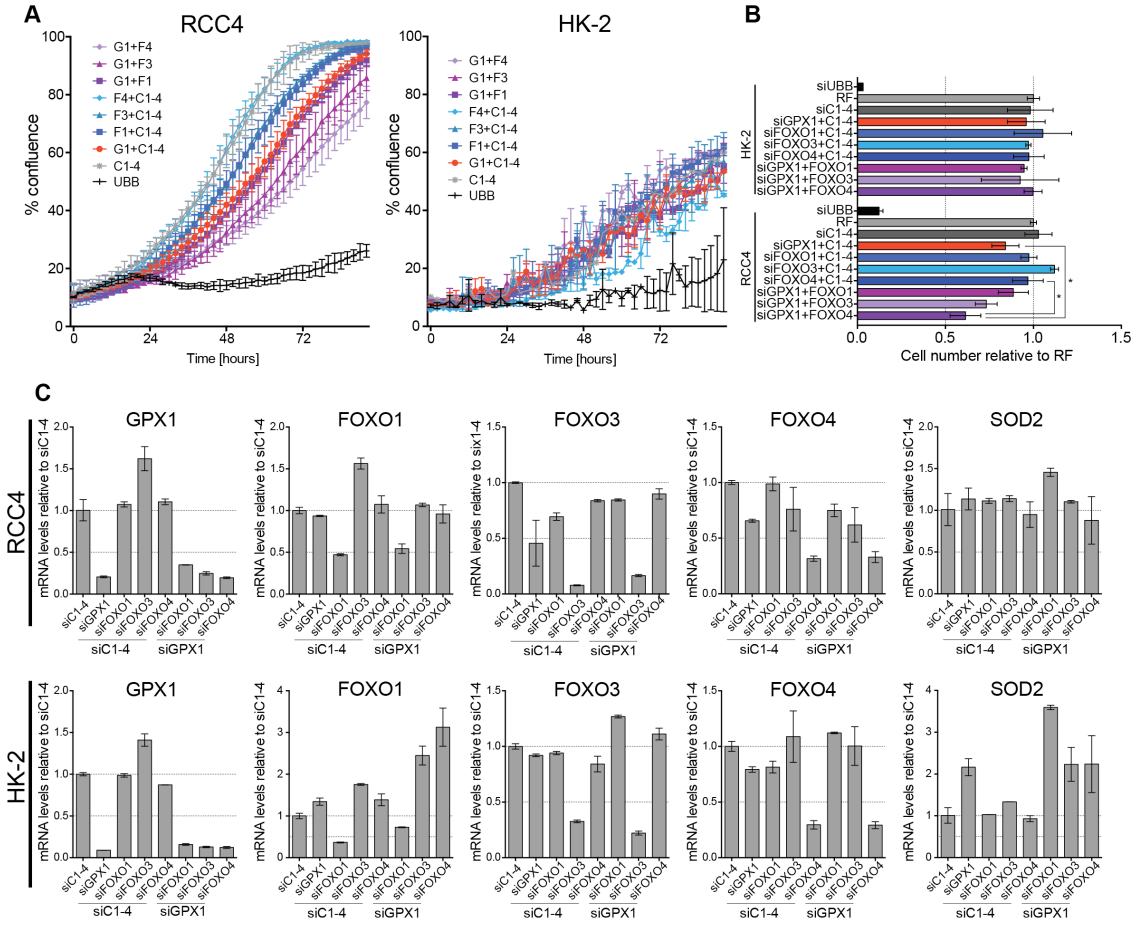

Figure 5.16: Co-silencing of GPX1 with FOXO4 has an additive negative effect on ccRCC proliferation

(A-B) RCC4 and HK-2 cells were reverse (co-)transfected with 37.5 nM siRNA (i.e. 18.75uM of each of the 2 SMARTpools) targeting GPX1 and FOXO1 (F1), FOXO3 (F3) or FOXO4 (F4) and monitored for cell proliferation using an IncuCyte live cell imaging system. siUBB (ubiquitin B) serves as positive, siC1-4 as negative control. (A) Curves show average cell proliferation over time generated from confluence measurements every 2 h for 92 h in total of triplicate wells ± SD. (B) Bar graphs represent average endpoint cell number of triplicate wells from (A) normalised to RISC-free (RF) ± SD. Asterisks indicate statistically significant difference in cell number loss upon co-silencing of GPX1 and FOXO4 compared to ablation of either alone (2-way ANOVA analysis with Dunnett multiple-comparison testing; *, $p \geq 0.05$). (C) Knockdown efficiency of GPX1/FOXO co-silencing 48 h post transfection. Bar graphs represent average of duplicate C_T measurements normalised to respective ACTB mRNA levels ± SD and are displayed relative to control silencing (siC1-4).

5.9 Silencing of GPX1, GPX3 and SOD1 leads to ROS accumulation in RCC4 but not in HK-2 cells

As GPX proteins are important regulators of cellular anti-oxidant response, the effect of GPX1, GPX3 and SOD1 depletion on ROS accumulation was determined in RCC4, CAKI1 and HK-2 cells using an H_2DCFDA fluorescence-activated cell-sorting (FACS)

assay. Only RCC4 cells showed a 1.5-fold increase in DCFDA immunofluorescence upon GPX1 and SOD1 ablation and a 1.25-fold increase upon GPX3 ablation compared to scrambled control. In CAKI1 cells, only siGPX1 #4 lead to a significant ROS accumulation compared to control, wheras there was no significant change detectable in HK-2 cells (Figure 5.17).

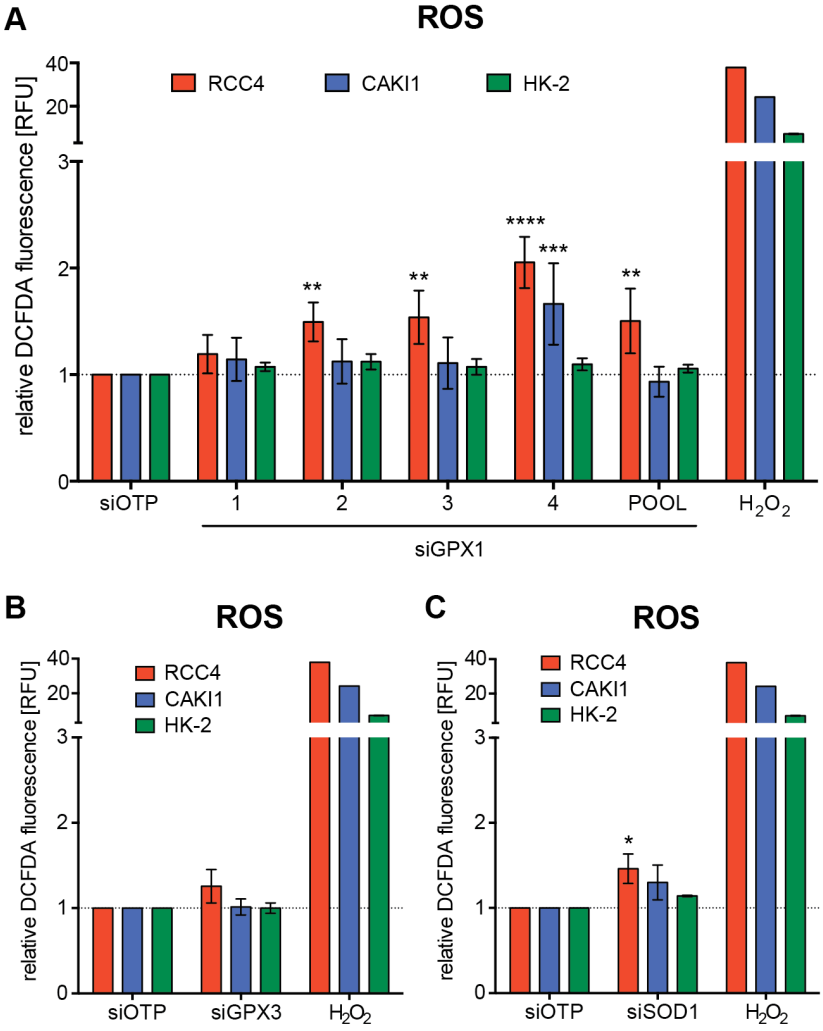

Figure 5.17: Ablation of GPX1 and SOD1 causes accumulation of ROS in RCC4 but not in CAKI1 and HK-2 cells

(A) RCC4, CAKI1 and HK-2 cells were reverse transfected with 37.5 nM siRNA targeting GPX1 (SMARTpool and the 4 individual siRNA sequences). Treatment with 1 mM H_2O_2 for 10 min prior to H_2DCFDA addition served as positive control. 48 h post transfection, cells were analysed for accumulation of DCFDA fluorescence using FACS. Bars represent mean cellular DCFDA intensities normalised to the respective negative siOTP control of three independent experiments. Error bars represent ± SEM. (B-C) Cells from the same experiment as in (A) treated in the same way but with siRNA SMARTpools against (B) GPX3 and (C) SOD1. Asterisks indicate statistically significant increase in fluorescent DCFDA accumulation for each cell line when compared to scrambled silencing (2-way ANOVA analysis with Dunnett multiple comparison testing; *, $p \leq 0.05$).

Next, RCC4 and HK-2 cells were subjected to a FACS assay that allows simultaneous detection of O_2^- and other ROS species (H_2O_2, $ONNOO^-$, $HO^\bullet$, NO, $ROO^\bullet$). Comparing untreated RCC4 and HK-2 cells for basal oxidative stress, the non-tumourigenic HK-2 cells seemed to have higher ROS and slightly lower O_2^- levels than the RCC4 cells (Figure 5.18A). GPX1 knockdown caused a 3-fold increase of ROS and a 1.5-fold increase in O_2^- in RCC4 cells but not in HK-2 cells compared to control silencing. This increase in ROS but not the increase in O_2^- was attenuated by addition of either NAC or GSH in RCC4 cells, though not statistically significant. Surprisingly, supplementation of HK-2 cells with GSH following siGPX1 seemed to increase ROS levels (Figure 5.18B). Ablation of GPX3 resulted in an almost 2-fold increase in ROS in both RCC4 and HK-2 cells compared to control silencing. Supplementation with NAC seemed to have an inhibitory effect on ROS accumulation, though this trend needs further investigation. O_2^- levels also increased 1.5-fold after GPX3 silencing compared to control in both cell lines, but NAC achieved rescue only in the HK-2 cells (Figure 5.18C). Interestingly, silencing of cytosolic SOD1 only increased ROS and O_2^- levels in RCC4 cells but not in HK-2 cells (Figure 5.18D).

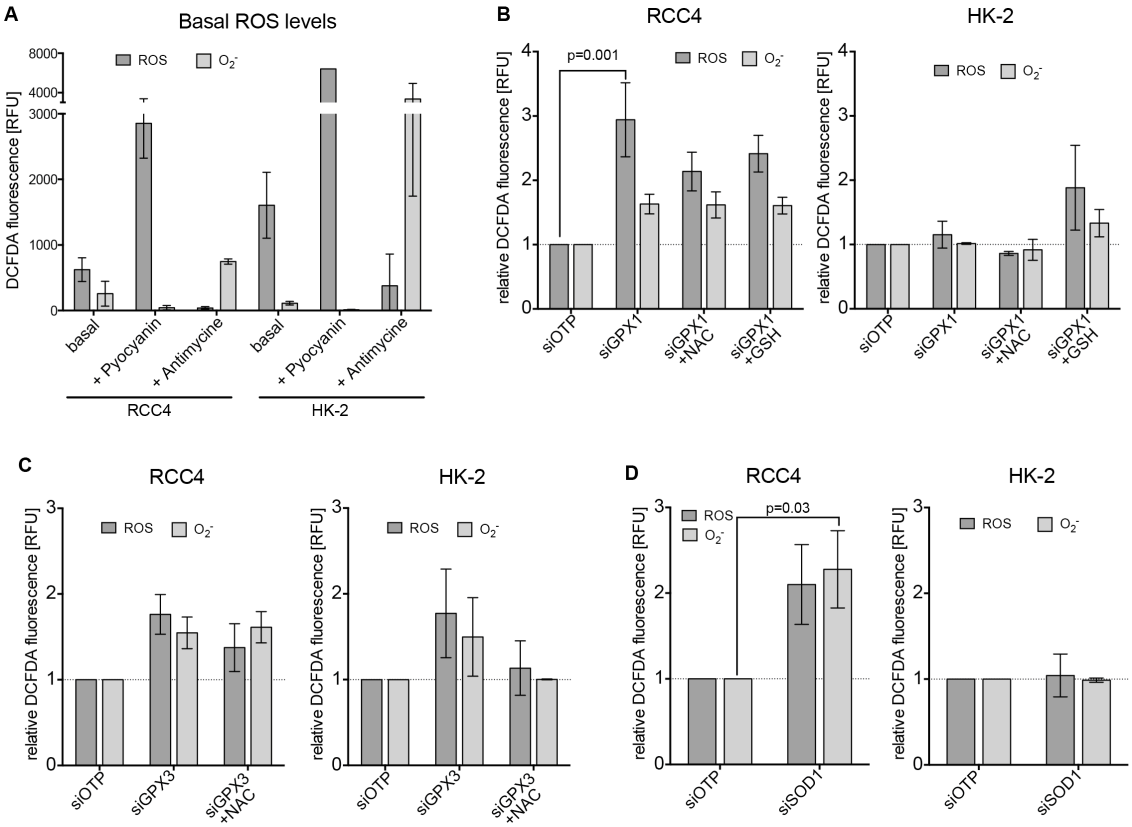

Figure 5.18: ROS accumulation following GPX1 and GPX3 depletion can be partially rescued by small-molecule inhibitors.

(A) Control conditions for (B-D). RCC4 and HK-2 cells were treated with 200 μM Pyocyanin (ROS inducer) and Antimycine A (O_2^- inducer) respectively as positive controls. Bars represent mean raw intensities of ROS (dark grey) and O_2^- (light grey) fluorescent dye per treated or untreated cell of ≥2 independent experiments ± SEM. (B) RCC4 and HK-2 cells were reverse transfected with 37.5 nM siRNA against GPX1 and treated with 1 mM NAC or 5 mM GSH the next day. Accumulation of ROS / O_2^- was determined 72 h later via FACS analysis. Bars represent mean intensities of ROS and O_2^- fluorescent dye per cell normalised to control treatment (siOTP1-4) of 3 independent experiments. Error bars represent ± SEM. (C-D) Same conditions and treatment strategies (where applicable) as in (B) but for (C) siGPX3 treatment and (D) siSOD1 treatment. Bar graphs represent mean intensities of ROS and O_2^- fluorescent dye per cell normalised to control treatment (siOTP1-4) of 3 independent experiments ± SEM. RFU, relative fluorescent units. Asterisks indicate statistically significant changes in ROS / O_2^- accumulation upon GPX1, GPX3 and SOD1 ablation compared to control (siOTP) or following antioxidant treatment compared to untreated (2-way ANOVA analysis with Dunnett multiple comparison test; *, $p \leq 0.05$).

In summary, it can be concluded that RCC4 cells accumulated comparatively more ROS and O_2^- following silencing of GPX1, GPX3 or SOD1 than HK-2 cells. Furthermore, ROS accumulation could be, at least partially, rescued through supplementation with the antioxidant NAC and in some cases also through addition of GSH. These results suggest that GPX1, GPX3 and SOD1 are important components of the anti-oxidant system in ccRCC cells. In contrast, non-tumourigenic HK-2 cells, although having slightly elevated basal ROS levels compared to RCC4 cells, do not seem to be dependant on these proteins for maintenance of their redox balance.

5.10 Antioxidants have only limited effect on cell number loss following GPX1, GPX3 and SOD1 depletion in RCC4 cells

As NAC and GSH were able to partially rescue ROS levels in RCC4 and HK-2 cells it was assessed whether these or other antioxidants could also prevent the cell number loss phenotype upon silencing of GPX1, GPX3 or SOD1. Hence, RCC4 and HK-2 cells were treated with increasing amounts of GSH, NAC, TEMPOL and the GPX-mimetic Ebselen following transfection with siGPX1, siGPX3 and siSOD1. TEMPOL (4-Hydroxy-TEMPO, a TEMPO derivative) is an antioxidant that specifically catalyses the disproportionation of O_2^- thereby acting as a SOD mimetic (Wilcox and Pearlman, 2008). Ebselen is a Se-containing small-molecule that, similarly to Se-dependent GPXs, neutralises H_2O_2 and (phospho-) lipid hydroperoxides using thiols (e.g. GSH) as cofactors (Maiorino et al., 1988).

Within the concentration range tested, hardly any positive effect on cell number could be seen upon treatment with any of the four antioxidants. Only treatment with 5 mM GSH (Figure 5.19A) and 10 μM TEMPOL (Figure 5.19C) following SOD1 ablation in RCC4 cells was able to significantly increase enpoint cell number. In contrast, treatment of control silenced RCC4 cells with 5 mM GSH, 1 mM NAC or 10 μM TEMPOL resulted in a small but significant cell number loss, suggesting that under control conditions RCC4 cells are in a redox balanced state, which is perturbed by external addition of antioxidants resulting in cell number loss due to reductive stress. Interestingly, HK-2 cells seem to be generally sensitive to GSH, NAC and Ebselen supplementation, as a prominent cell number loss was observed with increasing concentrations of any of these antioxidants and independent of the protein ablated (Figure 5.19A, B, D), while TEMPOL supplementation had a milder negative effect and was significant only upon ablation of GPX1 and GPX3 (Figure 5.19C).

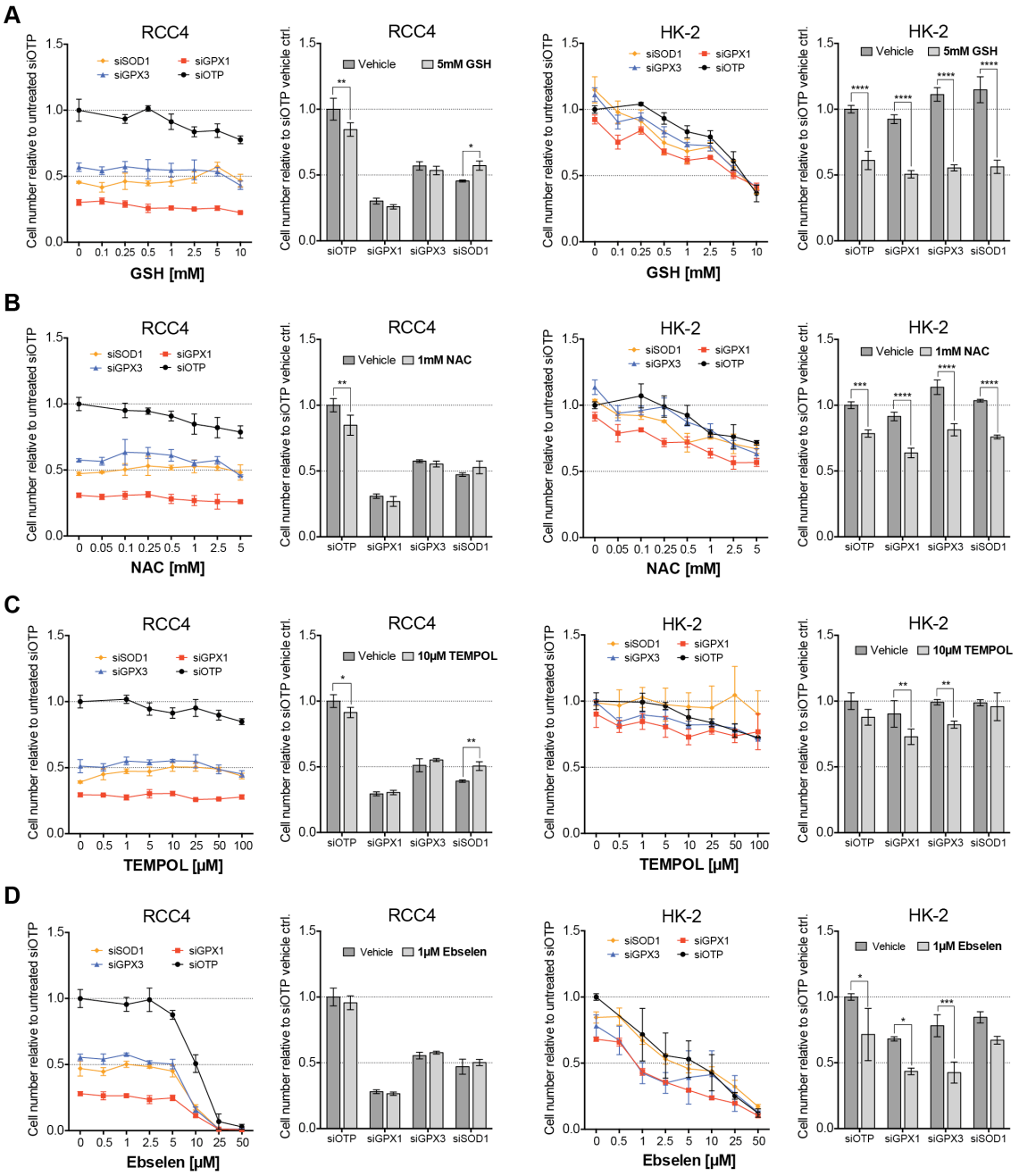

Figure 5.19: Antioxidants have only a limited effect on cell number loss upon ablation of GPX1, GPX3 and SOD1 in RCC4 cells and are detrimental for HK-2 cells

(A-D) RCC4 and HK-2 cells were reverse transfected with 37.5 nM siRNA against GPX1, GPX3 and SOD1 in a 96-well format. The next day, increasing doses of (A) glutathione (GSH), (B) the ROS scavenger N-acetylcysteine (NAC), (C) the superoxide scavenger TEMPOL and (D) the GPX mimetic Ebselen were added. Dose response curves (respective left-hand panel for each cell line) represent average endpoint cell numbers of triplicate wells normalised to the respective vehicle control (0 mM) 72 h post treatment. Error bars represent ± SD. Bar graphs (respective right-hand panel for each cell line) depict average cell numbers from the most effective concentration extracted from the respective dose response curve in (A-D). Bars represent average cell numbers of triplicate wells normalised to the control silenced (siOTP) vehicle treated condition. Error bars represent ± SD. Asterisks represent statistically significant changes in cell number for the indicated antioxidant treatment compared to vehicle control (2-way ANOVA analysis with Bonferroni multiple comparison test; *, $p \leq 0.05$).

The experiment was repeated in RCC4 and HK-2 cells with the most promising antioxidant concentrations and under monitoring cell proliferation and death in an IncuCyte live-cell imaging system. Figure 5.20A-F summarises growth curves and accumulation of apoptotic cells. Reassuringly, the mostly neutral effect of NAC and TEMPOL on GPX1, GPX3 and SOD1 ablation could be at least maintained if not strengthened to a positive effect on cell number as compared to vehicle treatment. In contrast, the previously neutral to positive effect of GSH and Ebselen following ablation of GPX1, GPX3 and SOD1 observed in RCC4 cells was reversed (Figure 5.20G). Treatment with these antioxidants resulted in increased apoptosis in these cells compared to treatment with vehicle as an accumulation of the fluorescent Caspase-3/7 substrate was observed (Figure 5.20A-F centre and right-hand panel graphs). Furthermore, the negative effect of the tested antioxidants on cell number in HK-2 cells could be confirmed and was due to increased apoptosis (Figure 5.20A-F centre and right-hand panel graphs) hinting further to a potential reductive stress that the normal cells might face and have difficulty to cope with. Although TEMPOL, which showed no difference in endpoint cell number compared to vehicle, was an exception (Figure 5.20H).

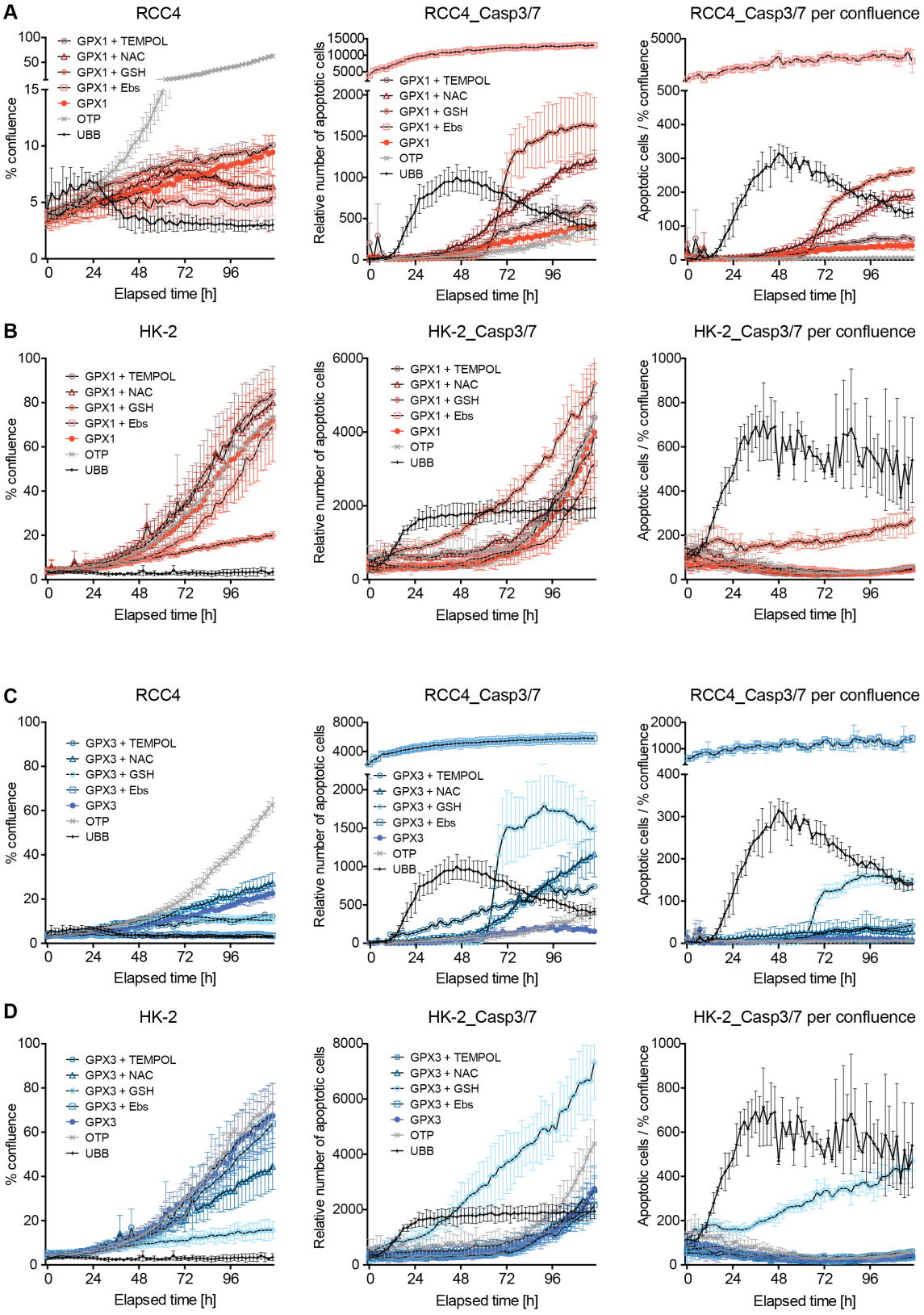
A
RCC4
RCC4_Casp3/7
RCC4_Casp3/7 per confluence
B
HK-2
HK-2_Casp3/7
HK-2_Casp3/7 per confluence
C
RCC4
RCC4_Casp3/7
RCC4_Casp3/7 per confluence
D
HK-2
HK-2_Casp3/7
HK-2_Casp3/7 per confluence
% confluence
Relative number of apoptotic cells
Apoptotic cells / % confluence
Elapsed time [h]
GPX1 + TEMPOL
GPX1 + NAC
GPX1 + GSH
GPX1 + Ebs
GPX1
OTP
UBB
GPX3 + TEMPOL
GPX3 + NAC
GPX3 + GSH
GPX3 + Ebs
GPX3
OTP
UBB

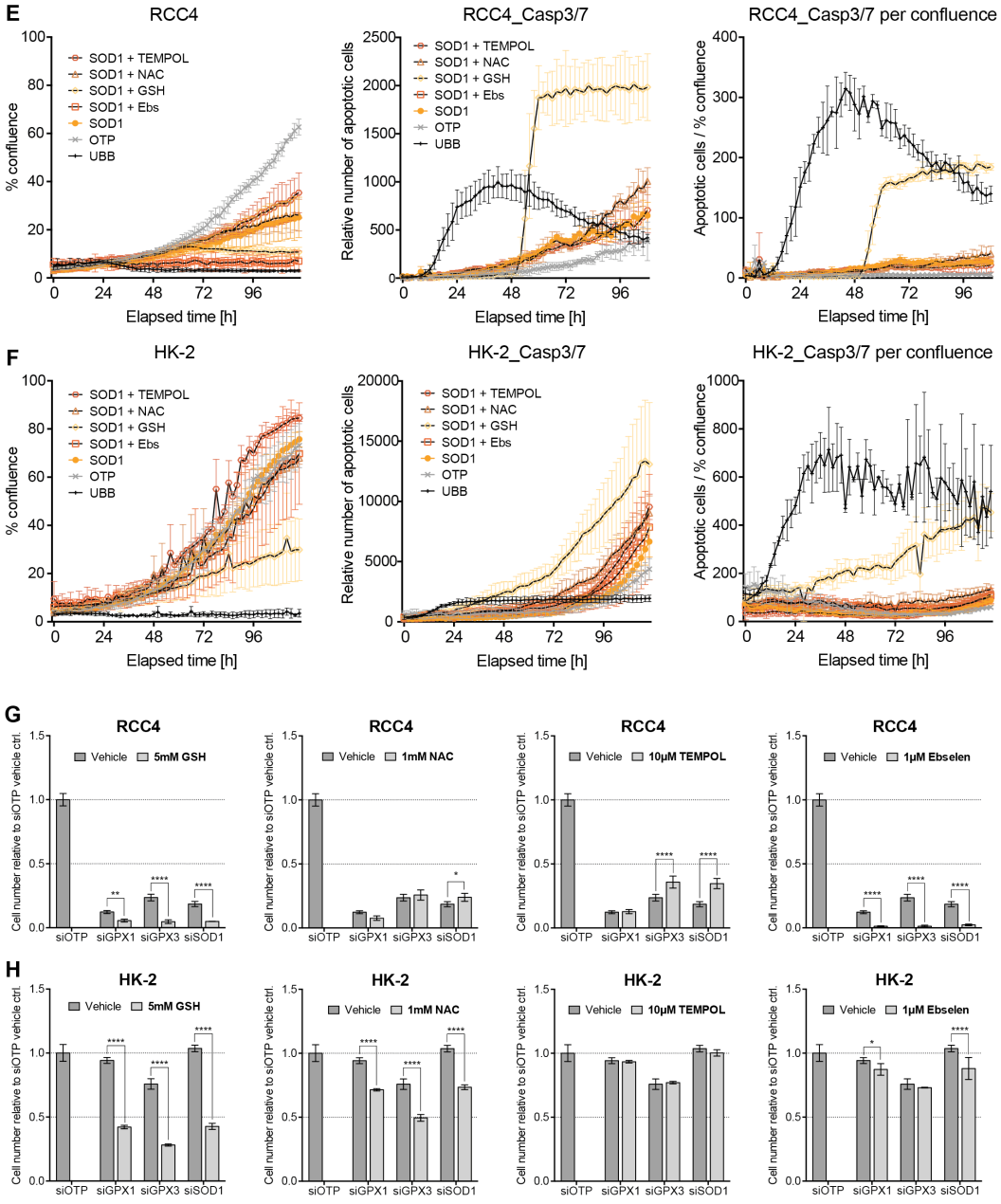

Figure 5.20: Antioxidants cannot rescue cell number loss phenotype upon siGPX1, siGPX3 and siSOD1

(A-F) RCC4 and HK-2 cells were reverse transfected with 37.5 nM siRNA targeting (A, B) GPX1, (C, D) GPX3 and (E, F) SOD1 in a 96-well format. 12 h post transfection, glutathione (GSH, 5 mM), the ROS scavenger N-acetylcysteine (NAC, 1 mM), the superoxide scavenger TEMPOL (10 µM) and the GPX mimetic Ebselen (1 µM) was added together with 5 µM of a fluorescent Caspase-3/7 substrate (ESSEN BioScience) to monitor real time cell death in an IncuCyte live cell imaging system. siUBB (targets ubiquitin B) serves as positive apoptosis-inducing control, siOTP as negative control. Left-hand panel line graphs represent average confluence measurements of triplicate wells ± SD generated every 2 h for 120 h in total. Center panel graphs represent number of cells that accumulate the converted and now fluorescent Caspase-3/7 substrate; average of triplicate wells ± SD. Right-hand panel graphs depict the ratio of apoptotic cells normalised to measured confluence; average of triplicate wells ± SD. (G-H) Bar graphs represent average endpoint cell numbers 5.5 d post transfection of the triplicate wells from (A-F) normalised to vehicle treated control silenced cells (siOTP) ± SD. Asterisks indicate statistically significant cell number changes upon treatment with Ebselen, GSH, NAC or TEMPOL compared to vehicle control (2-way ANOVA analysis with Dunnett multiple comparison test; *, $p \leq 0.05$).

In summary, although NAC and GSH treatment attenuated ROS/O_2^- levels to some extent in RCC4 cells, their ability to alleviate also the cell number loss phenotype resulting from GPX1, GPX3 or SOD1 knockdown was only limited and variable. This was unexpected, as the GPX mimetic Ebselen should substitute for the reduced expression of GPX enzymes while TEMPOL should replace SOD1 function. However, interpretation of the results was compromised by the high toxicity observed with the compounds used. In particular, it became apparent that the non-tumourigenic HK-2 cells are highly sensitive to treatment with GSH, NAC and Ebselen, pointing to increased sensitivity towards reductive stress. Furthermore, the exact timing of gene silencing and compound addition could also affect the outcome of the experiment. Overall, it seems that deregulation of antioxidant metabolism, either by depletion of GPX/SOD proteins or by addition of antioxidants, can perturb the cellular redox balance, ultimately negatively influencing cell survival.

5.11 GPX expression is heterogeneous in ccRCCs

Expression of different ROS detoxifying enzymes in the different ccRCC cell lines on mRNA levels was very heterogeneous and did not follow a clear pattern as can be seen from Figure 5.12. RCC4, 786-O, UMRC3, TK10 and ACHN cells seemed to be most compromised in their expression of antioxidant enzymes, judging from their mRNA levels relative to HK-2 cells. UMRC2, A704, CAKI2 and A498 cells showed higher levels of anti-oxidant gene expression compared to HK-2 cells. GPX2, GPX3, GPX5, GPX6 and SOD2 mRNA levels were generally lower in ccRCC cell lines compared to HK-2 cells, while GPX8, CAT and SOD1 showed a tendency to have marginally higher expression levels in the cancer cells. In contrast to SOD1 and SOD2, where mRNA levels were a good indicator of protein levels, GPX1 mRNA levels did not reflect protein expression in most cell lines (Figure 5.21C). GPX1 protein expression was generally reduced in ccRCC cells compared to non-malignant HK-2 cells (Figure 5.21C). This discrepancy might be due to the extensive post-transcriptional regulatory mechanisms that control GPX mRNA and protein levels (see section 5.1.2).

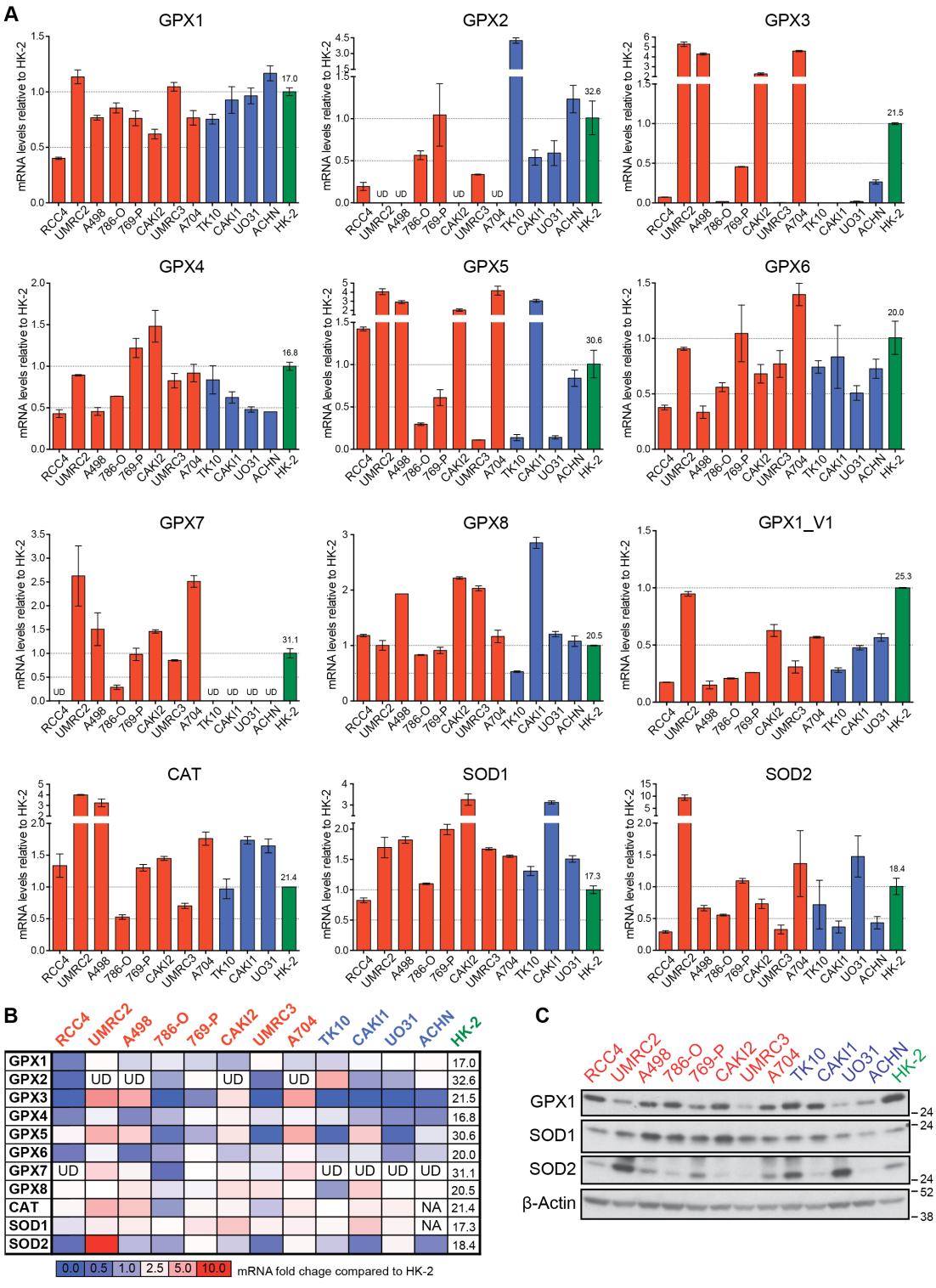

Figure 5.21: GPX, SOD and CAT expression is heterogeneous in ccRCC

(A) Basal mRNA expression of indicated ROS detoxifying enzymes analysed via RT-qPCR of total mRNA samples. Bar graphs represent average of duplicate measurements normalised to respective ACTB levels ± SD and are displayed relative to HK-2 cells. Numbers above HK-2 bars represent mean ΔC_T value for comparison. (B) Heat map summarising fold-change differences in mRNA abundance relative to HK-2 cells shown as bar graphs in (A). Numbers in HK-2 column represent average ΔC_T value for comparison. UD, undetermined. (C) Whole cell lysates were subjected to SDS/PAGE and analysed for basal GPX1, SOD1 and SOD2 protein expression levels. β-actin serves as loading control.

5.12 GPX activity is reduced in ccRCC cell lines compared to HK-2 cells

To assess total GPX activity across the cell line panel, an enzymatic assay that measures the ratio of GSH-dependent peroxidation of cumene hydroperoxide over time was used. This assay showed that GPX activity is substantially (approx. 4-fold) lower in the 12 cancer cell lines compared to non-malignant HK-2 cells (Figure 5.22B).

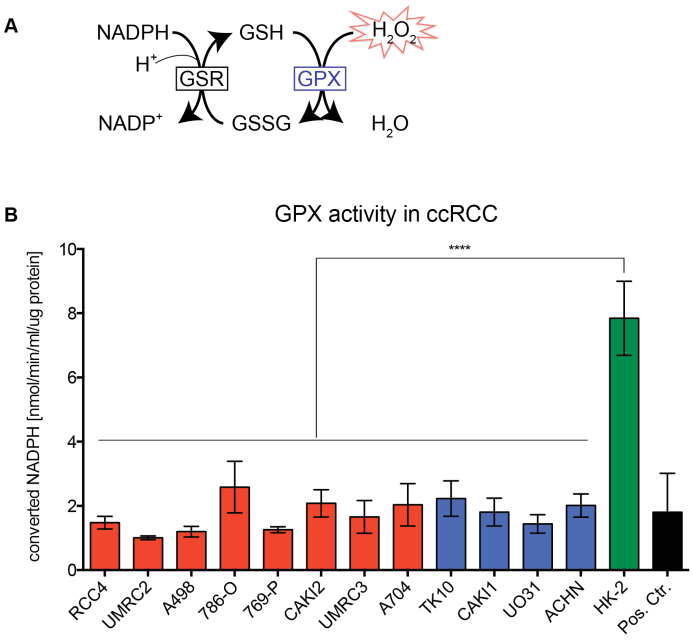

Figure 5.22: ccRCC cells have significantly less basal GPX activity than HK-2 cells
(A) Schematic of working principle of the Abcam GPX activity assay. GPX uses reduced glutathione (GSH) as cosubstrate to neutralise Cumene hydroperoxide (H_2O_2). The generated oxidised glutathione (GSSG) is recycled to GSH by glutathione reductase (GSR) under consumption of NADPH. Hence, GPX and GSR activity are supposedly proportional to each other and the decrease in auto-fluorescence emitted by NADPH at OD = 340nm should be proportional to GPX activity. All components but GPX are provided in excess in the reaction mix. (B) Basal GPX activity as measured with the GPX activity assay explained in (A). Bars represent mean calculated converted NADPH in nM/min/ml normalised to complete protein content assayed of three independent experiments. Error bars represent SEM. Asterisks indicate statistically significant reduction in GPX activity in ccRCC compared to HK-2 cells (One-way Anova, ****, $p \leq 0.001$); Pos. Ctr. = purified GPX protein.

Irrespective of expression and basal activity of GPX proteins, the results so far indicated that depleting GPX1 or GPX3 causes oxidative stress and compromises cell viability in ccRCC cells. In contrast, depletion of individual GPX proteins in HK-2 cells may not substantially impact on total GPX activity in HK-2 cells, therefore explaining the fact that these cells can tolerate the silencing of GPX1 and GPX3.

5.13 ccRCCs show mixed sensitivity to different ROS stimuli and inducer

With four times less GPX activity compared to the non-tumourigenic HK-2 cells, ccRCC cells should be more susceptible to oxidative stress. To assess this, the cell line panel was treated with increasing doses of H_2O_2, tert-Butyl hydroperoxide (tBuOOH, an organic peroxide), Pyocyanin, Rotenone or Antimycin A. Pyocyanin, a toxin produced and secreted by *Pseudomonas aeruginosa*, a pathogen involved in respiratory complications in cystic fibrosis, has strong redox activity and generates ROS (Hassan and Fridovich, 1980). In the cystic fibrosis lung, cytoplasmic pyocyanin reduces NADPH to $NADP^+$ to convert molecular oxygen to superoxide radicals ($O_2^{\bullet}$) causing a double negative effect: a) generating highly reactive ROS and b) depletion of the NADPH pool necessary to reduce GSSG to GSH. Hence, the lung upregulates CAT and SODs to keep the increased ROS in check (Ran et al., 2003). Furthermore, pyocyanin negatively regulates CAT via both direct interaction and inhibition of gene transcription. Reduced catalase activity results in H_2O_2 accumulation, which has a negative impact on the glutathione pool as GSH gets depleted (Muller, 2002). Rotenone, a herbal ketonic compound, and Antimycin A, a secondary metabolite produced by *Streptomyces*, affect components of the mitochondrial ETC, indirectly leading to the generation of ROS. Rotenone inhibits electron transfer from complex I to ubiquinone (CoQ) causing an accumulation of electrons in the mitochondrial intermembrane space such that NADH cannot be reduced any more and molecular oxygen gets converted into highly reactive O_2^-. Antimycin A has similar effects but its target is complex III, where it binds to cytochrome c reductase, inhibits oxidation of ubiquinol and causes an electron accumulation and subsequent O_2^- generation.

The rational behind stimulating O_2^- production is, to have a more constant endogenous source of H_2O_2 accumulation, as O_2^- is quickly converted to H_2O_2 by one of the SOD isoforms. Furthermore, this experiment was designed to delineate which source of ROS would be most detrimental for ccRCC cells.

Surprisingly, ccRCC cells seemed to be less sensitive to external ROS assault compared to HK-2 cells (Figure 5.23). CAKI2 and TK10 cells seemed to be particularly resistant to hydrogen peroxide species challenge (Figure 5.23A, B). Pyocyanin treatment evoked

a similar reaction pattern as do the two hydrogen peroxide species - although RCC4 and ACHN cells displayed higher sensitivity, while HK-2 cells were more tolerant to this ROS inducer compared to the hydrogen peroxides (Figure 5.23B). Rotenone seemed to be tolerated only by RCC4, A704 and TK10 cells, while HK-2 cells showed high sensitivity towards this compound (Figure 5.23D). Antimycin A had the most detrimental effect of all ROS inducers tested on HK-2 cell survival compared to ccRCC cells. RCC4, A704 and TK10 cells are more, ACHN cells are less sensitive to inhibition of complex III compared to inhibition of complex I (Figure 5.23E). This observation is also in accordance with the findings of the screen, where ablation of ND3 and ND6, two components of complex I, emerged as detrimental for ccRCC cell survival (Figure 4.16). Taken these results together, it seems that ccRCC cell lines can tolerate increased levels of cytoplasmic ROS (induced by treatment with H_2O_2, tBuOOH or Pyocyanin) relatively well; on average better than the non-transformed HK-2 cells. In contrast, counteracting endogenous O_2^- generation caused by inhibitors of respiratory complexes in the mitochondria is more problematic for all kidney epithelial cell lines tested, irrespective of their tumourigenic or non-tumourigenic status.

The decreased sensitivity of ccRCC cells towards cytoplasmic oxidants could indicate increased activity of GPX proteins, as this type of ROS is generally neutralised by the GPX reaction. In contrast, detoxification of mitochondrial ROS requires the activity of CAT and SOD2, two enzymes for which no selective dependency between ccRCC and non-malignant cells was detected.

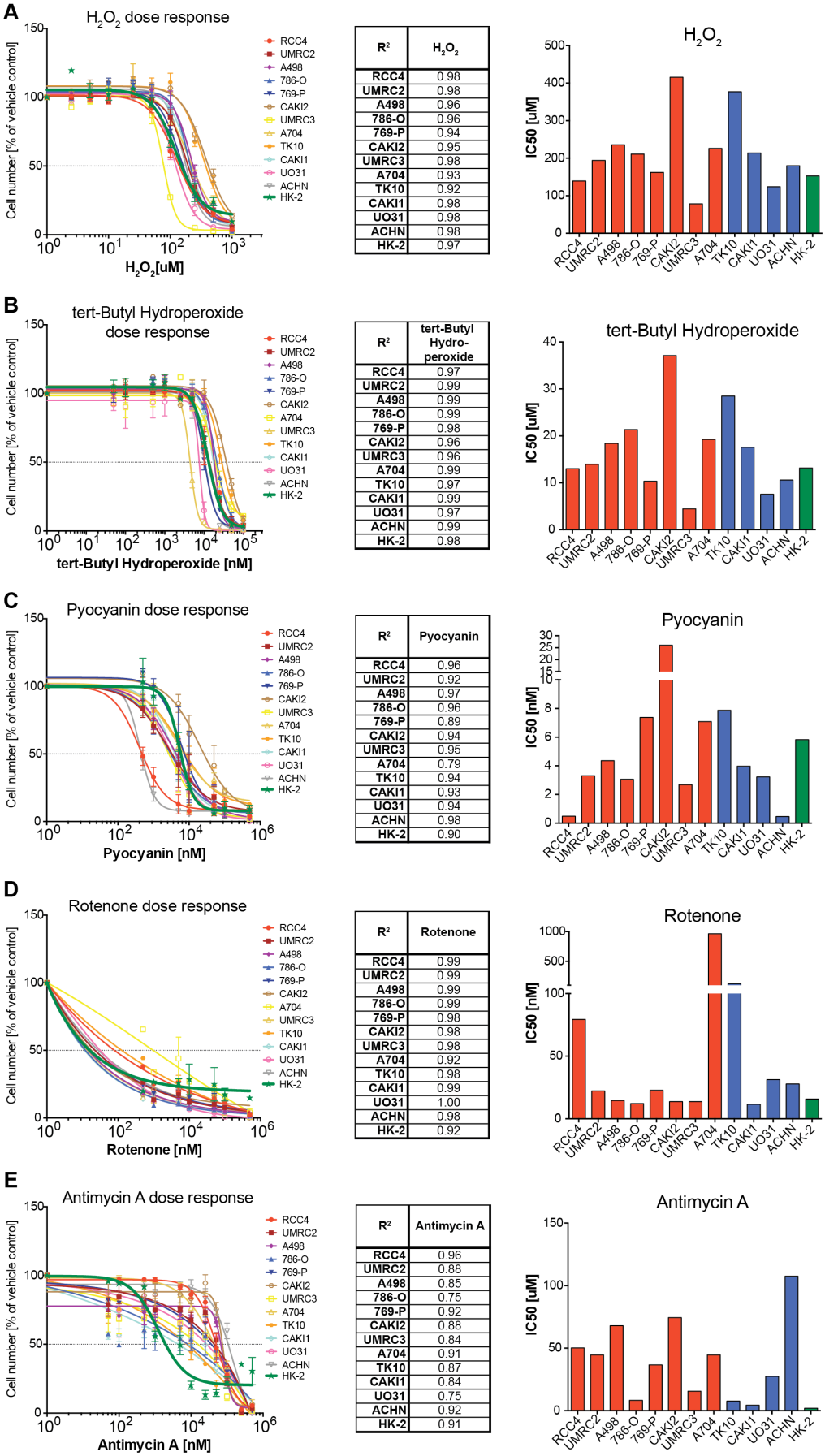

R²	H_2O_2
RCC4	0.98
UMRC2	0.98
A498	0.96
786-O	0.96
769-P	0.94
CAKI2	0.95
UMRC3	0.98
A704	0.93
TK10	0.92
CAKI1	0.98
UO31	0.98
ACHN	0.98
HK-2	0.97

R²	tert-Butyl Hydro-peroxide
RCC4	0.97
UMRC2	0.99
A498	0.99
786-O	0.99
769-P	0.98
CAKI2	0.96
UMRC3	0.96
A704	0.99
TK10	0.97
CAKI1	0.99
UO31	0.97
ACHN	0.99
HK-2	0.98

R²	Pyocyanin
RCC4	0.96
UMRC2	0.92
A498	0.97
786-O	0.96
769-P	0.89
CAKI2	0.94
UMRC3	0.95
A704	0.79
TK10	0.94
CAKI1	0.93
UO31	0.94
ACHN	0.98
HK-2	0.90

R²	Rotenone
RCC4	0.99
UMRC2	0.99
A498	0.99
786-O	0.99
769-P	0.98
CAKI2	0.98
UMRC3	0.98
A704	0.92
TK10	0.98
CAKI1	0.99
UO31	1.00
ACHN	0.98
HK-2	0.92

R²	Antimycin A
RCC4	0.96
UMRC2	0.88
A498	0.85
786-O	0.75
769-P	0.92
CAKI2	0.88
UMRC3	0.84
A704	0.91
TK10	0.87
CAKI1	0.84
UO31	0.75
ACHN	0.92
HK-2	0.91

Figure 5.23: ccRCC cells are less sensitive to ROS/ O_2^- stress than HK-2 cells
ccRCC cells were treated with increasing concentrations of (A) H_2O_2, (B) tert-Butyl hydroperoxide, (C) Pyocyanin, (D) Rotenone and (E) Antimycine A for 72 h. Dose response curves (respective left-hand panel) represent mean endpoint cell numbers of 3 independent experiments performed in triplicates ± SEM and result from non-linear regression modelling in GraphPad Prism 6. Accuracy of curve fitting (respective R^2-values) to determined endpoint cell numbers for each cell line is depicted in respective center-panneled tables. Bar graphs (respective right-hand panel) represent IC50 values for each ROS/O_2^- inducer that were extracted from the dose response curves.

5.14 ccRCC cells have higher GSH:GSSG ratio compared to HK-2 cells

Knowing that ccRCC cell lines have lower GPX activity than HK-2 cells but, at the same time, are less sensitive to peroxide species as well as O_2^--inducers, it was considered whether this phenomenon could be explained by variations in the glutathione pool as glutathione is a co-factor for GPX functionality. Therefore, basal glutathione levels were determined in all cell lines of the panel. Total amount of glutathione (GSH + GSSG) did not show major differences between the different cell lines (Figure 5.24A). The same was true for the amount of oxidised GSSG (Figure 5.24B). However, GSH levels derived by subtraction of oxidised GSSG from total glutathione, showed a trend towards higher levels in most of the ccRCC cell lines as compared to HK-2 cells (Figure 5.24C). Comparison of the ratio of reduced GSH and oxidised GSSG revealed a trend towards in average higher GSH:GSSG ratios in ccRCC cells than in HK-2 cells (Figure 5.24D), despite considerable variation between different experiments. This difference could indeed explain the increased tolerance of cancer cells to the ROS inducers tested compared to non-malignant HK-2 cells (Figure 5.23). As the amount of total glutathione (GSH + GSSG) was similar in both ccRCC and non-malignant cells, the increased GSH:GSSG ratio is indicative of lower levels of basal oxidative stress in cancer cells, which deplete the GSH pool. However, it is more likely that the processes that lead to the restoration of GSH could be more efficient in the cancer cells, resulting in higher GSH levels and increased resistance to oxidative insults.

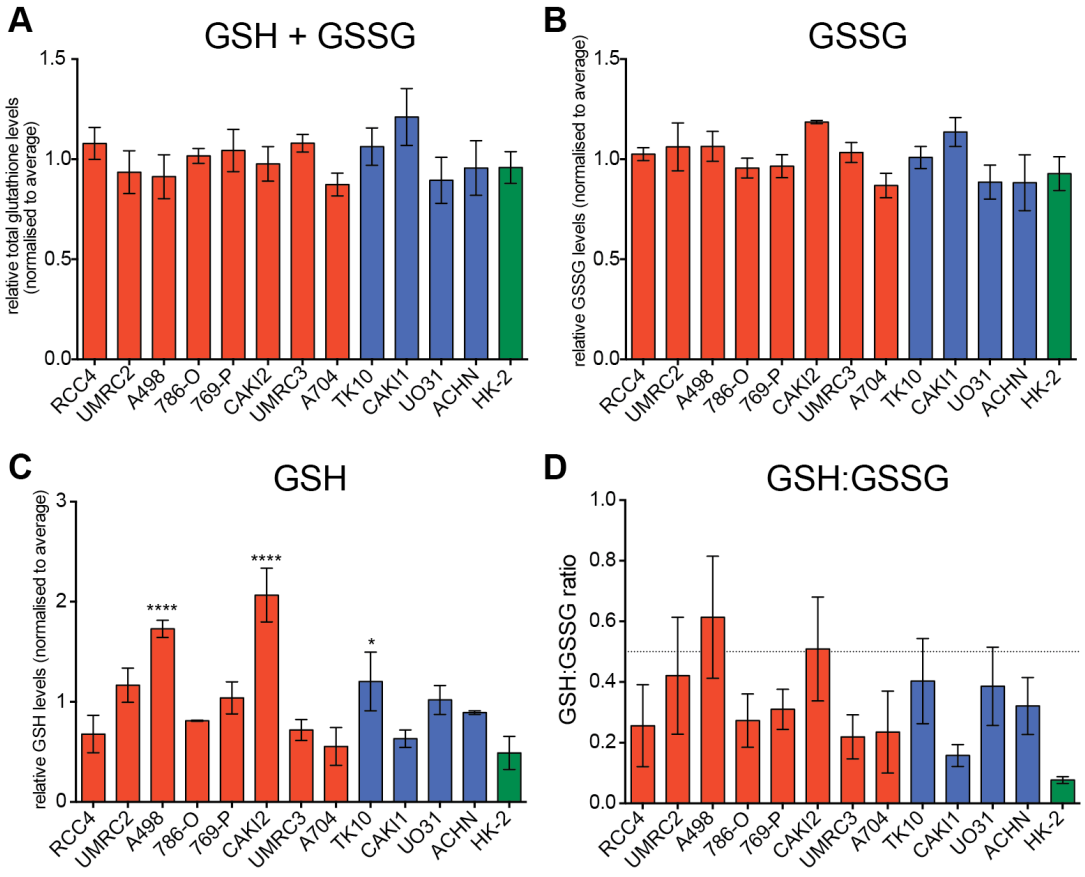

Figure 5.24: ccRCC cells have higher GSH levels and higher GSH:GSSG ratio as HK-2 cells

(A) Total glutathione (GSH + GSSG) and (B) oxidised glutathione (GSSG) were determined using a glutathione fluorometric assay kit (Biovision). (C) GSH levels were determined through subtraction of measured GSSG from measured total glutathione (GSSG + GSH). In each of the three independent experiments, the determined values were divided by the average value of all cell lines in order to being able to cross-compare between experiments. Error bars indicate ± SEM. (D) Calculated GSH:GSSG ratio from values determined in (A) and (B). Bar graphs represent average of ratios formed in each of the 3 individual experiments ± SEM. Asterisks indicate significant difference of respective ccRCC cell line compared to HK-2 cells in total glutathione, GSSG, GSH and GSH:GSSG (2-way ANOVA analysis with Dunnett multiple comparison testing.. *,$p \leq 0.05$).

For the maintenance of an active glutathione pool, oxidised GSSG can be recycled to reduced GSH. This reaction is accomplished by glutathione reductase (GSR) under consumption of NADPH. One cytosolic source of NADPH is the oxidative arm of the PPP (Figure 1.4 and 5.3). Hence, mRNA expression levels for GSR and G6PD, one of the two NADPH producing enzymes of the PPP, were examined. Indeed, HK-2 cells showed comparatively high levels of GSR mRNA, which is exeded only in UMRC2, 769-P and CAKI2 cells. G6PD mRNA expression was more variable in the cell line panel and did not reveal an obvious trend (Figure 5.25A).

Importantly, depletion of GSR or G6PD in ccRCC cell lines severely diminished their survival (Figure 5.25B). Indeed, most ccRCC cell lines showed more than 50% reduction in cell number following depletion of GSR or G6PD. In contrast, HK-2 cells were hardly impacted by silencing of these enzymes. This result indicated that the glutathione recycling system in the cancer cells could be more vulnerable to perturbations than that of HK-2 cells.

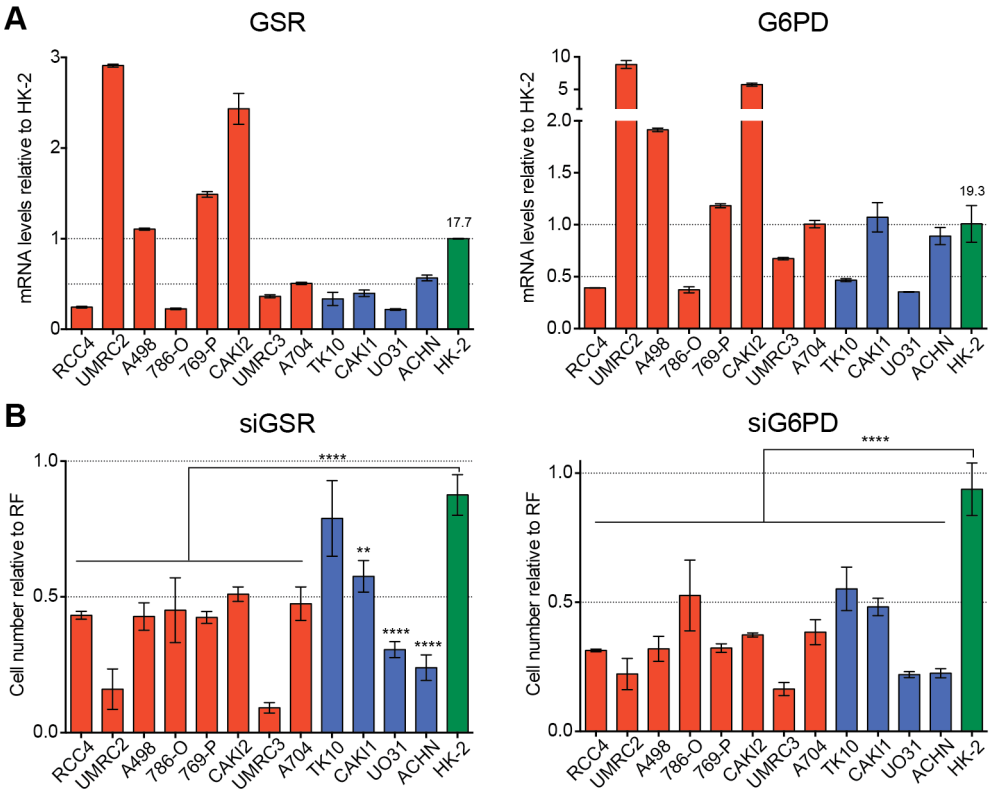

Figure 5.25: ccRCC cells have a less efficient GSH recycling system than HK-2 cells

(A) Total mRNA was extracted from untreated cells and analysed via RT-qPCR for glutathione reductase (GSR) and glucose-6-phosphate dehydrogenase (G6PD) expression levels. Bar graphs represent average of duplicate measurements normalised to respective ACTB levels ± SD and are displayed relative to HK-2 cells. Numbers above HK-2 bars represent average ΔC_T values for comparison. (B) ccRCC and HK-2 cells were reverse transfected with 37.5 nM siRNA against GSR or G6PD for 96 h in a 96-well format. Bar graphs represent average endpoint cell numbers normalised to RISC-free (RF) of 3 individual experiments performed in triplicates ± SEM. Asterisks indicate statistically significant cell number reduction in the respective ccRCC cell line compared to HK-2 cells (2-way ANOVA analysis with Dunnett multiple comparison testing; *, $p \leq 0.05$).

Unfortunately, due to time restrictions, complementary evaluation of the cellular $NADP^+$/NADPH pool to fully elucidate the reductive potential of ccRCC cells relative to HK-2 cells could not be carried out yet, but is an imminent future objective.

5.15 Perturbation of the active GSH pool is not tolerated by ccRCC cells and causes ROS accumulation

As mentioned in more detail in the introduction, GSH is a tripeptide composed of three amino acids, glutamate, cysteine and glycine and it is generated in a two-step process mediated firstly by the GCLC/GCLM complex and then by GSS (Figure 5.3). Glutamate is generated by GLS from L-glutamine, a nutrient contained in food. During the cell characterisation process, it was established that ccRCC cells are highly sensitive to glutamine deprivation (Figure 3.11). Hence, it was considered that glutamine addiction could be linked to GSH production in ccRCC cells.

Knockdown of GLS, GSS or GSR in a selection of ccRCC cell lines and HK-2 cells was performed and cell proliferation was monitored using an IncuCyte live cell imaging system. Contrary to HK-2 cells, all of the ccRCC cell lines tested showed reduced proliferation rates with significant endpoint cell number loss following ablation of GLS, GSS or GSR compared to control silencing. Loss of GSS had the strongest negative effect on ccRCC proliferation and overlapped in most cases with the dependency on GPX1, confirming the importance of glutathione for a functional GPX pathway in ccRCC cells. Furthermore, UMRC2, UMRC3 and ACHN cells were particularly sensitive to GLS ablation, suggesting a strong dependency on glutamate in these cells (Figure 5.26).

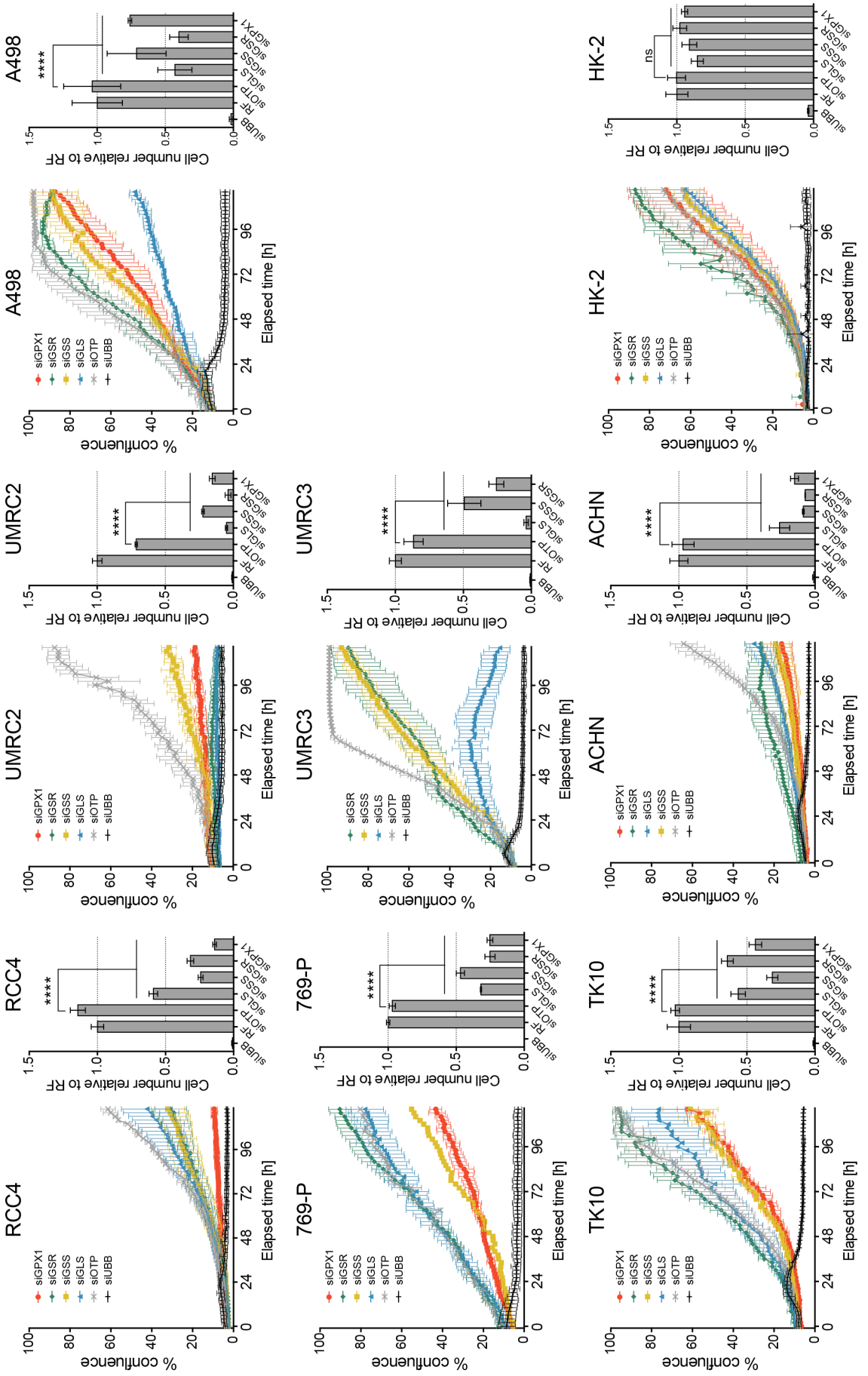
A498
HK-2
UMRC2
ACHN
UMRC3
TK10
RCC4
769-P
% confluence
Elapsed time [h]
Cell number relative to RF
siGPX1
siGSR
siGSS
siGLS
siOTP
siUBB
RF
****
ns

Figure 5.26: RNAi-mediated ablation of components of GSH biosynthesis and its recycling system negatively affect ccRCC proliferation

Indicated cell lines were reverse transfected with 37.5 nM siRNA targeting GPX1, glutathione reductase (GSR), glutathione synthetase (GSS) and glutaminase (GLS) in a 96-well format and cell proliferation was monitored using an IncuCyte live cell imaging system. siUBB (ubiquitin B) served as positive, siOTP as negative control. Respective left-hand growth curve graphs represent mean confluence values from triplicate wells ± SD recorded every 2 h for 120 h in total. Respective left-hand bar graphs represent average endpoint cell numbers normalised to RISC-free (RF) of the triplicate wells ± SD 120h post transfection. Asterisks indicate significant cell number loss upon ablation of GLS, GSS, GSR or GPX compared to scrambled silencing (2-way ANOVA analysis with Dunnett multiple comparison testing; ****, $p \leq 0.001$; ns, not significant).

Knockdown of GLS and GSS in the whole cell line panel confirmed the cancer-specific negative effect on cell number and, although not significantly, GCLC ablation also showed a trend towards preferential cell number loss in ccRCC compared to HK-2 cells (Figure 5.27A).

Next, the cell line panel was treated with the GLS inhibitor BPTES and the GCLC inhibitor BSO to see if chemical inhibition would have a similar phenotype as RNAi-mediated ablation of these genes. Dose response curves and extracted IC50 values pointed to higher sensitivity towards BPTES for ccRCC cells compared to HK-2 cells (Figure 5.27B). Furthermore, apart from UMRC3, A704 and ACHN cells, the profile of the IC50 values matched the sensitivity of the cells towards GLS silencing (Figure 5.27A-B), confirming that cancer cells are indeed addicted to glutamate. BSO on the other hand, was less effective with IC50 values well above 100μM for the majority of the cell lines including HK-2 cells (Figure 5.27C). Also, a discrepancy between extracted IC50 values and GCLC RNAi results could be observed for the respective cell lines (Figure 5.27A, C).

Comparison of GLS, GCLC and GSS mRNA levels showed that there is a tendency of ccRCC cells expressing in average higher levels of GLS and lower levesl of GSS compared to HK-2 cells, possibly explaining the increased sensitivity of ccRCC cells towards GLS and GSS ablation/inhibition. GCLC expression on the other hand was highly variable across the cell line panel (Figure 5.27E). However, at least in UMRC2, A498 and CAKI2 cells, high GCLC mRNA levels correlated with reduced BSO sensitivity. In contrast, RCC4, 786-O and UMRC3 cells, which expressed low GCLC mRNA levels, appeared to be more sensitive to BSO treatment (Figure 5.27C-E).

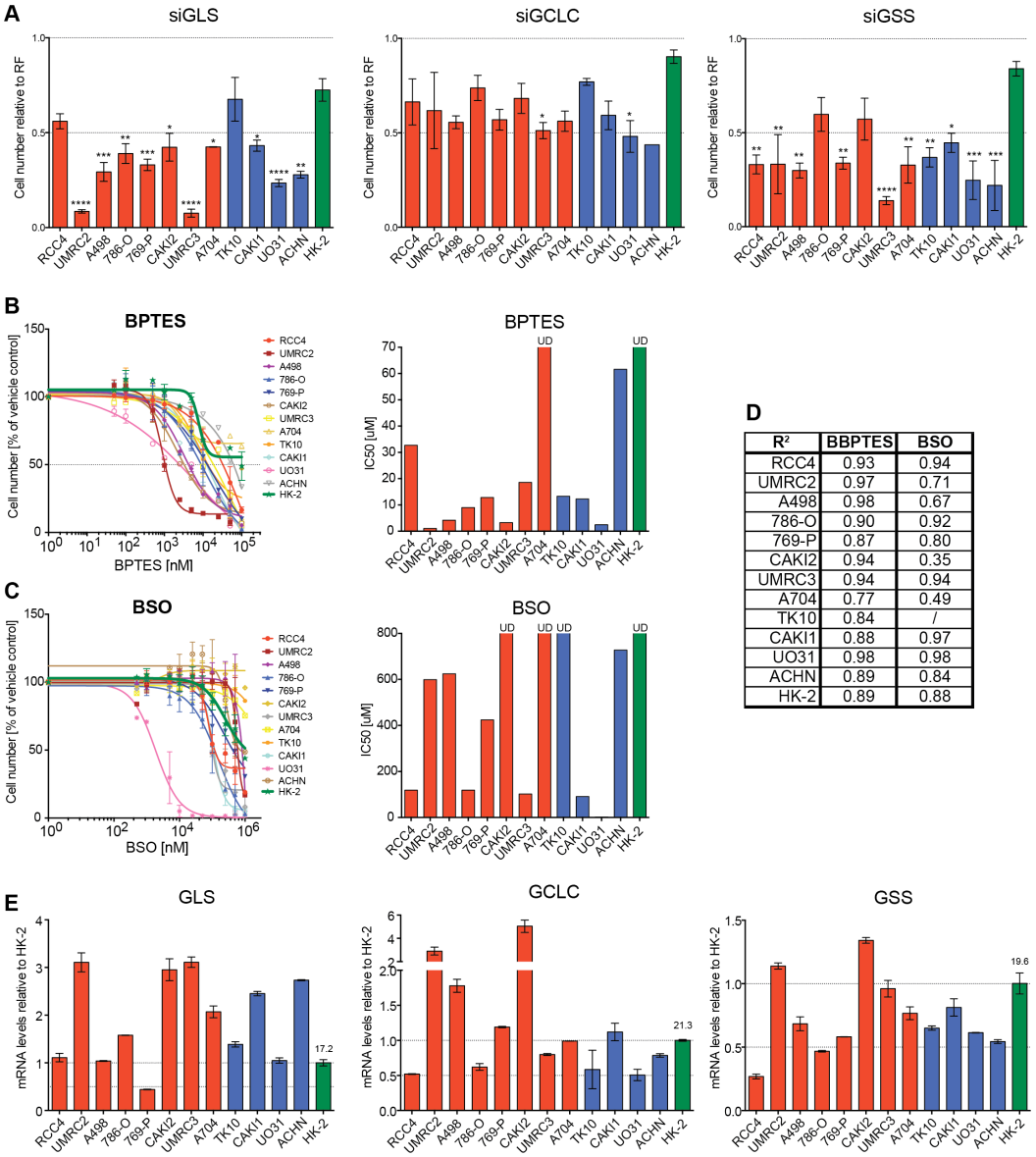

D		
R^2	BBPTES	BSO
RCC4	0.93	0.94
UMRC2	0.97	0.71
A498	0.98	0.67
786-O	0.90	0.92
769-P	0.87	0.80
CAKI2	0.94	0.35
UMRC3	0.94	0.94
A704	0.77	0.49
TK10	0.84	/
CAKI1	0.88	0.97
UO31	0.98	0.98
ACHN	0.89	0.84
HK-2	0.89	0.88

Figure 5.27: Ablation or inhibition of enzymes involved in GSH biosynthesis decreases ccRCC survival

(A) ccRCC cells were reverse transfected with 36.5 nM siRNA targeting glutathione synthetase (GSS), the catalytic subunit of glutamate-cysteine ligase (GCLC) and glutaminase (GLS) for 96 h in a 96-well format. Bar graphs represent mean endpoint cell numbers normalised to RISC-free (RF) of 3 independent experiments performed in triplicates ± SEM. Asterisks indicate statistically significant cell number loss upon GLS, GCLC or GSS ablation for the respective ccRCC cell line compared to HK-2 cells (2-way ANOVA analysis with Dunnett multiple comparison testig; *, $p \leq 0.05$). (B-C) ccRCC cell were treated for 72 h with increasing doses of (B) the GLS inhibitor BPTES or (C) the GCLC inhibitor BSO. Drug response curves (left-hand panel) represent mean endpoint cell numbers of 3 independent experiments performed in triplicates ± SEM and result from non-linear regression modelling in GraphPad Prism 6. Bar graphs (right-hand panel) represent IC50 values extracted from the dose response curves. UD, undetermined, i.e. 50% cell number reduction was not reached. (D) Table depicting R^2 values for the respective cell lines and drugs, which are indicative of goodness of fit of dose response curves to measured endpoint cell numbers. (E) Basal GLS, GCLC and GSS mRNA levels determined from total mRNA extraction by RT-qPCR, normalised to ACTB and displayed relative to HK-2 cells. Bars represent average of duplicate measurements ± SD. Numbers above HK-2 bars indicate average ΔC_T value for comparison.

Taken together, these data provide evidence that ccRCC cells rely on GSH production and maintenance for cell survival. Furthermore, they reiterate glutamate being an essential metabolite for these cancer cells but not so much for HK-2 cells.

To see if perturbation of GSH production phenocopied GPX1 and GPX3 ablation by slowing down the cell cycle, RCC4 and HK-2 cells were treated with increasing BSO concentrations. 48h BSO treatment resulted in distressed cells expressing increased p21 and p53 protein levels (Figure 5.28). Furthermore, cyclin A, cyclin D1, p27, cdk2 and cdk6 protein expression was elevated compared to vehicle control, indeed indicative of cell cycle arrest. A similar expression pattern could be observed upon silencing of *GPX1* and *GPX3* (Figure 5.13).

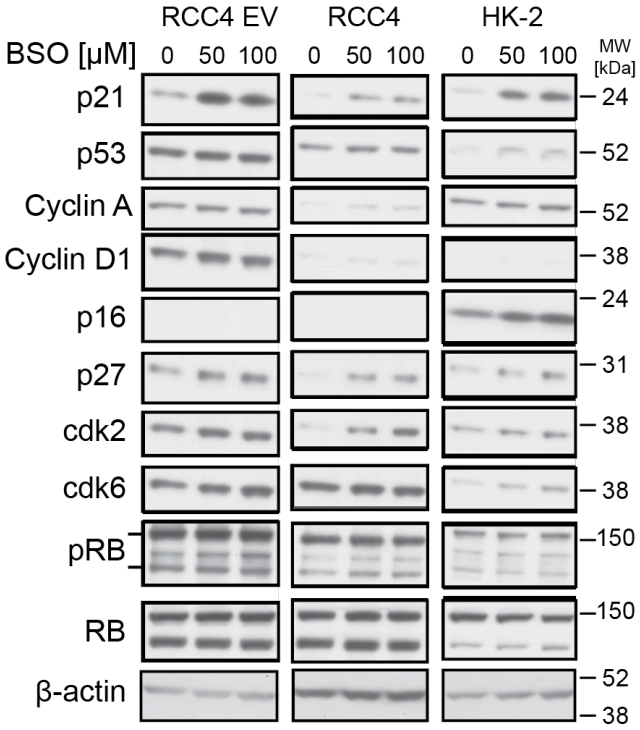

Figure 5.28: BSO phenocopies the cell cycle arrest phenotype caused by GPX1/GPX3 depletion

RCC4 EV, RCC4 and HK-2 cells were treated with increasing 50 µM and 100 µM BSO for 72 h; DMSO served as vehicle control (0 µM). Whole cell lysates were subjected to SDS/PAGE and analysed for expression of the indicated cell cycle regulators. β-actin serves as loading control.

Next, ROS levels were measured in RCC4 and HK-2 cells after BSO and BPTES treatment or after glutamine withdrawal to see if the cell cycle arrest phenotype correlates with ROS accumulation. A tendency towards increased ROS/O_2^- levels following BPTES treatment or glutamine withdrawl could be observed in RCC4 cells (Figure 5.29). However, in both cases, statistical significance was not reached due to high variability of the data. BSO treatment had no obvious effect on ROS but slightly

reduced O_2^- levels in RCC4 cells. Interestingly, both ROS and O_2^- induction following BPTES treatment could be rescued by NAC supplementation in RCC4 cells (Figure 5.29). Surprisingly, BSO caused substantial ROS accumulation in HK-2 cells, which could not be attenuated by NAC treatment. Although BPTES treatment alone did not alter ROS levels too much in HK-2 cells, in combination with NAC, however, a 2-fold increase in ROS levels could be observed. This ROS increase might be due to reductive stress - an assumption that needs further investigation.

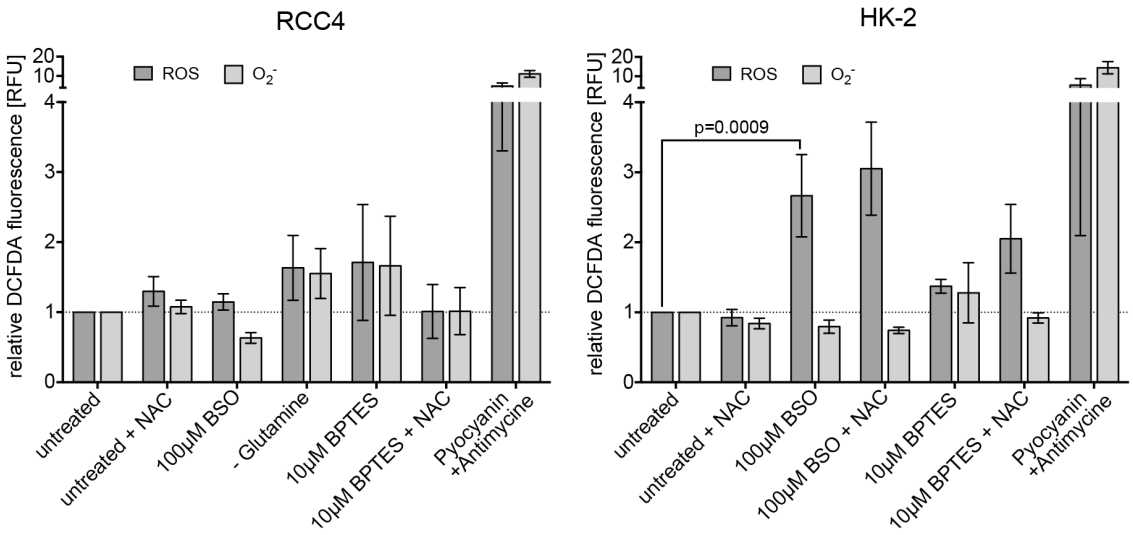

Figure 5.29: Inhibition of GSH production causes ROS accumulation in RCC4 and HK-2 cells

RCC4 and HK-2 cells were treated for 72 h with 100 µM BSO or 10 µM BPTES including 1 mM NAC (where applicable). Cellular ROS and O_2^- accumulation was measured via FACS. Treatment with 200 µM Antimycine A/Pyocyanin served as positive control. Bars represent mean cellular ROS/O_2^- intensities normalised to the respective untreated control of three independent experiments ± SEM. A 2-way ANOVA analysis with Dunnett multiple comparison testing was performed to check for statistically significant accumulation of ROS/O_2^- following BSO or BPTES treatment compared to untreated or ROS/O_2^- attenuation upon NAC addition. RFU, relative fluorescent units.

5.16 Glutamine and cysteine are essential nutrients for ccRCC

Ablation or inhibition of enzymes involved in GSH biosynthesis or recycling resulted in severe cell number loss in ccRCC cell lines compared to HK-2 cells. To see whether restriction of replenishment of GSH components has a similar effect on ccRCC cell proliferation, perturbation of glutamine and cystine uptake was examined. Glutamine and cystine uptake is facilitated by SLC1A5 and SLC7A9, respectively. Moreover, the

SLC7A11 antiporter shuttles extracellular cystine in exchange for intracellular glutamate.

Comparison of mRNA levels for these transporters revealed that ccRCC cells expressed on average lower levels of SLC1A5 mRNA, but higher levels of SLC7A11 and SLC7A9 mRNA compared to HK-2 cells. SLC7A9 is particularly highly upregulated in these cancer cell lines (Figure 5.30A). Knockdown of SLC1A5 and SLC7A11 resulted in significant cell number loss of ≥50% in most ccRCC cell lines, while HK-2 cells were only majourly affected by SLC7A11 (Figure 5.30B). Silencing of SLC7A9 caused a mixed result: about half the cancer cell lines showed a tendency towards increased cell number loss compared to HK-2 cells, while the other half remained relatively unaffected (Figure 5.30B).

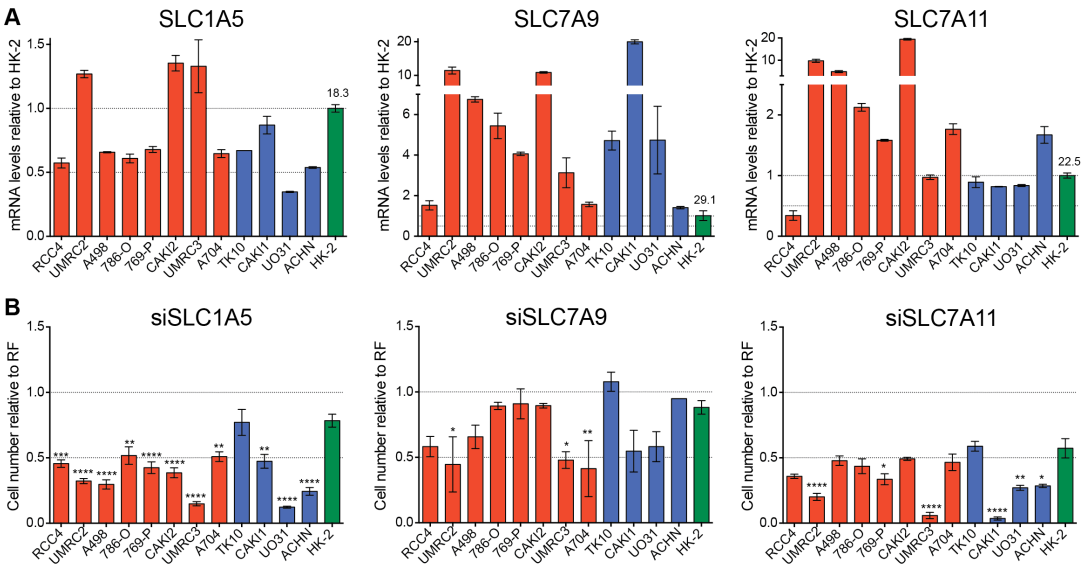

Figure 5.30: Ablation of glutamine or cystine transporters is detrimental to ccRCC cells
(A) Basal mRNA levels for SLC1A5 (glutamine transporter), SLC7A9 (cystine transporter) and SLC7A11 (glutamate/cysteine antiporter) determined via RT-qPCR and normalised to respective ACTB levels. Bars represent average of duplicate measurements ± SD and are displayed relative to HK-2 cells. Numbers above HK-2 bars indicate average ΔC_T value for comparison. (B) ccRCC and HK-2 cells were reverse transfected for 96 h with 37.5 nM siRNA targeting SLC1A5, SLC7A9 and SLC7A11 in a 96-well format. Bar graphs represent average endpoint cell number normalised to RISC-free (RF) of 3 independent experiments performed in triplicates ± SEM. Asterisks indicate statistically significant cell number loss in the respective ccRCC cell line compared to HK-2 cells resulting from SLC1A5, SLC7A9 or SLC7A11 knockdown (2-way ANOVA analysis with Dunnett multiple comparison testing; *, $p \leq 0.05$).

These results confirmed the previous observation that glutamate is a limiting factor for ccRCC cell proliferation. In addition, transporter-mediated uptake of cystine was also revealed as an essential process for both cancer and non-cancer cells.

In addition to its function as a precursor for GSH synthesis, glutamine can also be converted to α-KG and shuttled into the TCA cycle, thereby contributing to mitochondrial NADH and ATP synthesis, a process termed anaplerosis (Kovacevic and McGivan, 1983). Glutamate-derived α-KG can also contribute to lipid synthesis through reductive carboxylation (Figure 1.4) (Holleran et al., 1995, Metallo et al., 2012, Mullen et al., 2012). In an attempt to delineate whether in ccRCC cells glutamine is preferentially used for energy production or GSH synthesis, RCC4, 786-O, CAKI1 and HK-2 cells were starved off glutamine or treated with BPTES and supplemented with increasing amounts of GSH, L-cysteine, NAC and α-KG. Rescue of cell number loss with one or more of the antioxidants would suggest a preferred shuttling of glutamine into the GSH biosynthesis pathway, while rescue with α-KG would indicate that glutamine is mainly used to supplement the TCA cycle. Figure 5.31 illustrates the dose response curves for the respective treatments.

Supplementation of glutamine-deprived cells with increasing amouts of either GSH or NAC resulted in an upward trend with regard to cell proliferation in both cancer and HK-2 cells, although statistical significance could not be reached for the cancer cells due to high variability. Interestingly, HK-2 cells grown in glutamine-deprived DMEM displayed the strongest positive effect upon GSH and NAC addition. Supplementation with increasing doses of L-cysteine or α-KG on the other hand did not affect the cell number loss phenotype much in any of the four cell lines (Figure 5.31A).

In contrast, addition of GSH and NAC to all BPTES treated cells improved cell survival significantly (almost) in a dose dependent manner. Except for RCC4 cells, low concentrations of L-cysteine increased proliferation, while higher concentrations of L-cysteine were detrimental to 786-O, CAKI1 and HK-2 cells in the presence of 7.5 μM BPTES. Interestingly, all four cell lines responded similarly positive to α-KG supplementation independent of increasing doses (Figure 5.31B).

These results suggest that in ccRCC and HK-2 cells a fair amount of glutamine is needed for antioxidant purposes and point to the possibility of shunting a majour part of the generated glutamate into GSH production for antioxidant supply and only to a lower extend into the TCA cycle for energy production. However, a more extended examination, for example by using isotopomer flux analysis of stable isotope labelled glutamine, will be necessary to confirm this hypothesis.

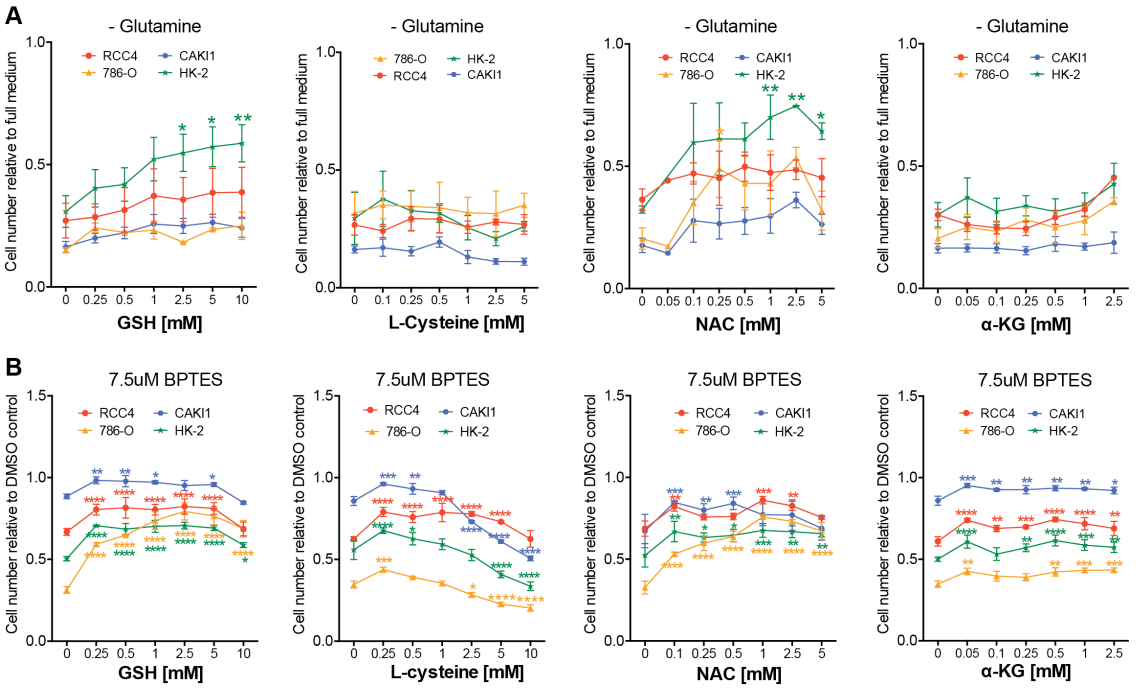

Figure 5.31: BPTES-induced cell number loss can be partially rescued by antioxidants and α-KG

(A) RCC4, 786-O, CAKI1 and HK-2 cells were treated for 72 h with increasing concentrations of GSH, L-cysteine, NAC and α-KG in glutamine-depleted growth medium. Curves represent average cell numbers normalised to untreated standard growth medium of 3 independent experiments performed in triplicates ± SEM. (B) RCC4, 786-O, CAKI1 and HK-2 cells were treated as in (A) in full growth medium supplemented with 7.5 µM BPTES. Curves represent average cell number of triplicate wells normalised to vehicle treated cells ± SD. Asterisks indicate statistically significant change in cell number upont GSH, L-cysteine, NAC or α-KG treatment compared to vehicle treatment for the respective cell line (2-way ANOVA analysis with Dunnett multiple comparison testing; *, $p \leq 0.05$).

5.17 Deregulation of GPX1, GLS, GCL, GSR, SLC1A5 and SLC7A9 correlates with clinical parameters in ccRCC

In order to examine whether expression of GPXs or enzymes involved in GSH biosynthesis are deregulated in clinical samples of human ccRCC, mRNA levels of these genes were examined in a public gene expression dataset. In 2013, a comprehensive study on ccRCC was published by The Cancer Genome Atlas (TCGA) consortium, which summarised DNA copy number, RNA and protein expression data from almost 450 individual ccRCC patient samples. This data set was used to decipher potential connections between the processes identified in this study and clinical parameters in renal cancer. Initial analysis of DNA copy number data revealed a

significant copy number loss for GPX1 and a copy number gain for GPX3 in ccRCC samples compared to samples of unaffected kidney tissue (Figure 5.32).

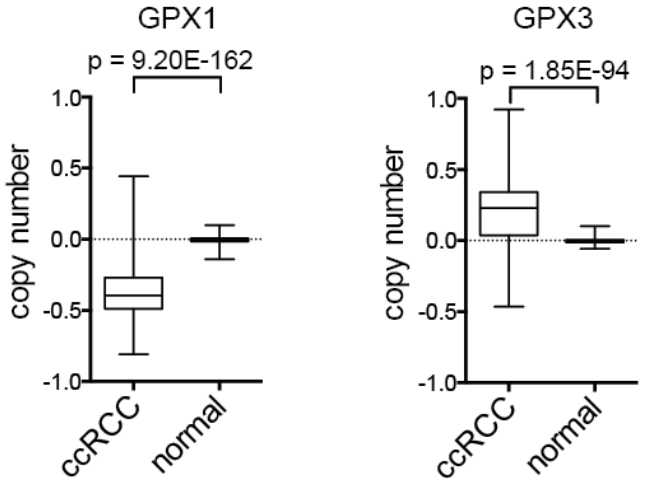

Figure 5.32: ccRCCs show DNA copy number loss for GPX1 and gain for GPX3 compared to normal adjacent tissue

Box plots summarise DNA copy number data ± range for GPX1 and GPX3 extracted from the Oncomine TCGA renal2 dataset (Cancer Genome Atlas Research, 2013).

Next, a detailed analysis of the RNA sequencing data provided within the TCGA dataset was performed by Richard Mitter from the LRI Bioinformatics and Biostatistics Service (BABS). Kaplan-Meier Plots were generated that correlate patient survival with low, medium and high expression of GPX1, GPX3, SOD1, GLS, GCLC, GCLM, GSS, GSR, G6PD, SLC1A5, SLC7A9 and SLC7A11 mRNA, respectively (Figure 5.33). Interestingly, poor survival correlates with high mRNA expression levels of GPX1 and SLC1A5 but with low mRNA levels of GLS, GCLC, GCLM, GSR and SLC7A9..

Additional analysis of protein expression of the different enzymes by immunohistochemistry or measurement of *in situ* GPX activity complemented with GSH and NADPH levels will be needed to establish the exact activation state of this pathway in ccRCC tissue.

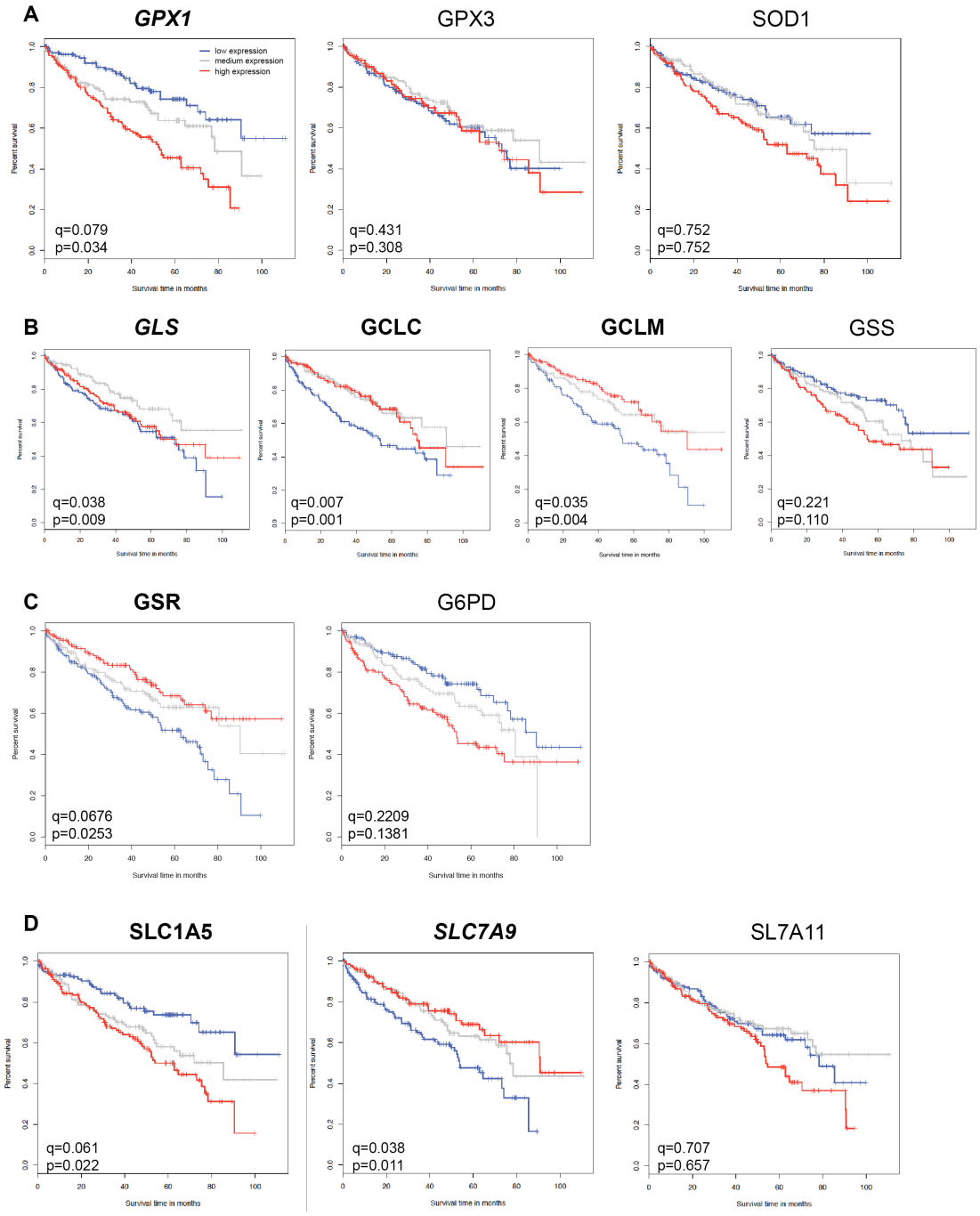

Figure 5.33: Deregulation of GPX1, GLS, GCL, GSR, SLC1A5 and SLC7A9 correlate with patient survival

(A-D) Analysis of RNA sequencing data from ccRCC patient samples (n = 419) published by The Cancer Genome Atlas Research Network (Cancer Genome Atlas Research, 2013) to identify associations of expression levels with poor survival. Kaplan-Meier survival curves for the indicated genes were produced. For each gene, the associated expression scores across all patients were split into tertiles representing high (red), medium (grey) and low (blue) expression. p-values/q-values represent the significance of difference between the three curves. Highlighted in bold are genes where mRNA expression levels correlate statistically significant with survival. (A) ROS detoxifying enzymes, (B) GSH biosynthesis enzymes, (C) enzymes involved in GSH recycling and (D) glutamine and cystine transporters.

5.18 Discussion

The aim of this study was to identify genes associated with metabolic functions, including enzymes, nutrient transporters and metabolic regulators that are essential for proliferation and survival of ccRCC cells. RNAi-mediated gene silencing in a panel of 12 ccRCC cell lines revealed that depletion of members of the GPX family, in particular GPX1 and GPX3, resulted in reduced cell proliferation. Moreover, depletion of the cytoplasmic SOD1, which also contributes to the detoxification of cytoplasmic ROS, but not the mitochondrial SOD2 isoform negatively influenced cell proliferation. Importantly, it was found that this effect was independent of pVHL status of the cells but was specific to cancer cells, as the non-transformed kidney epithelial cell line HK-2 was not affected by ablation of these genes (Figure 5.8). The observed loss in cell number was not due to induction of apoptosis, as no apoptotic markers could be detected (Figure 5.10 and 5.11). Instead, loss of cell number is more likely to be caused by inhibited cell cycle progression leading to a G1 cell cycle arrest (Figure 5.12 and 5.13). A likely cause for the G1 cell cycle arrest upon GPX1, GPX3 and SOD1 ablation is ROS-induced DNA damage, as both, a moderate increase in ROS levels and focal accumulation of the DDR proteins γH2.AX and 53BP1 were observed in RCC4 cells but not in HK-2 cells following GPX1 or GPX3 ablation (Figure 5.14, 5.17 and 5.18). Further evidence is required to substantiate these findings, for example confirmation of ROS-induced DNA damage could be provided by the detection of increased levels of 7,8-dihydro-8-oxo-2'-deoxyguanosine (8-oxo-dG), a biomarker of oxidative DNA damage (Mangal et al., Valavanidis et al., 2009).

Initial analysis of the cell line panel for mRNA expression of several components of the antioxidant system (GPX1-8, SOD1/2, CAT, NRF2) revealed an overall heterogeneous expression pattern (Figure 5.21). This could be due to the heterogeneity of the ccRCC cell line panel and the disease itself. However, no correlation of expression with sensitivity towards RNAi targeting different antioxidant enzymes or the response to exogenous ROS-insults (i.e. treatment with H_2O_2, tert-Butyl, Rotenone, AntimycinA or Pyocyanin) could be observed (Figure 5.23). This could be due to compensatory mechanisms carried out by other antioxidant enzymes not investigated in this study, such as components of the PRX or TRX system. Furthermore, it was found that,

especially with regard to GPX1, mRNA levels in ccRCC cells did not correlate with protein expression (Figure 5.21). However, the GPX activity analysis clearly showed that ccRCC cells were severely restricted in their GPX activity compared to the non-tumourigenic HK-2 cells, when measured using an enzymatic assay (Figure 5.22). In contrast, ccRCC cells were found to have higher levels of GSH than HK-2 cells (Figure 5.24), which could provide reducing capacity not only for the GPX reaction but also for other GSH-dependent antioxidant enzymes. Moreover, GSH on its own with its thiol group is already a potent antioxidant and can contribute to the antioxidant activity in ccRCC cells. The vital role of GSH in ccRCC homeostasis was revealed by the finding that perturbation of the GSH biosynthesis pathway was detrimental to most ccRCC cell lines, while proliferation of HK-2 cells was unaffected (Figure 5.26 and 5.27). The most severe effect on ccRCC cell viability was seen upon disruption of glutamate and cysteine supply. In particular, ablation of the glutamine transporter SLC1A5 or the glutamate/cystine antiporter SLC7A11 diminished ccRCC cell proliferation. However, the effect of silencing of SLC7A11 was not cancer specific, as HK-2 cells were affected to the same extent as the ccRCC cell lines (Figure 5.30). This suggests that SLC7A11 could be essential for kidney epithelial function in general. In fact, the kidney shows high expression of SLC7A11 as this antiporter is needed for the maintenance of acid-base balance. In the ccRCC cell line panel used here, SLC7A11 was highly expressed in about half of the cell lines, with these lines showing higher expression levels compared to HK-2 cells (Figure 5.30). Cell number loss upon ablation of GLS and GSS was not due to apoptosis but due to decreased cell proliferation (Figure 5.26), indicating that perturbation of GSH synthesis is growth inhibitory rather than cytotoxic, at least under the experimental conditions used. It would be interesting to see if this growth arrest is only transient or will eventually lead to cell death or senescence in longer term assays.

It seems that most of the ccRCC cell lines might also have a compromised GSH recycling system, as all but UMRC2, A498, 769-P and CAKI2 cells express lower levels of GSR and G6PD mRNA compared to the non-tumourigenic HK-2 cells (Figure 5.25). Interestingly, ablation of GSR or G6PD resulted in reduced proliferation to similar extent in all ccRCC cell lines, independent of mRNA expression levels, while HK-2 cells were unaffected (Figure 5.25). One explanation for the detrimental effect of

GSR and G6PD depletion might be that the GSH recycling system is in constant demand in ccRCC cells, potentially due to increased ROS production. If this limited recycling capacity is further reduced by gene silencing it cannot provide sufficient ROS detoxification, resulting in compromised proliferation. It is possible that increased levels of GSH and the strong dependency on components of the GSH biosynthesis pathway provide an alternative for ccRCC cells to circumvent an impaired GSH recycling capacity. However, changes in the levels of GSH and GSSG as well as alterations in the rate of NADPH synthesis upon GSR, G6PD or GSS silencing would need to be determined to confirm this hypothesis.

The study of cellular ROS is challenging due to the lack of tools to accurately measure not only distinct/specific ROS species but also their temporal and spatial distribution. To compound matters further, ROS are highly dynamic in their formation and distribution. Furthermore, the cellular system is highly buffered not only with regard to pH but also with regard to redox potential. Using ROS reagents based on electron interference, poses the risk of unspecific reactivity, while subtle but biologically potentially highly relevant changes in the nM range might be beyond the detection limit. The H_2DCFDA ROS probe, for example, can react with a wide range of ROS species and has low substrate affinity, making it easily reducible, which accounts for accumulative probe enrichment. However, as the importance of ROS in cellular homeostasis and disease development is becoming more appreciated, novel ROS reporters are being developed. There are now probes available that are species-specific and allow the simultaneous tracing of more than one ROS species at a time. Moreover, probes that locate to different organelles allow the detection of spatially separated ROS (Woolley et al., 2013). These tools could be used for a more detailed study of ROS accumulated upon GPX1, GPX3 or SOD1 ablation. Moreover, the effect of ROS on different macromolecules such as proteins, DNA and lipids, could be established. Finally, it would be interesting to see whether ROS accumulate only within the cytoplasm or in specific organelles.

It is also important to consider that oxidative stress can alter the expression and activity of different components of the antioxidant system. To better understand the full impact

of ROS on the antioxidant system in ccRCC cells, protein and activity levels would need to be evaluated upon external ROS assaults using diverse agents (e.g. H_2O_2, Rotenone, Antimycin A, Paraquat). For comparison of basal response with antioxidant-perturbed response, this should be also done following GPX1, GPX3 and SOD1 ablation. Moreover, the effect of GSH depletion using chemical agents such as PEITEC, BITC or Imexon should be investigated. These analyses could give valuable insights into potential novel drug regimens, i.e. the combinatorial delivery of a ROS-inducing agent (i.e. chemotherapy) with simultaneous or time-delayed delivery of an antioxidant-depleting compound to achieve synergistic effects.

The findings from this study also suggest that increased antioxidant intake, for example in the form of dietary supplements, could provide a growth advantage to cancer cells. Indeed, studies exploring the benefits of antioxidant intake for both cancer prevention and cancer treatment have so far provided controversial results. The first large-scale randomized Linxian General Population Nutrition Intervention Trial investigated potential beneficial effects of daily intake of an antioxidant mix (β-carotene, α-tocopherol and selenium) for 5 years for prevention of gastrointestinal cancer in Chinese men and women at risk. Although initial results were promising in that antioxidant supplementation reduced the mortality rates of gastric but not oesophageal cancer, without lowering the risk of either, though. In the final results, however, published 10 years after supplementation ended, the beneficial effect of antioxidants on mortality risk was no longer visible (Blot et al., 1995, Qiao et al., 2009). The Selenium and Vitamine E Cancer Prevention Trial (SELECT), which investigated potential beneficial effects of dietary supplementation with selenium, vitamin E or the combination on prostate cancer risk, was stopped ~ 5 years earlier than planned as antioxidant supplementation did not reduce cancer risk. An updated report after 7 years (5.5 years ‘on’ plus 1.5 years ‘off’ supplementation) even showed a 17 % increase in prostate cancer incidents following vitamin E supplementation as compared to the control group. Selenium supplementation on its own and the combination of both vitamins did not have any effect (Klein, 2009, Lippman et al., 2009). These and similar results reiterate that the presumption that ROS are disease promoting and have to be prevented is not necessarily true. It also highlights that ROS regulation is far more

complicated and caution has to be applied when considering it as anti-cancer treatment (Lau and Chiu, 2009).

Importantly, while all experiments indicating a role for GPX proteins and the GSH biosynthesis pathway were performed using *in vitro* systems, analysis of copy number and mRNA expression from human tissue suggests clinical relevance of the findings. High levels of GPX1, SOD1 and SLC1A5 mRNA or low levels of GLS, GCLC, GCLM, GSR and SLC7A9 mRNA are associated with poorer overall survival of patients harbouring ccRCC. However, these findings should be substantiated by the analysis of protein levels using immunohistochemistry or *in situ* enzymatic activity in ccRCC tissue samples.

Overall, it can be concluded that the GPX system and the processes involved in the synthesis and restoration of GSH are highly relevant for the proliferation of ccRCC cells and could represent interesting targets for the development of novel therapeutic strategies, especially as they seem to be cancer specific.

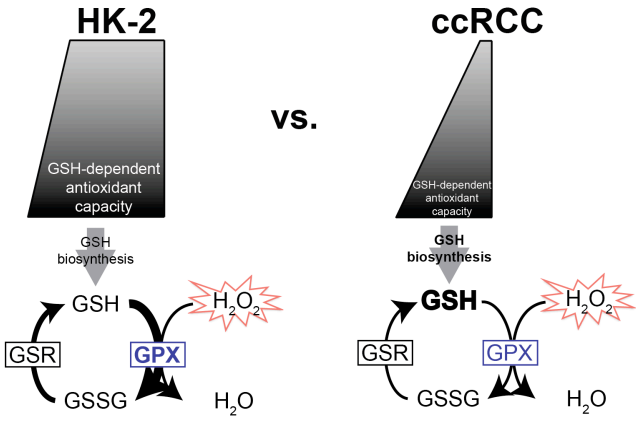

Figure 5.34: Proposed model
HK-2 cells showed high GPX activity and perturbation of neither GSH biosynthesis or recycling, nor GPX ablation had a major effect on their cell proliferation. In contrast, despite slightly higher GSH levels seen in most ccRCC cell lines tested, ablation of GPXs, especially GPX1 and GPX3, as well as perturbation of GSH biosynthesis and recycling had severe negative effects on ccRCC cell proliferation. The following assumption could offer a plausible explanation for the observations described in this chapter: In basal conditions, ccRCC cells already seem to work on the edge of their GSH-dependent antioxidant capacity and any perturbation that interferes with the highly optimised redox system drives these cancer cells over the edge causing e.g. unhealthy ROS accumulation accompanied by loss of proliferation. In contrast, HK-2 cells seem to have a relatively stable GSH-dependent antioxidant buffer capacity with enough leeway to allow for coping with exogenous perturbations before being overburdened and crashing.

Chapter 6: Discussion

The study presented here gives a more detailed insight into clear cell renal cell carcinoma (ccRCC) biology, especially with regard to the metabolic aspect. A panel of 12 ccRCC cell lines was examined for commonalities and differences with regard to their metabolic requirements and dependencies. Furthermore, a non-tumourigenic renal epithelial cell line, HK-2, was incorporated into the analysis to reveal cancer specific traits from common kidney physiology.

It could be shown, that ccRCC cells present a good example of the Warburg Effect, as these cancer cells showed characteristically high glycolytic activity, despite the presence of ample oxygen. This behaviour is mainly triggered by the constitutive activity of HIF due to functional loss of its negative regulator pVHL. Loss of functional pVHL is the central characteristic of ccRCC disease. HIF-dependency on the glycolytic phenotype was confirmed by the observation that reconstitution of functional pVHL expression was efficient in repressing HIF-α accumulation (Figure 3.3) and sufficient in decreasing glycolytic activity and increasing respiratory capacity as shown by decreased ECAR and increased OCR, respectively (Figure 3.6 and Figure 3.7). Furthermore, it was revealed that ccRCC cells are fairly stress-resistant with regards to metabolic perturbations. Oxygen deprivation (Figure 3.5), serum starvation (Figure 3.12) and lipid depletion (Figure 3.14) for several days compromised ccRCC cell proliferation only moderately, if at all, suggesting that this cancer type developed a highly dynamic metabolic network that allows quick adaptation to changes in nutrient availability. Having said that, there are two exceptions to the rule: glutamine and glucose withdrawal had severe negative effects on ccRCC cell proliferation (Figure 3.11). Glucose fuels the glycolytic pathway, which can serve as both, ATP/energy production or supply of precursors for anabolic pathways, such as the generation of nucleotides, phosphatidic acids or the biosynthesis of serine. Indeed, we established that ccRCC cells display high proliferation rates, which require high amounts of nucleotides for DNA replication. Glucose withdrawal could decrease nucleotide production to a critical level resulting in inhibition of proliferation. Glutamine is the most abundant amino acid, which can provide precursors for several anabolic pathways. Although Glutamine is a non-essential amino acid, i.e. can be synthesised by the cell, it has been established as an essential nutrient supplement for cancer cells as glutamine withdrawal from the medium severely compromises cell proliferation (De Berardinis et al., 2010). c-MYC-driven

tumours, including ccRCC, were found to be particularly sensitive to impaired glutamine supply (Fuchs and Bode, 2006, Garcia-Cao et al., 2012). However, the exact mechanism of how glutamine supports cancer cell survival and proliferation, i.e. whether it is its contribution to ATP/energy production via anaplerosis, its shunt into lipogenesis via reductive decarboxylation or its input to glutathione biosynthesis and redox homeostasis is not yet determined and provides room for investigation.

In an attempt to delineate the ccRCC-specific dependencies in the core glucose, amino acid and fatty acid metabolism and to identify associated metabolic vulnerabilities, a functional genomics approach was undertaken. Therefore, five ccRCC cell lines, including counterparts with reconstituted pVHL expression, were subjected to a functional siRNA screen targeting 240 genes that encode metabolic enzymes, regulators and nutrient transporters. This approach aimed at identifying not only general ccRCC metabolic vulnerabilities but also potential *VHL*-synthetic lethality. Furthermore, as the five isogenic cell lines that were chosen for the screen differ in their HIF-α isoform expression, putative correlations between metabolic essentialities and HIF-α isoform expression could also be elucidated.

Intriguingly, although we identified few cell line-specific *VHL*-synthetic lethal genes, none of the genes tested showed a strong, consistent cell number loss in all five cell lines upon silencing. Initially, this finding was puzzling, because it did not fit in with the assumptions that were made when planning the screen. Apart from functional pVHL loss, a prominent Warburgian metabolism is the other common feature in ccRCC. Hence, these two features could be expected, at some level, to influence each other. Several reasons could explain the lack of positive *VHL*-synthetic lethal genes. The screen only analysed 240 genes and it could be possible that the library did not contain the relevant *VHL*-synthetic lethal genes. Similarly, the readout used for this screen may have biased the results. Loss of cell number is a rather crude, though most definite readout, which, when exchanged by comparative analysis of more refined features such as changes in migration or redox-flux might have yielded more promising differential hits.

Recently, there is accumulating evidence for ccRCC to be a genetically highly instable disease. In addition to fractional LOH on chromosome 3p, fractional LOH of

chromosome 14q and gain of chromosome 5q as well as focal gene losses and gains across the genome were identified implicating substantial intertumour heterogeneity (Zbar et al., 1987, Presti et al., 1991b, Semenza, 2003, Shen et al., 2011, Cancer Genome Atlas Research, 2013, Sato et al., 2013). Indeed, although the ccRCC cell lines share some commonalities such as high glycolytic flux and growth inhibition upon glucose and glutamine withdrawal when compared to HK-2 cells, they show differences when compared amongst each other. In other words, despite having adapted to a metabolic switch from oxidative phosphorylation to glycolysis as a whole tumour subtype, the fine-tuning of this adaptation could be different in individual cell lines as consequence of their distinct genetic backgrounds. Hence, genetic heterogeneity between the different cell lines might not allow for one and the same *VHL*-synthetic lethal relationship. In line with this, pVHL is only one amongst many genes that is heterozygously lost upon fractional LOH of chromosome 3p, the initiating step in ccRCC tumourigenesis (Gerlinger et al., 2012a), and this could be another good reason for failing to identify metabolic genes that are exclusively synergistic-lethal with *VHL*. In fact, a systems biology approach that applied genome-scale metabolic modelling of cancer cells, revealed that the unique metabolic phenotype that distinguishes ccRCCs from other cancer types is due to recurrent LOH in multiple metabolic genes adjacent to *VHL*, such as choline dehydrogenase (CHDH), glycerol-3-phosphate dehydrogenase 1-like (GPD1L) or pyruvate dehydrogenase B (PDHB) (Gatto et al., 2014), putting the exclusivity of VHL into perspective, at least from a metabolic point of view.

We were also interested in identifying HIF-α isoform specific dependencies in ccRCC. However, correlation of loss of viability upon gene silencing and HIF-α expression was found in only few cases, probably because of the small number of cell lines analysed, and occurred almost predominantly in a HIF-2α specific manner. c-MYC was amongst the differential genes, which is in line with reports of HIF-2α/c-MYC cooperation in driving cell cycle progression in hypoxia (Gordan et al., 2007a). Indeed, when exposed to severe oxygen deprivation, the cell lines expressing only the HIF-2α isoform, 786-O and 769-P, showed steeper growth curves compared to the other cell lines expressing both HIF-α isoforms (Figure 3.5).

Given the heterogeneity that ccRCCs display, identifying vulnerabilities that are shared throughout the tumour subtype could provide leads for novel therapeutic windows. The screen described in this study was able to identify a number of genes whose silencing resulted in severe cell number loss in most, if not all, ccRCC cell lines. Amongst these 'general ccRCC killers' were many genes that belonged to the cholesterol or fatty acid biosynthesis pathway, genes that encoded glycolytic enzymes and also two AKT isoforms, AKT1 and AKT2. Intriguingly, these results are in line with the recently published comprehensive molecular characterisation of over 400 ccRCC patient samples within the TCGA network. The TCGA study highlighted that in ccRCCs the PI3K/AKT pathway is frequently mutated and that induced lipogenesis correlates with poor survival (Cancer Genome Atlas Research, 2013). These vulnerabilities were not only successfully recapitulated with the *in vitro* screen described in this study, but we were also able to identify specific targets in these metabolic processes that cause loss of viability upon ablation.

In addition, the screen identified a further metabolic vulnerability not addressed by the TCGA study: the strong dependency of ccRCC cells on a solid glutathione redox system. Loss of GPX1, GPX3 and SOD1 were identified to be detrimental in all tested ccRCC cell lines. Furthermore, comparison with the non-tumourigenic renal epithelial HK-2 cell line revealed that the observed effect was cancer-specific, as ablation of these proteins did not affect HK-2 cells. SOD1 is a cytosolic superoxide dismutase that converts highly reactive superoxide (O_2^-) to hydrogenperoxide (H_2O_2). GPXs, are a family of peroxidases that use glutathione (GSH) as co-factor to neutralise H_2O_2 to water. Subsequent analyses showed that although the different ccRCC cell lines showed heterogeneous expression of the different GPXs (Figure 5.21), all of them were found to have much lower GPX activity compared to HK-2 cells (Figure 5.22). This suggests that ccRCC cell lines must operate at the limit of GPX activity, as perturbing the already compromised GPX activity even further through ablation of GPX1 or GPX3 had severe consequences for cell proliferation (Figure 5.8 and Figure 5.10). In contrast, HK-2 cells must be able to accommodate GPX1 and GPX3 ablation easily as they were hardly affected in their proliferation (Figure 5.8 and Figure 5.10). Subsequent analysis to determine if availability of the co-substrate GSH is limited in ccRCC and contributes

to the impaired proliferation pattern seen upon GPX silencing, revealed that in comparison to HK-2 cells, ccRCC cells displayed higher levels of GSH with similar basal total glutathione levels across all cell lines (Figure 5.24). This accumulation of GSH in ccRCC cells seems to be partially dependent on GSH recycling but possibly more dependent on GSH production. Ablation of GSR, the enzyme that reduces oxidised GSSG to 2x GSH, using NADPH as co-factor, resulted in severe cell number loss in most ccRCC cells but not in HK-2 cells. The same result was obtained upon ablation of G6PD, a PPP enzyme that generates NADPH. Interestingly, two thirds of the cell lines displayed decreased GSR and half of them reduced G6PD mRNA levels compared to HK-2 cells (Figure 5.25), suggesting that activity of these enzymes, too, is close to the lowest limit tolerated in ccRCC cells while HK-2 cells have buffer capacity. Depletion of enzymes within the glutathione biosynthesis pathway, especially the first (GLS) and the last enzyme (GSS) in the cascade, though, not so much the actual rate limiting enzyme GCLC also resulted in severe cell number loss (Figure 5.27) implicating GSH biosynthesis to be essential for ccRCC proliferation. Interestingly, GLS, the enzyme that converts glutamine to glutamate, seemed to be induced in ccRCC cells at least on mRNA levels (Figure 5.27), suggesting a potential adaptation to increased glutamine utilisation. Intriguingly, ccRCC cells showed higher sensitivity to treatment with the GLS inhibitor BPTES (Figure 5.27), too. These findings tie in nicely with the observed sensitivity of ccRCC cells to glutamine withdrawal (Figure 3.11). In line with this, depletion of both the glutamine transporter SLC1A5 and the glutamate/cystine antiporter SLC7A11 resulted in ≥ 50% cell number loss in ccRCC cells, while depletion of the cystine transporter SLC7A9 showed this effect in only half the cell lines (Figure 5.30), reiterating the notion that glutamine is an essential nutrient for ccRCC proliferation. As mentioned above, glutamine is a universal amino acid that can be shunt into several anabolic pathways, the TCA cycle being one of them, GSH biosynthesis being another one. The data obtained so far strongly suggest an essentiality for glutamine in GSH production. Initial experiments support this idea, as supplementation of GSH, L-cysteine, NAC had a stronger positive effect on cell proliferation than α-KG following BPTES treatment (Figure 5.31). With the help of glutamine tracing techniques, it should be possible to delineate the contribution of glutamine to ATP/energy production, lipogenesis or GSH biosynthesis. This approach

could help to make a more informed call of whether, at least in ccRCC cells, glutamine addiction is due to an increased need for GSH production to maintain increased anti-oxidant capacity. This increased redox buffer is needed to accommodate increased ROS accumulation, which comes with high metabolic flux.

Finally, the inability to detect cell death upon silencing of GPX1, GPX3, SOD1 as well as genes encoding for enzymes in the GSH biosynthesis and recycling pathway suggests that loss of these proteins is not essential for survival but rather for proliferation, at least in the time frame analysed. Cell cycle analysis confirmed this assumption as RCC4 cells showed prolonged cell cycling upon silencing of GPX1, GPX3 and SOD1 as compared to control silencing (Figure 5.12). It will require further long-term assays to see whether this initial cytostatic effect seen in ccRCC during the four days of treatment will eventually result in senescence or cell death.

One reason for the delay in cell cycle progression could be due to the need to repair DNA damage (Figure 5.14) caused by accumulated ROS upon depleting GPX1, GPX3 and SOD1 (Figure 5.17, Figure 5.18) and possibly other enzymes involved in the GSH-ROS-detoxification system. And, although the antioxidant NAC was able to partially rescue ROS accumulation (Figure 5.18), cell proliferation upon ablation of GPX1, GPX3 or SOD1 could not be rescued with any of the antioxidants tried (Figure 5.19). Further analyses will be necessary to determine in more detail to what extend ROS accumulation and/or DNA damage response contribute to the phenotype seen upon GPX1, GPX3 and SOD1 depletion.

In conclusion, the presented study provides a detailed insight into the metabolic dependencies of ccRCC cells. It also provides evidence that the until recently prevailing dogma that ccRCC is exclusively caused by and defined as ‘loss of functional pVHL’ should be revised. Furthermore, the performed screen was not only able to recapitulate clinically relevant vulnerabilities of ccRCC, but also to identify the importance of the GSH-dependent anti-oxidant system for ccRCC cell proliferation, which provides also a novel lead for the development of diagnostic and/or therapeutic applications as it seems to be a cancer specific feature and does not affect normal cells.

The END

Bibliography

ABATE, C., PATEL, L., RAUSCHER, F. J., 3RD & CURRAN, T. 1990. Redox regulation of fos and jun DNA-binding activity in vitro. *Science,* 249**,** 1157-61.

AMBS, S., OGUNFUSIKA, M. O., MERRIAM, W. G., BENNETT, W. P., BILLIAR, T. R. & HARRIS, C. C. 1998. Up-regulation of inducible nitric oxide synthase expression in cancer-prone p53 knockout mice. *Proc Natl Acad Sci U S A,* 95**,** 8823-8.

ANDERSON, M. E. & MEISTER, A. 1980. Dynamic state of glutathione in blood plasma. *J Biol Chem,* 255**,** 9530-3.

ATSUMI, T., CHESNEY, J., METZ, C., LENG, L., DONNELLY, S., MAKITA, Z., MITCHELL, R. & BUCALA, R. 2002. High expression of inducible 6-phosphofructo-2-kinase/fructose-2,6-bisphosphatase (iPFK-2; PFKFB3) in human cancers. *Cancer Res,* 62**,** 5881-7.

AUGOFF, K. & GRABOWSKI, K. 2004. [Significance of lactate dehydrogenase measurements in diagnosis of malignancies]. *Pol Merkur Lekarski,* 17**,** 644-7.

AVISSAR, N., ORNT, D. B., YAGIL, Y., HOROWITZ, S., WATKINS, R. H., KERL, E. A., TAKAHASHI, K., PALMER, I. S. & COHEN, H. J. 1994. Human kidney proximal tubules are the main source of plasma glutathione peroxidase. *Am J Physiol,* 266**,** C367-75.

BAENKE, F., PECK, B., MIESS, H. & SCHULZE, A. 2013. Hooked on fat: the role of lipid synthesis in cancer metabolism and tumour development. *Dis Model Mech,* 6**,** 1353-63.

BELFI, C. A., CHATTERJEE, S., GOSKY, D. M., BERGER, S. J. & BERGER, N. A. 1999. Increased sensitivity of human colon cancer cells to DNA cross-linking agents after GRP78 up-regulation. *Biochem Biophys Res Commun,* 257**,** 361-8.

BENGOECHEA-ALONSO, M. T. & ERICSSON, J. 2007. SREBP in signal transduction: cholesterol metabolism and beyond. *Curr Opin Cell Biol,* 19**,** 215-22.

BENIZRI, E., GINOUVES, A. & BERRA, E. 2008. The magic of the hypoxia-signaling cascade. *Cell Mol Life Sci,* 65**,** 1133-49.

BERMANO, G., ARTHUR, J. R. & HESKETH, J. E. 1996. Selective control of cytosolic glutathione peroxidase and phospholipid hydroperoxide glutathione peroxidase mRNA stability by selenium supply. *FEBS Lett,* 387**,** 157-60.

BERRY, M. J., BANU, L., CHEN, Y. Y., MANDEL, S. J., KIEFFER, J. D., HARNEY, J. W. & LARSEN, P. R. 1991a. Recognition of UGA as a selenocysteine codon in type I deiodinase requires sequences in the 3' untranslated region. *Nature,* 353**,** 273-6.

BERRY, M. J., BANU, L. & LARSEN, P. R. 1991b. Type I iodothyronine deiodinase is a selenocysteine-containing enzyme. *Nature,* 349**,** 438-40.

BERTOUT, J. A., PATEL, S. A. & SIMON, M. C. 2008. The impact of O2 availability on human cancer. *Nat Rev Cancer,* 8**,** 967-75.

BLOT, W. J., LI, J. Y., TAYLOR, P. R., GUO, W., DAWSEY, S. M. & LI, B. 1995. The Linxian trials: mortality rates by vitamin-mineral intervention group. *Am J Clin Nutr,* 62**,** 1424S-1426S.

BOMMI-REDDY, A., ALMECIGA, I., SAWYER, J., GEISEN, C., LI, W., HARLOW, E., KAELIN, W. G., JR. & GRUENEBERG, D. A. 2008. Kinase requirements in human cells: III. Altered kinase requirements in VHL-/- cancer cells detected in a pilot synthetic lethal screen. *Proc Natl Acad Sci U S A,* 105**,** 16484-9.

BOUTROS, M., BRAS, L. P. & HUBER, W. 2006. Analysis of cell-based RNAi screens. *Genome Biol,* 7**,** R66.

BRISTOW, R. G. & HILL, R. P. 2008. Hypoxia and metabolism. Hypoxia, DNA repair and genetic instability. *Nat Rev Cancer,* 8**,** 180-92.

BROWN, M. S. & GOLDSTEIN, J. L. 1997. The SREBP pathway: regulation of cholesterol metabolism by proteolysis of a membrane-bound transcription factor. *Cell,* 89**,** 331-40.

BRUICK, R. K. & MCKNIGHT, S. L. 2001. A conserved family of prolyl-4-hydroxylases that modify HIF. *Science,* 294**,** 1337-40.

BUZZAI, M., BAUER, D. E., JONES, R. G., DEBERARDINIS, R. J., HATZIVASSILIOU, G., ELSTROM, R. L. & THOMPSON, C. B. 2005. The glucose dependence of Akt-transformed cells can be reversed by pharmacologic activation of fatty acid beta-oxidation. *Oncogene,* 24**,** 4165-73.

CANCER GENOME ATLAS RESEARCH, N. 2013. Comprehensive molecular characterization of clear cell renal cell carcinoma. *Nature,* 499**,** 43-9.

CARLSON, S. A. & JONES, B. D. 1998. Inhibition of Salmonella typhimurium invasion by host cell expression of secreted bacterial invasion proteins. *Infect Immun,* 66**,** 5295-300.

CEBRIAN, A., PHAROAH, P. D., AHMED, S., SMITH, P. L., LUCCARINI, C., LUBEN, R., REDMAN, K., MUNDAY, H., EASTON, D. F., DUNNING, A. M. & PONDER, B. A. 2006. Tagging single-nucleotide polymorphisms in antioxidant defense enzymes and susceptibility to breast cancer. *Cancer Res,* 66**,** 1225-33.

CHANDEL, N. S., MALTEPE, E., GOLDWASSER, E., MATHIEU, C. E., SIMON, M. C. & SCHUMACKER, P. T. 1998. Mitochondrial reactive oxygen species trigger hypoxia-induced transcription. *Proc Natl Acad Sci U S A,* 95**,** 11715-20.

CHANDEL, N. S., MCCLINTOCK, D. S., FELICIANO, C. E., WOOD, T. M., MELENDEZ, J. A., RODRIGUEZ, A. M. & SCHUMACKER, P. T. 2000a. Reactive oxygen species generated at mitochondrial complex III stabilize hypoxia-inducible factor-1alpha during hypoxia: a mechanism of O2 sensing. *J Biol Chem,* 275**,** 25130-8.

CHANDEL, N. S., TRZYNA, W. C., MCCLINTOCK, D. S. & SCHUMACKER, P. T. 2000b. Role of oxidants in NF-kappa B activation and TNF-alpha gene transcription induced by hypoxia and endotoxin. *J Immunol,* 165**,** 1013-21.

CHANDEL, N. S., VANDER HEIDEN, M. G., THOMPSON, C. B. & SCHUMACKER, P. T. 2000c. Redox regulation of p53 during hypoxia. *Oncogene,* 19**,** 3840-8.

CHEN, F., KISHIDA, T., DUH, F. M., RENBAUM, P., ORCUTT, M. L., SCHMIDT, L. & ZBAR, B. 1995. Suppression of growth of renal carcinoma cells by the von Hippel-Lindau tumor suppressor gene. *Cancer Res,* 55**,** 4804-7.

CHORLEY, B. N., CAMPBELL, M. R., WANG, X., KARACA, M., SAMBANDAN, D., BANGURA, F., XUE, P., PI, J., KLEEBERGER, S. R. & BELL, D. A. 2012. Identification of novel NRF2-regulated genes by ChIP-Seq: influence on retinoid X receptor alpha. *Nucleic Acids Res,* 40**,** 7416-29.

CHU, F. F., DOROSHOW, J. H. & ESWORTHY, R. S. 1993. Expression, characterization, and tissue distribution of a new cellular selenium-dependent glutathione peroxidase, GSHPx-GI. *J Biol Chem,* 268**,** 2571-6.

CHU, F. F., ESWORTHY, R. S., CHU, P. G., LONGMATE, J. A., HUYCKE, M. M., WILCZYNSKI, S. & DOROSHOW, J. H. 2004. Bacteria-induced intestinal cancer in mice with disrupted Gpx1 and Gpx2 genes. *Cancer Res,* 64**,** 962-8.

CHU, F. F., ESWORTHY, R. S., DOROSHOW, J. H., DOAN, K. & LIU, X. F. 1992. Expression of plasma glutathione peroxidase in human liver in addition to kidney, heart, lung, and breast in humans and rodents. *Blood,* 79**,** 3233-8.

CLIFFORD, S. C., COCKMAN, M. E., SMALLWOOD, A. C., MOLE, D. R., WOODWARD, E. R., MAXWELL, P. H., RATCLIFFE, P. J. & MAHER, E. R. 2001. Contrasting effects on HIF-1alpha regulation by disease-causing pVHL mutations correlate with patterns of tumourigenesis in von Hippel-Lindau disease. *Hum Mol Genet,* 10**,** 1029-38.

COPELAND, P. R., FLETCHER, J. E., CARLSON, B. A., HATFIELD, D. L. & DRISCOLL, D. M. 2000. A novel RNA binding protein, SBP2, is required for the translation of mammalian selenoprotein mRNAs. *EMBO J,* 19**,** 306-14.

COVELLO, K. L., KEHLER, J., YU, H., GORDAN, J. D., ARSHAM, A. M., HU, C. J., LABOSKY, P. A., SIMON, M. C. & KEITH, B. 2006. HIF-2alpha regulates Oct-4: effects of hypoxia on stem cell function, embryonic development, and tumor growth. *Genes Dev,* 20**,** 557-70.

COWAN, D. B., WEISEL, R. D., WILLIAMS, W. G. & MICKLE, D. A. 1993. Identification of oxygen responsive elements in the 5'-flanking region of the human glutathione peroxidase gene. *J Biol Chem,* 268**,** 26904-10.

CULLY, M., YOU, H., LEVINE, A. J. & MAK, T. W. 2006. Beyond PTEN mutations: the PI3K pathway as an integrator of multiple inputs during tumorigenesis. *Nat Rev Cancer,* 6**,** 184-92.

CURI, R., NEWSHOLME, P. & NEWSHOLME, E. A. 1988. Metabolism of pyruvate by isolated rat mesenteric lymphocytes, lymphocyte mitochondria and isolated mouse macrophages. *Biochem J,* 250**,** 383-8.

DALGLIESH, G. L., FURGE, K., GREENMAN, C., CHEN, L., BIGNELL, G., BUTLER, A., DAVIES, H., EDKINS, S., HARDY, C., LATIMER, C., TEAGUE, J., ANDREWS, J., BARTHORPE, S., BEARE, D., BUCK, G., CAMPBELL, P. J., FORBES, S., JIA, M., JONES, D., KNOTT, H., KOK, C. Y., LAU, K. W., LEROY, C., LIN, M. L., MCBRIDE, D. J., MADDISON, M., MAGUIRE, S., MCLAY, K., MENZIES, A., MIRONENKO, T., MULDERRIG, L., MUDIE, L., O'MEARA, S., PLEASANCE, E., RAJASINGHAM, A., SHEPHERD, R., SMITH, R., STEBBINGS, L., STEPHENS, P., TANG, G., TARPEY, P. S., TURRELL, K., DYKEMA, K. J., KHOO, S. K.,

PETILLO, D., WONDERGEM, B., ANEMA, J., KAHNOSKI, R. J., TEH, B. T., STRATTON, M. R. & FUTREAL, P. A. 2010. Systematic sequencing of renal carcinoma reveals inactivation of histone modifying genes. *Nature,* 463**,** 360-3.

DALTON, T. P., DIETER, M. Z., YANG, Y., SHERTZER, H. G. & NEBERT, D. W. 2000. Knockout of the mouse glutamate cysteine ligase catalytic subunit (Gclc) gene: embryonic lethal when homozygous, and proposed model for moderate glutathione deficiency when heterozygous. *Biochem Biophys Res Commun,* 279**,** 324-9.

DANG, C. V. 2009. MYC, microRNAs and glutamine addiction in cancers. *Cell Cycle,* 8**,** 3243-5.

DANG, C. V. 2012. MYC on the path to cancer. *Cell,* 149**,** 22-35.

DE BERARDINIS, E., BUSETTO, G. M., ANTONINI, G., GIOVANNONE, R. & GENTILE, V. 2010. Extracorporeal shock wave therapy in the treatment of Peyronie's disease: long-term results. *Arch Ital Urol Androl,* 82**,** 128-33.

DE HAAN, J. B., BLADIER, C., GRIFFITHS, P., KELNER, M., O'SHEA, R. D., CHEUNG, N. S., BRONSON, R. T., SILVESTRO, M. J., WILD, S., ZHENG, S. S., BEART, P. M., HERTZOG, P. J. & KOLA, I. 1998. Mice with a homozygous null mutation for the most abundant glutathione peroxidase, Gpx1, show increased susceptibility to the oxidative stress-inducing agents paraquat and hydrogen peroxide. *J Biol Chem,* 273**,** 22528-36.

DEBERARDINIS, R. J. & CHENG, T. 2010. Q's next: the diverse functions of glutamine in metabolism, cell biology and cancer. *Oncogene,* 29**,** 313-24.

DEBERARDINIS, R. J., MANCUSO, A., DAIKHIN, E., NISSIM, I., YUDKOFF, M., WEHRLI, S. & THOMPSON, C. B. 2007. Beyond aerobic glycolysis: transformed cells can engage in glutamine metabolism that exceeds the requirement for protein and nucleotide synthesis. *Proc Natl Acad Sci U S A,* 104**,** 19345-50.

DRANE, P., BRAVARD, A., BOUVARD, V. & MAY, E. 2001. Reciprocal down-regulation of p53 and SOD2 gene expression-implication in p53 mediated apoptosis. *Oncogene,* 20**,** 430-9.

DUFFIELD-LILLICO, A. J., DALKIN, B. L., REID, M. E., TURNBULL, B. W., SLATE, E. H., JACOBS, E. T., MARSHALL, J. R., CLARK, L. C. & NUTRITIONAL PREVENTION OF CANCER STUDY, G. 2003. Selenium supplementation, baseline plasma selenium status and incidence of prostate cancer: an analysis of the complete treatment period of the Nutritional Prevention of Cancer Trial. *BJU Int,* 91**,** 608-12.

DUFOUR, E., GAY, F., AGUERA, K., SCOAZEC, J. Y., HORAND, F., LORENZI, P. L. & GODFRIN, Y. 2012. Pancreatic tumor sensitivity to plasma L-asparagine starvation. *Pancreas,* 41**,** 940-8.

EBERLE, D., HEGARTY, B., BOSSARD, P., FERRE, P. & FOUFELLE, F. 2004. SREBP transcription factors: master regulators of lipid homeostasis. *Biochimie,* 86**,** 839-48.

ELBASHIR, S. M., HARBORTH, J., LENDECKEL, W., YALCIN, A., WEBER, K. & TUSCHL, T. 2001. Duplexes of 21-nucleotide RNAs mediate RNA interference in cultured mammalian cells. *Nature,* 411**,** 494-8.

ELORZA, A., SORO-ARNAIZ, I., MELENDEZ-RODRIGUEZ, F., RODRIGUEZ-VAELLO, V., MARSBOOM, G., DE CARCER, G., ACOSTA-IBORRA, B., ALBACETE-ALBACETE, L., ORDONEZ, A., SERRANO-OVIEDO, L., GIMENEZ-BACHS, J. M., VARA-VEGA, A., SALINAS, A., SANCHEZ-PRIETO, R., MARTIN DEL RIO, R., SANCHEZ-MADRID, F., MALUMBRES, M., LANDAZURI, M. O. & ARAGONES, J. 2012. HIF2alpha acts as an mTORC1 activator through the amino acid carrier SLC7A5. *Mol Cell,* 48**,** 681-91.

ESPENSHADE, P. J., LI, W. P. & YABE, D. 2002. Sterols block binding of COPII proteins to SCAP, thereby controlling SCAP sorting in ER. *Proc Natl Acad Sci U S A,* 99**,** 11694-9.

FAGEGALTIER, D., HUBERT, N., YAMADA, K., MIZUTANI, T., CARBON, P. & KROL, A. 2000. Characterization of mSelB, a novel mammalian elongation factor for selenoprotein translation. *EMBO J,* 19**,** 4796-805.

FAN, J., YE, J., KAMPHORST, J. J., SHLOMI, T., THOMPSON, C. B. & RABINOWITZ, J. D. 2014. Quantitative flux analysis reveals folate-dependent NADPH production. *Nature,* 510**,** 298-302.

FANTIN, V. R., ST-PIERRE, J. & LEDER, P. 2006. Attenuation of LDH-A expression uncovers a link between glycolysis, mitochondrial physiology, and tumor maintenance. *Cancer Cell,* 9**,** 425-34.

FERBER, E. C., PECK, B., DELPUECH, O., BELL, G. P., EAST, P. & SCHULZE, A. 2012. FOXO3a regulates reactive oxygen metabolism by inhibiting mitochondrial gene expression. *Cell Death Differ,* 19**,** 968-79.

FERON, O. 2009. Pyruvate into lactate and back: from the Warburg effect to symbiotic energy fuel exchange in cancer cells. *Radiother Oncol,* 92**,** 329-33.

FORRESTER, K., AMBS, S., LUPOLD, S. E., KAPUST, R. B., SPILLARE, E. A., WEINBERG, W. C., FELLEY-BOSCO, E., WANG, X. W., GELLER, D. A., TZENG, E., BILLIAR, T. R. & HARRIS, C. C. 1996. Nitric oxide-induced p53 accumulation and regulation of inducible nitric oxide synthase expression by wild-type p53. *Proc Natl Acad Sci U S A,* 93**,** 2442-7.

FOSTER, C. B., ASWATH, K., CHANOCK, S. J., MCKAY, H. F. & PETERS, U. 2006. Polymorphism analysis of six selenoprotein genes: support for a selective sweep at the glutathione peroxidase 1 locus (3p21) in Asian populations. *BMC Genet,* 7**,** 56.

FRANOVIC, A., HOLTERMAN, C. E., PAYETTE, J. & LEE, S. 2009. Human cancers converge at the HIF-2alpha oncogenic axis. *Proc Natl Acad Sci U S A,* 106**,** 21306-11.

FREED-PASTOR, W. A., MIZUNO, H., ZHAO, X., LANGEROD, A., MOON, S. H., RODRIGUEZ-BARRUECO, R., BARSOTTI, A., CHICAS, A., LI, W., POLOTSKAIA, A., BISSELL, M. J., OSBORNE, T. F., TIAN, B., LOWE, S. W., SILVA, J. M., BORRESEN-DALE, A. L., LEVINE, A. J., BARGONETTI, J. & PRIVES, C. 2012. Mutant p53 disrupts mammary tissue architecture via the mevalonate pathway. *Cell,* 148**,** 244-58.

FREW, I. J. & KREK, W. 2008. pVHL: a multipurpose adaptor protein. *Sci Signal,* 1**,** pe30.

FREW, I. J., MINOLA, A., GEORGIEV, S., HITZ, M., MOCH, H., RICHARD, S., VORTMEYER, A. O. & KREK, W. 2008. Combined VHLH and PTEN mutation causes genital tract cystadenoma and squamous metaplasia. *Mol Cell Biol,* 28**,** 4536-48.

FU, L., WANG, G., SHEVCHUK, M. M., NANUS, D. M. & GUDAS, L. J. 2011. Generation of a mouse model of Von Hippel-Lindau kidney disease leading to renal cancers by expression of a constitutively active mutant of HIF1alpha. *Cancer Res,* 71**,** 6848-56.

FUCHS, B. C. & BODE, B. P. 2006. Stressing out over survival: glutamine as an apoptotic modulator. *J Surg Res,* 131**,** 26-40.

GAO, P., TCHERNYSHYOV, I., CHANG, T. C., LEE, Y. S., KITA, K., OCHI, T., ZELLER, K. I., DE MARZO, A. M., VAN EYK, J. E., MENDELL, J. T. & DANG, C. V. 2009. c-Myc suppression of miR-23a/b enhances mitochondrial glutaminase expression and glutamine metabolism. *Nature,* 458**,** 762-5.

GARCIA-CAO, I., SONG, M. S., HOBBS, R. M., LAURENT, G., GIORGI, C., DE BOER, V. C., ANASTASIOU, D., ITO, K., SASAKI, A. T., RAMEH, L., CARRACEDO, A., VANDER HEIDEN, M. G., CANTLEY, L. C., PINTON, P., HAIGIS, M. C. & PANDOLFI, P. P. 2012. Systemic elevation of PTEN induces a tumor-suppressive metabolic state. *Cell,* 149**,** 49-62.

GATTO, F., NOOKAEW, I. & NIELSEN, J. 2014. Chromosome 3p loss of heterozygosity is associated with a unique metabolic network in clear cell renal carcinoma. *Proc Natl Acad Sci U S A,* 111**,** E866-75.

GEBHARD, R. L., CLAYMAN, R. V., PRIGGE, W. F., FIGENSHAU, R., STALEY, N. A., REESEY, C. & BEAR, A. 1987. Abnormal cholesterol metabolism in renal clear cell carcinoma. *J Lipid Res,* 28**,** 1177-84.

GERLINGER, M., ROWAN, A. J., HORSWELL, S., LARKIN, J., ENDESFELDER, D., GRONROOS, E., MARTINEZ, P., MATTHEWS, N., STEWART, A., TARPEY, P., VARELA, I., PHILLIMORE, B., BEGUM, S., MCDONALD, N. Q., BUTLER, A., JONES, D., RAINE, K., LATIMER, C., SANTOS, C. R., NOHADANI, M., EKLUND, A. C., SPENCER-DENE, B., CLARK, G., PICKERING, L., STAMP, G., GORE, M., SZALLASI, Z., DOWNWARD, J., FUTREAL, P. A. & SWANTON, C. 2012a. Intratumor heterogeneity and branched evolution revealed by multiregion sequencing. *N Engl J Med,* 366**,** 883-92.

GERLINGER, M., SANTOS, C. R., SPENCER-DENE, B., MARTINEZ, P., ENDESFELDER, D., BURRELL, R. A., VETTER, M., JIANG, M., SAUNDERS, R. E., KELLY, G., DYKEMA, K., RIOUX-LECLERCQ, N., STAMP, G., PATARD, J. J., LARKIN, J., HOWELL, M. & SWANTON, C. 2012b. Genome-wide RNA interference analysis of renal carcinoma survival regulators identifies MCT4 as a Warburg effect metabolic target. *J Pathol,* 227**,** 146-56.

GLOIRE, G., LEGRAND-POELS, S. & PIETTE, J. 2006. NF-kappaB activation by reactive oxygen species: fifteen years later. *Biochem Pharmacol,* 72**,** 1493-505.

GORDAN, J. D., BERTOUT, J. A., HU, C. J., DIEHL, J. A. & SIMON, M. C. 2007a. HIF-2alpha promotes hypoxic cell proliferation by enhancing c-myc transcriptional activity. *Cancer Cell,* 11**,** 335-47.

GORDAN, J. D., LAL, P., DONDETI, V. R., LETRERO, R., PAREKH, K. N., OQUENDO, C. E., GREENBERG, R. A., FLAHERTY, K. T., RATHMELL, W. K., KEITH, B., SIMON, M. C. & NATHANSON, K. L. 2008. HIF-alpha effects on c-Myc distinguish two subtypes of sporadic VHL-deficient clear cell renal carcinoma. *Cancer Cell,* 14**,** 435-46.

GORDAN, J. D., THOMPSON, C. B. & SIMON, M. C. 2007b. HIF and c-Myc: sibling rivals for control of cancer cell metabolism and proliferation. *Cancer Cell,* 12**,** 108-13.

GOUGH, D. R. & COTTER, T. G. 2011. Hydrogen peroxide: a Jekyll and Hyde signalling molecule. *Cell Death Dis,* 2**,** e213.

GRESNER, P., GROMADZINSKA, J. & WASOWICZ, W. 2007. Polymorphism of selected enzymes involved in detoxification and biotransformation in relation to lung cancer. *Lung Cancer,* 57**,** 1-25.

GU, Y. Z., MORAN, S. M., HOGENESCH, J. B., WARTMAN, L. & BRADFIELD, C. A. 1998. Molecular characterization and chromosomal localization of a third alpha-class hypoxia inducible factor subunit, HIF3alpha. *Gene Expr,* 7**,** 205-13.

GUAN, J., LO, M., DOCKERY, P., MAHON, S., KARP, C. M., BUCKLEY, A. R., LAM, S., GOUT, P. W. & WANG, Y. Z. 2009. The xc- cystine/glutamate antiporter as a potential therapeutic target for small-cell lung cancer: use of sulfasalazine. *Cancer Chemother Pharmacol,* 64**,** 463-72.

GUO, G., GUI, Y., GAO, S., TANG, A., HU, X., HUANG, Y., JIA, W., LI, Z., HE, M., SUN, L., SONG, P., SUN, X., ZHAO, X., YANG, S., LIANG, C., WAN, S., ZHOU, F., CHEN, C., ZHU, J., LI, X., JIAN, M., ZHOU, L., YE, R., HUANG, P., CHEN, J., JIANG, T., LIU, X., WANG, Y., ZOU, J., JIANG, Z., WU, R., WU, S., FAN, F., ZHANG, Z., LIU, L., YANG, R., LIU, X., WU, H., YIN, W., ZHAO, X., LIU, Y., PENG, H., JIANG, B., FENG, Q., LI, C., XIE, J., LU, J., KRISTIANSEN, K., LI, Y., ZHANG, X., LI, S., WANG, J., YANG, H., CAI, Z. & WANG, J. 2012. Frequent mutations of genes encoding ubiquitin-mediated proteolysis pathway components in clear cell renal cell carcinoma. *Nat Genet,* 44**,** 17-9.

HAN, D., HANAWA, N., SABERI, B. & KAPLOWITZ, N. 2006. Hydrogen peroxide and redox modulation sensitize primary mouse hepatocytes to TNF-induced apoptosis. *Free Radic Biol Med,* 41**,** 627-39.

HANAHAN, D. & WEINBERG, R. A. 2000. The hallmarks of cancer. *Cell,* 100**,** 57-70.

HANAHAN, D. & WEINBERG, R. A. 2011. Hallmarks of cancer: the next generation. *Cell,* 144**,** 646-74.

HANUKOGLU, I. 2006. Antioxidant protective mechanisms against reactive oxygen species (ROS) generated by mitochondrial P450 systems in steroidogenic cells. *Drug Metab Rev,* 38**,** 171-96.

HARA, S., HAMADA, J., KOBAYASHI, C., KONDO, Y. & IMURA, N. 2001. Expression and characterization of hypoxia-inducible factor (HIF)-3alpha in human kidney: suppression of HIF-mediated gene expression by HIF-3alpha. *Biochem Biophys Res Commun,* 287**,** 808-13.

HARDIE, L. J., BRIGGS, J. A., DAVIDSON, L. A., ALLAN, J. M., KING, R. F., WILLIAMS, G. I. & WILD, C. P. 2000. The effect of hOGG1 and glutathione peroxidase I genotypes and 3p chromosomal loss on 8-hydroxydeoxyguanosine levels in lung cancer. *Carcinogenesis,* 21**,** 167-72.

HASSAN, H. M. & FRIDOVICH, I. 1980. Mechanism of the antibiotic action pyocyanine. *J Bacteriol,* 141**,** 156-63.

HERNANDEZ-MONTES, E., POLLARD, S. E., VAUZOUR, D., JOFRE-MONTSENY, L., ROTA, C., RIMBACH, G., WEINBERG, P. D. & SPENCER, J. P. 2006. Activation of glutathione peroxidase via Nrf1 mediates genistein's protection against oxidative endothelial cell injury. *Biochem Biophys Res Commun,* 346**,** 851-9.

HIGA, A. & CHEVET, E. 2012. Redox signaling loops in the unfolded protein response. *Cell Signal,* 24**,** 1548-55.

HOFFMAN, M. A., OHH, M., YANG, H., KLCO, J. M., IVAN, M. & KAELIN, W. G., JR. 2001. von Hippel-Lindau protein mutants linked to type 2C VHL disease preserve the ability to downregulate HIF. *Hum Mol Genet,* 10**,** 1019-27.

HOLLERAN, A. L., BRISCOE, D. A., FISKUM, G. & KELLEHER, J. K. 1995. Glutamine metabolism in AS-30D hepatoma cells. Evidence for its conversion into lipids via reductive carboxylation. *Mol Cell Biochem,* 152**,** 95-101.

HORTON, J. D. 2002. Sterol regulatory element-binding proteins: transcriptional activators of lipid synthesis. *Biochem Soc Trans,* 30**,** 1091-5.

HSU, T. 2012. Complex cellular functions of the von Hippel-Lindau tumor suppressor gene: insights from model organisms. *Oncogene,* 31**,** 2247-57.

HU, R., DAI, A. & TAN, S. 2002. Hypoxia-inducible factor 1 alpha upregulates the expression of inducible nitric oxide synthase gene in pulmonary arteries of hyposic rat. *Chin Med J (Engl),* 115**,** 1833-7.

HU, Y. J. & DIAMOND, A. M. 2003. Role of glutathione peroxidase 1 in breast cancer: loss of heterozygosity and allelic differences in the response to selenium. *Cancer Res,* 63**,** 3347-51.

HU, Y. J., DOLAN, M. E., BAE, R., YEE, H., ROY, M., GLICKMAN, R., KIREMIDJIAN-SCHUMACHER, L. & DIAMOND, A. M. 2004. Allelic loss at the GPx-1 locus in cancer of the head and neck. *Biol Trace Elem Res,* 101**,** 97-106.

HUSSAIN, S. P., AMSTAD, P., HE, P., ROBLES, A., LUPOLD, S., KANEKO, I., ICHIMIYA, M., SENGUPTA, S., MECHANIC, L., OKAMURA, S., HOFSETH, L. J., MOAKE, M., NAGASHIMA, M., FORRESTER, K. S. & HARRIS, C. C. 2004. p53-induced up-regulation of MnSOD and GPx but not catalase increases oxidative stress and apoptosis. *Cancer Res,* 64**,** 2350-6.

HWANG, C., SINSKEY, A. J. & LODISH, H. F. 1992. Oxidized redox state of glutathione in the endoplasmic reticulum. *Science,* 257**,** 1496-502.

ILIOPOULOS, O., KIBEL, A., GRAY, S. & KAELIN, W. G., JR. 1995. Tumour suppression by the human von Hippel-Lindau gene product. *Nat Med,* 1**,** 822-6.

ISHIMOTO, T., NAGANO, O., YAE, T., TAMADA, M., MOTOHARA, T., OSHIMA, H., OSHIMA, M., IKEDA, T., ASABA, R., YAGI, H., MASUKO, T., SHIMIZU, T., ISHIKAWA, T., KAI, K., TAKAHASHI, E., IMAMURA, Y., BABA, Y., OHMURA, M., SUEMATSU, M., BABA, H. & SAYA, H. 2011. CD44 variant regulates redox status in cancer cells by stabilizing the xCT subunit of system xc(-) and thereby promotes tumor growth. *Cancer Cell,* 19**,** 387-400.

JAAKKOLA, P., MOLE, D. R., TIAN, Y. M., WILSON, M. I., GIELBERT, J., GASKELL, S. J., VON KRIEGSHEIM, A., HEBESTREIT, H. F., MUKHERJI, M., SCHOFIELD, C. J., MAXWELL, P. H., PUGH, C. W. & RATCLIFFE, P. J. 2001. Targeting of HIF-alpha to the von Hippel-Lindau ubiquitylation complex by O2-regulated prolyl hydroxylation. *Science,* 292**,** 468-72.

JABLONSKA, E., CHLOSTA, M. & PAWLEGA, J. 2004. [Ovarian cancer--therapeutic options after the failure of the first line of treatment]. *Ginekol Pol,* 75**,** 58-64.

JIANG, B. H., RUE, E., WANG, G. L., ROE, R. & SEMENZA, G. L. 1996. Dimerization, DNA binding, and transactivation properties of hypoxia-inducible factor 1. *J Biol Chem,* 271**,** 17771-8.

JOHNSON, T. M., YU, Z. X., FERRANS, V. J., LOWENSTEIN, R. A. & FINKEL, T. 1996. Reactive oxygen species are downstream mediators of p53-dependent apoptosis. *Proc Natl Acad Sci U S A,* 93**,** 11848-52.

KAELIN, W. G., JR. 2005. The concept of synthetic lethality in the context of anticancer therapy. *Nat Rev Cancer,* 5**,** 689-98.

KAELIN, W. G., JR. 2008. The von Hippel-Lindau tumour suppressor protein: O2 sensing and cancer. *Nat Rev Cancer,* 8**,** 865-73.

KAELIN, W. G., JR. & RATCLIFFE, P. J. 2008. Oxygen sensing by metazoans: the central role of the HIF hydroxylase pathway. *Mol Cell,* 30**,** 393-402.

KEISARI, Y., BRAUN, L. & FLESCHER, E. 1983. The oxidative burst and related phenomena in mouse macrophages elicited by different sterile inflammatory stimuli. *Immunobiology,* 165**,** 78-89.

KEITH, B., JOHNSON, R. S. & SIMON, M. C. 2012. HIF1alpha and HIF2alpha: sibling rivalry in hypoxic tumour growth and progression. *Nat Rev Cancer,* 12**,** 9-22.

KELLOFF, G. J., HOFFMAN, J. M., JOHNSON, B., SCHER, H. I., SIEGEL, B. A., CHENG, E. Y., CHESON, B. D., O'SHAUGHNESSY, J., GUYTON, K. Z., MANKOFF, D. A., SHANKAR, L., LARSON, S. M., SIGMAN, C. C., SCHILSKY, R. L. & SULLIVAN, D. C. 2005. Progress and promise of FDG-PET imaging for cancer patient management and oncologic drug development. *Clin Cancer Res,* 11**,** 2785-808.

KESSLER, R., BLEICHERT, F., WARNKE, J. P. & ESCHRICH, K. 2008. 6-Phosphofructo-2-kinase/fructose-2,6-bisphosphatase (PFKFB3) is up-regulated in high-grade astrocytomas. *J Neurooncol,* 86**,** 257-64.

KIM, D. J., KATAOKA, K., SANO, S., CONNOLLY, K., KIGUCHI, K. & DIGIOVANNI, J. 2009. Targeted disruption of Bcl-xL in mouse keratinocytes inhibits both UVB- and chemically induced skin carcinogenesis. *Mol Carcinog,* 48**,** 873-85.

KIM, J., LEE, J. H. & IYER, V. R. 2008. Global identification of Myc target genes reveals its direct role in mitochondrial biogenesis and its E-box usage in vivo. *PLoS One,* 3**,** e1798.

KIM, J. W., TCHERNYSHYOV, I., SEMENZA, G. L. & DANG, C. V. 2006. HIF-1-mediated expression of pyruvate dehydrogenase kinase: a metabolic switch required for cellular adaptation to hypoxia. *Cell Metab,* 3**,** 177-85.

KIM, W. Y. & KAELIN, W. G. 2004. Role of VHL gene mutation in human cancer. *J Clin Oncol,* 22**,** 4991-5004.

KIM, Y. J., AHN, J. Y., LIANG, P., IP, C., ZHANG, Y. & PARK, Y. M. 2007. Human prx1 gene is a target of Nrf2 and is up-regulated by hypoxia/reoxygenation: implication to tumor biology. *Cancer Res,* 67**,** 546-54.

KISHIDA, T., STACKHOUSE, T. M., CHEN, F., LERMAN, M. I. & ZBAR, B. 1995. Cellular proteins that bind the von Hippel-Lindau disease gene product: mapping of binding domains and the effect of missense mutations. *Cancer Res,* 55**,** 4544-8.

KLEIN, E. A. 2009. Selenium and vitamin E: interesting biology and dashed hope. *J Natl Cancer Inst,* 101**,** 283-5.

KNAUTH, K., BEX, C., JEMTH, P. & BUCHBERGER, A. 2006. Renal cell carcinoma risk in type 2 von Hippel-Lindau disease correlates with defects in pVHL stability and HIF-1alpha interactions. *Oncogene,* 25**,** 370-7.

KONDO, K., YAO, M., YOSHIDA, M., KISHIDA, T., SHUIN, T., MIURA, T., MORIYAMA, M., KOBAYASHI, K., SAKAI, N., KANEKO, S., KAWAKAMI, S., BABA, M., NAKAIGAWA, N., NAGASHIMA, Y., NAKATANI, Y. & HOSAKA, M. 2002. Comprehensive mutational analysis of the VHL gene in sporadic renal cell carcinoma: relationship to clinicopathological parameters. *Genes Chromosomes Cancer,* 34**,** 58-68.

KOPS, G. J., DANSEN, T. B., POLDERMAN, P. E., SAARLOOS, I., WIRTZ, K. W., COFFER, P. J., HUANG, T. T., BOS, J. L., MEDEMA, R. H. & BURGERING, B. M. 2002a. Forkhead transcription factor FOXO3a protects quiescent cells from oxidative stress. *Nature,* 419**,** 316-21.

KOPS, G. J., MEDEMA, R. H., GLASSFORD, J., ESSERS, M. A., DIJKERS, P. F., COFFER, P. J., LAM, E. W. & BURGERING, B. M. 2002b. Control of cell cycle exit and entry by protein kinase B-regulated forkhead transcription factors. *Mol Cell Biol,* 22**,** 2025-36.

KOSHIJI, M., KAGEYAMA, Y., PETE, E. A., HORIKAWA, I., BARRETT, J. C. & HUANG, L. E. 2004. HIF-1alpha induces cell cycle arrest by functionally counteracting Myc. *EMBO J,* 23**,** 1949-56.

KOUKOURAKIS, M. I., KONTOMANOLIS, E., GIATROMANOLAKI, A., SIVRIDIS, E. & LIBERIS, V. 2009. Serum and tissue LDH levels in patients with breast/gynaecological cancer and benign diseases. *Gynecol Obstet Invest,* 67**,** 162-8.

KOVACEVIC, Z. & MCGIVAN, J. D. 1983. Mitochondrial metabolism of glutamine and glutamate and its physiological significance. *Physiol Rev,* 63**,** 547-605.

KRYUKOV, G. V., CASTELLANO, S., NOVOSELOV, S. V., LOBANOV, A. V., ZEHTAB, O., GUIGO, R. & GLADYSHEV, V. N. 2003. Characterization of mammalian selenoproteomes. *Science,* 300**,** 1439-43.

LATIF, F., TORY, K., GNARRA, J., YAO, M., DUH, F. M., ORCUTT, M. L., STACKHOUSE, T., KUZMIN, I., MODI, W., GEIL, L. & ET AL. 1993. Identification of the von Hippel-Lindau disease tumor suppressor gene. *Science,* 260**,** 1317-20.

LAU, A. T. & CHIU, J. F. 2009. Biomarkers of lung-related diseases: current knowledge by proteomic approaches. *J Cell Physiol,* 221**,** 535-43.

LE, A., LANE, A. N., HAMAKER, M., BOSE, S., GOUW, A., BARBI, J., TSUKAMOTO, T., ROJAS, C. J., SLUSHER, B. S., ZHANG, H., ZIMMERMAN, L. J., LIEBLER, D. C., SLEBOS, R. J., LORKIEWICZ, P. K., HIGASHI, R. M., FAN, T. W. & DANG, C. V. 2012. Glucose-independent glutamine metabolism via TCA cycling for proliferation and survival in B cells. *Cell Metab,* 15**,** 110-21.

LEI, C., NIU, X., WEI, J., ZHU, J. & ZHU, Y. 2009. Interaction of glutathione peroxidase-1 and selenium in endemic dilated cardiomyopathy. *Clin Chim Acta,* 399**,** 102-8.

LEI, X. G., EVENSON, J. K., THOMPSON, K. M. & SUNDE, R. A. 1995. Glutathione peroxidase and phospholipid hydroperoxide glutathione peroxidase are differentially regulated in rats by dietary selenium. *J Nutr,* 125**,** 1438-46.

LESLIE, N. R., BENNETT, D., LINDSAY, Y. E., STEWART, H., GRAY, A. & DOWNES, C. P. 2003. Redox regulation of PI 3-kinase signalling via inactivation of PTEN. *EMBO J,* 22**,** 5501-10.

LEWIS, C. A., PARKER, S. J., FISKE, B. P., MCCLOSKEY, D., GUI, D. Y., GREEN, C. R., VOKES, N. I., FEIST, A. M., VANDER HEIDEN, M. G. & METALLO, C. M. 2014. Tracing compartmentalized NADPH metabolism in the cytosol and mitochondria of mammalian cells. *Mol Cell,* 55**,** 253-63.

LI, F., WANG, Y., ZELLER, K. I., POTTER, J. J., WONSEY, D. R., O'DONNELL, K. A., KIM, J. W., YUSTEIN, J. T., LEE, L. A. & DANG, C. V. 2005. Myc stimulates nuclearly encoded mitochondrial genes and mitochondrial biogenesis. *Mol Cell Biol,* 25**,** 6225-34.

LI, L., ZHANG, L., ZHANG, X., YAN, Q., MINAMISHIMA, Y. A., OLUMI, A. F., MAO, M., BARTZ, S. & KAELIN, W. G., JR. 2007. Hypoxia-inducible factor linked to differential kidney cancer risk seen with type 2A and type 2B VHL mutations. *Mol Cell Biol,* 27**,** 5381-92.

LI, S., BROWN, M. S. & GOLDSTEIN, J. L. 2010. Bifurcation of insulin signaling pathway in rat liver: mTORC1 required for stimulation of lipogenesis, but not inhibition of gluconeogenesis. *Proc Natl Acad Sci U S A,* 107**,** 3441-6.

LIPPMAN, S. M., KLEIN, E. A., GOODMAN, P. J., LUCIA, M. S., THOMPSON, I. M., FORD, L. G., PARNES, H. L., MINASIAN, L. M., GAZIANO, J. M., HARTLINE, J. A., PARSONS, J. K., BEARDEN, J. D., 3RD, CRAWFORD, E. D., GOODMAN, G. E., CLAUDIO, J., WINQUIST, E., COOK, E. D., KARP, D. D., WALTHER, P., LIEBER, M. M., KRISTAL, A. R., DARKE, A. K., ARNOLD, K. B., GANZ, P. A., SANTELLA, R. M., ALBANES, D., TAYLOR, P. R., PROBSTFIELD, J. L., JAGPAL, T. J., CROWLEY, J. J., MEYSKENS, F. L., JR., BAKER, L. H. & COLTMAN, C. A., JR. 2009. Effect of selenium and vitamin E on risk of prostate cancer and other cancers: the Selenium and Vitamin E Cancer Prevention Trial (SELECT). *JAMA,* 301**,** 39-51.

LIU, J., HINKHOUSE, M. M., SUN, W., WEYDERT, C. J., RITCHIE, J. M., OBERLEY, L. W. & CULLEN, J. J. 2004. Redox regulation of pancreatic cancer cell growth: role of glutathione peroxidase in the suppression of the malignant phenotype. *Hum Gene Ther,* 15**,** 239-50.

LIU, Z., LU, H., SHI, H., DU, Y., YU, J., GU, S., CHEN, X., LIU, K. J. & HU, C. A. 2005. PUMA overexpression induces reactive oxygen species generation and proteasome-mediated stathmin degradation in colorectal cancer cells. *Cancer Res,* 65**,** 1647-54.

LIVAK, K. J. & SCHMITTGEN, T. D. 2001. Analysis of relative gene expression data using real-time quantitative PCR and the 2(-Delta Delta C(T)) Method. *Methods,* 25**,** 402-8.

LJUNGBERG, B., CAMPBELL, S. C., CHOI, H. Y., JACQMIN, D., LEE, J. E., WEIKERT, S. & KIEMENEY, L. A. 2011. The epidemiology of renal cell carcinoma. *Eur Urol,* 60**,** 615-21.

LO, M., LING, V., LOW, C., WANG, Y. Z. & GOUT, P. W. 2010. Potential use of the anti-inflammatory drug, sulfasalazine, for targeted therapy of pancreatic cancer. *Curr Oncol,* 17**,** 9-16.

LOCASALE, J. W. 2013. Serine, glycine and one-carbon units: cancer metabolism in full circle. *Nat Rev Cancer,* 13**,** 572-83.

LONERGAN, K. M., ILIOPOULOS, O., OHH, M., KAMURA, T., CONAWAY, R. C., CONAWAY, J. W. & KAELIN, W. G., JR. 1998. Regulation of hypoxia-inducible mRNAs by the von Hippel-Lindau tumor suppressor protein requires binding to complexes containing elongins B/C and Cul2. *Mol Cell Biol,* 18**,** 732-41.

LONSER, R. R., GLENN, G. M., WALTHER, M., CHEW, E. Y., LIBUTTI, S. K., LINEHAN, W. M. & OLDFIELD, E. H. 2003. von Hippel-Lindau disease. *Lancet,* 361**,** 2059-67.

LOS, M., SCHENK, H., HEXEL, K., BAEUERLE, P. A., DROGE, W. & SCHULZE-OSTHOFF, K. 1995. IL-2 gene expression and NF-kappa B activation through CD28 requires reactive oxygen production by 5-lipoxygenase. *EMBO J,* 14**,** 3731-40.

LOW, S. C. & BERRY, M. J. 1996. Knowing when not to stop: selenocysteine incorporation in eukaryotes. *Trends Biochem Sci,* 21**,** 203-8.

LOW, S. C., HARNEY, J. W. & BERRY, M. J. 1995. Cloning and functional characterization of human selenophosphate synthetase, an essential component of selenoprotein synthesis. *J Biol Chem,* 270**,** 21659-64.

LU, Y. P., LOU, Y. R., YEN, P., NEWMARK, H. L., MIROCHNITCHENKO, O. I., INOUYE, M. & HUANG, M. T. 1997. Enhanced skin carcinogenesis in transgenic mice with high expression of glutathione peroxidase or both glutathione peroxidase and superoxide dismutase. *Cancer Res,* 57**,** 1468-74.

LUNT, S. Y. & VANDER HEIDEN, M. G. 2011. Aerobic glycolysis: meeting the metabolic requirements of cell proliferation. *Annu Rev Cell Dev Biol,* 27**,** 441-64.

MADDOCKS, O. D., BERKERS, C. R., MASON, S. M., ZHENG, L., BLYTH, K., GOTTLIEB, E. & VOUSDEN, K. H. 2013. Serine starvation induces stress and p53-dependent metabolic remodelling in cancer cells. *Nature,* 493**,** 542-6.

MAHON, P. C., HIROTA, K. & SEMENZA, G. L. 2001. FIH-1: a novel protein that interacts with HIF-1alpha and VHL to mediate repression of HIF-1 transcriptional activity. *Genes Dev,* 15**,** 2675-86.

MAIORINO, M., ROVERI, A., COASSIN, M. & URSINI, F. 1988. Kinetic mechanism and substrate specificity of glutathione peroxidase activity of ebselen (PZ51). *Biochem Pharmacol,* 37**,** 2267-71.

MANDRIOTA, S. J., TURNER, K. J., DAVIES, D. R., MURRAY, P. G., MORGAN, N. V., SOWTER, H. M., WYKOFF, C. C., MAHER, E. R., HARRIS, A. L., RATCLIFFE, P. J. & MAXWELL, P. H. 2002. HIF activation identifies early lesions in VHL kidneys: evidence for site-specific tumor suppressor function in the nephron. *Cancer Cell,* 1**,** 459-68.

MANGAL, D., VUDATHALA, D., PARK, J. H., LEE, S. H., PENNING, T. M. & BLAIR, I. A. 2009. Analysis of 7,8-dihydro-8-oxo-2'-deoxyguanosine in cellular DNA during oxidative stress. *Chem Res Toxicol,* 22**,** 788-97.

MARANCHIE, J. K., VASSELLI, J. R., RISS, J., BONIFACINO, J. S., LINEHAN, W. M. & KLAUSNER, R. D. 2002. The contribution of VHL substrate binding and HIF1-alpha to the phenotype of VHL loss in renal cell carcinoma. *Cancer Cell,* 1**,** 247-55.

MARINHO, H. S., ANTUNES, F. & PINTO, R. E. 1997. Role of glutathione peroxidase and phospholipid hydroperoxide glutathione peroxidase in the reduction of lysophospholipid hydroperoxides. *Free Radic Biol Med,* 22**,** 871-83.

MARTINEZ, P., BIRKBAK, N. J., GERLINGER, M., MCGRANAHAN, N., BURRELL, R. A., ROWAN, A. J., JOSHI, T., FISHER, R., LARKIN, J., SZALLASI, Z. & SWANTON, C. 2013. Parallel evolution of tumour subclones mimics diversity between tumours. *J Pathol,* 230**,** 356-64.

MAXWELL, P. H., WIESENER, M. S., CHANG, G. W., CLIFFORD, S. C., VAUX, E. C., COCKMAN, M. E., WYKOFF, C. C., PUGH, C. W., MAHER, E. R. & RATCLIFFE, P. J. 1999. The tumour suppressor protein VHL targets hypoxia-inducible factors for oxygen-dependent proteolysis. *Nature,* 399**,** 271-5.

MAYNARD, M. A., EVANS, A. J., HOSOMI, T., HARA, S., JEWETT, M. A. & OHH, M. 2005. Human HIF-3alpha4 is a dominant-negative regulator of HIF-1 and is down-regulated in renal cell carcinoma. *FASEB J,* 19**,** 1396-406.

MAYNARD, M. A. & OHH, M. 2004. Von Hippel-Lindau tumor suppressor protein and hypoxia-inducible factor in kidney cancer. *Am J Nephrol,* 24**,** 1-13.

MEDES, G., THOMAS, A. & WEINHOUSE, S. 1953. Metabolism of neoplastic tissue. IV. A study of lipid synthesis in neoplastic tissue slices in vitro. *Cancer Res,* 13**,** 27-9.

MENENDEZ, J. A. & LUPU, R. 2007. Fatty acid synthase and the lipogenic phenotype in cancer pathogenesis. *Nat Rev Cancer,* 7**,** 763-77.

METALLO, C. M., GAMEIRO, P. A., BELL, E. L., MATTAINI, K. R., YANG, J., HILLER, K., JEWELL, C. M., JOHNSON, Z. R., IRVINE, D. J., GUARENTE, L., KELLEHER, J. K., VANDER HEIDEN, M. G., ILIOPOULOS, O. & STEPHANOPOULOS, G. 2012. Reductive glutamine metabolism by IDH1 mediates lipogenesis under hypoxia. *Nature,* 481**,** 380-4.

MINCHENKO, O. H., OCHIAI, A., OPENTANOVA, I. L., OGURA, T., MINCHENKO, D. O., CARO, J., KOMISARENKO, S. V. & ESUMI, H. 2005. Overexpression of 6-phosphofructo-2-kinase/fructose-2,6-bisphosphatase-4 in the human breast and colon malignant tumors. *Biochimie,* 87**,** 1005-10.

MITSUISHI, Y., TAGUCHI, K., KAWATANI, Y., SHIBATA, T., NUKIWA, T., ABURATANI, H., YAMAMOTO, M. & MOTOHASHI, H. 2012. Nrf2 redirects glucose and glutamine into anabolic pathways in metabolic reprogramming. *Cancer Cell,* 22**,** 66-79.

MONTERO, A. J., EAPEN, S., GORIN, B. & ADLER, P. 2012. The economic burden of metastatic breast cancer: a U.S. managed care perspective. *Breast Cancer Res Treat,* 134**,** 815-22.

MORENO-SANCHEZ, R., RODRIGUEZ-ENRIQUEZ, S., MARIN-HERNANDEZ, A. & SAAVEDRA, E. 2007. Energy metabolism in tumor cells. *FEBS J,* 274**,** 1393-418.

MULLEN, A. R., WHEATON, W. W., JIN, E. S., CHEN, P. H., SULLIVAN, L. B., CHENG, T., YANG, Y., LINEHAN, W. M., CHANDEL, N. S. & DEBERARDINIS, R. J. 2012. Reductive carboxylation supports growth in tumour cells with defective mitochondria. *Nature,* 481**,** 385-8.

MULLER, M. 2002. Pyocyanin induces oxidative stress in human endothelial cells and modulates the glutathione redox cycle. *Free Radic Biol Med,* 33**,** 1527-33.

MYHRSTAD, M. C., CARLSEN, H., NORDSTROM, O., BLOMHOFF, R. & MOSKAUG, J. O. 2002. Flavonoids increase the intracellular glutathione level by transactivation of the gamma-glutamylcysteine synthetase catalytical subunit promoter. *Free Radic Biol Med,* 32**,** 386-93.

NEMOTO, S., TAKEDA, K., YU, Z. X., FERRANS, V. J. & FINKEL, T. 2000. Role for mitochondrial oxidants as regulators of cellular metabolism. *Mol Cell Biol,* 20**,** 7311-8.

NEUMANN, H. P. & BENDER, B. U. 1998. Genotype-phenotype correlations in von Hippel-Lindau disease. *J Intern Med,* 243**,** 541-5.

NEVE, J. 1995. Human selenium supplementation as assessed by changes in blood selenium concentration and glutathione peroxidase activity. *J Trace Elem Med Biol,* 9**,** 65-73.

NOGUEIRA, V., PARK, Y., CHEN, C. C., XU, P. Z., CHEN, M. L., TONIC, I., UNTERMAN, T. & HAY, N. 2008. Akt determines replicative senescence and oxidative or oncogenic premature senescence and sensitizes cells to oxidative apoptosis. *Cancer Cell,* 14**,** 458-70.

O'DWYER, P. J., HAMILTON, T. C., LACRETA, F. P., GALLO, J. M., KILPATRICK, D., HALBHERR, T., BRENNAN, J., BOOKMAN, M. A., HOFFMAN, J., YOUNG, R. C., COMIS, R. L. & OZOLS, R. F. 1996. Phase I trial of buthionine sulfoximine in combination with melphalan in patients with cancer. *J Clin Oncol,* 14**,** 249-56.

OKAR, D. A. & LANGE, A. J. 1999. Fructose-2,6-bisphosphate and control of carbohydrate metabolism in eukaryotes. *Biofactors,* 10**,** 1-14.

OKAR, D. A., MANZANO, A., NAVARRO-SABATE, A., RIERA, L., BARTRONS, R. & LANGE, A. J. 2001. PFK-2/FBPase-2: maker and breaker of the essential biofactor fructose-2,6-bisphosphate. *Trends Biochem Sci,* 26**,** 30-5.

PENG, S. Y., LAI, P. L., PAN, H. W., HSIAO, L. P. & HSU, H. C. 2008. Aberrant expression of the glycolytic enzymes aldolase B and type II hexokinase in hepatocellular carcinoma are predictive markers for advanced stage, early recurrence and poor prognosis. *Oncol Rep,* 19**,** 1045-53.

PETERSON, T. R., SENGUPTA, S. S., HARRIS, T. E., CARMACK, A. E., KANG, S. A., BALDERAS, E., GUERTIN, D. A., MADDEN, K. L., CARPENTER, A. E., FINCK, B. N. & SABATINI, D. M. 2011. mTOR complex 1 regulates lipin 1 localization to control the SREBP pathway. *Cell,* 146**,** 408-20.

PIETERS, R., HUNGER, S. P., BOOS, J., RIZZARI, C., SILVERMAN, L., BARUCHEL, A., GOEKBUGET, N., SCHRAPPE, M. & PUI, C. H. 2011. L-asparaginase treatment in acute lymphoblastic leukemia: a focus on Erwinia asparaginase. *Cancer,* 117**,** 238-49.

POLYAK, K., XIA, Y., ZWEIER, J. L., KINZLER, K. W. & VOGELSTEIN, B. 1997. A model for p53-induced apoptosis. *Nature,* 389**,** 300-5.

PORPORATO, P. E., DHUP, S., DADHICH, R. K., COPETTI, T. & SONVEAUX, P. 2011. Anticancer targets in the glycolytic metabolism of tumors: a comprehensive review. *Front Pharmacol,* 2**,** 49.

PORSTMANN, T., SANTOS, C. R., GRIFFITHS, B., CULLY, M., WU, M., LEEVERS, S., GRIFFITHS, J. R., CHUNG, Y. L. & SCHULZE, A. 2008. SREBP activity is regulated by mTORC1 and contributes to Akt-dependent cell growth. *Cell Metab,* 8**,** 224-36.

PREALL, J. B., HE, Z., GORRA, J. M. & SONTHEIMER, E. J. 2006. Short interfering RNA strand selection is independent of dsRNA processing polarity during RNAi in Drosophila. *Curr Biol,* 16**,** 530-5.

PRESTI, J. C., JR. & CARROLL, P. R. 1991. Bilateral spontaneous renal hemorrhage due to polyarteritis nodosa. *West J Med,* 155**,** 527-8.

PRESTI, J. C., JR., RAO, P. H., CHEN, Q., REUTER, V. E., LI, F. P., FAIR, W. R. & JHANWAR, S. C. 1991a. Histopathological, cytogenetic, and molecular characterization of renal cortical tumors. *Cancer Res,* 51**,** 1544-52.

PRESTI, J. C., JR., REUTER, V. E., GALAN, T., FAIR, W. R. & CORDON-CARDO, C. 1991b. Molecular genetic alterations in superficial and locally advanced human bladder cancer. *Cancer Res,* 51**,** 5405-9.

PRITCHETT, T. L., BADER, H. L., HENDERSON, J. & HSU, T. 2014. Conditional inactivation of the mouse von Hippel-Lindau tumor suppressor gene results in wide-spread hyperplastic, inflammatory and fibrotic lesions in the kidney. *Oncogene,* 0.

PURDUE, M. P., JOHANSSON, M., ZELENIKA, D., TORO, J. R., SCELO, G., MOORE, L. E., PROKHORTCHOUK, E., WU, X., KIEMENEY, L. A., GABORIEAU, V., JACOBS, K. B., CHOW, W. H., ZARIDZE, D., MATVEEV, V., LUBINSKI, J., TRUBICKA, J., SZESZENIA-DABROWSKA, N., LISSOWSKA, J., RUDNAI, P., FABIANOVA, E., BUCUR, A., BENCKO, V., FORETOVA, L., JANOUT, V., BOFFETTA, P., COLT, J. S., DAVIS, F. G., SCHWARTZ, K. L., BANKS, R. E., SELBY, P. J., HARNDEN, P., BERG, C. D., HSING, A. W., GRUBB, R. L., 3RD, BOEING, H., VINEIS, P., CLAVEL-CHAPELON, F., PALLI, D., TUMINO, R., KROGH, V., PANICO, S., DUELL, E. J., QUIROS, J. R., SANCHEZ, M. J., NAVARRO, C., ARDANAZ, E., DORRONSORO, M., KHAW, K. T., ALLEN, N. E., BUENO-DE-MESQUITA, H. B., PEETERS, P. H., TRICHOPOULOS, D., LINSEISEN, J., LJUNGBERG, B., OVERVAD, K., TJONNELAND, A., ROMIEU, I., RIBOLI, E., MUKERIA, A., SHANGINA, O., STEVENS, V. L., THUN, M. J., DIVER, W. R., GAPSTUR, S. M., PHAROAH, P. D., EASTON, D. F., ALBANES, D., WEINSTEIN, S. J., VIRTAMO, J., VATTEN, L., HVEEM, K., NJOLSTAD, I., TELL, G. S., STOLTENBERG, C., KUMAR, R., KOPPOVA, K., CUSSENOT, O., BENHAMOU, S., OOSTERWIJK, E., VERMEULEN, S. H., ABEN, K. K., VAN DER MAREL, S. L., YE, Y., WOOD, C. G., PU, X., MAZUR, A. M., BOULYGINA, E. S., CHEKANOV, N. N., FOGLIO, M., LECHNER, D., GUT, I., HEATH, S., BLANCHE, H., HUTCHINSON, A., THOMAS, G., WANG, Z., YEAGER, M., FRAUMENI, J. F., JR., SKRYABIN, K. G., MCKAY, J. D., et al. 2011. Genome-wide association

study of renal cell carcinoma identifies two susceptibility loci on 2p21 and 11q13.3. *Nat Genet,* 43**,** 60-5.

QIAO, Y. L., DAWSEY, S. M., KAMANGAR, F., FAN, J. H., ABNET, C. C., SUN, X. D., JOHNSON, L. L., GAIL, M. H., DONG, Z. W., YU, B., MARK, S. D. & TAYLOR, P. R. 2009. Total and cancer mortality after supplementation with vitamins and minerals: follow-up of the Linxian General Population Nutrition Intervention Trial. *J Natl Cancer Inst,* 101**,** 507-18.

RAN, H., HASSETT, D. J. & LAU, G. W. 2003. Human targets of Pseudomonas aeruginosa pyocyanin. *Proc Natl Acad Sci U S A,* 100**,** 14315-20.

RANKIN, E. B., TOMASZEWSKI, J. E. & HAASE, V. H. 2006. Renal cyst development in mice with conditional inactivation of the von Hippel-Lindau tumor suppressor. *Cancer Res,* 66**,** 2576-83.

RATNASINGHE, D., TANGREA, J. A., ANDERSEN, M. R., BARRETT, M. J., VIRTAMO, J., TAYLOR, P. R. & ALBANES, D. 2000. Glutathione peroxidase codon 198 polymorphism variant increases lung cancer risk. *Cancer Res,* 60**,** 6381-3.

RAVAL, R. R., LAU, K. W., TRAN, M. G., SOWTER, H. M., MANDRIOTA, S. J., LI, J. L., PUGH, C. W., MAXWELL, P. H., HARRIS, A. L. & RATCLIFFE, P. J. 2005. Contrasting properties of hypoxia-inducible factor 1 (HIF-1) and HIF-2 in von Hippel-Lindau-associated renal cell carcinoma. *Mol Cell Biol,* 25**,** 5675-86.

RIVERA, A. & MAXWELL, S. A. 2005. The p53-induced gene-6 (proline oxidase) mediates apoptosis through a calcineurin-dependent pathway. *J Biol Chem,* 280**,** 29346-54.

ROS, S., SANTOS, C. R., MOCO, S., BAENKE, F., KELLY, G., HOWELL, M., ZAMBONI, N. & SCHULZE, A. 2012. Functional metabolic screen identifies 6-phosphofructo-2-kinase/fructose-2,6-biphosphatase 4 as an important regulator of prostate cancer cell survival. *Cancer Discov,* 2**,** 328-43.

SANTOS, C. R. & SCHULZE, A. 2012. Lipid metabolism in cancer. *FEBS J,* 279**,** 2610-23.

SANTOS, C. X., TANAKA, L. Y., WOSNIAK, J. & LAURINDO, F. R. 2009. Mechanisms and implications of reactive oxygen species generation during the unfolded protein response: roles of endoplasmic reticulum oxidoreductases, mitochondrial electron transport, and NADPH oxidase. *Antioxid Redox Signal,* 11**,** 2409-27.

SASAKI, H., SATO, H., KURIYAMA-MATSUMURA, K., SATO, K., MAEBARA, K., WANG, H., TAMBA, M., ITOH, K., YAMAMOTO, M. & BANNAI, S. 2002. Electrophile response element-mediated induction of the cystine/glutamate exchange transporter gene expression. *J Biol Chem,* 277**,** 44765-71.

SATO, Y., YOSHIZATO, T., SHIRAISHI, Y., MAEKAWA, S., OKUNO, Y., KAMURA, T., SHIMAMURA, T., SATO-OTSUBO, A., NAGAE, G., SUZUKI, H., NAGATA, Y., YOSHIDA, K., KON, A., SUZUKI, Y., CHIBA, K., TANAKA, H., NIIDA, A., FUJIMOTO, A., TSUNODA, T., MORIKAWA, T., MAEDA, D., KUME, H., SUGANO, S., FUKAYAMA, M., ABURATANI, H., SANADA, M., MIYANO, S., HOMMA, Y. & OGAWA, S. 2013. Integrated molecular analysis of clear-cell renal cell carcinoma. *Nat Genet,* 45**,** 860-7.

SCARPULLA, R. C. 2011. Metabolic control of mitochondrial biogenesis through the PGC-1 family regulatory network. *Biochim Biophys Acta,* 1813**,** 1269-78.

SCHODEL, J., OIKONOMOPOULOS, S., RAGOUSSIS, J., PUGH, C. W., RATCLIFFE, P. J. & MOLE, D. R. 2011. High-resolution genome-wide mapping of HIF-binding sites by ChIP-seq. *Blood,* 117**,** e207-17.

SCHOFIELD, C. J. & RATCLIFFE, P. J. 2004. Oxygen sensing by HIF hydroxylases. *Nat Rev Mol Cell Biol,* 5**,** 343-54.

SCHULZE, A. & HARRIS, A. L. 2012. How cancer metabolism is tuned for proliferation and vulnerable to disruption. *Nature,* 491**,** 364-73.

SEILER, A., SCHNEIDER, M., FORSTER, H., ROTH, S., WIRTH, E. K., CULMSEE, C., PLESNILA, N., KREMMER, E., RADMARK, O., WURST, W., BORNKAMM, G. W., SCHWEIZER, U. & CONRAD, M. 2008. Glutathione peroxidase 4 senses and translates oxidative stress into 12/15-lipoxygenase dependent- and AIF-mediated cell death. *Cell Metab,* 8**,** 237-48.

SELAK, M. A., ARMOUR, S. M., MACKENZIE, E. D., BOULAHBEL, H., WATSON, D. G., MANSFIELD, K. D., PAN, Y., SIMON, M. C., THOMPSON, C. B. & GOTTLIEB, E. 2005. Succinate links TCA cycle dysfunction to oncogenesis by inhibiting HIF-alpha prolyl hydroxylase. *Cancer Cell,* 7**,** 77-85.

SEMENZA, G. L. 1999a. Perspectives on oxygen sensing. *Cell,* 98**,** 281-4.

SEMENZA, G. L. 1999b. Regulation of mammalian O2 homeostasis by hypoxia-inducible factor 1. *Annu Rev Cell Dev Biol,* 15**,** 551-78.

SEMENZA, G. L. 2003. Targeting HIF-1 for cancer therapy. *Nat Rev Cancer,* 3**,** 721-32.

SEMENZA, G. L. 2011. Oxygen sensing, homeostasis, and disease. *N Engl J Med,* 365**,** 537-47.
SHAO, X., SOMLO, S. & IGARASHI, P. 2002. Epithelial-specific Cre/lox recombination in the developing kidney and genitourinary tract. *J Am Soc Nephrol,* 13**,** 1837-46.
SHEN, C., BEROUKHIM, R., SCHUMACHER, S. E., ZHOU, J., CHANG, M., SIGNORETTI, S. & KAELIN, W. G., JR. 2011. Genetic and functional studies implicate HIF1alpha as a 14q kidney cancer suppressor gene. *Cancer Discov,* 1**,** 222-35.
SHI, M., YANG, H., MOTLEY, E. D. & GUO, Z. 2004. Overexpression of Cu/Zn-superoxide dismutase and/or catalase in mice inhibits aorta smooth muscle cell proliferation. *Am J Hypertens,* 17**,** 450-6.
SHI, Z. Z., OSEI-FRIMPONG, J., KALA, G., KALA, S. V., BARRIOS, R. J., HABIB, G. M., LUKIN, D. J., DANNEY, C. M., MATZUK, M. M. & LIEBERMAN, M. W. 2000. Glutathione synthesis is essential for mouse development but not for cell growth in culture. *Proc Natl Acad Sci U S A,* 97**,** 5101-6.
SINGER, E. A., GUPTA, G. N., MARCHALIK, D. & SRINIVASAN, R. 2013. Evolving therapeutic targets in renal cell carcinoma. *Curr Opin Oncol,* 25**,** 273-80.
SOM, P., ATKINS, H. L., BANDOYPADHYAY, D., FOWLER, J. S., MACGREGOR, R. R., MATSUI, K., OSTER, Z. H., SACKER, D. F., SHIUE, C. Y., TURNER, H., WAN, C. N., WOLF, A. P. & ZABINSKI, S. V. 1980. A fluorinated glucose analog, 2-fluoro-2-deoxy-D-glucose (F-18): nontoxic tracer for rapid tumor detection. *J Nucl Med,* 21**,** 670-5.
SUBBARAMAIAH, K., ALTORKI, N., CHUNG, W. J., MESTRE, J. R., SAMPAT, A. & DANNENBERG, A. J. 1999. Inhibition of cyclooxygenase-2 gene expression by p53. *J Biol Chem,* 274**,** 10911-5.
SUNDE, R. A., RAINES, A. M., BARNES, K. M. & EVENSON, J. K. 2009. Selenium status highly regulates selenoprotein mRNA levels for only a subset of the selenoproteins in the selenoproteome. *Biosci Rep,* 29**,** 329-38.
SUZUKI, K., KOIKE, H., MATSUI, H., ONO, Y., HASUMI, M., NAKAZATO, H., OKUGI, H., SEKINE, Y., OKI, K., ITO, K., YAMAMOTO, T., FUKABORI, Y., KUROKAWA, K. & YAMANAKA, H. 2002. Genistein, a soy isoflavone, induces glutathione peroxidase in the human prostate cancer cell lines LNCaP and PC-3. *Int J Cancer,* 99**,** 846-52.
SUZUKI, S., TANAKA, T., POYUROVSKY, M. V., NAGANO, H., MAYAMA, T., OHKUBO, S., LOKSHIN, M., HOSOKAWA, H., NAKAYAMA, T., SUZUKI, Y., SUGANO, S., SATO, E., NAGAO, T., YOKOTE, K., TATSUNO, I. & PRIVES, C. 2010. Phosphate-activated glutaminase (GLS2), a p53-inducible regulator of glutamine metabolism and reactive oxygen species. *Proc Natl Acad Sci U S A,* 107**,** 7461-6.
TAGUCHI, K., MOTOHASHI, H. & YAMAMOTO, M. 2011. Molecular mechanisms of the Keap1-Nrf2 pathway in stress response and cancer evolution. *Genes Cells,* 16**,** 123-40.
TAN, M., HEIZMANN, C. W., GUAN, K., SCHAFER, B. W. & SUN, Y. 1999. Transcriptional activation of the human S100A2 promoter by wild-type p53. *FEBS Lett,* 445**,** 265-8.
TANG, S. W., CHANG, W. H., SU, Y. C., CHEN, Y. C., LAI, Y. H., WU, P. T., HSU, C. I., LIN, W. C., LAI, M. K. & LIN, J. Y. 2009. MYC pathway is activated in clear cell renal cell carcinoma and essential for proliferation of clear cell renal cell carcinoma cells. *Cancer Lett,* 273**,** 35-43.
THAKER, N. G., MCDONALD, P. R., ZHANG, F., KITCHENS, C. A., SHUN, T. Y., POLLACK, I. F. & LAZO, J. S. 2010. Designing, optimizing, and implementing high-throughput siRNA genomic screening with glioma cells for the discovery of survival genes and novel drug targets. *J Neurosci Methods,* 185**,** 204-12.
THOMPSON, C. B., BAUER, D. E., LUM, J. J., HATZIVASSILIOU, G., ZONG, W. X., ZHAO, F., DITSWORTH, D., BUZZAI, M. & LINDSTEN, T. 2005. How do cancer cells acquire the fuel needed to support cell growth? *Cold Spring Harb Symp Quant Biol,* 70**,** 357-62.
TONG, W. H., SOURBIER, C., KOVTUNOVYCH, G., JEONG, S. Y., VIRA, M., GHOSH, M., ROMERO, V. V., SOUGRAT, R., VAULONT, S., VIOLLET, B., KIM, Y. S., LEE, S., TREPEL, J., SRINIVASAN, R., BRATSLAVSKY, G., YANG, Y., LINEHAN, W. M. & ROUAULT, T. A. 2011. The glycolytic shift in fumarate-hydratase-deficient kidney cancer lowers AMPK levels, increases anabolic propensities and lowers cellular iron levels. *Cancer Cell,* 20**,** 315-27.
TONKS, N. K. 2005. Redox redux: revisiting PTPs and the control of cell signaling. *Cell,* 121**,** 667-70.
TOPPO, S., FLOHE, L., URSINI, F., VANIN, S. & MAIORINO, M. 2009. Catalytic mechanisms and specificities of glutathione peroxidases: variations of a basic scheme. *Biochim Biophys Acta,* 1790**,** 1486-500.
TRINEI, M., GIORGIO, M., CICALESE, A., BAROZZI, S., VENTURA, A., MIGLIACCIO, E., MILIA, E., PADURA, I. M., RAKER, V. A., MACCARANA, M., PETRONILLI, V., MINUCCI, S.,

BERNARDI, P., LANFRANCONE, L. & PELICCI, P. G. 2002. A p53-p66Shc signalling pathway controls intracellular redox status, levels of oxidation-damaged DNA and oxidative stress-induced apoptosis. *Oncogene,* 21**,** 3872-8.

TUJEBAJEVA, R. M., COPELAND, P. R., XU, X. M., CARLSON, B. A., HARNEY, J. W., DRISCOLL, D. M., HATFIELD, D. L. & BERRY, M. J. 2000. Decoding apparatus for eukaryotic selenocysteine insertion. *EMBO Rep,* 1**,** 158-63.

VALAVANIDIS, A., VLACHOGIANNI, T. & FIOTAKIS, C. 2009. 8-hydroxy-2' -deoxyguanosine (8-OHdG): A critical biomarker of oxidative stress and carcinogenesis. *J Environ Sci Health C Environ Carcinog Ecotoxicol Rev,* 27**,** 120-39.

VAN DER HORST, A. & BURGERING, B. M. 2007. Stressing the role of FoxO proteins in lifespan and disease. *Nat Rev Mol Cell Biol,* 8**,** 440-50.

VANDER HEIDEN, M. G., CANTLEY, L. C. & THOMPSON, C. B. 2009. Understanding the Warburg effect: the metabolic requirements of cell proliferation. *Science,* 324**,** 1029-33.

VANDER HEIDEN, M. G., LUNT, S. Y., DAYTON, T. L., FISKE, B. P., ISRAELSEN, W. J., MATTAINI, K. R., VOKES, N. I., STEPHANOPOULOS, G., CANTLEY, L. C., METALLO, C. M. & LOCASALE, J. W. 2011. Metabolic pathway alterations that support cell proliferation. *Cold Spring Harb Symp Quant Biol,* 76**,** 325-34.

VARELA, I., TARPEY, P., RAINE, K., HUANG, D., ONG, C. K., STEPHENS, P., DAVIES, H., JONES, D., LIN, M. L., TEAGUE, J., BIGNELL, G., BUTLER, A., CHO, J., DALGLIESH, G. L., GALAPPATHTHIGE, D., GREENMAN, C., HARDY, C., JIA, M., LATIMER, C., LAU, K. W., MARSHALL, J., MCLAREN, S., MENZIES, A., MUDIE, L., STEBBINGS, L., LARGAESPADA, D. A., WESSELS, L. F., RICHARD, S., KAHNOSKI, R. J., ANEMA, J., TUVESON, D. A., PEREZ-MANCERA, P. A., MUSTONEN, V., FISCHER, A., ADAMS, D. J., RUST, A., CHAN-ON, W., SUBIMERB, C., DYKEMA, K., FURGE, K., CAMPBELL, P. J., TEH, B. T., STRATTON, M. R. & FUTREAL, P. A. 2011. Exome sequencing identifies frequent mutation of the SWI/SNF complex gene PBRM1 in renal carcinoma. *Nature,* 469**,** 539-42.

VEAL, E. A., DAY, A. M. & MORGAN, B. A. 2007. Hydrogen peroxide sensing and signaling. *Mol Cell,* 26**,** 1-14.

VERMEULEN, A., BEHLEN, L., REYNOLDS, A., WOLFSON, A., MARSHALL, W. S., KARPILOW, J. & KHVOROVA, A. 2005. The contributions of dsRNA structure to Dicer specificity and efficiency. *RNA,* 11**,** 674-82.

VICHAI, V. & KIRTIKARA, K. 2006. Sulforhodamine B colorimetric assay for cytotoxicity screening. *Nat Protoc,* 1**,** 1112-6.

WANG, J. B., ERICKSON, J. W., FUJI, R., RAMACHANDRAN, S., GAO, P., DINAVAHI, R., WILSON, K. F., AMBROSIO, A. L., DIAS, S. M., DANG, C. V. & CERIONE, R. A. 2010. Targeting mitochondrial glutaminase activity inhibits oncogenic transformation. *Cancer Cell,* 18**,** 207-19.

WARBURG, O. 1956a. On respiratory impairment in cancer cells. *Science,* 124**,** 269-70.

WARBURG, O. 1956b. On the origin of cancer cells. *Science,* 123**,** 309-14.

WILCOX, C. S. & PEARLMAN, A. 2008. Chemistry and antihypertensive effects of tempol and other nitroxides. *Pharmacol Rev,* 60**,** 418-69.

WINGLER, K., BOCHER, M., FLOHE, L., KOLLMUS, H. & BRIGELIUS-FLOHE, R. 1999. mRNA stability and selenocysteine insertion sequence efficiency rank gastrointestinal glutathione peroxidase high in the hierarchy of selenoproteins. *Eur J Biochem,* 259**,** 149-57.

WISE, D. R., DEBERARDINIS, R. J., MANCUSO, A., SAYED, N., ZHANG, X. Y., PFEIFFER, H. K., NISSIM, I., DAIKHIN, E., YUDKOFF, M., MCMAHON, S. B. & THOMPSON, C. B. 2008. Myc regulates a transcriptional program that stimulates mitochondrial glutaminolysis and leads to glutamine addiction. *Proc Natl Acad Sci U S A,* 105**,** 18782-7.

WOLF, A., AGNIHOTRI, S., MICALLEF, J., MUKHERJEE, J., SABHA, N., CAIRNS, R., HAWKINS, C. & GUHA, A. 2011. Hexokinase 2 is a key mediator of aerobic glycolysis and promotes tumor growth in human glioblastoma multiforme. *J Exp Med,* 208**,** 313-26.

WOOLLEY, J. F., STANICKA, J. & COTTER, T. G. 2013. Recent advances in reactive oxygen species measurement in biological systems. *Trends Biochem Sci,* 38**,** 556-65.

XIA, X., LEMIEUX, M. E., LI, W., CARROLL, J. S., BROWN, M., LIU, X. S. & KUNG, A. L. 2009. Integrative analysis of HIF binding and transactivation reveals its role in maintaining histone methylation homeostasis. *Proc Natl Acad Sci U S A,* 106**,** 4260-5.

XU, D., ROVIRA, II & FINKEL, T. 2002. Oxidants painting the cysteine chapel: redox regulation of PTPs. *Dev Cell,* 2**,** 251-2.

YAHAGI, N., SHIMANO, H., HASEGAWA, K., OHASHI, K., MATSUZAKA, T., NAJIMA, Y., SEKIYA, M., TOMITA, S., OKAZAKI, H., TAMURA, Y., IIZUKA, Y., OHASHI, K., NAGAI, R., ISHIBASHI, S., KADOWAKI, T., MAKUUCHI, M., OHNISHI, S., OSUGA, J. & YAMADA, N. 2005. Co-ordinate activation of lipogenic enzymes in hepatocellular carcinoma. *Eur J Cancer,* 41**,** 1316-22.

YAMAMOTO, T., SEINO, Y., FUKUMOTO, H., KOH, G., YANO, H., INAGAKI, N., YAMADA, Y., INOUE, K., MANABE, T. & IMURA, H. 1990. Over-expression of facilitative glucose transporter genes in human cancer. *Biochem Biophys Res Commun,* 170**,** 223-30.

YANT, L. J., RAN, Q., RAO, L., VAN REMMEN, H., SHIBATANI, T., BELTER, J. G., MOTTA, L., RICHARDSON, A. & PROLLA, T. A. 2003. The selenoprotein GPX4 is essential for mouse development and protects from radiation and oxidative damage insults. *Free Radic Biol Med,* 34**,** 496-502.

YECIES, J. L. & MANNING, B. D. 2011. mTOR links oncogenic signaling to tumor cell metabolism. *J Mol Med (Berl),* 89**,** 221-8.

YOON, K. A., NAKAMURA, Y. & ARAKAWA, H. 2004. Identification of ALDH4 as a p53-inducible gene and its protective role in cellular stresses. *J Hum Genet,* 49**,** 134-40.

YOON, S., LEE, M. Y., PARK, S. W., MOON, J. S., KOH, Y. K., AHN, Y. H., PARK, B. W. & KIM, K. S. 2007. Up-regulation of acetyl-CoA carboxylase alpha and fatty acid synthase by human epidermal growth factor receptor 2 at the translational level in breast cancer cells. *J Biol Chem,* 282**,** 26122-31.

YUNEVA, M., ZAMBONI, N., OEFNER, P., SACHIDANANDAM, R. & LAZEBNIK, Y. 2007. Deficiency in glutamine but not glucose induces MYC-dependent apoptosis in human cells. *J Cell Biol,* 178**,** 93-105.

ZAVACKI, A. M., MANSELL, J. B., CHUNG, M., KLIMOVITSKY, B., HARNEY, J. W. & BERRY, M. J. 2003. Coupled tRNA(Sec)-dependent assembly of the selenocysteine decoding apparatus. *Mol Cell,* 11**,** 773-81.

ZBAR, B., BRAUCH, H., TALMADGE, C. & LINEHAN, M. 1987. Loss of alleles of loci on the short arm of chromosome 3 in renal cell carcinoma. *Nature,* 327**,** 721-4.

ZHANG, H., GAO, P., FUKUDA, R., KUMAR, G., KRISHNAMACHARY, B., ZELLER, K. I., DANG, C. V. & SEMENZA, G. L. 2007. HIF-1 inhibits mitochondrial biogenesis and cellular respiration in VHL-deficient renal cell carcinoma by repression of C-MYC activity. *Cancer Cell,* 11**,** 407-20.

ZHANG, W., TRACHOOTHAM, D., LIU, J., CHEN, G., PELICANO, H., GARCIA-PRIETO, C., LU, W., BURGER, J. A., CROCE, C. M., PLUNKETT, W., KEATING, M. J. & HUANG, P. 2012. Stromal control of cystine metabolism promotes cancer cell survival in chronic lymphocytic leukaemia. *Nat Cell Biol,* 14**,** 276-86.

ZHOU, L. Z., JOHNSON, A. P. & RANDO, T. A. 2001. NF kappa B and AP-1 mediate transcriptional responses to oxidative stress in skeletal muscle cells. *Free Radic Biol Med,* 31**,** 1405-16.

ZIMMER, M., DOUCETTE, D., SIDDIQUI, N. & ILIOPOULOS, O. 2004. Inhibition of hypoxia-inducible factor is sufficient for growth suppression of VHL-/- tumors. *Mol Cancer Res,* 2**,** 89-95.

Appendix

Table 7.1: siRNA oligonucleotides used in customised Dharmacon siRNA library

Gene Symbol	Gene ID	Plate	Well	Pool Number	Duplex Number	Sequence
HK1	3098	1	A03	MU-006820-01	D-006820-01	GGAAGGAGAUGAAGAAUGG
					D-006820-03	GAAGUUACCUGUGGGAUUC
					D-006820-04	GCACAACAAUGCCGUGGUU
					D-006820-05	GACCGAGAAUGGUGACUUC
HK2	3099	1	A04	MU-006735-01	D-006735-05	GCGGAUGUGUAUCAAUAUG
					D-006735-02	GAAGUUGGCCUCAUUGUUG
					D-006735-03	GCAGAAGGUUGACCAGUAU
					D-006735-04	CAAGCUACAUCCUCACUUU
GCK	2645	1	A05	MU-010819-01	D-010819-05	CCACGAUGAUCUCCUGCUA
					D-010819-01	GCAAGCAGAUCUACAACAU
					D-010819-02	GCUCAUAGGUGGCAAGUAC
					D-010819-04	GCACGAAGACAUCGAUAAG
PKLR	5313	1	A06	MU-006780-01	D-006780-01	GUGAAGAGGUUUGAUGAAA
					D-006780-02	GGGCAAGCCUGUUGUCUGU
					D-006780-03	GUGGAGAGCUUUGCAGGUU
					D-006780-04	GAAGGACACGGCAUCAAGA
PKM2	5315	1	A07	MU-006781-02	D-006781-05	GCAUUGAGAUUCCUGCAGA
					D-006781-01	GAAAGAACAUCAAGAUUAU
					D-006781-02	UUAGGAAGGUCCUGGGAGA
					D-006781-03	GCAAGAAGGGUGUGAACCU
PC	5091	1	A08	MU-008950-02	D-008950-01	GAAAGCAGAUGAAGCCUAU
					D-008950-03	GAGCUGAUGUGGUGGAUGU
					D-008950-18	GGAUAAUGCUUCCGCCUUC
					D-008950-19	UCUCUGAGCGAGCGGACUU
PDHA1	5160	1	A09	MU-010329-02	D-010329-02	GCUCUAGCCUGUAAGUAUA
					D-010329-04	GCUCACGGCUUUACUUUCA
					D-010329-05	AAGCAGAUCAGCUGUAUAA
					D-010329-06	AAUAAUCGCUAUGGAAUGG
PDHA2	5161	1	A10	MU-023925-01	D-023925-01	UAAGAGGGAUCCUAUAAUA
					D-023925-02	GAUGAGAUCUGUUUGACUU
					D-023925-03	GCAGAUAGCCGAAGCUUUC
					D-023925-04	GCUCAUGGUGUGUGCUAUA
PDHB	5162	1	A11	MU-008803-01	D-008803-01	CAAAUCAUCUUGUAACUGU
					D-008803-02	GGUCAAAGACAUCAUAUUU
					D-008803-03	GAAAGGCAAGGAACACAUA
					D-008803-04	GAGAAUGAAUUGAUGUAUG
DLD	1738	1	A12	MU-009509-01	D-009509-04	GUACAAAGUUGGGAAAUUC
					D-009509-01	GAAGUUCGCUUGAAUUUAG
					D-009509-02	UAUUAAAGCUGCCCAGUUA
					D-009509-03	CAAUGGAUAUGGAAAGAUA
DLAT	1737	1	B03	MU-008490-00	D-008490-01	GCACAGCGAUUAAUGCAAU
					D-008490-02	CAACCGAAGUAACAGAUUU
					D-008490-03	GGAUUGAUCUUACACAAGU
					D-008490-04	GUACGGAAAGAACUUAAUA
ACACA	31	1	B04	MU-004551-02	D-004551-01	GAAAGCAGGUCAACUAUGA
					D-004551-03	CAGCAAACCUGGAUUCUGA
					D-004551-04	GCAGAUGACUUCCCUAAUC
					D-004551-09	GCAAUUAGAUUCGUUGUCA
LDHA	3939	1	B05	MU-008201-01	D-008201-01	GGAGAAAGCCGUCUUAAUU
					D-008201-02	GGCAAAGACUAUAAUGUAA
					D-008201-03	GAAGAGGCCCGUUUGAAGA
					D-008201-04	CUACGUGGCUUGGAAGAUA
LDHB	3945	1	B06	MU-009779-01	D-009779-01	GAAAGUCUCUGGCUGAUGA
					D-009779-02	GGAAGGAAGUGCAUAAGAU
					D-009779-03	GAACUGACAAUGAUAGUGA
					D-009779-04	CAUGGGAGCUUAUUUCUUC
LDHC	3948	1	B07	MU-008759-02	D-008759-01	GGAUUUGGCUGAUGAACUU
					D-008759-03	GUUAAGGGAUUAUAUGGAA
					D-008759-04	GGAAUGGUGUCUCAGAUGU
					D-008759-05	CGUAAUGUGGCUAUAAUGA
CS	1431	1	B08	MU-009334-01	D-009334-01	GCAAAGAUCUACCGAAAUC
					D-009334-03	GGACUGGUCUCACAAUUUC
					D-009334-04	GCAAAGCUACCUUGUGUUG
					D-009334-17	GGAAGACUGAUCCGCGAUA

Gene Symbol	Gene ID	Plate	Well	Pool Number	Duplex Number	Sequence
ACLY	47	1	B09	MU--004915-00	D-004915-01	CCAACGAGCUCAACAAUAU
					D-004915-02	GACCAAAGAUGGAGUCUAU
					D-004915-03	UCAACGAGCUGGCAAACUA
					D-004915-04	CCACUCCUCUGCUCGAUUA
G6PD	2539	1	B10	MU-008181-02	D-008181-05	UGACCUACGGCAACAGAUA
					D-008181-01	GAGAGUGGGUUUCCAGUAU
					D-008181-02	CAACAUCGCCUGCGUUAUC
					D-008181-03	CGUGAGGCCUGGCGUAUUU
FASN	2194	1	B11	MU-003954-04	D-003954-01	GAGCGUAUCUGUGAGAAAC
					D-003954-03	UGACAUCGUCCAUUCGUUU
					D-003954-04	CCAUGGAGCGUAUCUGUGA
					D-003954-08	GCAACUCACGCUCCGGAAA
CHKA	1119	1	B12	MU-006704-01	D-006704-01	GAAUUAAGUUUGCCAGAUA
					D-006704-02	CAGAUGAGGUCCUGUAAUA
					D-006704-03	GAGCAAACAUCCGGAAGUA
					D-006704-04	GAAUACAGCAGUUACAAUU
CHKB	1120	1	C03	MU-006705-00	D-006705-01	GGAAUGGCCUUUCUACAAA
					D-006705-02	GUGAGUGGGUUUAUGAUUA
					D-006705-03	CCACGAAGAUGGCGCAAUU
					D-006705-04	CAUAGAAUUUGGUUACUUG
HMGCS1	3157	1	C04	MU-009808-01	D-009808-01	GAAGACACCUACUUUGAUA
					D-009808-04	GAUAUUAACUCUCUUUGCA
					D-009808-17	GCCAAAUGUACUCGAAUGA
					D-009808-18	CAGAGACAAUCAUCGACAA
HMGCS2	3158	1	C05	MU-010179-01	D-010179-01	AAACUGACCUGGAGAAGUA
					D-010179-02	ACACAAACCAGCUUAUAUA
					D-010179-03	AGAGAGCAAUUCUACCAUA
					D-010179-04	GGGCAUAGAUACCACCAAU
HMGCR	3156	1	C06	MU-009811-02	D-009811-03	UGAAGAAUGUCUACAGAUA
					D-009811-04	CCAGAAAUGUGAUUCAGUA
					D-009811-06	GAGCAGUGACAUUAUAAUU
					D-009811-19	GAUGGAAACUCAUGAGCGU
SLC2A4	6517	1	C07	MU-007517-02	D-007517-01	CAGAUAGGCUCCGAAGAUG
					D-007517-02	GCAUGGGUUUCCAGUAUGU
					D-007517-03	UCAACCAACUGGCCAUUGU
					D-007517-05	ACAGAUAGGCUCCGAAGAU
SLC2A1	6513	1	C08	MU-007509-01	D-007509-02	CCAAGAGUGUGCUAAAGAA
					D-007509-03	CAUCGUGGCUGAACUCUUC
					D-007509-04	GAGCAUCGUGGCCAUCUUU
					D-007509-05	GUAUGUGGGUGAAGUGUCA
SREBF1	6720	1	C09	MU-006891-01	D-006891-01	UGACUUCCCUGGCCUAUUU
					D-006891-02	ACAUUGAGCUCCUCUCUUG
					D-006891-03	GCGCACUGCUGUCCACAAA
					D-006891-04	ACACAGACGUGCUCAUGGA
SREBF2	6721	1	C10	MU-009549-00	D-009549-01	GAGCGGAGCUGGUCUGUGA
					D-009549-02	GAAGAGAGCUGUGAAUUCU
					D-009549-03	GCACAAGUCUGGCGUUCUG
					D-009549-04	AAACUCAGCUGCAACAACA
PRKAA1	5562	1	C11	MU-005027-02	D-005027-01	CAAAGUCGACCAAAUGAUA
					D-005027-02	GUAGAGCAAUCAAACAAUU
					D-005027-03	GACAAGCACUUACUCCAAA
					D-005027-05	ACAAUUGGAUUAUGAAUGG
PRKAA2	5563	1	C12	MU-005361-02	D-005361-02	GUACCUACGUUAUUUAAGA
					D-005361-03	GGAAGGUAGUGAAUGCAUA
					D-005361-04	GACAGAAGAUUCGCAGUUU
					D-005361-05	ACAGAAGAUUCGCAGUUUA
HIF1A	3091	1	D03	MU-004018-05	D-004018-01	GGACACAGAUUUAGACUUG
					D-004018-06	UCACCAAAGUUGAAUCAGA
					D-004018-03	GAUGGAAGCACUAGACAAA
					D-004018-05	CGUGUUAUCUGUCGCUUUG
AKT2	208	1	D05	MU-003001-02	D-003001-05	GUACUUCGAUGAUGAAUUU
					D-003001-06	GCAAAGAGGGCAUCAGUGA
					D-003001-07	GGGCUAAAGUGACCAUGAA
					D-003001-08	GCAGAAUGCCAGCUGAUGA
AKT3	10000	1	D06	MU-003002-02	D-003002-09	GAAAGAUUGUGUACCGUGA
					D-003002-10	GGACUACUGUUAUAGAGAG
					D-003002-11	UGAGACAGAUACUAGAUAU
					D-003002-12	GCUCAUUCAUAGGAUAUAA

Gene Symbol	Gene ID	Plate	Well	Pool Number	Duplex Number	Sequence
ILVBL	10994	1	D07	MU-009658-02	D-009658-03	UGACUGCGGUGAAGAAUGC
					D-009658-20	CCUGGUAUUUAGAGAAUUA
					D-009658-21	CGUCAAUCGUAAUCGGGAA
					D-009658-22	GCUACAGCCUCAUCGAAUU
PHGDH	26227	1	D08	MU-009518-01	D-009518-01	GAACAUCCCUGAAGAAUGC
					D-009518-02	GAACUCACUUGUGGAAUGA
					D-009518-03	GGAAAGACCCUGGGAAUUC
					D-009518-04	GGAAGGGCAUCUUGGUUAU
MDH1	4190	1	D09	MU-009264-00	D-009264-01	CAAAGGAACUGACAGAAGA
					D-009264-02	CAUCAAGGCUCGAAAACUA
					D-009264-03	GUUGAAGGUCUCCCUAUUA
					D-009264-04	AAGGUGAAAUUGCAAGGAA
MDH2	4191	1	D10	MU-008439-00	D-008439-01	CCAGAACAAUGCUAAAGUA
					D-008439-02	CAACACCAAUGCCACGAUU
					D-008439-03	CAAGAAGCAUGGAGUGUAC
					D-008439-04	CCUGAAAGGUUGUGAUGUG
GPD1	2819	1	D11	MU-008782-01	D-008782-02	AGAAAGAGUUGCUGAAUGG
					D-008782-04	GAUCGUGGGUGGCAAUGCA
					D-008782-17	AGAUGAUAGCCUUCGCCAA
					D-008782-18	CCCAUCAGUUCAUCGGCAA
GPD2	2820	1	D12	MU-009843-02	D-009843-01	UGAAUGAAGUGCGUAAUUA
					D-009843-02	GAACCUGGCCUAUGUUAAA
					D-009843-03	GAUAUGAUUUCACGUCGUA
					D-009843-05	GAGAGUGGCCUUAUUACUA
PRPS1	5631	1	E03	MU-006784-00	D-006784-01	GCAAAUAUGCUAUCUGUAG
					D-006784-02	UGGAGGAACUGCACUAUUG
					D-006784-03	GUGAUUGACAUCUCUAUGA
					D-006784-04	CCAUGCAGCUGACAAACUU
PRPS2	5634	1	E04	MU-004877-02	D-004877-05	GAUCUUGGCCGAAGCAAUC
					D-004877-01	AUACAGGGAUUCUUUGAUA
					D-004877-03	CAAAGUGUAUGCUAUCCUU
					D-004877-04	CAGAGUAACUGCCGUGAUC
PPAT	5471	1	E05	MU-006003-01	D-006003-01	GAAAUGGUCUGGAAUGUUU
					D-006003-02	GGUAAAUGCUGCUCGAUUA
					D-006003-03	GGGAAUGGGUCUUGUAAAU
					D-006003-05	GAAUGGGUCUUGUAAAUCA
UMPS	7372	1	E06	MU-009828-01	D-009828-02	GAACUAAGCGUCUUGUAGA
					D-009828-04	GAAGACUCAUGUAGAUAUU
					D-009828-17	AUUUCUGGCUCCCGAGUAA
					D-009828-18	UGAUAUUUGAAGACCGGAA
SLC1A5	6510	1	E07	MU-007429-01	D-007429-02	GGAUGUGGGUUUACUCUUU
					D-007429-03	GUUCUGGUCUCCUGGAUCA
					D-007429-17	GAGAGGAAUAUCACCGGAA
					D-007429-18	CAGUCAACCUCCCGGUCGA
SLC7A5	8140	1	E08	MU-004953-01	D-004953-01	GAUCCCAACUUCUCAUUUG
					D-004953-03	UGACCAACCUGGCCUACUU
					D-004953-17	GUGAACUGCUACAGCGUGA
					D-004953-18	UGAAAACUCUGGUACGAAU
PFKL	5211	1	E09	MU-006822-00	D-006822-01	UGAAGAUGCUGGCACAAUA
					D-006822-02	GCACAAUACCGCAUCAGUA
					D-006822-03	CACAAUACCGCAUCAGUAU
					D-006822-04	UGCUGAAGAUGCUGGCACA
GAPDH	2597	1	E10	MU-004253-02	D-004253-01	CAACGGAUUUGGUCGUAUU
					D-004253-03	GACCUCAACUACAUGGUUU
					D-004253-04	UGGUUUACAUGUUCCAAUA
					D-004253-05	GUCAACGGAUUUGGUCGUA
GAPDS	26330	1	E11	MU-009671-01	D-009671-01	CAAGGGAAGUGUGGAAUUC
					D-009671-02	GGACAACCAUGAGAUCUCU
					D-009671-03	UGGUGUACAUGUUUAAGUA
					D-009671-04	CCAUGAACAUUGUGAGCAA
PGK1	5230	1	E12	MU-006767-01	D-006767-05	GAAGCGGGUCGUUAUGAGA
					D-006767-01	CAAAAUUGAUGAUCCAUUA
					D-006767-02	UUGAUGAUCCAUUAAGUAA
					D-006767-04	GCACAGCAUCUCAGCUCAU
PGK2	5232	1	F03	MU-006768-02	D-006768-05	GGAAUGGGCCGUUAGGAGU
					D-006768-02	GCAGACAAGAUCCAACUUA
					D-006768-03	CAAGAUCCCUCUGGAAAGA
					D-006768-04	UGACAAAUAUUCCUUAGCA

Gene Symbol	Gene ID	Plate	Well	Pool Number	Duplex Number	Sequence
ENO1	2023	1	F04	MU-004034-02	D-004034-03	CAAACUGAUGAUCGAGAUG
					D-004034-04	AAUGAUAAGACUCGCUAUA
					D-004034-01	GAACGUCACAGAACAAGAG
					D-004034-02	GAUAAGACUCGCUAUAUGG
IDH1	3417	1	F05	MU-008296-00	D-008294-03	GUACAUAACUUUGAAGAAG
					D-008294-04	CAAGAUAAGUCAAUUGAAG
					D-008294-01	GAGCAAAGCUUGAUAACAA
					D-008294-02	GGACUUGGCUGCUUGCAUU
IDH2	3418	1	F06	MU-004013-00	D-004013-01	CAAGAACUAUGACGGAGAU
					D-004013-02	GCGCCACUAUGCCGACAAA
					D-004013-03	AACGAGCACUUCCUGAACA
					D-004013-04	GACAUCCAGCUAAAGUAUU
OGDH	4967	1	F07	MU-009679-02	D-009679-03	GCUAGGACAUUUCAACAGA
					D-009679-05	CAGACAAACUUGGGUUCUA
					D-009679-18	UCUAGAAGGCUGCGAGGUA
					D-009679-19	CUGAUGAGGGCUCCGGAGA
SDHA	6389	1	F08	MU-009398-02	D-009398-01	GAGGGAGGCAUUCUCAUUA
					D-009398-03	CGAAGGACCUGGCGUCUAG
					D-009398-04	UGAGAAAGAUCACGUCUAC
					D-009398-14	CGAAAGGUUUAUGGAGCGA
SDHB	6390	1	F09	MU-011773-02	D-011773-01	GGUAUUGGAUGCUUUAAUC
					D-011773-02	GAACAUCAAUGGAGGCAAC
					D-011773-19	GUGAGAAACUGGACGGGCU
					D-011773-20	GCUACUGGUGGAACGGAGA
SDHC	6391	1	F10	MU-011385-01	D-011385-17	GGGCUUAGAUAGAAAGUCU
					D-011385-18	AGUUAAAGCUGUGGGUCGA
					D-011385-19	GAAAAGAAGUGACGCAUGU
					D-011385-20	UCGAAGUAAUGUACCCUUU
SDHD	6392	1	F11	MU-006305-00	D-006305-01	GGACCGACCUAUCCCAGAA
					D-006305-02	GCUUUGCUAUUUCAACUAU
					D-006305-03	ACUUUCAGCUUUAACCUUU
					D-006305-04	CAGACCUGCUCAUAUCUCA
FH	2271	1	F12	MU-009512-00	D-009512-01	GAUCUACGAUGAACUUUAA
					D-009512-02	UCAACAAGCUGAUGAAUGA
					D-009512-03	GCACAGAUCAUCAAGAUUG
					D-009512-04	AGCCAGAGCUCAAAUGAUA
CHPT1	56994	1	G03	MU-009775-02	D-009775-01	GAACUUAUCCUGACUGGUU
					D-009775-06	UUUCAGGCAUGUUGAGAUU
					D-009775-19	GCGCUCAUUGGCAGACUUA
					D-009775-20	CUUCAUUUGAUAUGGUGAU
MVK	4598	1	G04	MU-006749-00	D-006749-01	UGGAAGAGCUCAUUGACAU
					D-006749-02	ACACCAAAGUCCCUCGCAA
					D-006749-03	GCUCAAGUUCCCAGAGAUC
					D-006749-04	ACCAAAGUCCCUCGCAAUA
PMVK	10654	1	G05	MU-006782-01	D-006782-01	UUUAUCCGCUCCAGACUUU
					D-006782-02	CGAGAACCAUGGAGUUGAA
					D-006782-03	GCGAAACCCUGCCAUAUCC
					D-006782-04	AAUGUGGCCUGGACAACUU
MVD	4597	1	G06	MU-006748-00	D-006748-01	GACCGGAUUUGGCUGAAUG
					D-006748-02	ACAUCGCGGUCAUCAAGUA
					D-006748-03	GCCCAUCUCUUACCUCAAU
					D-006748-04	CAGCAUCGCUCGGCAAGUG
GGPS1	9453	1	G08	MU-016477-02	D-016477-03	CAAAUUAGGGAUGAUUAUG
					D-016477-04	UAAAACCGCUACUUAAUAC
					D-016477-20	GGGACAAGGCCUAGAUAUU
					D-016477-21	CCAAUUGGGAAGCGGAAAA
LSS	4047	1	G09	MU-008624-00	D-008624-01	GGACUGCGCUCAACUAUGU
					D-008624-02	GCAGAAGGCUCAUGAGUUC
					D-008624-03	GAAGCUGUAUGAACACAUU
					D-008624-04	UGCAGGCGCUUAAGUAUUU
DHCR7	1717	1	G10	MU-020182-01	D-020182-01	GGCCAAGACUCCACCUAUA
					D-020182-02	GAACAAGUAUCAGAUCAAC
					D-020182-03	CAUCAUGGCUUGUGACCAG
					D-020182-04	GCCCAGCUCUAUACCUUGU
PRKAG2	51422	1	G11	MU-009693-01	D-009693-02	GCAAUAAGCUGGAAAUACU
					D-009693-03	CCACAACAUUGCCUUCAUA
					D-009693-17	CGGAGUGACCGCCGUGAAU
					D-009693-18	CCACAGAUUGCCCGUUAUU

Gene Symbol	Gene ID	Plate	Well	Pool Number	Duplex Number	Sequence
PRKAG3	53632	1	G12	MU-009859-01	D-009859-01	UCUAUGAGAUUGAACAACA
					D-009859-02	GGGAAGUGAUCGACAGGAU
					D-009859-03	ACAAACGCCUGCUCAAGUU
					D-009859-05	GCUCCAAGCUAGUCAUCUU
PRKAB1	5564	1	H03	MU-007675-00	D-007675-01	CAGAAGCCACAAUAACUUU
					D-007675-02	CAACAACUGGAGUAAACUU
					D-007675-03	UGUCUGAGCUGUCCAGUUC
					D-007675-04	GGAAGGAGAGCAUCAGUAC
PRKAB2	5565	1	H04	MU-007672-00	D-007672-01	GUUCGAUGCUUUAAAGUUA
					D-007672-02	UAAGAGCCAUAAUGACUUU
					D-007672-03	GCAAGGAGGUCUUCAUCUC
					D-007672-04	GCACCAAGAUUCCACUGAU
PRKAG1	5571	1	H05	MU-009056-01	D-009056-01	GGACAUCUACUCCAAGUUU
					D-009056-02	GAUGCUGUCUCUUCAUUAA
					D-009056-03	CAACAUCGAUCACAUUACU
					D-009056-04	GUGUAUACUUCCUUCAUGA
EPAS1	2034	1	H06	MU-004814-01	D-004814-05	ACACAUCUUUGGAUAACGA
					D-004814-02	GCAAAUGUACCCAAUGAUA
					D-004814-03	GAGCGGGACUUCUUCAUGA
					D-004814-04	AGACGGAGGUGUUCUAUGA
MT-ND1	4535	1	H07	MU-012827-00	D-012827-01	UAACCUCCCUGUUCUUAUG
					D-012827-02	UGAUUUAUCUCCACACUAG
					D-012827-03	CUAAUAAGUGGCUCCUUUA
					D-012827-04	CCGAAUACACAAACAUUAU
MT-ND2	4536	1	H08	MU-012828-00	D-012828-01	GCGCUAAGCUCGCACUGAU
					D-012828-02	UAACCAAUACUACCAAUCA
					D-012828-03	CAAUAUACUCUCCGGACAA
					D-012828-04	CCAUAUCUAACAACGUAAA
MT-ND3	4537	1	H09	MU-012829-00	D-012829-01	CAACUAACCUGCCACUAAU
					D-012829-02	CCGCGUCCCUUUCUCCAUA
					D-012829-03	CUUAGUAGCUAUUACCUUC
					D-012829-04	CAACUCAACGGCUACAUAG
MT-ND4	4538	1	H10	MU-012830-00	D-012830-01	CUAGGCGGCUAUGGUAUAA
					D-012830-02	GACCUAAAAUCGCUCAUUG
					D-012830-03	GAGCCAAUAACUUAAUAUG
					D-012830-04	UAACCACGUUCUCCUGAUC
MT-ND5	4540	1	H11	MU-012831-00	D-012831-01	UGAGAGGGCGUAGGAAUUA
					D-012831-02	GCCUAUAGCACUCGAAUAA
					D-012831-03	CUAGGACUCAUAAUAGUUA
					D-012831-04	CUACUCCACUCAAGCACUA
MT-ND6	4541	1	H12	MU-012832-00	D-012832-01	GGUCGGGUGUGUUAUUAUU
					D-012832-02	GAAUGAUGGUUGUCUUUGG
					D-012832-03	CGAUGGCUAUUGAGGAGUA
					D-012832-04	GAUUAUGGGCGUUGAUUAG
GALK1	2584	2	A03	M-007728-01	D-007728-03	GACCAGUUCAUCUCACUUA
					D-007728-04	GCGCCAAUGUGAAGAAGUG
					D-007728-05	GGGAACACACGGACUACAA
					D-007728-06	GAGCCAAGGUGCUGUGCUU
GALK2	2585	2	A04	M-006725-00	D-006725-01	GCUAAUAACAUCCAGAUUG
					D-006725-02	GCACAACUAUUUCUUAUGU
					D-006725-03	GGAAAUAUCCCACCAAGUU
					D-006725-04	GGACCAGUCUAUAUCAUUU
GALT	2592	2	A05	M-010327-00	D-010327-01	AAACAAAGGUGCCAUGAUG
					D-010327-02	GAUCUAGCCUCCAUCAUGA
					D-010327-03	GAUCUCAGCAGGCCUAUAA
					D-010327-04	GCAAACGACCAUCAGCAUA
PGM1	5236	2	A06	M-010925-00	D-010925-01	CGAAUCGUCUUCCGACUGA
					D-010925-02	GUACAUCGAUAGCUAUGAG
					D-010925-03	CGACUGAAGAUCCGUAUUG
					D-010925-04	GGAAAUUGUGGAUUCGGUA
PGM3	5238	2	A07	M-013912-00	D-013912-01	GAGGUCAAUUCCAUGAUUA
					D-013912-02	GGAUUUAGGUGCUAUUACA
					D-013912-03	GGGCAAACUCAAUCAUUUA
					D-013912-04	GACAAGAUAGCAACGUUAA
GLUD1	2746	2	A08	M-004032-02	D-004032-01	GCAACCAUGUGCUGAGUCU
					D-004032-02	UAAAUCAUGUCAGCUAUGG
					D-004032-05	CAAUGAAGCUUCUUACAUG
					D-004032-19	GAAAUUAAGGUUAGCGGAU

Gene Symbol	Gene ID	Plate	Well	Pool Number	Duplex Number	Sequence
GLUD2	2747	2	A09	M-009067-02	D-009067-01	CAAUGAAGCUUCUUACAUG
					D-009067-04	GGACGCAUCUCUGCUACUG
					D-009067-05	CAAGGGAGGUAUCCGUUAC
					D-009067-18	CUUUAUUGGUCCUGGCGUU
HK3	3101	2	A10	M-006736-00	D-006736-01	GGAAUGCGAUGUCUCCUUA
					D-006736-02	GCAGUUGACUCGUGUCUGA
					D-006736-03	GACAGGAGCACCCUCAUUU
					D-006736-04	UCACGUUCCUGCAGUCAGA
GPI	2821	2	A11	M-004900-01	D-004900-01	GGAAAUACAUCACCAAAUC
					D-004900-03	CAACCAAAGUGAAGGAGUU
					D-004900-04	GAUGAUACCCUGUGACUUC
					D-004900-05	UCACGACGCUUCUACCAAU
PFKM	5213	2	A12	M-006765-01	D-006765-01	UCAAGAAUCUGGUGGUUAA
					D-006765-03	GAUCAUGGAAAUUGUAGAU
					D-006765-04	CAGAAGACAUCAAGAAUCU
					D-006765-05	GGAUAUGACACCCGGGUUA
PFKP	5214	2	B03	M-010253-01	D-010253-01	GAAAUCGGCUGGACAGAUG
					D-010253-02	CAACGUAGCUGUCAUCAAC
					D-010253-03	GAAGAGAUCGCCACACAGA
					D-010253-05	GGAACGGCCAGAUCGAUAA
PFKFB1	5207	2	B04	M-006761-01	D-006761-01	UAAAGAGAAUUGAGUGCUA
					D-006761-03	UAAUGACCCUGGCAUAAUU
					D-006761-04	GCUAUGAGGUCAACUACCA
					D-006761-17	UACCAGAGAACGACGGUCA
PFKFB2	5208	2	B05	M-006762-02	D-006762-01	GAACUUUGCUGAACAGAAU
					D-006762-02	GAACAGAGAGAACGUGAUG
					D-006762-03	CCAAUAUUCUGGAGGUUAA
					D-006762-18	CGGCAUGGAGAAAGCGAGU
PFKFB3	5209	2	B06	M-006763-01	D-006763-01	GGACCUAACCCGCUCAUGA
					D-006763-02	GAGGAUCAGUUGCUAUGAA
					D-006763-03	AAAGCUACCUGGCGAAAGA
					D-006763-17	ACAAGUACUAUUACCGCUA
PFKFB4	5210	2	B07	M-006764-01	D-006764-01	GAGCGACCAUCUUUAAUUU
					D-006764-02	GAAAUGACCUACGAGGAAA
					D-006764-04	CAUCGUAUAUUACCUCAUG
					D-006764-17	GGGACAGGCCUCAGAACGU
ALDOA	226	2	B08	M-010376-01	D-010376-02	GGACAAAUGGCGAGACUAC
					D-010376-03	UUGAAGCGCUGCCAGUAUG
					D-010376-04	GGCGUUGUGUGCUGAAGAU
					D-010376-05	UGACAUCGCUCACCGCAUC
ALDOB	229	2	B09	M-010990-01	D-010990-01	CCAAAGCCCUGGAAACUAA
					D-010990-02	GGACAUGCCUGCACCAAGA
					D-010990-04	GAAGAAGGAGCUCUCAGAA
					D-010990-05	CCAAAGGACAGUAUGUUCA
ALDOC	230	2	B10	M-012697-01	D-012697-01	GAAAGAUGAUAAUGGUGUU
					D-012697-02	GCGCUUACCUUCUCCUAUG
					D-012697-03	GCACAGUCACUCUACAUUG
					D-012697-04	AAACGUUGUCAGUAUGUUA
TPI1	7167	2	B11	M-009776-02	D-009776-01	GCAAGGUCGUCCUGGCCUA
					D-009776-02	GCUCAGAGCACCCGUAUCA
					D-009776-05	AGAGAGAAGGCAUGUCUUU
					D-009776-06	GAUCAAAGACUGCGGAGCC
PGAM4	441531	2	B12	M-034271-00	D-034271-13	GCACAGGUUCUCAGUCUAA
					D-034271-14	CCUCAUACCAAUAUAGGAU
					D-034271-15	CAUGCUAAGCCACGACCAA
					D-034271-16	CAGAAGAGAGUGAUCCGGA
PGAM1	5223	2	C03	M-008883-01	D-008883-02	GGACAAGAACUUGAAGCCU
					D-008883-03	CCAUGCAGUUUCUGGGGGA
					D-008883-04	UGAAGAGACGGUGCGCAAA
					D-008883-05	GGUCUAACCGGUCUCAAUA
PGAM2	5224	2	C04	M-008712-02	D-008712-01	GAUCAAGGCCGGCAAGCGA
					D-008712-03	CCAAGAUGGAGUUUGACAU
					D-008712-18	UGUCAGACCAGGCGAUCAU
					D-008712-19	GGAUGUCAGACCAGGCGAU
BPGM	669	2	C05	M-008917-02	D-008917-02	GAAAGCUCCUGGCGUCUAA
					D-008917-03	GGAAUAAGGAGAACCGUUU
					D-008917-04	GGAGGAAGCUCGGAACUGU
					D-008917-18	CAACUGCCACGGUCGGAAA

Gene Symbol	Gene ID	Plate	Well	Pool Number	Duplex Number	Sequence
ENO2	2026	2	C06	M-009777-01	D-009777-04	CUGAACGUCUGGCUAAAUA
					D-009777-17	GGACAUAACUUCCGUAAUC
					D-009777-18	CCACUGAUCCUUCCCGAUA
					D-009777-19	CCUCAGAGUUUUAUCGUGA
ENO3	2027	2	C07	M-009718-02	D-009718-02	CUAUGAGGCUCUGGAACUA
					D-009718-03	GGGUGAACAUCCAGAUUGU
					D-009718-04	GCAAUGGGAAGUACGAUCU
					D-009718-05	CGGAGCGUCUGGCCAAAUA
LDHAL6A	160287	2	C08	M-008760-01	D-008760-01	GGAGAAACACGCCUUGAUU
					D-008760-02	CCAGAUAUAGGAACUGAUA
					D-008760-03	GGAGUGGUGUGAACAUUGC
					D-008760-04	GAAGAGGAGGCCAUUCAUC
LDHAL6B	92483	2	C09	M-008908-02	D-008908-01	UGGAAUAGAUGAAGAAGUA
					D-008908-03	AGUAAGGUCUCCAUCAUAG
					D-008908-04	GACGAUGGAUCUUCAACAU
					D-008908-17	GAGUGAGCUUAUUGAGCGU
PDK3	5165	2	C10	M-005021-02	D-005021-02	GUUGGUAUAUGCAGAGUUU
					D-005021-03	UAAGAUCAGUGACCUAGGU
					D-005021-05	CGGGAGAGAUAAUGCAUGU
					D-005021-06	GUUCAGAGUUGGUAUAUGC
PDK4	5166	2	C11	M-019425-02	D-019425-01	AAAGAAGACCUUACCAUUA
					D-019425-02	GAAAUAGACACCAUAAUGU
					D-019425-03	CGACAAGAAUUGCCUGUGA
					D-019425-04	GACCGCCUCUUUAGUUAUA
PDP1	54704	2	C12	M-008718-00	D-008718-01	CGACUGAUAUUGAUGUUAA
					D-008718-02	GAACUGAGCAGGAUCUAUG
					D-008718-03	GCAUCCAAAUUGUACUUUA
					D-008718-04	GCAAGUUGGUGAUCCUAAU
PDP2	57546	2	D03	M-022572-00	D-022572-01	CAACAGAGGAAGAUGAUUU
					D-022572-02	GCAAACCAAUGGACUGAUG
					D-022572-03	GGAACAGCAUUGCCACAUU
					D-022572-04	GAAGAAGCAUUAAUGUACU
ACO1	48	2	D04	M-010037-00	D-010037-01	GCAAACAGGUCGUGAUGAA
					D-010037-02	GAACAUAGAAGUGCCAUUU
					D-010037-03	GUAGGAAUGUUUCGAGAUU
					D-010037-04	GAGAUUCGGUAACAACUGA
ACO2	50	2	D05	M-009566-00	D-009566-01	CAAUCUAGCUGAUGAAUUC
					D-009566-02	CCACUUCCGUGUUCCCUUA
					D-009566-03	GCAGUGCCCUCAACAGAAU
					D-009566-04	GGACGGCUAUGCACAGAUC
LOC441996	441996	2	D06	M-035153-01	D-035153-09	CAGGCAAGGAUGGCAAGAA
					D-035153-10	GGUCAGUUGCACAGAAAGG
					D-035153-11	GCAGGAGAAGAACAUAAUU
					D-035153-12	GCAGAUCCGUGCCUCCAUU
IDH3A	3419	2	D07	M-008753-00	D-008753-01	GCAGAAAGCUGUAAAGAUA
					D-008753-02	GAACGUCACUGCCAUUCAA
					D-008753-03	GGAAAGAGCUUGACAAAAG
					D-008753-04	GCUAAAGAGUCCAUGGAUA
IDH3B	3420	2	D08	M-009596-00	D-009596-01	UGAAGAAGGUGAUCAAAGU
					D-009596-02	GCAUCUUAAUCUUGAGUAU
					D-009596-03	GCAGUGGGCAGGAAUAUAG
					D-009596-04	UUGAGACAAUGAUCAUAGA
IDH3G	3421	2	D09	M-009361-00	D-009361-01	GCAAGAGUAUCGCCAAUAA
					D-009361-02	GGACAUAGACAUCCUCAUU
					D-009361-03	GCACGUGAGUUCCAAUGCU
					D-009361-04	GAACACAGAGGGCGAGUAC
DLST	1743	2	D10	M-009941-02	D-009941-01	GCAGGAAGGUUGUCAUUAA
					D-009941-02	GCAGAGAGGCUGUGACUUU
					D-009941-05	GAUGAGGGCUCGGCACAAA
					D-009941-19	CAAAAUCAAGGCAGCGGUA
LOC283398	283398	2	D11	M-026908-01	D-026908-01	UAAAGGAAGCUCAAGUAUA
					D-026908-02	CAAAUUACGAAGCUGUAUA
					D-026908-03	GGACGACAAAUCAGAGAAU
					D-026908-04	ACUAGAAACUUCCAGUCAA
SUCLG2	8801	2	D12	M-008918-01	D-008918-01	AAAGGAAGCUCAAGUAUAU
					D-008918-02	AAAUGAAGCUGCCAAAUAU
					D-008918-04	GGACUAGAUGGGAACAUUG
					D-008918-17	GGUACAAUCUAGCGACAAA

Gene Symbol	Gene ID	Plate	Well	Pool Number	Duplex Number	Sequence
SUCLG1	8802	2	E03	M-008677-01	D-008677-01	GAAAUUCCCUUGGUUGUGU
					D-008677-02	AGAGAAUGCUGCAGAAUUU
					D-008677-03	GGGCUUACCUGUCUUUAAU
					D-008677-04	GAUCUGGCACCCUGACUUA
SUCLA2	8803	2	E04	M-008237-00	D-008237-01	GCAAAGGAAUCUCUCACUA
					D-008237-02	GGAUGAAGCUGCUAGAAUG
					D-008237-03	UCAAGGUCCUGUAUUAAUA
					D-008237-04	GGGAAGUUCUGGAUUGUUU
GOT1	2805	2	E05	M-011673-01	D-011673-01	GAGCAUAUCGCACGGAUGA
					D-011673-02	UUAAAGACAUUCGGUCCUA
					D-011673-03	UAGCCUAAAUCACGAGUAU
					D-011673-17	GAACAGGUGCACUUCGAAU
GOT2	2806	2	E06	M-011674-02	D-011674-01	GCAUGCAGCUACAAGGUUA
					D-011674-03	AACAUGGGCUUAUAUGGUG
					D-011674-04	CUUGAAGAGUGGCCGGUUU
					D-011674-18	UGAGAAACAGCACACGUUA
SLC25A11	8402	2	E07	M-007470-00	D-007470-01	GGACUCAGGCUACUUCUCU
					D-007470-02	GGGAUGGGAGCUACAGUUU
					D-007470-03	CAGAACAUGCGGAUGAUUG
					D-007470-04	UCUAUACCGUGCUGUUUGA
GPD1L	23171	2	E08	M-008514-01	D-008514-01	GGAAGACCAUUGAAGAGUU
					D-008514-02	GGCUGAAGCUCAUUUCUGA
					D-008514-03	GUUGCCAUGUCAAAUCUUA
					D-008514-04	GCAGACCAGUUCAAGAGAU
ME3	10873	2	E09	M-008499-01	D-008499-01	CAACAAUGCUGAAUUCUUG
					D-008499-02	ACAAAUACCGUAACAAGUA
					D-008499-03	GGAGCCACCUGAACCAUGA
					D-008499-04	CUAAAGGGCUCAUUGUCAA
GLUL	2752	2	E10	M-008228-01	D-008228-01	GCACGUGUCUUCUCAAUGA
					D-008228-02	GAAGAAGGGUUACUUUGAA
					D-008228-03	GCACACCUGUAAACGGAUA
					D-008228-04	CAUGAAACCUCCAACAUCA
GPT	2875	2	E11	M-031622-00	D-031622-01	GAAGAAGCCUUUCACCGAG
					D-031622-02	GAACAUGGACGCUGCAGUG
					D-031622-03	GCGCAGUGCAGGUGGAUUA
					D-031622-04	CCGAGCAGGUCUUCAAUGA
GPT2	84706	2	E12	M-004173-02	D-004173-01	UCAAAUGGCUCCAGACAUG
					D-004173-03	GUGAAAGACUUCCACAUCA
					D-004173-04	UCAAGAAGGUGCUGUACGA
					D-004173-18	GUGAAAAGGUUAAAUCGUA
DDO	8528	2	F03	M-009311-01	D-009311-02	CAGCACGGAUUGCAGUUGU
					D-009311-03	UCAGAGAAACCUUUAAUCA
					D-009311-17	GGACCUAUGCAGAUUUAUA
					D-009311-18	GGUGUAACAUGUAAGCUGA
AGXT	189	2	F04	M-008925-01	D-008925-01	GGAGAGACAUCGUCAGCUA
					D-008925-02	GCAAGGAUAUGUACCAGAU
					D-008925-04	UAGACCACUUCGACAUUGA
					D-008925-05	GGUCAUCUCUGGCUCGGGA
AGXT2	64902	2	F05	M-009818-00	D-009818-01	GGAAAGAAGAGCUAAGUAA
					D-009818-02	GGACCUACAUGUUACUAAA
					D-009818-03	GGAAGCAGAUACCUGGAUU
					D-009818-04	CAUAACCACUCCAGAGAUU
PSAT1	29968	2	F06	M-010398-02	D-010398-21	UUUAAGAGUGCCAGGCGAA
					D-010398-22	GAGAAUCUUGUGCGGGAAU
					D-010398-23	GCGCAAAUGAGACGGUGCA
					D-010398-24	GGACUAUAAAUAUCGUUCA
CAD	790	2	F07	M-009471-01	D-009471-01	GAGGGUCUCUUCUUAAGUA
					D-009471-17	GGAAGGAGAUUGAGUACGA
					D-009471-18	CCAACAGAUAAGCGGAUUU
					D-009471-19	AUUAAGACUCCACGGGUAU
ODC1	4953	2	F08	M-006668-00	D-006668-01	GAGCAGACCUUUAUGUAUU
					D-006668-02	CGAAAGAGCUAAAUAUCGA
					D-006668-03	GAAGUUGAGUUGAUGAAAG
					D-006668-04	GAAGAGAUCACCGGCGUAA
SHMT1	6470	2	F09	M-004617-00	D-004617-01	GAGCUGGCAUGAUCUUCUA
					D-004617-02	GGAGAACGCACGCCUCUUC
					D-004617-03	CCUAGGCUCUUGCUUAAAU
					D-004617-04	UACGGAAGAUUGCAGAUGA

Gene Symbol	Gene ID	Plate	Well	Pool Number	Duplex Number	Sequence
SHMT2	6472	2	F10	M-004906-01	D-004906-01	GGAGAUCCCUUACACAUUU
					D-004906-02	GGUCAGGGCUCAUCUUCUA
					D-004906-03	GGACAGUGAUCCUGAGAUG
					D-004906-04	AAACUGGCCUCAUUGACUA
TKT	7086	2	F11	M-004734-01	D-004734-01	GAAAAUGCCAUCAUCUAUA
					D-004734-03	GAACUAGCCGCCAAUACAA
					D-004734-04	CUGCCGAACUGCUGAAGAA
					D-004734-05	GGAACUAGCCGCCAAUACA
TKTL1	8277	2	F12	M-004736-01	D-004736-01	GCAAGUACCGCUCUAAUUU
					D-004736-02	GGAAUUCCCUUCGCUGUUU
					D-004736-03	GCAGAAAGUUGGCAUGCAA
					D-004736-04	GGAAUUAGUGCCAGACAUA
DKFZP 434L1717	84076	2	G03	M-004735-01	D-004735-01	CGACAGAGCAUGCUAUUUA
					D-004735-02	GUGAAUUGCUGGAUAUGUU
					D-004735-03	GAUAAAGUCACAGUAAUUG
					D-004735-04	GUAAUUGGAGCUGGAGUUA
PGLS	25796	2	G04	M-020023-00	D-020023-01	GAUUGUGGCUCCCAUCAGU
					D-020023-02	CACACUACCUGUCCUGAAU
					D-020023-03	GCAAGGCAGCUGUUCUGAA
					D-020023-04	CGGCUGAGGACUACGCCAA
H6PD	9563	2	G05	M-004692-01	D-004692-01	CCGAGGAGCUGAUCUCUAA
					D-004692-02	GCAGCCCUCUGUCCGAUUA
					D-004692-03	GGACAUGUCUCCAUAAUCC
					D-004692-04	GGGCUACGCUCGGAUCUUG
PGD	5226	2	G06	M-008371-00	D-008371-01	GAUCAUCUCUUACGCUCAA
					D-008371-02	UAAUAGGACUGUCUCCAAA
					D-008371-03	GAAAUCACAGCCAAUAUUC
					D-008371-04	GAAAUUGGUACCAUUGUUG
RPIA	22934	2	G07	M-016428-01	D-016428-01	GGAAGUGGUUCUACAAUUG
					D-016428-02	GCGAAUAGCUGAAAGGGUG
					D-016428-03	GCUAGUCGCUUCAUCGUGA
					D-016428-04	CAAAUGGAGUGAAGUGAAU
PRPS1L1	221823	2	G08	M-006804-00	D-006804-01	GCAAAUAUGCUCUCUAUAG
					D-006804-02	GAAAUCAACGACAGUCUAA
					D-006804-03	CAACACUGCAUGCUUUGAA
					D-006804-04	CAACCAGAGUUUAUGCUAU
GPAM	57678	2	G09	M-009946-01	D-009946-01	GGAAAGAUGUUCUCUAUAG
					D-009946-02	GAUAAUACCUGUUGGAAUC
					D-009946-03	GUUCAUAGAUCCCAUAUUG
					D-009946-04	AGAAAGAAAUGUUGCAGUA
AGPAT1	10554	2	G10	M-003810-01	D-003810-01	AUGAAGAUCUUGCGUCUAA
					D-003810-03	CGUGGCGCCUUCCAUCUUG
					D-003810-04	UCGAGAACAUGAAGAUCUU
					D-003810-05	UCAAAUACCUGUACGGGAU
AGPAT2	10555	2	G11	M-003811-02	D-003811-01	GUGCGAAGCUUCAAGUACU
					D-003811-03	GCCGGACGGUGGAGAACAU
					D-003811-21	CGGCCGAGUUCUACGCCAA
					D-003811-22	GCGCUGUGCUUCACGGUGU
AGPAT6	137964	2	G12	M-010300-00	D-010300-01	GAAAUUGGAGCCACAGUUU
					D-010300-02	UUAAGGAGUUCAUGAGUAA
					D-010300-03	GAACCUGCAUCAAUAAUAC
					D-010300-04	GAGAAGAACCACCAGCUUU
UNQ1849	253558	2	H03	M-010307-00	D-010307-01	GGAAUUGCCUGAUGCGAUA
					D-010307-02	UCGAAGACAUGAUUGAUUA
					D-010307-03	GCCUAUAUCUUCAUUCAUA
					D-010307-04	GAAAGAAGUGUCAUUAUCA
AGPAT3	56894	2	H04	M-008620-00	D-008620-01	GCUCCAAGGUCCUCGCUAA
					D-008620-02	GGGAGCAGCUUCCUUUGGA
					D-008620-03	UCCAGGAGAUAUAUAAUCA
					D-008620-04	GCAGCUGUCUAUGAUGUAA
AGPAT4	56895	2	H05	M-009283-01	D-009283-01	AGAAAGAGCUGGCCUAUGU
					D-009283-02	GGAGUUCGAUGGAUGAUUG
					D-009283-03	GCACACGGUUCACGGAGAA
					D-009283-04	AAAUGUAGUUUCAGCUGUA
PPAP2A	8611	2	H06	M-019098-01	D-019098-01	GAGGAGGACUCUCAUACAA
					D-019098-03	CUACAUAUGUCGAGGGAAU
					D-019098-04	CAACAACUGGGAAUCACUA
					D-019098-17	CUGUAUAUGUAUCGGAUUU

Gene Symbol	Gene ID	Plate	Well	Pool Number	Duplex Number	Sequence
PPAP2C	8612	2	H07	M-011500-00	D-011500-01	UGACAGACCUGGCCAAGUA
					D-011500-02	GCACGACUCUGUUGGAAGU
					D-011500-03	GCUCGGACUUCAACAACUA
					D-011500-04	CCGCGUGUCUGAUUACAAA
PPAP2B	8613	2	H08	M-017312-01	D-017312-01	GGGACUGUCUCGCGUAUCA
					D-017312-02	UCUAUUACCUGAAGAAGUC
					D-017312-03	CAGUUCACCUUGAUCAUGA
					D-017312-05	GGAAUUCUACCGGAUCUAU
PCYT1A	5130	2	H09	M-008642-01	D-008642-01	GGAGAGGGUUGACAAAGUA
					D-008642-02	UGAAACAUAUGCUGAAAGA
					D-008642-04	GGAGAAGUCCCGAGAAUUC
					D-008642-17	UGUGAGAGUUUAUGCCGAU
PCYT1B	9468	2	H10	M-009611-01	D-009611-02	GGACAUCAUUACCAGAAUU
					D-009611-03	AAAGAGCCAUGAUCUAAUU
					D-009611-17	GGAAAUAACUAAUGCCUAU
					D-009611-18	CUUAGUCACCUGUGCGAAA
PLD1	5337	2	H11	M-009413-00	D-009413-01	UAACUGAGCUUAUCUAUGU
					D-009413-02	GAAGAACAAUUCCUUGGUA
					D-009413-03	GAAGAUUACUUGACAAAGA
					D-009413-04	GGUAAUCAGUGGAUAAAUU
PLD2	5338	2	H12	M-005064-01	D-005064-01	GGACAACCAAGAAGAAAUA
					D-005064-02	GGACCGGCCUUUCGAAGAU
					D-005064-03	GACCUGCACUACCGACUGA
					D-005064-04	CAGCAUGGCGGGACUAUAU
ACAS2L	84532	3	A03	M-008549-00	D-008549-01	CCACCAAGAUCGCCAAAUA
					D-008549-02	GAUCGGAGCUGUCCACACA
					D-008549-03	GAAGAUCAAUCAGUUCUAU
					D-008549-04	UGAGGAAGAUCAUCACUAG
ACAS2	55902	3	A04	M-010396-00	D-010396-01	GAGAAGGGUUUCCCAGUAA
					D-010396-02	GAGACAACCUACUUUAAGA
					D-010396-03	CCACAACCUUCAAGUAUGU
					D-010396-04	GCACCUGGCUUGCCUAAAA
ACACB	32	3	A05	M-004759-02	D-004759-01	GAACAUCCCUGCACAGAAA
					D-004759-05	CCACAAAGGAUUUAAAUAC
					D-004759-18	GAACUUAACCGGAUGCGUA
					D-004759-19	AGAUACAUGAUCACGGAUA
MT	27349	3	A06	M-014204-01	D-014204-01	GAAGAAUUCCUCUAAGUUU
					D-014204-02	UAAAGGCAGUCGACAUUAA
					D-014204-04	AGACGAUGCAUGCCAUAUA
					D-014204-17	GCUGGCCGCUGUCGAGAAA
THEDC1	55301	3	A07	M-004796-01	D-004796-01	GGGCAGAUCUGAACAUUGU
					D-004796-02	GGAUAAACCAUUUGCAUUU
					D-004796-04	CCAAGGAAUUUGUGAAACA
					D-004796-17	GGAUCCUGCGAACGAGAAA
FLJ20604	54995	3	A08	M-031860-00	D-031860-01	GGAGACUCAUUUAGAUUUA
					D-031860-02	GGUCAGCAUUCGAUAUAAA
					D-031860-03	GCAAUUGGCAUGGGAAUGA
					D-031860-04	UCUCAACUAUGUUCCACUA
ELOVL6	79071	3	A09	M-008861-01	D-008861-01	CAAUGGACCUGUCAGCAAA
					D-008861-02	GGUCGGCACCUAAUGAAUA
					D-008861-03	CGAACUAGGAGAUACAAUA
					D-008861-17	GGGUGUAUAUCUAGAACGA
SCD	6319	3	A10	M-005061-01	D-005061-02	GAUAUGCUGUGGUGCUUAA
					D-005061-04	AGAAUGAUGUCUAUGAAUG
					D-005061-05	CGACAUUCGCCCUGAUAUA
					D-005061-06	GGAGUACGCUAGACUUGUC
SCD5	79966	3	A11	M-008416-03	D-008416-03	CAUAUUGGGUGGCUGUUUG
					D-008416-20	AGAACAUCGUCUGGAGGAA
					D-008416-21	GAGAAAGCUUGACGUCACU
					D-008416-22	CAGAAUGACAUCUUCGAGU
ACAT1	38	3	A12	M-009408-00	D-009408-01	GAAAUGAACAGGACGCUUA
					D-009408-02	GGGUAAAGCUUGAAGAUUU
					D-009408-03	GCAAAGAAGCUGAAUAUUG
					D-009408-04	GCGAAGAGGCUCAAUGUUA
ACAT2	39	3	B03	M-010001-01	D-010001-01	UCACUUGGCUUACUUGAGA
					D-010001-02	GGAAUUCCCUACUCUGUUC
					D-010001-03	GAAGCCAUGUCCAAGCUAA
					D-010001-04	GCAUCUGGCUGUCGAAUUC

Gene Symbol	Gene ID	Plate	Well	Pool Number	Duplex Number	Sequence
AACS	65985	3	B04	M-009458-01	D-009458-02	CGAAAGGAAUCGCAGAUGU
					D-009458-04	GGCAAGAAGUGGCUUUGUU
					D-009458-17	CGUAUACGCUCAACGGCAA
					D-009458-18	GGAACGAUGAGAACGGCAA
IDI1	3422	3	B05	M-009357-00	D-009357-01	GAACAUUGAGAAAGGAUUA
					D-009357-02	GAGGAAGAAUGUAACUUUG
					D-009357-03	UAAGAUAACGCCAUGGUUU
					D-009357-04	UAAAUGGUGGGAUAACUUA
IDI2	91734	3	B06	M-008463-00	D-008463-01	GUAGUAGCCACCCAUUAUA
					D-008463-02	GGAAUUGCCAUCUGAACGA
					D-008463-03	UGGAGGAAAUGCUGAUUGU
					D-008463-04	UCACGUUUCCUGGGUAUUU
FDFT1	2222	3	B07	M-009442-02	D-009442-01	GGAAGAGAUUUAUCAUAGA
					D-009442-03	GGACAAGUACUGCCACUAU
					D-009442-04	CCACUUUGGCUGCCUGUUA
					D-009442-05	GUUUGGAGCAGGUAUGUUA
SQLE	6713	3	B08	M-009646-01	D-009646-04	UAUUGAAGGUGUUGUGUUA
					D-009646-17	UUUCAAACUUGGUGGCGAA
					D-009646-18	CAAACUUGGUGGCGAAUGU
					D-009646-19	GAGAUACAGUGGAAGGUCU
CYP51A1	1595	3	B09	M-009215-01	D-009215-01	CAGCAUACAUCCUCAACUA
					D-009215-02	CCACUAUGCUUCGUUUAUA
					D-009215-03	GAAGGGAGUUGCAUACGAU
					D-009215-17	GGUAGGGAAUAAUCGAACA
NSDHL	50814	3	B10	M-008448-00	D-008448-01	UGACAGGCCUCAAUUAUGA
					D-008448-02	GCCAAGAGAUGCACAGUGA
					D-008448-03	GAUAUGCUGUCAAUGUAUU
					D-008448-04	GCAGUUAGCGAGCCAAUGA
HSD17B7	51478	3	B11	M-008140-02	D-008140-02	GAAGAUGGACCUAGAUGAA
					D-008140-03	GGAAUUCUGCCUCCGUUUA
					D-008140-18	CAAUAUUGCUACUUCGCUU
					D-008140-19	GCAUUCACUUUGACACCAU
EBP	10682	3	B12	M-012282-01	D-012282-01	GAAAGAGUAUGCCAAGGGA
					D-012282-03	GCCGAUACAUCCUGGGUGA
					D-012282-04	ACGAAGACCUGCUUGGAGA
					D-012282-17	CCCACAGUUUGGAGGGACA
SC5DL	6309	3	C03	M-009745-01	D-009745-01	CAAAUUACAUGAUGACCUA
					D-009745-02	GAAGAUUCCUACUCCAUUU
					D-009745-03	GGAAGGGACCGCUCAGUUA
					D-009745-04	GUGCAACACUGAGCUAUUA
DHCR24	1718	3	C04	M-010222-01	D-010222-01	CAACACAUCUGCACUGCUU
					D-010222-02	GAAAUGAGGCAGAGCUCUA
					D-010222-03	GGAGUACAUUCCCUUGAGA
					D-010222-04	CAUCAUCCCUGCCAAGAAG
SOD1	6647	3	C05	M-008364-01	D-008364-05	UCGUUUGGCUUGUGGUGUA
					D-008364-06	ACAAAGAUGGUGUGGCCGA
					D-008364-07	GUGCAGGGCAUCAUCAAUU
					D-008364-08	UUAAUCCUCUAUCCAGAAA
SOD2	6648	3	C06	M-009784-02	D-009784-03	AAAGAUACAUGGCUUGCAA
					D-009784-04	GUAAUCAACUGGGAGAAUG
					D-009784-19	ACCAGGAGGCGUUGGCCAA
					D-009784-20	GGAUUGAUGUGUGGGAGCA
SOD3	6649	3	C07	M-009741-01	D-009741-01	GCGCCAAGCUCGACGCCUU
					D-009741-02	ACGCCAAGGUCACGGAGAU
					D-009741-03	GCGGAGUGGAUCCGAGACA
					D-009741-04	AAGAAGCGGCGGCGCGAGA
CAT	847	3	C08	M-010021-01	D-010021-01	CACAUGACAUUACCAAAUA
					D-010021-02	GGAAUCCAGUUAAUUACUU
					D-010021-03	GAGCACAGCAUCCAAUAUU
					D-010021-04	GGACAUCGCCACAUGAAUG
GPX6	257202	3	C09	M-019309-00	D-019309-01	GCAAGCACGUCCUGUUUGU
					D-019309-02	GCAGUUCAAUACCCACUAG
					D-019309-03	GCGAGGAGUACAUCCAAUU
					D-019309-04	AUAGGAAGGUGGAUUGCAA

Gene Symbol	Gene ID	Plate	Well	Pool Number	Duplex Number	Sequence
GPX1	2876	3	C10	M-008982-00	D-008982-01 D-008982-02 D-008982-03 D-008982-04	GCAAGGUACUACUUAUCGA UGAAUUCCCUCAAGUACGU GGAGAACGCCAAGAACGAA GCAACCAGUUUGGGCAUCA
GPX2	2877	3	C11	M-011675-00	D-011675-01 D-011675-02 D-011675-03 D-011675-04	GAACGAGCAUCCUGUCUUC GAAGGUAGAUUUCAAUACG CAGGAGAACUGUCAGAAUG GCAGGGCCGUGCUGAUUGA
GPX3	2878	3	C12	M-006485-01	D-006485-01 D-006485-02 D-006485-03 D-006485-04	GUACGGAGCCCUCACCAUU GGAUGUCAAUGGAGAGAAA AGGAAGAGCUUGCACCAUU GAGGCUUUGUCCCUAAUUU
GPX4	2879	3	D03	M-011676-01	D-011676-01 D-011676-03 D-011676-04 D-011676-17	CAACGUGGCCUCCCAGUGA GUAACGAAGAGAUCAAAGA CGUCAAAUUCGAUAUGUUC GCUGCGUGGUGAAGCGCUA
GPX5	2880	3	D04	M-009445-01	D-009445-03 D-009445-04 D-009445-17 D-009445-18	GCAAGCACAUCCUCUUCGU UGGCGUACUUGAAGCAAUU AGGCCAUCGCACUUAAUAA GGGAGGAUUUGUACCUAGU
GPX7	2882	3	D05	M-009875-01	D-009875-01 D-009875-02 D-009875-03 D-009875-04	GAAGCGAGAAGACUUAUAA ACAAGGAGAUUGAGAGCUU GCACCUACAGUGUCUCAUU GGACUUCUACGACUUCAAG
SCO2	9997	3	D06	M-011987-01	D-011987-01 D-011987-02 D-011987-03 D-011987-04	GCAGAUCGGCUGAGCAGAU GAACAGAAGCCCUGCGCCA GAACCCGGCUGCUGAUCAC ACAGUUACCGCGUGUACUA
ATPIF1	93974	3	D07	M-017220-00	D-017220-01 D-017220-02 D-017220-03 D-017220-04	AAGAAGAAAUCGUUCAUCA AGAGAGAGCAGGCUGAAGA GCCAUAAGCAGAAGAUCAA GGGCGUGAGGACCAUGCAA
COX4I1	1327	3	D08	M-011625-00	D-011625-01 D-011625-02 D-011625-03 D-011625-04	UGUACGAGCUCAUGAAAGU GCAGAAGCACUAUGUGUAC CGAGUUGUAUCGCAUUAAG CCAAGUGGGACUACGAAAA
COX4I2	84701	3	D09	M-013590-00	D-013590-01 D-013590-02 D-013590-03 D-013590-04	GCACAGAACUCAACGCUGA UCGCAGCUCUGGUGAUUUG GCAGCGGGUCUACGUAUUU GAUGAACCGUCGCUCCAAU
COX5A	9377	3	D10	M-011940-00	D-011940-01 D-011940-02 D-011940-03 D-011940-04	GAACUUAGACCAACUUUAA ACACACUUGUUACCUAUGA GCAUGCAGACGGUUAAAUG GAUAUAGAUGCCUGGGAAU
C12ORF5	57103	3	D11	M-020597-01	D-020597-01 D-020597-02 D-020597-03 D-020597-04	AAUCACAGCUCUAAAGUUA GAUAUGACGGUAAAGUAUG GAAAUACGGGGUUGUAGAA GAGUCACGGUGCUUACAUG
OXCT1	5019	3	D12	M-004045-00	D-004045-01 D-004045-02 D-004045-03 D-004045-04	GAACGACAGUACUUAUCUG UUAUGUACAUCGCCUUAUA UGUGUCAACCGCAUUAUUA UCAACCGCAUUAUUACUGA
OXCT2	64064	3	E03	M-013881-00	D-013881-01 D-013881-02 D-013881-03 D-013881-04	UUAUGUAGAUCGCGUGAUA CCAAGAUCAUGGAGAAAUG ACGCGCAGCUCUGGAAUUU GCGCUUAACGAUCCUGAAA
SLC16A7	9194	3	E04	M-007409-01	D-007409-01 D-007409-02 D-007409-04 D-007409-17	GGAUUUAACUGGAGAAUAU GAUAGCAGGAGGCUUAUUA CAGCAAAUAUUCCACACUA CGGAAGAUGUUAACGUCAA
SLC16A3	9123	3	E05	M-005126-03	D-005126-03 D-005126-04 D-005126-05 D-005126-06	GGCAACUUCUUCUGCAUUA CGACCCACGUCUACAUGUA CAUGGUGGCUGCGUCCUUU GCUCACCUCCUCCCUGAUU
SLC16A8	23539	3	E06	M-007410-01	D-007410-02 D-007410-03 D-007410-04 D-007410-17	GCACGUCCCGUAUCUGUUC CCAAAGCCGUGAGCGUCUU UGUACGCCGUCACCAAGUU CUGCCUGCGUUGUGCUAAA

Gene Symbol	Gene ID	Plate	Well	Pool Number	Duplex Number	Sequence
SLC16A4	9122	3	E07	M-007406-00	D-007406-01	GACAGGAGCCCUUAUAUUA
					D-007406-02	GAAACACACUGCCAUGAGA
					D-007406-03	GAAGAAAGUGAUAAGGUUA
					D-007406-04	UGACAUACUUGGAGAGAAA
TALDO1	6888	3	E08	M-008996-02	D-008996-01	GAGCAGAAAUACUAAAGAA
					D-008996-02	CAGCACAGAUGCCCGCUUA
					D-008996-05	CACAAGAGGACCAGAUUAA
					D-008996-18	CCACAGAAGUAGACGCAAG
RPE	6120	3	E09	M-012767-00	D-012767-01	GGGCUAAUCAGAUAGAUAU
					D-012767-02	GAGCUAACAUGAUUGUGUC
					D-012767-03	GUUCCCAUCUUUGGAUAUA
					D-012767-04	CCAUAAAUGUGCAGAGGCA
GFPT1	2673	3	E10	M-008833-01	D-008833-02	GGACGAGGCUAUCAUUAUG
					D-008833-03	UGAAACGGCUGCCUGAUUU
					D-008833-17	GAGCAUGGAUGACGAAAUU
					D-008833-18	CAUGCAAGAAAGACGCAAA
GFPT2	9945	3	E11	M-010390-01	D-010390-01	UCGCCAAGCUGAUUAAAUA
					D-010390-03	GAUCAUCCGUGGCUUGAGA
					D-010390-04	AGACAAAGGCAACGAAUUU
					D-010390-17	CGAUGGGAAUAAUCACGAA
GNPNAT1	64841	3	E12	M-005239-01	D-005239-02	CGGCAACUCUGAUUAUAGA
					D-005239-03	CUACAUGUGUCGGAGGUUU
					D-005239-04	GUACUGCUGACUUAAAUAG
					D-005239-17	GGAUUACAUAUGUCGGCUA
UAP1	6675	3	F03	M-017160-01	D-017160-01	GAACAAAGUUUCUAUGGCU
					D-017160-02	UGAGAGAUGUUGUCAAUGU
					D-017160-03	CUACUACGUUUCUGGAAUG
					D-017160-04	ACCCAAGGACAGUUAAUUA
OGT	8473	3	F04	M-019111-00	D-019111-01	GCAGUUCGCUUGUAUCGUA
					D-019111-02	CGACAUGCAUUGCGUCUCA
					D-019111-03	GAUUAAGCCUGUUGAAGUC
					D-019111-04	CCGAGAAAUUGGCUUAUAU
PGM1	5236	3	F05	M-010925-00	D-010925-01	CGAAUCGUCUUCCGACUGA
					D-010925-02	GUACAUCGAUAGCUAUGAG
					D-010925-03	CGACUGAAGAUCCGUAUUG
					D-010925-04	GGAAAUUGUGGAUUCGGUA
PGM3	5238	3	F06	M-013912-00	D-013912-01	GAGGUCAAUUCCAUGAUUA
					D-013912-02	GGAUUUAGGUGCUAUUACA
					D-013912-03	GGGCAAACUCAAUCAUUUA
					D-013912-04	GACAAGAUAGCAACGUUAA
WBSCR14	51085	3	F07	MU-009253-00	D-009253-01	GACACUCUCUUCACCAUGAUU
					D-009253-02	ACAAGUGGCGCAUCUACUAUU
					D-009253-03	GGGCACAUCUACCAGUAUCUU
					D-009253-04	GCCCAUGCCUUCAAACUUCUU
SLC25A10	1468	3	F08	MU-007469-00	D-007469-01	GCAGACAGAUGACCUACUCUU
					D-007469-02	GUACCUCUCUGACAACAUCUU
					D-007469-03	CCGCGUAGCUCGUGAAGAGUU
					D-007469-04	CUGAAGACUCGCCUGAUGUU
ME1	4199	3	F09	MU-009348-02	D-009348-02	CAUCUGACAUUGAGAAAUU
					D-009348-03	AGUAAGAGGUUCUGAAUAU
					D-009348-19	CCUUGCAGCUCUUCGAAUA
					D-009348-05	GGUAAAUUGGCUCUAUAUA
ME2	4200	3	F10	MU-009461-00	D-009461-01	GAAGAAGCAUAUACACUUAUU
					D-009461-02	UGAAAGGCCUGUAAUAUUUUU
					D-009461-03	GAACAUGGCGGAGUGAAUAUU
					D-009461-04	GAAACGAGAUCGCACACAAUU
GLS	2744	3	F11	MU-004548-00	D-004548-01	AGACAUGGUUGGUAUAUUAUU
					D-004548-02	UGAAUAAGAUGGCUGGUAAUU
					D-004548-03	GGUGGUUUCUGCCCAAUUAUU
					D-004548-04	GAAUAACACUCCCAUGGAUUU
GLS2	27165	3	F12	MU-012500-00	D-012500-01	UCAAACUGCUUCAAGAUUAUU
					D-012500-02	GAACUUAGAAAGCAUGGUAUU
					D-012500-03	CAAGUGGCCUGCGCUACAAUU
					D-012500-04	GCCAUCGGCUAUUAUCUCAUU

Gene Symbol	Gene ID	Plate	Well	Pool Number	Duplex Number	Sequence
PIK3CA	5290	3	G03	MU-003018-03	D-003018-07 D-003018-08 D-003018-24 D-003018-25	GGACAACUGUUUCAUAUAG GCCAGUACCUCAUGGAUUA CUUGAAGAGUGUCGAAUUA GCUUGAAGAGUGUCGAAUU
MYLCD	23417	3	G04	MU-009626--01	D-009626-01 D-009626-02 D-009626-03 D-009626-04	GGAAUGAACUCUUUACAGA GAACAUCCUCCAUCAGAAA UGAAAGGAAUGCUCUCAGA UCAACUGGAUGGCGGAUGU
IRS1	3667	3	G08	MU-003015-01	D-003015-05 D-003015-06 D-003015-07 D-003015-08	AAAGAGGUCUGGCAAGUGA GAACCUGAUUGGUAUCUAC CCACGGCGAUCUAGUGCUU GUCAGUCUGUCGUCCAGUA
PTEN	5728	3	G12	MU-003023-01	D-003023-05 D-003023-06 D-003023-07 D-003023-08	GUGAAGAUCUUGACCAAUGUU GAUCAGCAUACACAAAUUAUU GGCGCUAUGUGUAUUAUUAUU GUAUAGAGCGUGCAGAUAAUU
MYC	4609	3	H03	MU-003282-07	D-003282-14 D-003282-15 D-003282-16 D-003282-35	AACGUUAGCUUCACCAACA GGAACUAUGACCUCGACUA GAACACACAACGUCUUGGA CUACCAGGCUGCGCGCAAA
RPTOR	57521	3	H04	MU-004107-00	D-004107-01 D-004107-02 D-004107-03 D-004107-04	GAAACCAUCGGUGCAAAUUUU AGAAGGGCAUUACGAGAUUUU UGGAGAAGCGUGUCAGAUAUU GCCCGUCGAUCUUCGUCUAUU
RICTOR	253260	3	H05	MU-016984-01	D-016984-01 D-016984-02 D-016984-03 D-016984-04	UCAACGAGCUCACAUAUGAUU GUACGAAGACUACUUUAUUUU UGACCGAUCUGGACCCAUAUU GUACUUGGGCUCAUAGCUAUU
SLC16A1	6566	3	H06	MU-007402-02	D-007402-01 D-007402-02 D-007402-05 D-007402-18	GCAGUAUCCUGGUGAAUAA AGAGGAAGCUUUCUAAUUC GGUAAUUGGAGCUUUCAUU GCCAAUAAGACCUCGAAUU
SLC25A1	6576	3	H07	MU-007468-01	D-007468-01 D-007468-02 D-007468-05 D-007468-06	CCAUAGUGUUUGUCAUCUA GCCUGGAGGCGCACAAAUA GCGCACAAAUACCGGAACA UGAAGCUGCUCAACAAAGU
PDK1	5163	3	H08	MU-005019-00	D-005019-01 D-005019-02 D-005019-03 D-005019-04	GGAAGUCCAUCUCAUCGAAUU GGAACACCAUGCCAACAGAUU GAUCAGAAACCGACACAAUUU GAUCAGUGAAUGCUUGUGAUU
PDK2	5164	3	H09	MU-005020-00	D-005020-01 D-005020-02 D-005020-03 D-005020-04	CAAAGAUGCCUACGACAUGUU GCACGGAGCCCAAGAACACUU GCUCCUGUGUGACAAGUAUUU CCAGCACACCCUCAUCUUUUU
CPT1a	1374	3	H10	MU-009749-02	D-009749-01 D-009749-02 D-009749-05 D-009749-18	GAGAGAACCUCAUCAAUUU GAAGAAGGAUACAGAAGUG GGACAGCUACGCCAAAUCU UGACAACGAUGUACGCCAA
CPT1b	1375	3	H11	MU-010266-01	D-010266-04 D-010266-17 D-010266-18 D-010266-19	CAAGUAACUAUGUGAGUGA GAUCAUGUAUCGCCGUAAA GGACUGAGACUGUGCGUUC CAUGAUUGCAGGCGAGAAC
AKT1 AKT2 AKT3	207 208 209	3	H12	MU-003000-03 MU-003001-02 MU-003002-02	D-003000-05 D-003000-07 D-003000-08	GACAAGGACGGGCACAUUA GCUACUUCCUCCUCAAGAA GACCGCCUCUGCUUUGUCA